



TS Fuzzy Approach for Modeling, Analysis and Design of Non-smooth Dynamical Systems

Kamyar Mehran

School of Electrical, Electronic and Computer Engineering
Department of Science and Engineering
Newcastle University

Thesis submitted for the partial fulfilment of degree of
Doctor of Philosophy · 2010 ·

Abstract

There has been growing interest in the past two decades in studying the physical model of dynamical systems that can be described by nonlinear, non-smooth differential equations, i.e. non-smooth dynamical systems. These systems exhibit more colourful and complex dynamics compared to their smooth counterparts; however, their qualitative analysis and design are not yet fully developed and still open to exploration. At the same time, Takagi-Sugeno (TS) fuzzy systems have been shown to have a great ability to represent a large class of nonlinear systems and approximate their inherent uncertainties. This thesis explores an area of TS fuzzy systems that have not been considered before; that is, modelling, stability analysis and design for non-smooth dynamical systems.

TS fuzzy model structures capable of representing or approximating the essential discontinuous dynamics of non-smooth systems are proposed in this thesis. It is shown that by incorporating discrete event systems, the proposed structure for TS fuzzy models, which we will call non-smooth TS fuzzy models, can accurately represent the smooth (or continuous) as well as non-smooth (or discontinuous) dynamics of different classes of electrical and mechanical non-smooth systems including (sliding and non-sliding) Filippov's systems and impacting systems. The different properties of the TS fuzzy modelling (or formalism) are discussed. It is highlighted that the TS fuzzy formalism, taking advantage of its simple structure, does not need a special platform for its implementation.

Stability in its new notion of structural stability (stability of a periodic solution) is one of the most important issues in the qualitative analysis of non-smooth systems. An important part of this thesis is focused on addressing stability issues by extending non-smooth Lyapunov theory for verifying the stability of local orbits, which the non-smooth TS fuzzy models can contain. Stability conditions are proposed for Filippov-type and impacting systems and it is shown that by formulating the conditions as Linear Matrix inequalities (LMIs), the onset of non-smooth bifurcations or chaotic phenomena can be detected by solving a feasibility problem. A number of examples are given to validate the proposed approach. Stability robustness of non-smooth TS fuzzy systems in the presence of model uncertainties is discussed in terms of non-smoothness rather than traditional observer design.

The LMI stabilization problem is employed as a building block for devising design strategies to suppress the unwanted chaotic behaviour in non-smooth TS fuzzy models. There have been a large number of control applications in which the overall closed-loop system can be stabilized by switching between pre-designed sub-controllers. Inspired by this idea, the design part of this thesis concentrates on fuzzy-chaos control strategies for Filippov-type systems. These strategies approach the design problem by switching between local state-feedback controllers such that the closed-loop TS fuzzy system of interest rapidly converges to the stable periodic solution of the system. All control strategies are also automated as a design problem recast on linear matrix inequality conditions to be solved by modern optimization techniques.

Keywords: Takagi-Sugeno fuzzy systems, non-smooth Lyapunov theory, non-smooth dynamical systems, piecewise-smooth dynamical systems, structural stability, discontinuity-induced bifurcation, chaos controllers, dc-dc converters, Filippov's system, impacting system, linear matrix inequalities.

Contents

Acknowledgments	x
1 Introduction	1
1.1 Motivation	1
1.2 Smooth nonlinear dynamical systems	2
1.3 Non-smooth dynamical systems	3
1.4 Takagi-Sugeno fuzzy systems	5
1.5 Contributions	6
1.6 Publications	7
1.7 Organization of the thesis	7
2 Background	9
2.1 Non-smooth dynamical systems - Case studies	10
2.1.1 Case Study I: DC-DC electronic converters	10
2.1.2 Case Study II: A hard-impact oscillator	13
2.1.3 Case Study III: A dry-friction oscillator	16
2.2 Theory and concepts of NSDS	18
2.2.1 Classification	18
2.2.2 Smooth bifurcations	20
2.2.3 Discontinuity-induced bifurcation: a unique bifurcation phenomenon	23
2.2.4 Structural stability of an invariant set	25
2.2.5 Discontinuity map: a prevailing tool to study impacting dynamics	31
2.2.6 Sliding motions in Filippov-type systems	33
2.3 Summary	36
3 Takagi-Sugeno fuzzy modeling	38
3.1 Models for smooth dynamical systems	38
3.1.1 TS fuzzy model structure	38
3.1.2 Constructing smooth TS fuzzy models	41
3.1.3 The stimulating example	46
3.2 Models for non-smooth dynamical systems	49
3.2.1 Discrete-event dynamical systems	49
3.2.2 Non-smooth TS fuzzy model structure	50
3.2.3 Evolution of states in a non-smooth TS fuzzy model	55
3.2.4 The possibility of representing sliding dynamics	56
3.2.5 Sufficient conditions for existence and uniqueness	57
3.2.6 Constructing non-smooth TS fuzzy models	64
3.2.7 Numerical simulation	85
3.3 Summary	87

4	Stability Analysis	89
4.1	Lyapunov's stability for smooth TS fuzzy systems	89
4.1.1	Existing formulations for stability analysis	93
4.2	Structural stability analysis	97
4.2.1	Non-smooth Lyapunov functions	98
4.3	Stability theorems for Filippov-type systems	100
4.3.1	Substitution of confined regions with LMI quadratic forms	105
4.4	Stability theorems for impacting systems	108
4.5	Substituting flexible regions by quadratic inequalities	109
4.5.1	Region Ω restricted by hyperplanes	110
4.5.2	Bifurcation analysis of the case studies	114
4.5.3	Numerical Complexity	125
4.6	Robustness	126
4.6.1	Model uncertainties in switch sets	126
4.6.2	Model uncertainties in selecting fuzzy sub-vector fields	128
4.7	Summary	129
5	Controller design for DC-DC converters	131
5.1	General motive	131
5.2	Literature on Fuzzy-chaos control	132
5.3	Design problem	134
5.4	Fuzzy switching (gain-scheduling) strategy	135
5.5	Summary	153
6	Concluding Remarks	155
6.1	Overview and Summary of Contributions	155
6.2	Topics for Future Research	157
	Appendices	159
A	Modeling and analysis of current-mode controlled Ćuk converter	160
A.1	TS fuzzy model of the Ćuk converter	162
A.2	Structural stability analysis	165
B	Linear Matrix Inequalities	167
B.1	The formal definition	167
B.1.1	Some standard LMI problems	168
B.1.2	\mathcal{S} -procedure	168
B.2	Nonlinear matrix inequalities	169
B.2.1	Bilinear matrix inequalities	169
B.2.2	Quadratic matrix inequalities	169
B.3	Finding a solution to strict inequalities	170
B.4	LMI solvers	173
C	Parameter Values	174
C.1	DC-DC Converters	174
C.2	Forced hard impact oscillator	175
C.3	Forced dry-friction oscillator	175
	Bibliography	175

List of Figures

2.1	Single-diode DC-DC (a) boost and (b) buck power electronic converters along with their control circuits. R , L , C , D and S stand for resistance, inductance, capacitance, diode and switch in both circuits. r_{VD} , r_S , r_L and r_C are the parasitic resistance of the diode, switch, inductance and capacitance respectively in the boost converter circuit. All the parameter values can be found in Appendix C.	10
2.2	Nominal stable period-1 operation of the current-mode controlled boost converter. The period of the regulated output signals of (a) voltage and (b) current of the boost converter are equal to the period of the PWM signal. .	12
2.3	In nominal stable period-1 operation of the voltage-mode controlled buck converter, the period of the regulated output signals of (a) voltage and (b) current, are equal to the period of the ramp signal v_{ramp}	12
2.4	Periodic orbit of the boost converter: (a) period-1 stable operation with $V_{in} = 50V$, (b) period-2 operation with $V_{in} = 35.7V$ and (c) chaotic operation with $V_{in} = 20V$. The symbol (inside the bracket in labels) represents the variable of the respective label not the unit.	12
2.5	Periodic orbit of the buck converter: (a) period-1 stable operation with $V_{in} = 23V$, (b) period-2 operation with $V_{in} = 24.53V$ and (c) chaotic operation with $V_{in} = 33V$. The symbol (inside the bracket in labels) represents the variable of the respective label not the unit.	13
2.6	The bifurcation diagram summarizes the simulated dynamics upon varying the input voltage V_{in} as a parameter of the buck converter. The narrow band starting very close to the operating point $V_{in} = 24.16$ shows that a period-3 attractor can coexist with the stable period-1 orbit (coexisting attractors). This condition cannot be visible in the experimental setup of the converter [1] but it is well observed in numerical simulations where a large number of initial conditions are chosen randomly.	13
2.7	A one-degree-of-freedom hard impact oscillator.	14
2.8	Periodic solutions of the hard-impact oscillator (2.5)-(2.6) when (a) period-1 stable with $F = 0.275N$ and $\varpi = 2.97$, (b) chaotic with $F = 0.276N$ and $\varpi = 2.97$. The symbol (inside the bracket in labels) represents the variable of the respective label not the unit.	15
2.9	The bifurcation diagram (a) shows the ω -limit set for increasing $F \in (0.2, 0.34)$ for $\varpi = 2.97$, (b) magnified to show the qualitative change of the solution (u, v) from a stable periodic behaviour when $F = 0.275N$ and $\varpi = 2.97$ to a chaotic behaviour when $F = 0.276N$ and $\varpi = 2.97$ [2].	16
2.10	A model of forced dry-friction oscillator [3]	17
2.11	A simpler model: an unforced dry-friction oscillator.	17
2.12	Solution trajectories of the unforced dry-friction oscillator (model (2.9)). . .	18
2.13	If the forcing function amplitude is set to $F = 0.1$, then (a) $4T$ stable periodic orbit at the forcing frequency $\omega = 1.70781$, (b) chaotic orbit induced by grazing the boundary of sliding region (grazing-sliding event) at the forcing frequency $\omega = 1.7077997$ where the discontinuity-induced bifurcation occurs.	19

2.14	The bifurcation diagram shows the grazing-sliding bifurcation where there is a sudden transition to a chaotic attractor.	19
2.15	The classification of non-smooth dynamical systems (NSDS). The number in brackets associated with each block represents the degree of smoothness (DoS).	20
2.16	(a) A saddle-node bifurcation, (b) A transcritical bifurcation. <i>eig</i> is denoted as an eigenvalue of the Jacobian (2.15).	22
2.17	(a) A supercritical pitchfork bifurcation, (b) A subcritical pitchfork bifurcation.	22
2.18	(a) A supercritical Hopf bifurcation, and (b) A subcritical Hopf bifurcation.	23
2.19	The bifurcation diagram for the logistic map $x_{n+1} = \rho x_n(1 - x_n)$ under a range of parameter variation of $\rho \in [2.4, 4]$. The asymptotic behaviour of the sampled state variable x , plotted as discrete points, shows Feigenbaum's cascade of period-doubling bifurcation leading to chaos.	23
2.20	The 3-dimensional view illustrates how the periodic solution $\Gamma(t)$ is mapped to the fixed point x^* of the discrete-time map; that is, the Poincaré map.	28
2.21	On the onset of a DIB, the eigenvalues of the Poincaré map undergo a jump (a) through the real axis (b) through the imaginary axis.	30
2.22	The fate of the orbit $\Phi(t, x_0)$ when a perturbation δ is added to its initial conditions to become $\tilde{x}_0 = x_0 + \delta$. $\tilde{x}(t)$ is assumed to cross the switching manifold Σ_{ij} at the point $\tilde{x}(t_\Sigma)$ but it actually crosses Σ_{ij} at the point $\tilde{x}(\tilde{t}_\Sigma)$ where there is a small time lag $\delta t = \tilde{x}(\tilde{t}_\Sigma) - \tilde{x}(t_\Sigma)$, producing an error in the derivation of the Poincaré map.	31
2.23	Behaviour of the periodic orbit $\Phi(t, x)$ close to the switching manifold Σ_{ij} for the impacting system in case study II: (a) the periodic orbit initiating at some initial condition $x_0 \in \Xi$ close to x^* do not intersect Σ_{ij} meaning the impact has not occurred yet, (b) the periodic orbit grazes Σ_{ij} , and (c) the periodic orbit intersect Σ_{ij} twice, meaning the impact has occurred. In this case a smooth reset map $R : x \mapsto R(x)$ applies to explain the discontinuous jump of the state to a new position.	32
2.24	Zero-time discontinuity mapping close to grazing in an impacting system. The solid line represents the actual trajectory while the dashed line represents the extended ones. The ZDM is the map $x_1 \mapsto x_4$	33
2.25	Illustration of sliding motion using Filippov's convex combination method.	36
2.26	Illustration of Utkin's equivalent control method where $F^{eq} := F_{12}$	36
3.1	Membership functions for the off-equilibrium linearization method. Variables z_1 and z_2 represent the equivalent fuzzy variables for system states x_1 and x_2 , respectively.	42
3.2	The surface function of (a) the original system (3.8) (white mesh) and it's TS fuzzy model (grey mesh underneath), (b) the error between the original system and its TS fuzzy model.	43
3.3	Membership functions for the sector nonlinearity method.	45
3.4	The surface function of (a) the original system (3.8) (white mesh) and it's TS fuzzy model (grey mesh underneath), (b) the error between the original system and its TS fuzzy model.	45
3.5	Vector fields of the original system (3.10) along with its TS fuzzy approximation obtained using off-equilibrium linearization, (a) with the first set of linearization points, (b) with the more granular set of linearization points.	47
3.6	Suitable membership functions defined for (a) first set of linearization points, (b) the more granular set of linearization points.	48
3.7	The evolution of the state variables of a discrete-event system (a) by events at time k , and (b) in real time t_k	50

3.8	Trajectories evolve in a non-smooth TS fuzzy model based on different fuzzy sub-vector fields whose global state spaces (or regions) are separated from each other. Changing of the discrete state m will result in moving from one state space to another state space containing a smooth flow, represented by a fuzzy sub-vector field F_{m_i} , $i = 0, 1, 2, \dots, N$. Each fuzzy state space region \mathcal{F}_i , $i = 0, 1, 2, \dots$, can also be locally divided to different operating regions resulting from the piece-wise linear structure of the membership functions.	55
3.9	The shaded surface depicts the (measure-zero) sliding manifold S , formed by coinciding $S_{i,k}$ and $S_{k,i}$ at certain fuzzy states and the opposite direction of the flows of F_{m_i} and F_{m_k} . In this case an infinite number of rapid switches between the two discrete states m_i and m_k associated with the fuzzy sub-vector fields F_{m_i} and F_{m_k} can occur.	56
3.10	Another Possible scenario of coinciding switch sets $S_{i,k}$ and $S_{k,i}$ in a non-smooth TS fuzzy system would result the formation of a non-measure-zero sliding region.	57
3.11	Membership functions defined for Example 3.4	61
3.12	(a) The response of a non-smooth TS fuzzy system as a oscillatory closed orbit. (b) Changing the location of switching manifolds can result in a stable TS fuzzy system.	63
3.13	Switchings between stable fuzzy subsystems may lead to an unstable system.	64
3.14	Waveform of the inductor current $i_L(t)$ in the boost converter.	68
3.15	Output current time responses of the boost converter: (a) the original system in period-1 operation ($V_{in} = 45V$), (b) its TS Fuzzy model in period-1 operation ($V_{in} = 45V$), (c) the original system in an unstable period-2 operation ($V_{in} = 36V$), (d) its TS Fuzzy model in period-2 operation ($V_{in} = 36V$) (e) the original system in an unstable period-4 operation ($V_{in} = 34V$), (f) its TS Fuzzy model in period-4 operation ($V_{in} = 34V$) (g) the original system operating in chaos ($V_{in} = 20V$), and (h) its TS Fuzzy model ($V_{in} = 20V$).	69
3.16	Output voltage time responses of the boost converter: (a) the original system in period-1 operation ($V_{in} = 45V$), (b) its TS Fuzzy model in period-1 operation ($V_{in} = 45V$), (c) the original system in an unstable period-2 operation ($V_{in} = 36V$), (d) its TS Fuzzy model in period-2 operation ($V_{in} = 36V$) (e) the original system in an unstable period-4 operation ($V_{in} = 34V$), (f) its TS Fuzzy model in period-4 operation ($V_{in} = 34V$) (g) the original system operating in chaos ($V_{in} = 20V$), and (h) its TS Fuzzy model ($V_{in} = 20V$).	70
3.17	The long term behaviour of the boost converter for $V_{in} \in (10, 50)$ is shown via bifurcation diagrams (using switch-on sampling) in (a) the original system, (b) and (c) its TS fuzzy model.	71
3.18	The bifurcation diagram for $V_{in} \in (22, 33)$ shows the long-time behaviour of the TS fuzzy model of the buck converter.	73
3.19	Output voltage and current time responses of the buck converter when (a) operating in stable period-1 ($V_{in} = 24V$), (b) operating in period-2 ($V_{in} = 25V$), (c) operating in period-4 ($V_{in} = 32V$). Small differences between the original system 's output (solid line) and it's TS fuzzy model (dashed line) were intentionally introduced for the sake of visibility, otherwise there exists no error in modeling.	73
3.20	The coexisting stable (thick line) and unstable (narrow line) periodic orbit of the TS fuzzy model of the buck converter for $V_{in} = 25V$	74

3.21	Time responses, produced from (a) the original impacting system ($\varpi = 2.97$, $F = 0.275N$) when the system is stable, (b) its TS fuzzy model ($\varpi = 2.97$, $F = 0.275N$), (c) the original impacting system ($\varpi = 2.97$, $F = 0.2759N$) when the system becomes chaotic, (d) its TS fuzzy model ($\varpi = 2.97$, $F = 0.276N$), (e) the original impacting system ($\varpi = 2.97$, $F = 0.277N$) when the system becomes stable again, and (f) its TS fuzzy model ($\varpi = 2.97$, $F = 0.277N$).	77
3.22	The bifurcation diagrams (b-f) shows the dynamics close to grazing in the original impact oscillator when (b) $\varpi = 1$, (c) $\varpi = 2$, (d) $\varpi = 3$, (e) $\varpi = 4$, and (f) $\varpi = 5$. The diagrams (g-j) show the corresponding TS fuzzy model figures.	78
3.23	The grazing bifurcation in (a) the impact oscillator, and (b) its TS fuzzy model when $\varpi = 2.97$	79
3.24	$4T$ -periodic ($8\pi/\omega$) orbit of the non-smooth TS fuzzy model (3.42) when (a) it's stable and grazing does not take place, (b) grazes the switching manifold where a sliding region is formed, (c) becomes chaotic due to the grazing-sliding DIB.	81
3.25	Time responses, produced from (a) the original dry-friction oscillator, and (b) its TS fuzzy model, when the system is stable at the forcing frequency $\omega = 1.70781$. The time responses when (c) the original dry-friction oscillator and (d) its TS fuzzy model, becomes chaotic at the frequency $\omega = 1.70779$	81
3.26	Bifurcation diagram obtained from the direct simulation of the TS fuzzy model (3.42) shows the grazing-sliding DIB at the frequency $\omega = 1.70778$	82
3.27	Membership functions for Example 3.9	84
3.28	Comparing (a) the original system and (b) the TS fuzzy model using the approach of Taylor Expansion for constructing non-smooth TS fuzzy models.	84
4.1	Geometrical notion of Lyapunov stability where solution trajectory 1 is stable, solution trajectory 2 is unstable, solution trajectory 3 is asymptotically stable and solution trajectory 4 is exponentially stable.	92
4.2	The non-smooth Lyapunov function candidate is non-smooth at region Λ_{45} (where the switching $S_{i,j}$ occurs) and piecewise-continuous with respect to time in every region Ω_q where the local functions V_q should be reduced to prove stability.	100
4.3	The white region Ω is substituted with a region representing semi-definite conditions $x^T Z_1 x \geq 0$, $x^T Z_2 x \geq 0$ and $x^T Z_3 x \geq 0$, each of which limited by two hyperplanes $(f^a)^T x \geq 0$ and $(f^b)^T x \geq 0$ requiring both set of states x_0 and $-x_0$ to be fulfilled for inequality conditions. The region Ω can be also substituted with semi-definite conditions whose property requires to fulfill just for set of states x_0	111
4.4	Shaded cubic region Ω restricted by two half-planes can also be substituted by an ellipsoid.	112
4.5	An illustration of region partitioning and estimated energy levels of the non-smooth Lyapunov function candidate in the local regions (dot-dashed curves) when sliding (local) orbit grazes the switching manifold.	124
5.1	Weighting function $w^j(\theta)$ for a specific value p of x_1 . The vertices of the weighting functions for a specific value p of x_1 are given by the intersection of the vertical $x_1 = p$ and the hyperplanes.	139
5.2	The cross-hatched regions are states fulfilling (left) $x^T(F_{m_1}P_1 + P_1F_{m_1})x \leq 0$, (middle) $x^T(F_{m_2}P_2 + P_2F_{m_2})x \leq 0$ and (right) $x^T(P_2 - P_1)x \leq 0$	139
5.3	The cross-hatched regions indicate states where both local Lyapunov functions decreases and the energy reduces when the switching occurs from $F_{m_1}x$ to $F_{m_2}x$ and $F_{m_2}x$ to $F_{m_1}x$	139

5.4	Switching anywhere in the cross-hatched regions leads to a stable closed-loop TS fuzzy system, if the sub-vector field switchings take place in the interior of the cross-hatched regions.	140
5.5	Switching from the fuzzy sub-vector field $F_{m_1}x$ to $F_{m_2}x$, at any place in the cross-hatched region, or inversely in the non-cross-hatched region, leads to a stable closed-loop fuzzy system. The solid-line solution trajectory is simulated with the manipulated switch sets ($k = 0.2$) against the dotted-dashed-line trajectory with initial switch sets. It is apparent that the convergence rate of the solid-line trajectory is faster than the dot-dashed trajectory. . .	141
5.6	Bifurcation diagrams varying reference current using (a),(b) the conventional control scheme, and (c), (d) the proposed TS fuzzy control scheme. .	144
5.7	Bifurcation diagrams varying supply voltage using (a),(b) the conventional control scheme and (c), (d) the proposed TS fuzzy control scheme.	144
5.8	System responses is (a),(b) chaotic under the conventional control scheme, and (d), (c) regulated under the proposed TS fuzzy control scheme.	145
5.9	Output current response of the close-loop system subject to a sudden supply voltage V_{in} change from 45V to 85V and 85V to 45V at 0.1s and 0.2s, respectively, with the fixed parameter $R = 30\Omega$ under (a),(b) the conventional control scheme, and (c), (d) the proposed TS fuzzy control scheme. (b) and (d) are the magnified rectangle area in (a) and (c), respectively. . .	146
5.10	Output current response of the close-loop system subject to a large reference current I_{ref} step change from 4A to 6A at 0.2s with the fixed parameter $V_{in} = 45V$ under (a),(b) the conventional control scheme and (c), (d) the proposed TS fuzzy control scheme. (b) and (d) are the magnified rectangle area in (a) and (c), respectively.	146
5.11	Output current response of the close-loop fuzzy system subject to a sudden load resistance R changing from 30Ω to 50Ω and 50Ω back to 30Ω at 0.1s and 0.2s respectively with the fixed parameters $V_{in} = 45V$ and $I_{ref} = 4A$ under (a), (b) the conventional control scheme and (c), (d) the proposed TS fuzzy control scheme. (b) and (d) are the magnified rectangle area in (a) and (c), respectively.	147
5.12	Output voltage response of the closed-loop fuzzy system subject to an abrupt variations of (b) supply voltage ($45V \rightarrow 85V \rightarrow 45V$), (d) the reference current ($4A \rightarrow 6A$), (f) load resistance ($30\Omega \rightarrow 50\Omega \rightarrow 30\Omega$), verses that of the conventional control scheme (a, b, and c) under the same abrupt variations.	148
5.13	System responses at $V_{in} = 24.16V$ is (a),(c) unstable with period-3 attractor under conventional control, (b),(d) regulated to period-1 orbit under the proposed TS fuzzy control.	150
5.14	System responses at $V_{in} = 25V$ (a),(c) unstable with period-2 attractor under conventional control, (b),(d) regulated to period-1 orbit under the proposed TS fuzzy control.	150
5.15	Bifurcation diagrams of output voltage v_C with the input voltage V_{in} as the bifurcation parameter for (a) conventional control, (b) proposed TS fuzzy control scheme. Evidently the proposed TS fuzzy control scheme can structurally stabilize the output voltage for a wide range of parameter variation.	151
5.16	Bifurcation diagrams of output current i_L with the input voltage V_{in} as bifurcation parameter for (a) conventional control, (b) proposed TS fuzzy control. Evidently the proposed TS fuzzy control scheme can structurally stabilize the output current for a wide range of parameter variation.	152

5.17	Output voltage response of (a), (b) the conventional control scheme subject to an abrupt variations of supply voltage ($20V \rightarrow 35V \rightarrow 20V$) versus (c), (d) the closed-loop TS fuzzy system scheme under the same conditions. (b) and (d) are the magnified rectangle area in (a) and (c), respectively.	153
5.18	Output voltage response of the closed-loop TS fuzzy control system subject to an abrupt variation of supply voltage ($20V \rightarrow 35V \rightarrow 20V$). The transient response is significantly improved using Theorem 5.1. (b) shows the magnified rectangle area in (a).	153
A.1	Current-mode controlled Ćuk converter.	160
A.2	Nominal stable period-1 operation of the current-mode controlled Ćuk converter. The period of the regulated output signals of (a) first inductor current and (b) sum of the inductor currents of the Ćuk converter are equal to the period of the PWM signal.	161
A.3	Periodic orbit of the Ćuk converter: (a) period-1 operation with $I_{\text{ref}} = 0.4A$, (b) period-2 operation with $I_{\text{ref}} = 0.51A$ and (c) chaotic operation with $I_{\text{ref}} = 0.7A$	161
A.4	The Monte carlo bifurcation diagram of the Ćuk converter shows how the circuit loses its stability to a period-2 and then to a chaotic attractor upon variation of the reference current I_{ref} as a bifurcation parameter.	162
A.5	The phase space diagram shows the transversal intersection of stable period-1 limit cycle.	163
A.6	The non-smooth TS fuzzy model (A.4) operates in (a) stable period-1 orbit when $I_{\text{ref}} = 0.4A$, (b) period-2 orbit when the reference current is varied to $I_{\text{ref}} = 0.5A$, and (c) chaotic orbit when the reference current is varied to $I_{\text{ref}} = 0.7A$	164
A.7	The Monte-carlo bifurcation diagram of the TS fuzzy model of the Ćuk converter (A.4) when the reference current I_{ref} is varied as a bifurcation parameter.	164
B.1	(a) The vector field is bidirectional between Ω_q^x and Ω_r^x . The circle on the surface show the turning point of the vector fields. (b) Two regions are split into four to avoid an implicit equality like $\tilde{P}_q = \tilde{P}_r$	172

List of Tables

2.1	The different types of non-smooth dynamical system	21
A.1	Different trials of partitioning of $\Omega \in \mathcal{F}$ shows too many region partitions may lead to a conservative result	165

Acknowledgments

The course of PhD studies can be synonymous with the subject of this thesis as I have understood and realized in many ways. In the initial stages, despite your enthusiasm, the subject of your research appears hazy and uncertain. The trajectory of your progress is nonlinear and I may say, non-smooth. At times you are filled with sheer joy of discovering novel ideas, which may follow with boredom and disappointment. Then for the unknown period of time, through testing and applying numerous ideas, you are face with unforeseen and possibly surprising aspects of your project. Although my academic achievement for this course of study, appears small, upon my discovery, the domain of my knowledge is infinitesimal compared to my unknowns, I could say, my life lessons have reached to a certain level of maturity. One of these lessons, which I can claim, is that nothing in this world is realizable without the collaboration and support of others, even in the seemingly individual, self-reliant endeavor of receiving a doctorate degree in engineering. I have truly been fortunate to receive the guidance and support from a number of people to whom I deeply indebted.

First, I would like to thank my supervisor, Dr. Damian Giaouris, for his great support and faith in my scientific curiosity and ideas. Without a doubt his stimulating, in-depth discussions and constructive criticism have polished my ideas to a presentable level.

I would also thank my other supervisor, Dr. Bashar Zahawi, for his valuable comments. The readability and consistency of a number of my publications, along with this thesis, are due to his efforts.

Furthermore, I would like to acknowledge Prof. Sumitro Banejee, from the Indian Institute of Technology (IIT), Kharagpur, for intermittent but valuable discussions on the subject of non-smooth dynamical systems. Also his depth of knowledge and humility to listen to novel ideas have been always a great source of inspiration to me.

I am grateful to Mr. Masud R. Mehran, my great uncle, for his financial contribution and constant encouragement for further education and the continuation of my family legacy. His presence has helped me a great deal to surpass the obstacles and to realize my goals and aspirations.

Many friends and colleagues have also helped me in bringing pleasant times. Among them, in no particular order: Dan Dan Ma, Graham Pannell, Dr. Mehregan Movassaghe, Arash Mojdehi and many others.

Chris, George, Andrew, Reza, Omid, Lawrence, I will never forget the coffee times!

I'm thankful to the school of Electrical, Electronic and Computer Engineering of Newcastle University for granting partial scholarship and enough facility for me to pursue my research effectively.

Specially, I am thankful to my parents, Hassan and Paricher, and my brother, Mazyar, his wife, Ladan, and his little son, Rastin, for their unconditional love and support in every imaginable way. Without them, tolerating the difficult times seem impossible to me. Extra specially, I wish to express my love and gratitude to my fiancé, Tara, to whom I have dedicated this thesis. Definitely, her love, affection and support have made my life incredibly joyous during the last year of this thesis.

Kamyar Mehran, July 2010.

Glossary

$:=$	Is equal to by definition.
$[\Gamma]^0$	Support of a fuzzy set Γ .
$[\Gamma]^\alpha$	α -level set for a fuzzy set.
$[w]^0$	Support set of continuous fuzzy states.
α, β	Class \mathcal{K} -function.
\bar{S}_i	The closed region S_i and its boundary.
χ	Function describing the change of discontinuous states.
ΔA^j	Parametric uncertainty matrix.
Γ^j	Fuzzy set or membership function (Chapter 3).
\hat{S}	Sliding region.
\in	Belong to.
λ^i	Additional parameters for quadratic inequalities representing flexible regions of fuzzy state space $\Omega \subseteq \mathcal{F}$; see, (4.28).
Λ_{qr}	A set representing boundary region or switching manifold.
\mathcal{D}_i	Jump set for discontinuous state; see Remark 3.3.
\mathcal{F}	Fuzzy state space.
$\hat{\mathbf{F}}$	A notation for non-smooth TS fuzzy system.
Ω, Ω_q	Flexible region of fuzzy state space.
ω_n	Natural frequency in an impacting system.
$\bar{\Phi}$	Notation for fundamental solution matrix.
Φ, Φ_i	Flow operator corresponding to $\dot{x} = F_i(x, \rho)$ or non-smooth TS fuzzy model $\dot{x} = F_m, m^+ = \xi(x, m)$.
\mathbb{R}^n	Space of real n -dimensional column vectors
$\mathbb{R}^{n \times m}$	Space of real $m \times n$ -dimensional matrices
ρ	System parameter.
Σ_{ij}, Σ	Discontinuity set or switching manifold.
\sup	Supremum Norm.

eig, eig_i	Eigenvalues of a matrix.
ODE	Ordinary differential equation.
\tilde{P}_q	Piece-wise quadratic matrix representing local Lyapunov functions.
ε	Infinitesimal perturbation is state variable x .
ϖ	Frequency ratio of the impacting system.
Ξ	Poincaré section.
ξ	Function describing the change of discrete states.
ζ	Viscous damping factor in an impacting system.
A_F	Maximum admissible region where a fuzzy sub-vector field can be selected.
ASR	Admissible switch region.
D	Domain of definition.
d, d_n	Duty ratio.
DP	General notation for Jacobian matrix of Poincaré map.
F	Forcing function amplitude.
f	Parameter of hyperplane confining a region Ω . General expression for a smooth vector field $\dot{x} = f(x)$.
F_m, F_{m_i}	Fuzzy sub-vector field; see Definition 3.1.
$g(t)$	Forcing function in an impacting system.
I_{ref}	Reference current.
I_Λ	A set of tuples.
$I_{n \times n}$	Identity matrix.
$J(m), J(m_i)$	Jump matrix for discontinuous state; see Remark 3.3.
m	Discrete state variable.
m^+	Notation describes the next state of discrete state m .
P	General notation for Poincaré map, $x \rightarrow P(x)$.
$Q(x)$	quadratic inequalities representing flexible regions of fuzzy state space $\Omega \subseteq \mathcal{F}$.
$R(k_1, k_2)$	Exponential region of attraction.
RoA	Region of attraction.
S	Saltation matrix. Sliding (measure-zero) manifold.
S_i	Open region of the phase space where dynamics governed by $\dot{x} = F_i(x, \rho)$ or $\dot{x} \rightarrow F_i(x, \rho)$.
$S_{i,j}$	Switch set describing the transition of discrete states; see Remark 3.2.
T	Period of clock pulse.

U_{eq}	Utkin's equivalent control for a Filippov system; see, (2.30).
$V(x)$	Non-smooth Lyapunov function. Common Lyapunov function.
$V_q(x)$	Local Lyapunov function in each flexible region $\Omega_q \subset \mathcal{F}$.
V_{in}	Input or supply voltage.
V_{ramp}	Periodic sawtooth waveform.
x^*	Equilibrium point of flow or fixed point of map.
$x^p, \Gamma(t)$	Periodic solution or limit cycle (Chapter 2).
BMI	Bilinear matrix inequalities.
DIB	Discontinuity-induced bifurcation.
DoS	Degree of smoothness.
LMI	Linear matrix inequalities.
LTi	Linear-time invariant.
LTV	Linear-time varying.
NMI	Nonlinear matrix inequalities.
NSDS	Non-smooth dynamical systems.
PDC	Parallel distributed compensation.
PDM	Poincaré-section discontinuity mapping.
PWM	Pulse-width modulation.
QMI	Quadratic matrix inequalities.
TS	Takagi-Sugeno.
ZDM	Zero-time discontinuity mapping.

Chapter 1

Introduction

In the subliminal ego, on the contrary, there reigns what I would call liberty, if one could give this name to the mere absence of discipline and to disorder born of chance...

HENRI POINCARÉ

In this introductory chapter, the motivation necessary to justify the writing of this thesis, is given. Non-smooth and smooth dynamical systems are introduced as classes of nonlinear systems, and Takagi-Sugeno fuzzy systems are discussed. The contributions and objectives of this thesis are then elucidated and a brief outline of each chapter is given.

1.1 Motivation

The roots of dynamical system theory goes back to Newtonian mechanics and the mathematics of multi-valued logic proposed in the early 1900's by Lukasiewicz. However, since the 1960's, chaos theory (discovered by Edward Lorenz [4]) and fuzzy set theory (originally introduced by Lotfi Zadeh [5]) have coincided to revolutionize research trends in this area both in theory and application. At first, the two ideas seem to have no or little common ground, fuzzy logic theory being about incorporating uncertainty into mathematical precision, and chaos theory being about unstable aperiodic behaviour in deterministic nonlinear dynamical systems. Nevertheless, over the course of the last 30 years, it has been revealed that chaotic behaviour is if anything, a more typical rather than a unique feature of the dynamics of general nonlinear systems [6, 7]. Furthermore, uncertainty and imprecision are inevitable properties of a considerably large number of physical processes and their dynamical models. It has also been recently discovered that non-smooth dynamical systems show a rich variety of nonlinear phenomena, including chaos, which are unique to this potentially important class of nonlinear dynamical systems. This has presented a strong motivation for the author to pursue the work presented in this thesis, namely *the design and analysis of non-smooth dynamical systems using the TS fuzzy approach*.

First of all, there are still many open problems in the area of non-smooth dynamical systems. The qualitative analysis of non-smooth dynamics demands specialized methods for modeling, simulation and design of these systems. Although, these methods have been attempted in some fields, they are still at an early stage of development. Secondly, having identified the extremely nonlinear behaviour as their main characteristic, there is an underlying uncertainty in the dynamics of these systems. Therefore, it seems unfeasible if one tries to look for any general solution for non-smooth systems merely based on precise information and the resulting numerical models.

Fuzzy systems based on the TS method of reasoning can be very useful and intuitive in the study of afore-mentioned problems. In fact, they can integrate qualitative knowledge representations with an ability to express quantitative but imprecise or uncertain information. Uncertainty for non-smooth dynamical systems is also a typical property inducing unique nonlinear phenomena. TS fuzzy systems are well-suited to mathematical analysis because of their functional consequent structure. As a result, TS fuzzy methods for non-smooth dynamical systems, are intuitive and advantageous in providing the possibility of a rigorous mathematical framework for stability analysis, leading to better controller designs. Most importantly, this body of work, can enhance the reputation of fuzzy methodologies by extending their abilities to deal with non-smooth dynamical systems in a more convincing way to the traditional control and nonlinear dynamics community. Therefore, the author believes that developing the TS fuzzy system in this respect is a step forward towards a general theory of uncertainty.

1.2 Smooth nonlinear dynamical systems

In the literature of control theory, the dominant class of nonlinear dynamical systems are smooth dynamical systems. In fact, the qualitative analysis of non-smooth systems relies on the understanding of smooth systems. Smooth systems can be represented as ordinary differential equations (or flows) [8]. To give a simple definition, a *smooth* system is a nonlinear mathematical model that can be described by a set of differential equations:

$$\dot{x} = f(x, \rho) \quad (1.1)$$

where f is differentiable everywhere in a given domain and ρ is a system parameter. Therefore, smooth nonlinear systems as a control problem have the general form

$$\begin{cases} \dot{x} = f(x, u, \rho) \\ y = g(x, u, \rho), \end{cases} \quad (1.2)$$

where $x \in \mathbb{R}^n$ is the state vector, $u \in \mathbb{R}^m$ is the control input, ρ is a system parameter and $y \in \mathbb{R}^p$ is the measurement vector. The qualitative theory of smooth nonlinear systems must be considered as a mature area of study [8, 9] where a wide range of analytical tools are available. Nonetheless, a generic control method valid for all types of smooth systems have yet to be developed, and most methods have been expanded for a particular class of smooth dynamical systems or employ linearization of some kind to take advantage of

well-established linear control techniques [10].

1.3 Non-smooth dynamical systems

Non-smooth dynamical systems (NSDS) (or in another widely-used terminology, *piece-wise smooth* dynamical system (PWS)) have been progressively the subject of attention in the past twenty years. A non-smooth dynamical system is described by a finite set of ordinary differential equations (ODEs) which are smooth in different regions S_i , $i = 1, 2, \dots, n$ of phase space but becomes non-smooth across the boundaries or intersection of the neighboring regions. The formal definition which according to diBernardo [7] can be given by a group of non-smooth flows:

$$\dot{x} = F_i(x, \rho), \quad \text{for } x \in S_i, \quad (1.3)$$

where $F : \mathbb{R}^{n+m} \rightarrow \mathbb{R}^n$ is a non-smooth function or flow, $\rho \in \mathbb{R}^m$ is a system parameter and $x \in \mathbb{R}^n$ is the vector of system states. Each vector field F_i is smooth in each phase space region S_i (each S_i has a non-empty interior) and described by a smooth, different functional form f_i or flow Φ_i . Each vector field F_i is non-smooth across the intersection $\Sigma_{ij} := \bar{S}_i \cap \bar{S}_j$, an \mathbb{R}^{n-1} -dimensional smooth manifold, which is also called a *discontinuity set* or *switching manifold*.

Generally speaking, these are dynamical systems mathematically modeled with non-smooth or discontinuous functions in their right-hand side¹. Dynamical systems of this sort are important due to the fact that problems to be modeled and solved with the help of non-smooth functions are practically ubiquitous. Examples includes switching electrical circuits, which will be treated in detail in this thesis, mechanical devices in which the parts experience impacts with each other (such as gear assemblies and impact oscillators), mechanical systems with dry friction, sliding or squealing, robotic systems controlled by any kind of switching mechanism and complex biological and financial models where an unexpected discrete action can change the whole system dynamics. Taking a closer look, all these problems share a common attribute. Triggered by an *event*, their continuous dynamic is abruptly changed to a completely different continuous dynamic. Therefore, the resulting model is piece-wise smooth in nature. For a long period of time, this group of systems had been ignored based on the assumption that the behavior of any problem can be defined with a dynamical system having smooth function of its argument. As a result, the qualitative theory of smooth systems have been exhaustively developed to explain the underlying nonlinear phenomena in many applications including fluid dynamics, population biology, computational astrophysics and some chaotic dynamics in meteorology. However, not until the Russian mathematician - Filippov - categorized and developed the theory of equations with discontinuous right-hand side [11], did researchers notice the existence of the broad category of non-smooth systems giving engineers access to the tools needed to analyze and understand these systems.

¹RHS or right-hand side is merely a name for a term as part of an expression; and they are in practice interchangeable since equality is symmetric. The equation on the right side/right part of the "=" sign is the right side of the equation and the left of the "=" is the left side/left part of equation. For instance, the right-hand side in (1.3) is " $F_i(x, \rho)$, for $x \in S_i$ " and the left-hand side in (1.3) is " \dot{x} ".

The original idea of systems whose continuous routines can be changed by the firing of an asynchronous discrete event, was theoretically recognized and applied by computer scientists in the 1930s. Alan Turing had an influential role in providing a mathematical framework to apply those concepts to modern computers in the form of finite automata [12] and Petri nets [13]. However, control theorists and engineers didn't show any interest in developing these ideas for dynamical systems, mainly due to the belief that all physical systems behave naturally as *smooth* functions. At the time, that was a reasonable assumption to make if the dynamics were to be viewed at large. In this case, the time period of a discrete event, i.e. an impact, would be so infinitesimal compared to the time span of the system evolution that any abrupt transition can be easily neglected and the overall dynamical model treated as a smooth system where complex but familiar scenarios occur. However, pursuing the radical work of Filippov with the tools developed earlier by Poincaré on the qualitative theory of differential equations, researches were becoming disillusioned with traditional ideas as a result of discovering that in many physical systems a completely separate set of dynamics, can arise because of a discontinuous or *non-smooth* transition. For example, an abrupt transition from a strongly stable periodic motion to full scale chaotic motion can frequently occur in a non-smooth system with a small variation in its parameters, whereas this phenomena is not observable in a smooth system unless it undergoes a series of period-doubling bifurcations, famously called a Feigenbaum cascade, leading to chaos. As a result, new modeling methods started to be introduced to consider the discontinuous behavior of non-smooth systems and the resulting rich mathematical structures. A number of proposals were made in the late 1980s mostly involved with synthesizing models where the continuous dynamics can interact with discrete events.

The main qualitative concepts of smooth nonlinear systems, such as structural stability, bifurcation and chaos [8], should also have been redefined to provide a test-bed for non-smooth systems and their unique dynamical phenomena. These extended, or in some cases, newly developed concepts, like *flows* and *discontinuous maps*, play an essential role in solving the engineering problems leading to these concepts. Even though the classification first proposed by Filippov [11] is able to describe an important group (Filippov's systems) of what is today considered a much larger group of non-smooth systems, the observed unique nonlinear phenomena in these systems demand a rather distinct but novel classification, formalism and even codimension for non-smooth dynamical systems. The classification needs to be inclusive enough to consider all different system topologies. The formalism needs to be general and all-embracing to describe a wide class of non-smooth systems with different degrees of smoothness and the resulting models should be able to handle the intricate web of discontinuity boundaries the phase space of a non-smooth system normally contains. Even for the most analytically-developed formalisms like, *complementarity systems* and *variational formulation* based on *differential inclusions*, there is no promise of characterizing the existence and uniqueness and hence the stability of the solution in all possible circumstances. In particular, investigation of the stability of periodic solutions demands a comprehensively-defined formulation to provide errorless modeling methods.

Control algorithms for non-smooth dynamical systems have evolved in tandem with

the qualitative analysis of these systems, specifically the stability in its classical notion (stability of equilibria) or in its structural notion (stability of invariant sets or periodic solution). The goal is to design control strategies to stabilize the system through proving the stability of some target state, which naturally would be either an equilibrium point or a limit cycle (period-I stable) [14–16]. Various ideas exist in the control theory literature based on some sort of switching mechanisms or somehow curbing the sliding dynamics of the system of interest. Nevertheless, successful attempts are largely focused on avoiding the bifurcation phenomenon or suppressing the unwanted chaotic behavior of the specific non-smooth systems in application like power electronic converters (see [1] and the references therein), walking robots [17, 18] and automotive systems [19]. The initial trend in controlling chaos was created by the idea of E. Ott, C. Grebogi, and J. A. Yorke [20, 21]. The control goal, based on this idea, can be achieved through a small perturbation of an accessible, time-independent parameter. However, the implementation of this strategy was found to be problematic on higher-dimensional systems, largely because of noise and the computational burden. Henceforth, other control strategies were proposed to resolve the practical issues of chaos control [22, 23]. Noticeably the most recent class of control strategies, specially for non-smooth systems, have been initiated in the area of control engineering. This class of controllers, chiefly employing state-feedback mechanisms, proved to be most successful in suppressing chaos or bifurcation while guaranteeing practically important factors like robustness to noise and external disturbances [24–26]. All in all, improving the design and robustness of feed-back control algorithms for non-smooth systems is intensively entangled with the qualitative analysis of the dynamics including numerical methods, modeling and stability. These, in turn, do not follow from the well-known methods for smooth nonlinear systems and there is still much to be discovered in the area of non-smooth dynamical systems.

1.4 Takagi-Sugeno fuzzy systems

As this thesis aims to enhance Takagi-Sugeno (TS) fuzzy systems for the design and analysis of non-smooth dynamical systems, TS systems must be properly treated. When TS fuzzy systems were first introduced by the pioneering work of Takagi and Sugeno [27], it was designed to model a smooth nonlinear system by means of fuzzy approximations. This modeling technique was later elaborated and named as the TS fuzzy modeling approach [28]. Regardless of how to obtain a TS fuzzy model, the overall system can be expressed as

$$\begin{aligned} \dot{x} &= \sum_{j=1}^l w^j(\theta)(A^j x + B^j u + a^j) \\ y &= \sum_{j=1}^l w^j(\theta)(C^j x + D^j u + c^j), \end{aligned} \quad (1.4)$$

where the matrices $A \in \mathbb{R}^{n \times n}$, $B \in \mathbb{R}^{n \times m}$, $C \in \mathbb{R}^{p \times n}$, $D \in \mathbb{R}^{p \times m}$, $a^j \in \mathbb{R}$, $c^j \in \mathbb{R}$, $\theta(t) \in \mathbb{R}^q$ is a vector of time-varying parameters, which is confined to a compact set $\theta \in \Theta$, and the *weighting functions* $w^j(\theta)$ denote a convex disintegration of Θ describe by a fuzzy rule base. Therefore, a TS fuzzy system can be viewed as the convex combination of the consequent parameter-varying affine local models (The structure of TS fuzzy systems will be discussed in detail in Chapter 3). There has been a consensus that the TS fuzzy

system of the form (1.4) is, in theory, able to model or approximate *any smooth nonlinear system* to an arbitrary accuracy [28].

1.5 Contributions

The scientific contributions of this thesis are highlighted as follows:

As mentioned in the last section, the TS fuzzy model structure of the form (1.4) is considered as universal approximators for nonlinear systems. However, this so-called universal approximation capability is limited to smooth dynamical systems. As a result, it is necessary to come up with a novel structure of TS fuzzy systems capable of modeling non-smooth dynamical systems and representing their ensuing unique nonlinear phenomena. The first contribution of this thesis is to propose and develop a TS fuzzy modeling structure suitable for the representation of the discontinuous nature of NSDS and all their complex nonlinearities. It will be shown that the proposed fuzzy formulation can accurately model important groups of non-smooth systems including Filippov's systems (sliding or non-sliding) as well as NSDS with discontinuous state jumps (impacts). Filippov systems mainly arise in models of electrical circuits with (ideal) diode elements, controlled systems with encoders or mechanical systems with dry friction. Impacting system embrace mechanical systems where there are impacts between rigid bodies. The dynamic behaviour, existence and the uniqueness of the novel TS fuzzy modeling solutions in terms of sliding motions and discontinuous state jumps (impacts) are also analyzed and discussed. Two major approaches for obtaining TS fuzzy models based on the new structure is also suggested in Chapter 3 for NSDS with affine or nonlinear vector fields.

The second major contribution of this thesis is providing a Lyapunov-based framework for the complicated *structural stability* analysis of limit cycles for non-smooth dynamical systems based on their TS fuzzy models. The new framework for structural stability, unlike the existing classical stability results for fuzzy systems (stability of equilibria) is able to analyze the stability of stable and unstable limit cycle and to locate the onset of bifurcation or chaotic orbits. It is also shown how the stability results are formulated as Linear Matrix Inequalities with partitioning of the fuzzy state space into flexible regions.

The stability robustness issues of the new structure of TS fuzzy systems and how the unmodeled system uncertainties can be compensated for by selecting specific sets of discrete events (or the fuzzy sub-vector fields) to insure structural stability are also discussed.

The third major contribution of this thesis, is to further develop the proposed structural stability analysis framework for a novel TS model-based design strategy, to suppress the chaotic behaviour in Filippov's systems exemplified by DC/DC electronic converters. The novel control scheme avails from the concepts of gain-scheduling and switching controllers to design state feed-back local controllers.

1.6 Publications

A number of papers and other publications, based on the work presented in this thesis, has already been published or submitted for publication. Here is the list of these publications:

1. K. Mehran, D. Giaouris, and B. Zahawi. Stability analysis and control of nonlinear phenomena in boost converter using model-based Takagi-Sugeno fuzzy approach. *IEEE Transactions in Circuits and Systems - I*, volume 57, number 1, pages 200-212, January 2010.
2. K. Mehran, B. Zahawi, and D. Giaouris. Fuzzy Logic for Non-smooth Dynamical Systems. Chapter in the book: *Kansei Engineering and Soft Computing: Theory and Practice*. To be published by IGI Global, 2010.
3. K. Mehran, D. Giaouris, and B. Zahawi. Modeling and Stability Analysis of Non-linear Phenomena in Impacting Systems via Model-based Takagi-Sugeno Fuzzy Approach. *IEEE Transactions in Fuzzy Systems - I*, submitted.
4. K. Mehran, D. Giaouris, and B. Zahawi. Modeling and stability analysis of dc-dc buck converter via takagi-sugeno fuzzy approach. In *IEEE Conference on Intelligent Systems and Knowledge Engineering*, volume 1, pages 401-406, Xiamen, China, November 2008.
5. K. Mehran, D. Giaouris, and B. Zahawi. Stability Analysis of DC-DC Buck Converter using Takagi-Sugeno Fuzzy Model-based Approach. Selected from ISKE'08, accepted for Journal of Donghua University (English version, EI indexed).
6. K. Mehran, D. Giaouris, and B. Zahawi. Modeling and Stability Analysis of Closed Loop Current-Mode Controlled Ćuk Converter using Takagi-Sugeno Fuzzy Approach. In *CHAOS09*, England, London, IFAC, June 2009.
7. K. Mehran, B. Zahawi, and D. Giaouris. A Hybrid TS Fuzzy Approach for Controlling Nonlinear Chaotic Systems, In *Postgraduate Conference (PGC2006)*, Newcastle upon Tyne, England, 2006.

1.7 Organization of the thesis

The outline of the chapters of this thesis is as follows:

Chapter 2 is dedicated to the back-ground study of non-smooth dynamical systems and existing analytical tools for their analysis. The major types of NSDS and their unique dynamics are studied through different case studies. The first case study is focused on a group of single-diode switching electronic converters, namely the dc-dc boost and buck converters, which are typical examples of Filippov systems exhibiting rich nonlinear phenomena. The second case study is an important mechanical impacting system, an hard impact oscillator, which is a non-smooth system with discontinues state jumps. The next case study is also a mechanical system with dry friction, showing a variety of siding dynamics. These case studies are representative of the major groups of non-smooth systems with a broad variety of complex dynamics. An overview of the existing qualitative theory and concepts for NSDS is then given where the notion of structural stability and non-smooth bifurcation, known as discontinuity-induced bifurcation, is formally introduced along with

a discussion of the tools, like discontinuity mapping, available for studying and analyzing these bifurcation phenomena.

Chapter 3 gives a brief review of the TS fuzzy modeling structure for smooth dynamical systems and the available methods for constructing such a model. The deficiencies of the current modeling approach in modeling a non-smooth system are then shown through a simple example. A novel TS fuzzy modeling structure is then synthesized to overcome the deficiency. After formalizing the definition of the new structure, the properties of the non-smooth TS fuzzy model (a term coined by the author) in terms of representing sliding motions and impacting dynamics are discussed. The sufficient conditions for guaranteeing the existence and uniqueness of the solutions are addressed as a supplement to the universal approximation theorem of fuzzy system to include non-smooth systems as well as smooth system. Two major approaches are proposed to obtain a non-smooth TS fuzzy model. The success of the modeling approaches are illustrated through a number of examples, including the case studies introduced in chapter 2. The chapter ends with a discussion of the direct numerical simulation technique that will be employed throughout the rest of the thesis for implementing the structure of non-smooth TS fuzzy modeling and investigating the dynamics of example systems.

Chapter 4 is chiefly concerned with the structural stability of non-smooth TS fuzzy systems in the Lyapunov sense. First, an overview is given of existing stability results for TS fuzzy system. Then different theorems for the bifurcation analysis (stability of limit cycles) of non-smooth TS fuzzy systems are proposed. The stability theorems are developed based on searching for non-smooth Lyapunov functions in different but flexible regions of fuzzy state space. All the stability theorems are then formulated as linear matrix inequalities (LMI) problems, to be solved by interior-point optimization methods. Through the different case studies, it is shown how by solving the LMI stability problems, the onset of bifurcation and chaos can be located. Stability robustness to guarantee stability in terms of the model uncertainties in selecting the location of the switching events and the fuzzy sub-vector fields, is discussed. Stability robustness issues arisen from model uncertainties are addresses and discussed.

Chapter 5 starts with a collective literature on fuzzy control strategies for controlling chaos. A model-based TS fuzzy control design problem, recast on LMIs, is developed to suppress the unwanted chaos or bifurcation. The control methodology is the direct application of LMI stability conditions proposed in chapter 4, inspired by gain-scheduling concepts for designing local switching controllers. The strength of the methodology is shown in dc-dc electronic converters where the stable period-1 behaviour is preserved for a long range of operating conditions.

Chapter 6 concludes the whole thesis. Several open problems are suggested for future research.

Three appendices are also included. Appendix A presents the modeling and analysis of the current-mode controlled Ćuk converter as an example of higher order non-smooth Filippov system. Appendix B includes description of linear matrix inequalities (LMIs) and how a non-conservative formulation can be obtained for the analysis proposed in Chapters 4 and 5. System parameters used in this thesis are given in Appendix C.

Chapter 2

Background

For a superficial observer, scientific truth is beyond the possibility of doubt; the logic of science is infallible, and if the scientists are sometimes mistaken, this is only from their mistaking its rule...

HENRI POINCARÉ

Lets explain the atypical behaviour of a non-smooth system by bringing a provocative example, the dynamics of mechanical impacts with a rigid body, which surprisingly has stimulated the historical development of the theory of non-smooth systems. The impacting behavior, as an engineering problem, can be found in a range of mechanical systems from a simple motion of an elastic bouncing ball to sophisticated walking robots. The impacting system, in its simplest form, is comprised of a hard wall positioned at a distance σ from the center of a mass which is subject to the instantaneous impact with the wall. Upon each impact with the hard wall, driven by a periodical external force, the mass experiences an instantaneous reversal of its velocity or simply a completely different behavior in the state evolution of the system. The overall dynamics of this example can be modeled in an event-driven fashion where the system states smoothly evolve until it's interrupted by an event, the sudden change in velocity, and the scenario repeats. To fully understand the dynamics of those subsequent events, the relation of the system states immediately before the event (impact) to the ones immediately after the event, needs to be known. One of the fundamental tools, to study this property, is *Poincaré* or *discrete-time discontinuity* mapping that can express the relation in a lower-dimension by sampling the system states at a fixed time. In case of the impacting system, the map is also non-smooth as the dynamics of the system just before the impact is different from when the impact occurs. Therefore, even in a simple impacting system with its seemingly-linear differential equation, by introducing instantaneous impacts, the system becomes a highly-nonlinear (and in some cases, transcendental) equation. These equations show a variety of interesting phenomena, including non-smooth bifurcation and abrupt transition to a chaotic behavior unseen in smooth dynamical systems.

2.1 Non-smooth dynamical systems - Case studies

To begin the detailed discussion of NSDS, these case studies will be examined as archetypal non-smooth systems exemplifying the colorful but complex dynamics of these systems.

2.1.1 Case Study I: DC-DC electronic converters

DC-DC power electronic converters are designed to convert electrical energy at high efficiency. They fulfill this purpose by employing switching components, such as transistors, diodes and energy-storing components such as inductors and capacitors. Although power electronic converters may not seem complicated from the viewpoint of circuit design, the combination of both type of components (passive and active) makes these circuits highly nonlinear, time-varying dynamical systems. Furthermore, the control circuits commercially used for DC-DC converters involve nonlinear components such as comparators, PWM generators, multipliers, phase-locked loops, monostables and digital controllers. When driven beyond their operating limits, these circuits become complex systems that can show a variety of nonlinear phenomena including period-doubling bifurcations and chaos [1, 29, 30]. As a result, they become a subject of interest from the mathematical point of view as they fall into the category of non-smooth Filippov systems, later introduce as equations with discontinuous right hand sides. The case studies selected as examples of electrical Filippov system in this section are the most conventional, single-diode DC-DC electronic converters, namely the boost and buck converters (2.1).

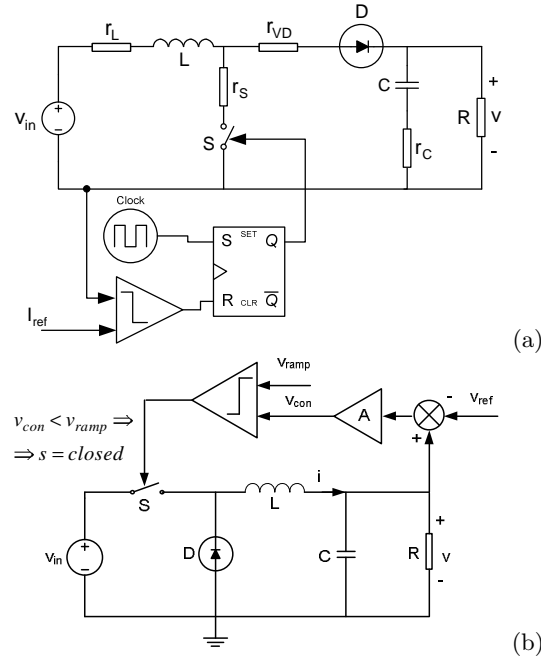


Figure 2.1: Single-diode DC-DC (a) boost and (b) buck power electronic converters along with their control circuits. R , L , C , D and S stand for resistance, inductance, capacitance, diode and switch in both circuits. r_{VD} , r_S , r_L and r_C are the parasitic resistance of the diode, switch, inductance and capacitance respectively in the boost converter circuit. All the parameter values can be found in Appendix C.

In the boost converter, shown in Fig. 2.1a, the current-mode control logic switches between the 'OFF' and 'ON' states. When the controlled switch S is in the ON state, the current through the inductor increases until it reaches the given reference current value I_{ref} . The controlled switch S is then turned OFF by an arriving clock pulse to reduce the inductor current and charge the output capacitor to a voltage higher than the input voltage. During the OFF period, any arriving clock pulse is ignored. The operation just described is assumed to be in continuous-conduction mode (CCM) where the inductor current never falls to zero. In this mode, the dynamics of the converter is governed by two sets of differential equations associated with the OFF and ON states:

$$\frac{di_L}{dt} = \begin{cases} \frac{V_{\text{in}}}{L} - \frac{i_L}{L}(r_L + r_{VD} + \frac{Rr_C}{R+r_C}) - v_C \frac{R}{L(R+r_C)}, & S \text{ is off}; \\ \frac{V_{\text{in}}}{L} - \frac{(r_L + r_{SW})}{L}i_L, & S \text{ is on} \end{cases} \quad (2.1)$$

$$\frac{dv_C}{dt} = \begin{cases} \frac{1}{C(R+r_C)}(Ri_L - v_C), & S \text{ is off}; \\ -\frac{v_C}{C(R+r_C)}, & S \text{ is on}. \end{cases} \quad (2.2)$$

where the inductor current i_L and output voltage v_C are the state variables.

In the buck converter circuit, the pulse-width modulation PWM scheme provides a *bi*-state logic for voltage-mode control to regulate the output voltage. In this way, a given value of reference voltage V_{ref} is subtracted from the output voltage $v(t)$, and the error is amplified by A , the gain of the feedback loop, to form the control signal $v_{\text{con}} = A(v(t) - V_{\text{ref}})$ ¹. The switching signal is then generated by comparing the control signal with the periodic sawtooth signal v_{ramp} . When $v_{\text{con}} < v_{\text{ramp}}$, the state of the switch S is ON, imposing the input voltage V_{in} across the LC circuit. The switch S is turned OFF when $v_{\text{con}} > v_{\text{ramp}}$ and the diode D conducts to keep the current flowing in the inductor. The dynamics of this circuits can also be described by two sets of differential equations as follows:

$$\frac{di_L}{dt} = \begin{cases} \frac{V_{\text{in}} - v}{L}, & S \text{ is off}; \\ -\frac{v}{L}, & S \text{ is on}. \end{cases} \quad (2.3)$$

$$\frac{dv}{dt} = \frac{1}{C}(i_L - \frac{v}{R}) \quad (2.4)$$

where the state variables are the inductor current i_L and output voltage v .

Under stable conditions, the close-loop control provides a regulated dc output for the converter, with a mean value close to the desired voltage (or a maximum dc value close to the desired current in the peak current-mode control boost converter) with a period equal to the period of the PWM signal. This condition is usually referred to as a period-1 stable condition (see Figs. 2.3 and 2.2 for the boost converter). However, if the system parameters are varied even slightly beyond specified operating limits, the system may undergo a period-doubling bifurcation leading to chaos [33]. This scenario is shown for the boost

¹It is possible to use PI controllers for controlling buck converters although this may increase system's dimensions to three due to the additional capacitor in the feedback loop. However, the conventional control method for the buck converter is the proportional controller that we study here which is also considered by others for an investigation of nonlinear phenomena [31,32] (also see [1] and the references therein)

and buck converter in the form of a phase plane diagram $v - i$ in Fig. 2.4 and Fig. 2.5 respectively, where a stable period-1 orbit upon the variation of input voltage V_{in} loses its stability to a period-2 orbit and then with a higher value of V_{in} , a chaotic orbit is born.

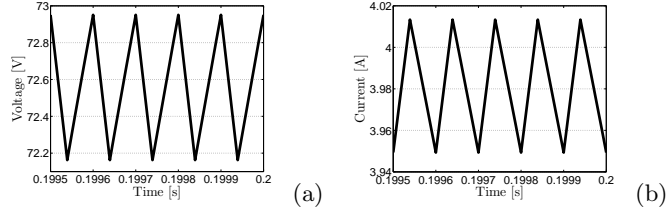


Figure 2.2: Nominal stable period-1 operation of the current-mode controlled boost converter. The period of the regulated output signals of (a) voltage and (b) current of the boost converter are equal to the period of the PWM signal.

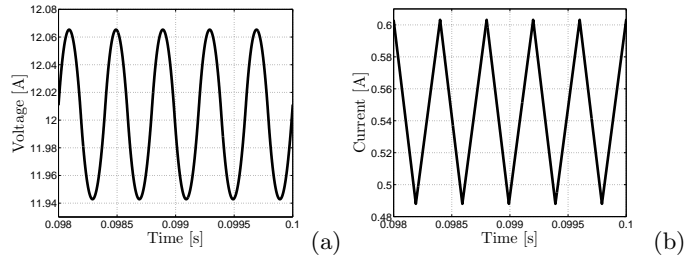


Figure 2.3: In nominal stable period-1 operation of the voltage-mode controlled buck converter, the period of the regulated output signals of (a) voltage and (b) current, are equal to the period of the ramp signal v_{ramp} .

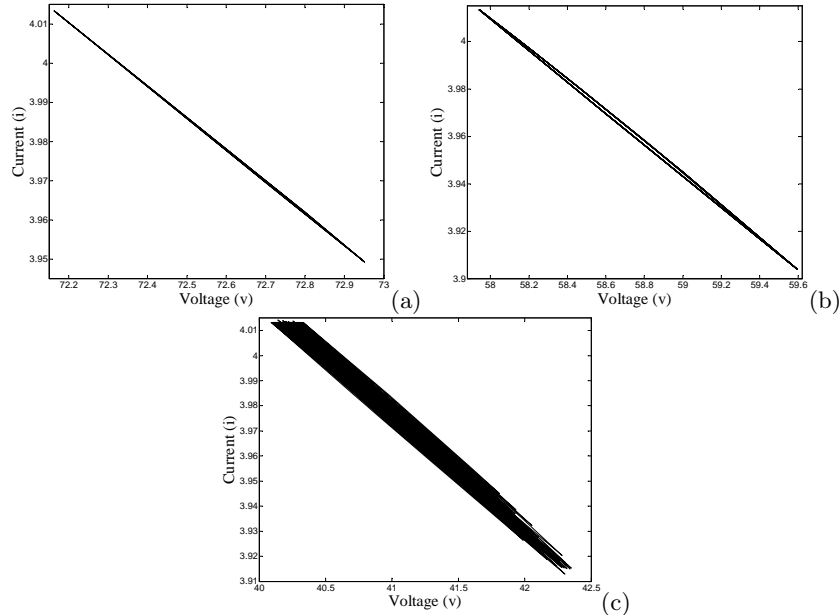


Figure 2.4: Periodic orbit of the boost converter: (a) period-1 stable operation with $V_{in} = 50V$, (b) period-2 operation with $V_{in} = 35.7V$ and (c) chaotic operation with $V_{in} = 20V$. The symbol (inside the bracket in labels) represents the variable of the respective label not the unit.

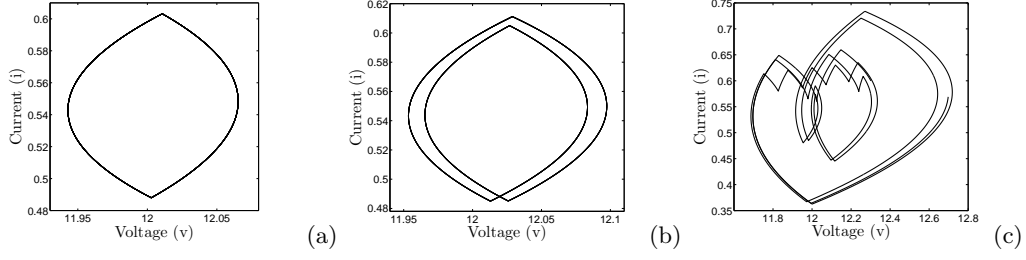


Figure 2.5: Periodic orbit of the buck converter: (a) period-1 stable operation with $V_{in} = 23\text{V}$, (b) period-2 operation with $V_{in} = 24.53\text{V}$ and (c) chaotic operation with $V_{in} = 33\text{V}$. The symbol (inside the bracket in labels) represents the variable of the respective label not the unit.

The long-term behaviour of a system upon the variation of a system's parameter is referred to as *bifurcation diagram* and the parameter is varied is called *bifurcation parameter*. For instance, the bifurcation diagram in Fig. 2.6 is derived from the repetitive sampling at the clock instance with the period of T , when the input voltage V_{in} is varied as a bifurcation parameter. Close to the operating point $V_{in} = 24.515$, a single periodic orbit undergoes a destabilizing period-doubling bifurcation, leading to a sudden large chaotic orbit (Fig. 2.4c) close to the operating point $V_{in} = 32.341$. The detection of such a sudden transition to the chaotic orbit is only possible if studying the *non-smooth* model of the converter [1]. It is also noticeable from the bifurcation diagram in Fig. 2.6, that for the range of parameter variation (from $V_{in} = 24$ to $V_{in} = 25$), other periodic orbits can coexist with the period-1 orbit [1, 34].

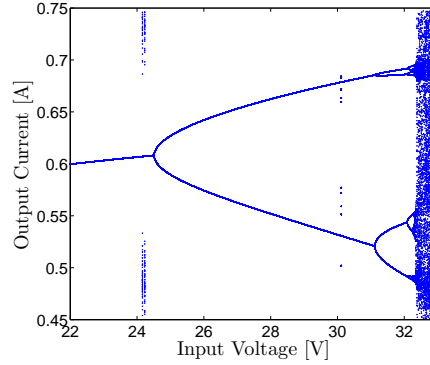


Figure 2.6: The bifurcation diagram summarizes the simulated dynamics upon varying the input voltage V_{in} as a parameter of the buck converter. The narrow band starting very close to the operating point $V_{in} = 24.16$ shows that a period-3 attractor can coexist with the stable period-1 orbit (coexisting attractors). This condition cannot be visible in the experimental setup of the converter [1] but it is well observed in numerical simulations where a large number of initial conditions are chosen randomly.

2.1.2 Case Study II: A hard-impact oscillator

From classical mechanics to modern systems, many cases can be found involving impacting behaviour (see [7, 35] and the references therein). The simplest impacting system may be considered as the motion of an elastic ball bouncing vertically on a rigid surface such as a table. The impacting system considered here is a one-degree-of-freedom hard impact

oscillator (Fig. 2.7). This system and its dynamics have been considered frequently in the study of non-smooth dynamical systems [36–42]. This hard impact oscillator is comprised of a hard wall positioned at a distance σ from the center of a mass, which is subjected to an instantaneous impact with the wall. The state evolution of the system can be fully described by the position $u(t)$ and the velocity $v(t) = \frac{du}{dt} = \dot{u}(t)$ of its center of mass.

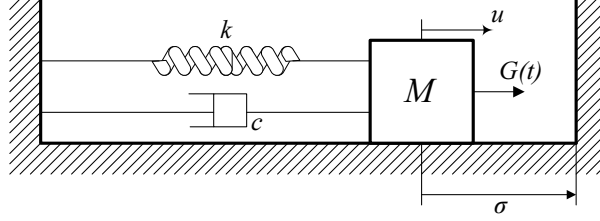


Figure 2.7: A one-degree-of-freedom hard impact oscillator.

Assuming a linear spring and a dashpot attaching the mass to a datum point, the free motion of impacts can be represented by the dimensionless differential equation

$$\frac{d^2u}{dt^2} + 2\zeta\omega_n \frac{du}{dt} + \omega_n^2 u = g(t), \quad \text{if } u > \sigma. \quad (2.5)$$

where $\zeta = c/2\sqrt{kM}$ is the viscous damping factor, $\omega_n = \sqrt{k/M}$ is the natural frequency of the oscillation and $g(t) = G(t)/M$ is the applied external force. It is possible to apply different types of forcing function $g(t)$ fed from the external flow or the solution of another problem [43]. However here, we apply a periodic sinusoidal forcing function, $g(t) = F\cos(\omega t)$ with period $T = 2\pi/\omega$ and amplitude F [7]. With mass and stiffness scaled to unity, in a free-motion condition in the region $u > \sigma$, the impact with a rigid obstacle takes place at some time t_0 at which the position of the mass $u = \sigma$. In fact, at $t = t_0$, the motion and the velocity just before the impact $(u(t_0), v(t_0)) := (u_-, v_-)$ are mapped to the zero-time motion and the zero-time velocity just after the impact (u^+, v^+) as:

$$u^+ = u^- \quad \text{and} \quad v^+ = -rv^-, \quad (2.6)$$

where $0 < r < 1$ is Newton's coefficient of restitution. The restitution law indicates the overall effect of a swift energy dissipation through the propagation of shock waves. Therefore, the value of r depends on the geometry of the system components as well as their material properties [44]. The impacting system here is assumed to have a perfect, instantaneous impact, though implementing such an impacting system in practice is arduous and needs a special setup [45].

The system (2.5) would be linear without the presence of instantaneous impacts so its solution will not be affected by parameter variation. However, the impacts, cause discontinuous changes in velocity (discontinuous state jumps) in the dynamics as described by (2.6), transforming the whole system to a non-smooth system. The system is, then, greatly influenced by a change in system parameters. This would become more clear if we observe the *periodic solutions* of the system (2.5) and (2.6) for different parameter values of, say, forcing function amplitudes F . A drastic qualitative change is observable when by slightly changing the value of F , the stable orbit (Fig. 2.8a) turns to a completely chaotic

orbit (Fig. 2.8b).

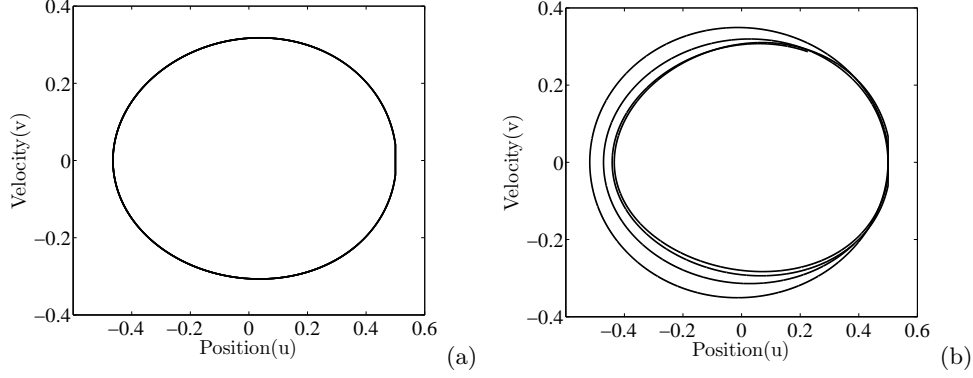


Figure 2.8: Periodic solutions of the hard-impact oscillator (2.5)-(2.6) when (a) period-1 stable with $F = 0.275N$ and $\varpi = 2.97$, (b) chaotic with $F = 0.276N$ and $\varpi = 2.97$. The symbol (inside the bracket in labels) represents the variable of the respective label not the unit.

In terms of its global dynamics, experimental results are also in close agreement with the solution of this idealized model of the impact oscillator [46]. These results are typically demonstrated via a bifurcation diagram where a range of the solution data is plotted against the parameter F . Looking at a much longer range of parameter variation in the bifurcation diagram of Fig. 2.9a, it can be observed that a verity of chaotic orbits exist with stable or unstable period- n orbits. This intermittent chaotic orbits interrupted by different periodic orbits (period-2 to period-8) is specifically noticeable in the range of $F \in [0.24, 0.28]$. However, focusing on the much narrower range of $F \in [0.275, 0.278]$ in Fig. 2.9, a unique bifurcation phenomenon is observable, where there is a sudden transition from a stable orbit to a large chaotic orbit.

This abrupt qualitative transition, called a *grazing* bifurcation, is associated with non-smooth systems, which later in this chapter, will be classified as a discontinuity-induced bifurcation (DIB) [7]. A DIB cannot be observed in smooth dynamical systems where a chaotic orbit can be met only after a (Feigenbaum) cascade of period-doubling bifurcations to $(2^k, 2^k)$ orbits, for $k = 1, 2, \dots, \infty$ [7, 8] (except in some rare cases which will be mentioned in Section 2.2.2). The grazing bifurcation, occurring at zero-velocity impact, is a crucial, difficult-to-analyze problem, which will be discussed later in this chapter.

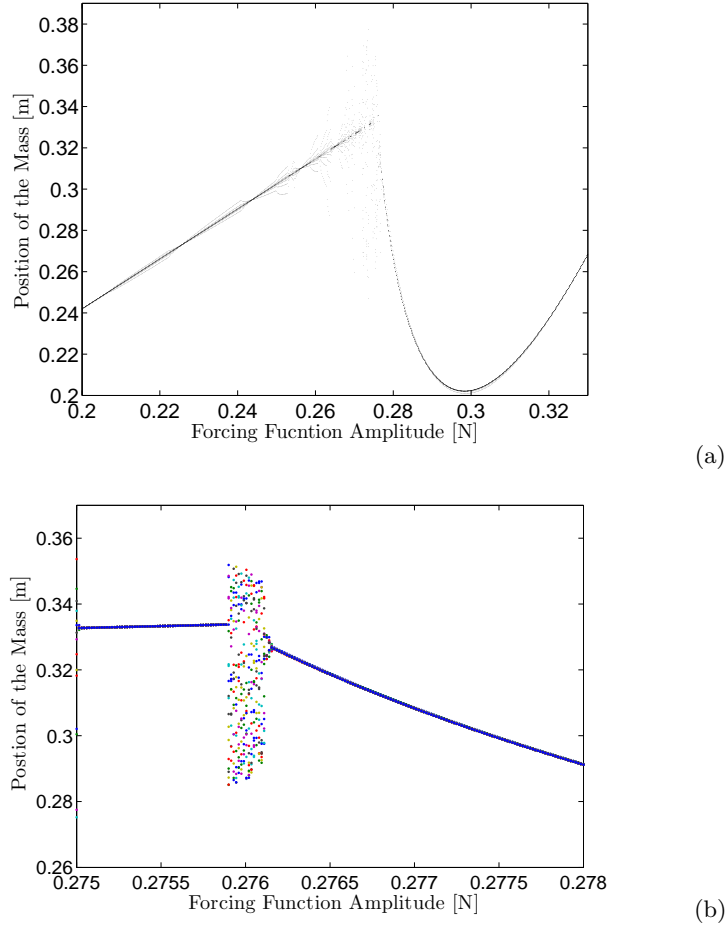


Figure 2.9: The bifurcation diagram (a) shows the ω -limit set for increasing $F \in (0.2, 0.34)$ for $\varpi = 2.97$, (b) magnified to show the qualitative change of the solution (u, v) from a stable periodic behaviour when $F = 0.275$ N and $\varpi = 2.97$ to a chaotic behaviour when $F = 0.276$ N and $\varpi = 2.97$ [2].

2.1.3 Case Study III: A dry-friction oscillator

Another important example of NSDS showing a different group of dynamics - sliding dynamics - is mechanical systems with dry friction or stick-slip vibrations. Several different systems of this type have been studied, looking for bifurcation phenomena and chaotic behavior [47–50]. The model of interest here is a forced one-degree-of-freedom dry-friction oscillator [3, 7], illustrated in Fig. 2.10.

This model consists of a mass M which can move freely on a surface that is attached to a fixed point through a spring with a stiffness coefficient of K . In the forced model, the mass M is subject to a sinusoidal force and placed on a driving belt moving with a constant velocity V such that the relative motion between the mass and the belt follows a kinematic dry-friction law. Therefore, the equations of motions can be expressed with a nonlinear Coulomb friction law as:

$$\ddot{u} + u = P(1 - \dot{u}) + F \cos(\omega t) \quad (2.7)$$

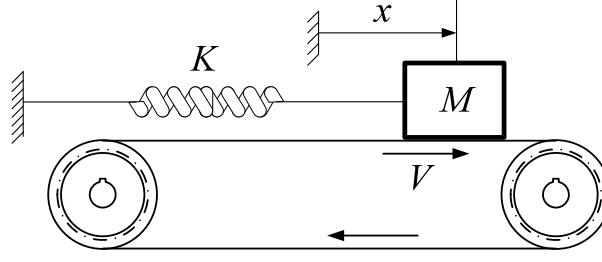


Figure 2.10: A model of forced dry-friction oscillator [3]

where

$$P(1 - \dot{u}) = \alpha_0 \operatorname{sgn}(1 - \dot{u}) - \alpha_1(1 - \dot{u}) + \alpha_2(1 - \dot{u})^3 \quad (2.8)$$

is a Coulomb friction law, $(1 - \dot{u})$ represents the relative velocity between the driving belt and the mass. α_i , $i = 0, 1, 2$ are positive constants determined by the material characteristics of the mass and the belt, which, in our case, are assumed to be $\alpha_0 = \alpha_1 = 1.5$ and $\alpha_2 = 0.45$. F is the amplitude and ω is the frequency of the sinusoidal forcing function. Without the loss of generality, the mass M , stiffness K and the velocity V can all be set to unity in (2.7).

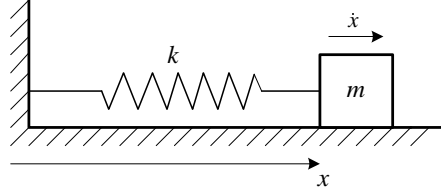


Figure 2.11: A simpler model: an unforced dry-friction oscillator.

To better understand the dynamics of dry-friction system, the equation of motion in the absence of sinusoidal forcing and with a simple Coulomb friction law (see Fig. 2.11) can be alternatively expressed by:

$$M\ddot{x} + P(\dot{x}) + Kx = 0, \quad (2.9)$$

where x is the displacement, M is the mass, K is the spring stiffness and the Coulomb friction law is

$$P(\dot{x}) = \begin{cases} P_0, & \text{if } \dot{x} > 0, \\ -P_0, & \text{if } \dot{x} < 0, \end{cases} \quad (2.10)$$

where P_0 is a positive constant. Therefore, system dynamics can be equivalently described by:

$$\dot{x}^2 + \frac{k}{m}(x + P_0/k)^2 = \frac{k}{m}c^2 \quad \text{if } \dot{x} > 0, \quad (2.11)$$

$$\dot{x}^2 + \frac{k}{m}(x - P_0/k)^2 = \frac{k}{m}c^2 \quad \text{if } \dot{x} < 0, \quad (2.12)$$

where $c \geq 0$. This dynamic behaviour is also depicted in Fig. 2.12 where a non-smoothness

is noticeable at the plane $\dot{x} = 0$ due to the Coulomb friction. Hence, the dynamic is undefinable at the surface $\dot{x} = 0$ (referred to as the *discontinuity surface* or the *switching manifold*) in the sense of smooth differential equations. However, the solution trajectories show a new type of motion called sliding motion, and the mode of behavior when sliding motions occur is called a sliding mode [7, 10, 51]. In real scenarios, sliding motions do not take place exactly at the manifold $\{\dot{x} = 0\}$ but in some neighborhood of it, called the *sliding region*. In our case, the switching manifold is the sliding region, where the vector fields closely above and below the switching manifold, are both attracted to $\dot{x} = 0$ and never leave this manifold (see Fig. 2.12).

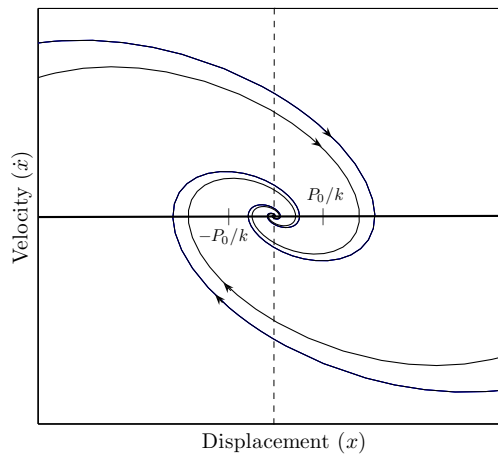


Figure 2.12: Solution trajectories of the unforced dry-friction oscillator (model (2.9)).

Returning to the forced model of (2.7) with the nonlinear Coulomb friction law (2.8), the sliding motion leads to an interesting phenomena when letting the frequency ω vary as a bifurcation parameter. For a frequency of $\omega \simeq 1.7078$, the oscillator undergoes a bifurcation visible in Fig. 2.14, which similar to the grazing bifurcation in the previous case study, is an abrupt transition to a chaotic orbit [52]. This discontinuity-induced bifurcation takes place when the stable sliding orbit at the forcing frequency of $\omega = 1.7077997$ becomes tangent (grazing) to the switching manifold, and the boundary of the sliding region where the set $\dot{u} = 1$ attracts the system trajectories (see Fig. 2.13). In a real system, this scenario is realizable when the dry-friction oscillator try to immediately enter a stick-slip phase from a purely slip phase. While in the chaotic region, the trajectory constantly enters the stick phase and always exit from it with a different phase but with the same velocity or position [52].

2.2 Theory and concepts of NSDS

2.2.1 Classification

The case studies described above represent different types of non-smooth systems (see Fig. 2.15). NSDS can be classified based on their *degree of smoothness* or DoS [7], which

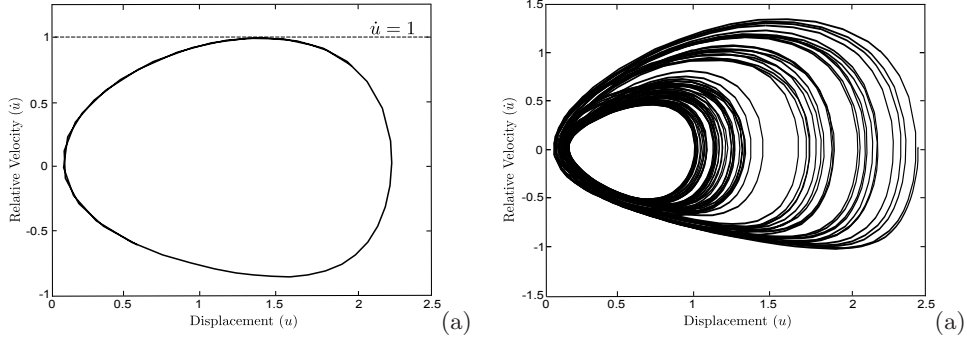


Figure 2.13: If the forcing function amplitude is set to $F = 0.1$, then (a) $4T$ stable periodic orbit at the forcing frequency $\omega = 1.70781$, (b) chaotic orbit induced by grazing the boundary of sliding region (grazing-sliding event) at the forcing frequency $\omega = 1.7077997$ where the discontinuity-induced bifurcation occurs.

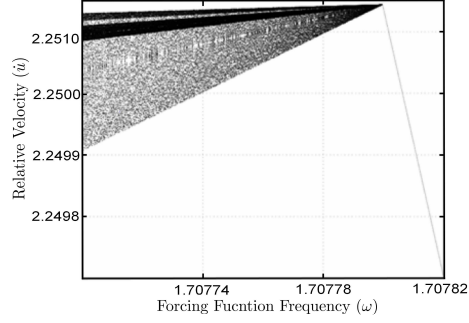


Figure 2.14: The bifurcation diagram shows the grazing-sliding bifurcation where there is a sudden transition to a chaotic attractor.

actually describes different dynamics with respect to the switching manifold (see Table 2.1). In brief, the degree of smoothness can be described by the partial derivatives of the non-smooth function F_i . If the equation (1.3) is redefined as:

$$\dot{x} = \begin{cases} F_1(x, \rho), & \text{for } x \in S_1 \\ F_2(x, \rho), & \text{for } x \in S_2 \\ \vdots \\ F_n(x, \rho), & \text{for } x \in S_n \end{cases} \quad (2.13)$$

where F_i , $i = 1, 2, \dots, n$ generates flows Φ_i , $i = 1, 2, \dots, n$. The 1st, 2nd and the 3rd partial differentiation of $F_i(x)$ will be

$$\begin{aligned} \left. \frac{\partial \Phi_i(x, t)}{\partial t} \right|_{t=0} &= F_i(x), \\ \left. \frac{\partial^2 \Phi_i(x, t)}{\partial t^2} \right|_{t=0} &= \frac{\partial F_i}{\partial \Phi_i} \frac{\partial \Phi_i}{\partial t}, \\ \left. \frac{\partial^3 \Phi_i(x, t)}{\partial t^3} \right|_{t=0} &= \frac{\partial^2 F_i}{\partial \Phi_i^2} \left(\frac{\partial \Phi_i}{\partial t} \right)^2 + \left(\frac{\partial F_i}{\partial \Phi_i} \right)^2 \frac{\partial \Phi_i}{\partial t}. \end{aligned}$$

Therefore, if the first partial derivative of flows $\left. \frac{\partial \Phi_i(x, t)}{\partial t} \right|_{t=0} \neq \left. \frac{\partial \Phi_j(x, t)}{\partial t} \right|_{t=0}$ at the discontinuity set Σ_{ij} , then the non-smooth system has a DoS of one. However, if the first partial derivative of flows $\left. \frac{\partial \Phi_i(x, t)}{\partial t} \right|_{t=0} = \left. \frac{\partial \Phi_j(x, t)}{\partial t} \right|_{t=0}$ but the second partial derivative of flows $\left. \frac{\partial^2 \Phi_i(x, t)}{\partial t^2} \right|_{t=0} \neq \left. \frac{\partial^2 \Phi_j(x, t)}{\partial t^2} \right|_{t=0}$ at the switching manifold Σ_{ij} , then we have DoS of two and so on.

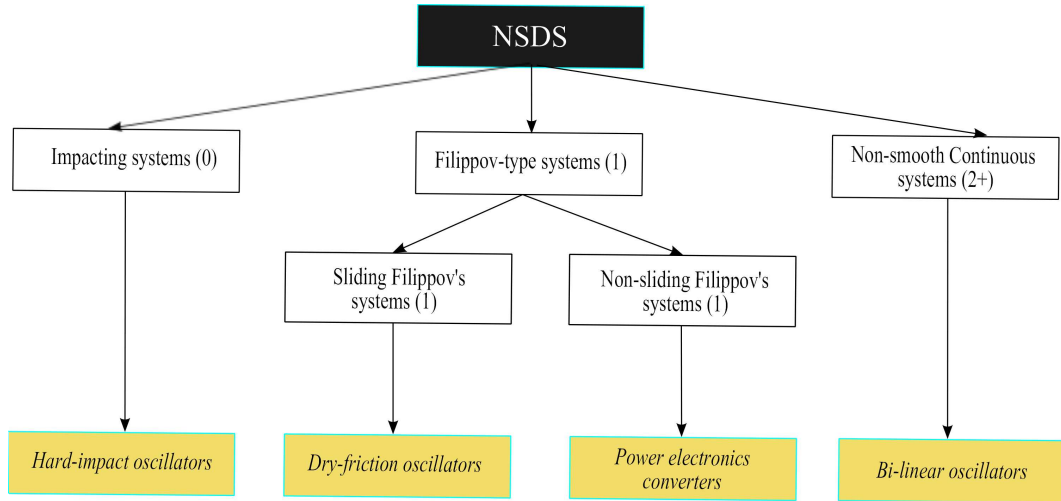


Figure 2.15: The classification of non-smooth dynamical systems (NSDS). The number in brackets associated with each block represents the degree of smoothness (DoS).

2.2.2 Smooth bifurcations

Smooth bifurcations arise in smooth dynamical systems of the form (1.2) (and smooth maps). These are basically bifurcation scenarios where upon any parameter variation, there are often involved period-doubling bifurcations leading to a chaotic orbit [8]. As introduced in Section 1.2, the system (1.1) is *smooth* if f is differentiable everywhere and up to any order in both x and ρ . Fixed points x^* of the smooth system (1.1) are solutions derived from solving the following algebraic equation:

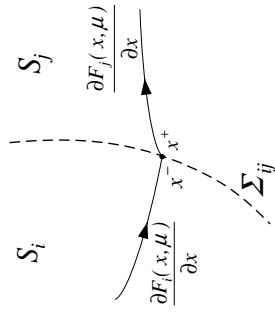
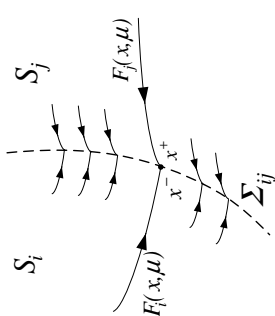
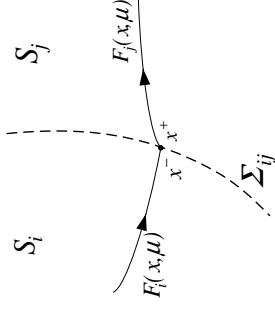
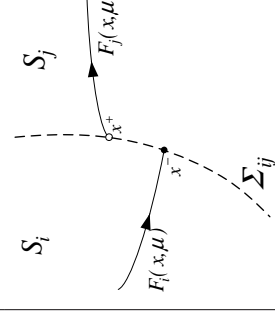
$$0 = f(x, \rho). \quad (2.14)$$

A diagram illustrating a scalar measure of the n -vector x versus the variation of a parameter ρ , where (x^*, ρ) is a solution of (2.14), is referred to as a *bifurcation diagram* [53]. In smooth systems, the bifurcation branches are *smooth* (curves of solutions (2.14) under variation of ρ) but can split into one or more branches, referred to as period-doubling bifurcations.

If we define a Jacobian of the system (1.1) as

$$\mathcal{J}(x, \rho) = \frac{\partial f(x, \rho)}{\partial x}, \quad (2.15)$$

Table 2.1: The different types of non-smooth dynamical system

DoS	2 or higher	1	1	0
model	bilinear oscillators Non-smooth continuous systems	dry friction oscillators Non-smooth Filippov-type systems with sliding dynamics	DC-DC converters Non-smooth Filippov-type systems	impact oscillators Non-smooth systems with discontinuous (jump) states
dynamics				
possible DIBs	Boundary equilibrium, Grazing of limit cycle	Boundary equilibrium, Boundary pseudo-equilibria, sliding/sticking	Boundary equilibrium, Boundary intersection crossing, Corner collision	Boundary equilibrium, Grazing of limit cycle

where the derivative exists for the smooth system (1.1), different bifurcations can result from the different (unique) paths of the *eigenvalues* of the Jacobian (2.15). These generic forms of smooth bifurcations can be categorized as pitchfork (or flip) bifurcations, saddle-node (or fold) bifurcations, transcritical bifurcations and Hopf bifurcations [6, 54] depending on the (continuous) path the eigenvalues take in phase space. These paths are depicted in Figs. 2.16, 2.17 and 2.18, where a solid line shows a stable branch (when the fixed points x^* are stable) and a dashed line shows an unstable branch (when the fixed points x^* are unstable). Fig. 2.16a shows a saddle-node bifurcation where the (continuous path of) eigenvalues of the Jacobian shows that the upper branch is stable while the lower one is unstable. In a transcritical bifurcation, two smooth branches exchange stability (Fig. 2.16b).

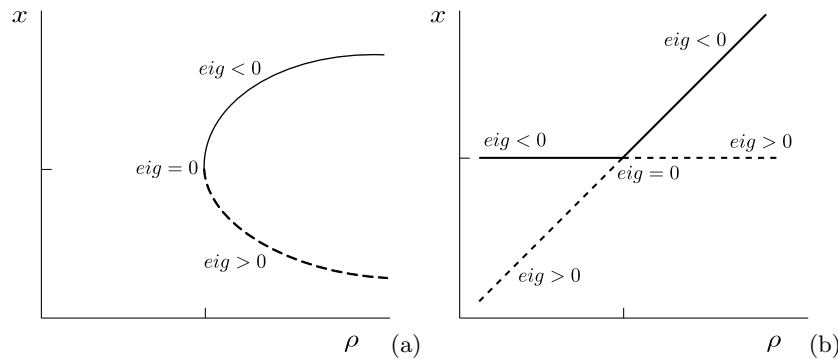


Figure 2.16: (a) A saddle-node bifurcation, (b) A transcritical bifurcation. eig is denoted as an eigenvalue of the Jacobian (2.15).

Fig. 2.17 shows how two stable branches intersect in a bifurcation point and form an unstable branch creating a supercritical pitchfork bifurcation (or vice-versa resulting in subcritical pitchfork bifurcation).

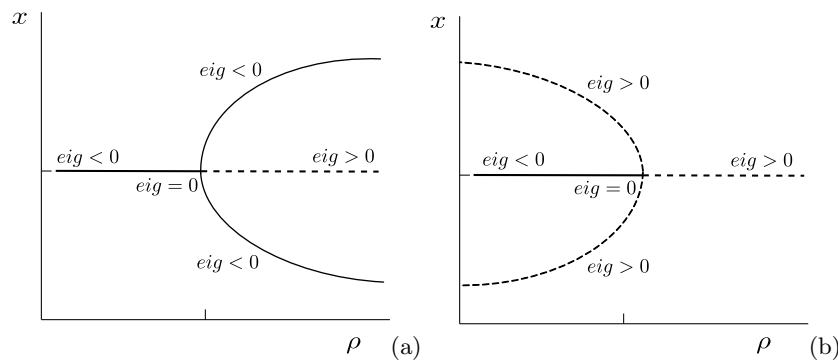


Figure 2.17: (a) A supercritical pitchfork bifurcation, (b) A subcritical pitchfork bifurcation.

In a Hopf bifurcation (Fig. 2.18), the fixed point loses its stability and as a result a periodic solution is born (or vice-versa).

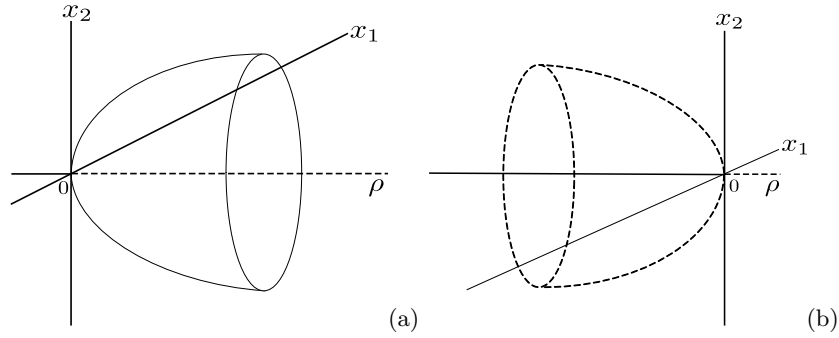


Figure 2.18: (a) A supercritical Hopf bifurcation, and (b) A subcritical Hopf bifurcation.

It is possible for a smooth bifurcation, in some rare cases, after having a short cascade of bifurcations (usually after three Hopf bifurcations), to reach a chaotic orbit [55]. For the period-doubling bifurcation cascade leading to chaos, the phase space of smooth flows must be at least three-dimensional; however, one of the most typical examples of a smooth bifurcation occurs in one-dimensional discrete system known as logistic maps (Fig. 2.19). In this smooth bifurcation, each cascade is a pitchfork bifurcation where a double-period stable orbit is born leaving behind an unstable orbit.

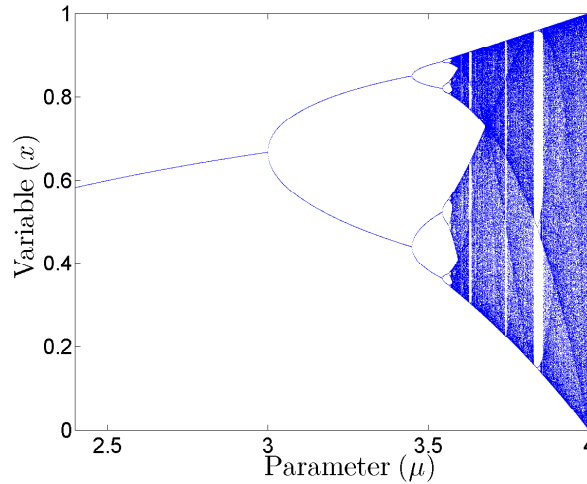


Figure 2.19: The bifurcation diagram for the logistic map $x_{n+1} = \rho x_n(1 - x_n)$ under a range of parameter variation of $\rho \in [2.4, 4]$. The asymptotic behaviour of the sampled state variable x , plotted as discrete points, shows Feigenbaum's cascade of period-doubling bifurcation leading to chaos.

2.2.3 Discontinuity-induced bifurcation: a unique bifurcation phenomenon

Even though the bifurcation scenarios in smooth systems can also be observed in non-smooth systems, the most remarkable nonlinear behaviour of non-smooth systems is the abrupt transition from a stable periodic orbit to chaos without any period-doubling or cascade of bifurcations, as shown in the different case studies introduced earlier in this

chapter. As a result, a different class of bifurcation has been introduced to study these new bifurcation phenomena; namely the, discontinuity-induced bifurcation (DIB). Understanding the dynamics of DIBs induced by a non-smooth transition with respect to the switching manifold, requires some preliminary but essential concepts, which are partly adopted from the qualitative theory of smooth dynamical system. These concepts can be defined from the viewpoint of system topology as follows.

Definition 2.1: Invariant set An *invariant set* of the system (1.3) is a subset of the state space such that any trajectory with the initial condition x_0 starts in the invariant set, will remain in the set for all future times $t \in T$ of system evolution. Therefore, the simplest form of the invariant set of the system (1.3) will be an equilibrium point x^* , which fulfills the flow condition $\Phi_i(x^{eq}, t) = \Phi_i(x^{eq}, 0)$ for $x \in S_i$, $i = 1, 2, \dots, n$. A more complex invariant set, called *periodic orbits* or *limit cycles*, is defined as non-trivial periodic solution when $\Phi_i(x^p, T) = x^p$ well defined in ∂S_i , $i = 1, 2, \dots, n$.

Definition 2.2: Piece-wise topological equivalence [7] Lets define two non-smooth systems of the form (2.13), which generate smooth flows $\Phi_i^1(x, t)$ and $\Phi_i^2(x, t)$ in the state space regions S_i^1 and S_i^2 , respectively for $i = 1, 2, \dots, n$. The two systems become topologically equivalent, if by continuous and invertible mapping of the orbits of the first system onto the second system via a homeomorphism $h : t \rightarrow s(t)$ as $\Phi_i^1(x, t) = h^{-1}(\Phi_i^2(h(x), s(t)))$, the flow remain the same while maintaining the direction of time. Moreover, each of the switching manifolds must be maintained by the mapping $h(\Sigma_{ij}^1) = \Sigma_{ij}^2$.

A DIB takes place whenever an infinitesimal perturbation of a vector field results in a system that is not *piecewise-topologically equivalent* to the system just before the perturbation. The above definitions emphasize different notions of topological equivalence, which is entirely based on topological changes rather than the stability of a specific invariant set. This is important considering the fact that a DIB cannot be considered as a bifurcation in the classical notion of *structural stability for smooth functions*. For instance, in an impacting system (Section 2.1.2), the grazing event occurs when an invariant set (limit cycle) becomes tangent to the switching manifold. Varying a parameter causes the invariant set to pass through a non-transversal intersection with the switching manifold leading to a grazing bifurcation (Fig. 2.9). However, in both analytical and topological senses of structural stability defined for smooth dynamical systems [53, 56], the invariant set is still stable; hence, there should not be a bifurcation [52, 53]. Feigin first discovered this kind of bifurcation, often termed as *C-bifurcation* in Russian Literature [57–59]. Later Weger et. al. [42] and di Bernardo et al. [60] reinvestigated in detail the C-bifurcation phenomenon in continuous-time, non-smooth systems as the so-called grazing bifurcation in impact oscillators.

Although the case studies presented in this chapter center around continuous-time systems, DIBs have also been observed in discrete-time non-smooth systems known as *discrete-time maps*. Nusse and Yorke, in a number of studies, classified DIBs in discrete-time piece-smooth maps as *border-collision* bifurcations [61–63]. Generally a border-

collision bifurcation comes about when the fixed points of a map cross a switching manifold. Banerjee and Grebogi further studied this kind of bifurcation in power electronics converters [64].

Grazing bifurcations (see Case study II in Section 2.1.2) have been considered as a separate group of DIBs whose prominence comes from the fact that they are difficult to analyze close to the grazing event due to the square-root singularity of the Jacobian matrix. Nordmark introduced a special approach, zero-time discontinuity mapping, to derive piece-wise smooth maps as *normal forms* where the dynamics of invariant sets local to the grazing can be investigated through iteration of the normal maps [65]. diBernardo et al. further employed the normal forms to study DIBs in all non-smooth systems classified in Table 2.1 [66–68]. Nonetheless, in the case of a hard impacting system, the square-root singularity, causing an infinite stretching of the phase space near the grazing orbit, present an obstacle to the direct application of existing tools to effectively analyze the grazing phenomena.

Grazing bifurcations have also been observed in sliding Filippov-type systems at the onset of sliding motions. This type of DIB normally leads to discontinuity maps with jumps in the derivatives of higher than linear order. However, the case of *grazing-sliding* bifurcation (Section 2.1.3) is unique in the sense that the dynamics local to the bifurcation point are governed by a piece-wise linear map which can be derived in normal form. However, this normal form map is not of the form originally studied by Feigin as it is singular on one side of the switching manifold.

All the aforementioned DIBs are induced by the interaction of an invariant set (equilibrium or limit cycle in the sense of Definition 2.1) with the switching manifold. However, there are possible DIB scenarios induced by the interaction of an invariant set with other invariant sets. Kuznetsov et al. studied this type of DIBs in two-dimensional Filippov systems having a single switching manifold [69].

To date, non-smooth bifurcation theory has paid attention to *codimension-one* bifurcation scenarios where there is only one parameter to be varied and at most two switching manifolds to be dealt with (see Table 2.1 for possible codimension-one DIBs observed in non-smooth system [7]). The resulting complex dynamics in the finite set of codimension-one equilibrium and limit cycle bifurcations have yet to be explored. Nevertheless, there is also literature on codimension-two *C*-bifurcations and higher codimension global bifurcation and the colorful dynamics they can exhibit (see [60] and all the references therein).

2.2.4 Structural stability of an invariant set

Considering Definitions 2.1 and 2.2, the stability of a periodic solution when a bifurcation occurs is associated with studying the dynamics of the periodic solution in question qualitatively. These qualitative dynamics, in turn, can be investigated in terms of equivalent dynamics when the system is subject to any variation of its parameters. Therefore, a new notion of *structural stability for non-smooth system* can be redefined as follows:

Definition 2.3: Structural stability A non-smooth system is called structurally stable if any perturbation, even for an infinitesimal size $\varepsilon > 0$ or any variation to the

system parameters, results in a piece-wise topologically equivalent system where its degree of smoothness (DoS), the number and position of its switching manifold remain intact.

So as an alternative to Definition 2.2 in defining the onset of a DIB, if any variation of system parameters results in a system that according to Definition 2.3 is not structurally stable, then a DIB occurs. The equivalent dynamics can then be realized by employing the idea of system *topology* in a mathematical sense [53] as, for instance, is defined in Definition 2.2 for a non-smooth dynamical system (1.3). It is important to know that, even though Definition 2.2 and consequently Definition 2.3 are defined in a sense of topological equivalence for smooth bifurcations [53], there have been not yet developed rigorous mathematical definitions for topological equivalence and structural stability of non-smooth systems. Hence, Definitions 2.2 and 2.3 can be accepted as existing definitions for practical purposes. In studying the stability of general nonlinear systems, the prevailing tendency is to linearize the system around an invariant set of interest as the study of the linearized system would be less complicated using established approaches. Practically, the linearization of a nonlinear dynamical system becomes mathematically justifiable if we define the system in a topological way. This is mainly because a dynamical system in the close neighborhood of an invariant set is topologically equivalent to the linearization of the system around that set. This concept is generally validated and formalized in the form of a theorem in the study of dynamical systems, the Hartman-Grobman theorem or the so-called linearization theorem. Nevertheless, before introducing this theorem, an essential concept of topological conjugacy should be properly defined using the established theorems for smooth dynamical systems.

Definition 2.4 (Topological conjugate [53]) If there exists two smooth (continuous and differentiable over the entire phase space) dynamical system $\dot{x} = f(x)$ and $\dot{y} = g(y)$, generating the flows $\Phi(x, t)$ and $\tilde{\Phi}(h(x), t)$, then the two flows are called topologically conjugate if a homeomorphism h

$$\Phi(x, t) = h^{-1}(\tilde{\Phi}(h(x), t))$$

holds for the flows.

Remark: A homeomorphism is an invertible map such that both the map and its inverse are continuous.

Although the definition above was originally used by Kuznetsov [53] as the basis of topological equivalence for structural stability of smooth systems, di Bernardo [7] redefines Definition 2.4 based on flow functions of the system.

Theorem 2.1 (Hartman-Grobman [70]) The behaviour of a dynamical system near a hyperbolic equilibrium point ² is qualitatively (topologically) equivalent to the behaviour of its linearization around that point. Hence, if there is a smooth map $f : \mathbb{R}^n \rightarrow \mathbb{R}^n$ as $x \mapsto f(x)$ whose fixed point is x^* , then the linearization of f in the neighborhood

²An equilibrium point is called hyperbolic if none of its eigenvalues lie on the imaginary axis

of x^* can be expressed as:

$$y \mapsto Ay$$

where $A = \left. \frac{df}{dx} \right|_{x^*}$ is the linearization of f at the fixed point x^* . Therefore, there exists a neighborhood U of x^* and a homeomorphism $h : U \rightarrow \mathbb{R}^n$ such that

$$f(x) = h^{-1}(A(h(x)));$$

that is, in the neighborhood U of x^* , the map f is topologically conjugate to its linearization A .

Theorem 2.1 emphasizes that analyzing the stability of periodic solutions, which are the main elements of the dynamics of nonlinear systems, can be done on a linearized map representing the equivalent dynamics close to the periodic solutions. This also implies that the stability of a periodic orbit can be investigated straightforwardly if an n -dimensional flow is mapped to an appropriately chosen $(n - 1)$ -dimensional map. One of the fundamental tools for this purpose is the Poincaré map, which transforms the flows of a continuous-time system (1.3) to a discrete-time map.

Definition 2.5 (Poincaré map) Consider an autonomous smooth system

$$\dot{x} = f(x), \quad x \in \mathbb{R}^n, \quad (2.16)$$

which generates the flow $\Phi(x, t)$ (or the solution at time t) as $f(\Phi(x, t)) = \frac{\partial \Phi(x, t)}{\partial t}$ with the initial condition $x(t_0) = x_0$. Let $\Gamma(t) = \Gamma(t + T)$ be a periodic solution with a period of $T > 0$. Let Ξ represents a hyperplane of dimension $n - 1$, called the *Poincaré section* where a periodic solution $\Gamma(t)$ crosses transversally at a point x^* as depicted in Fig. 2.20. The flow $\Phi(x, T)$ initiating in a small neighborhood of x^* , crosses Ξ sufficiently close to x^* after some time T . Therefore, if we let $U \subset \Xi$ be some neighborhood of $\Gamma(x^*)$ and $V \subset \Xi$ be another neighborhood of $\Gamma(x^*)$, the flow $\Phi(T, x)$ defines a Poincaré map $P : U \rightarrow V$ as

$$P(x^*) = \Phi(T, x^*), \quad (2.17)$$

where $T = T(x_0)$ is the time taken for the flow initiated at x_0 to first return to Ξ .

Remark: The formal definition above is for the periodic solution of an autonomous system of the form (1.3). For non-autonomous system, the discrete-time map, or so-called stroboscopic Poincaré map, samples the continuous-time orbit at known but fixed sampling interval T [1].

Using the definition 2.5, a periodic solution can be always related to a fixed point of the Poincaré map.

With the Poincaré map, the stability of a periodic solution $\Phi(x, t)$ can be simply examined via the linearization of the map at the fixed point x^* as

$$DP(x^*) = \frac{\partial P(x^*)}{\partial x^*} = \left[I - \frac{1}{\frac{\partial n_{\Xi}}{\partial x} \frac{\partial \Phi(T, x^*)}{\partial t}} \frac{\partial \Phi(T, x^*)}{\partial t} \frac{\partial n_{\Xi}}{\partial x} \right] \frac{\Phi(T, x^*)}{\partial x}, \quad (2.18)$$

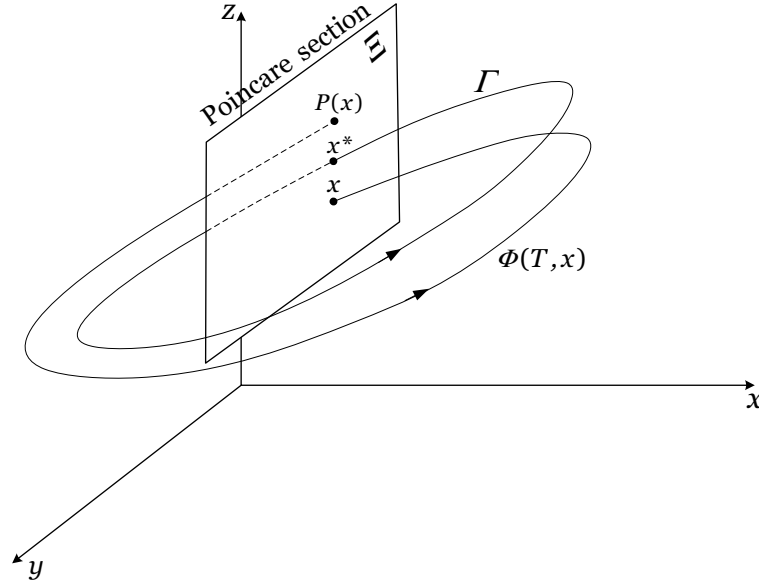


Figure 2.20: The 3-dimensional view illustrates how the periodic solution $\Gamma(t)$ is mapped to the fixed point x^* of the discrete-time map; that is, the Poincaré map.

where n_Ξ is the normal vector to Ξ . The matrix $DP(x^*)$ is the *Jacobian matrix* of P with respect to x^* . In general, investigating the *eigenvalues* of the matrix $DP(x^*)$, or the so-called *Floquet multipliers* $\lambda_i, i = 1, 2, \dots, n$ of $\frac{\partial \Phi(T, x^*)}{\partial x}$ in (2.18), referred to as *Monodromy matrix* plays an important role in the stability analysis of a fixed point x^* of the map, which in turn, determines the stability of the mapped limit cycle³. The stability of dynamical systems in its classical notion of *Lyapunov* stability precedes that of structural stability. Lyapunov theory is more concerned with the behaviour of a nonlinear system in the neighborhood of its equilibrium. In fact, the asymptotic stability (in the sense of Lyapunov) of an equilibrium (or invariant set) can be proven if a trajectory initiated close to an equilibrium (or invariant set), after any perturbation of initial conditions, returns and stays close to that equilibrium (or invariant set) for all future time [9]. Alternatively, asymptotic stability of a periodic solution can be investigated in terms of Floquet multipliers or as we shall henceforward refer to, multipliers.

Theorem 2.2 (Asymptotic stability of the periodic solutions of autonomous smooth systems [35]) Let $P(x)$ be a Poincaré map as defined by Definition 2.5, mapping the periodic solution $\Gamma(x)$ of an autonomous smooth system (2.16). $\text{eig}(DP(x^*))$ always includes one eigenvalue of zero value or the *Monodromy matrix* has always a multiplier $\lambda_1 = 1$. The periodic solution $\Gamma(x)$ is locally asymptotically stable if the magnitude of the rest of the eigenvalues of $DP(x^*)$ or $(n - 1)$ multipliers $\lambda_i, i = 2, \dots, n$ lie inside the unit circle ($|\lambda_i| < 1$, for $i = 2, \dots, n$).

Remark: The multipliers in the notion of the above Theorem, can also be determined from the fundamental solution matrix $\bar{\Phi}(T, x^*)$, related to the Jacobian of the Poincaré

³Note that the seemingly equal terms $\frac{\partial n_\Xi}{\partial x} \frac{\partial \Phi(T, x^*)}{\partial t}$ and $\frac{\partial \Phi(T, x^*)}{\partial t} \frac{\partial n_\Xi}{\partial x}$ in the numerator and the denominator of (2.18) are actually the inner product of two matrices resulted from perturbed trajectories; hence, they cannot be cancelled out.

map as [71]:

$$DP(x^*) = \frac{\partial P(x^*)}{\partial x^*} = \left[I - \frac{1}{n_{\Xi} \frac{\partial \Phi(T, x^*)}{\partial t}} \frac{\partial \Phi(T, x^*)}{\partial t} n_{\Xi} \right] \bar{\Phi}(T, x^*), \quad (2.19)$$

Remark: From $\text{eig}(DP(x^*)) = \text{eig}_i$, $i = 1, \dots, n$, $\text{eig}_1 = 0$ because the eigenvectors of DP are located in the tangent plane to the Poincaré section (see Fig. 2.20). This means that eig_1 is linearly independent from $\text{eig}_2, \dots, \text{eig}_n$. Similarly, from the multipliers λ_i , $i = 1, \dots, n$, $\lambda_i = 1$ because the limit cycle $\Gamma(x)$ of an autonomous system can be shifted in time [35].

However, according to Theorem 2.2, investigating asymptotic stability of multipliers located on the imaginary axis would become complicated even if the multipliers lie in the unit circle. In the case of NSDS, examining the asymptotic stability becomes more complicated as there are cases where an invariant set extends across the switching manifold or an equilibrium lies on the switching manifold dividing the two regions of S_i and S_j in (2.13) [16]. Therefore, in these cases, the Lyapunov approach can be a strong alternative, instead of the discrete mapping approach, as it deals with allocating Lyapunov (energy) functions for a perturbation of the invariant set of interest. The stability can then be verified if the value of the Lyapunov function reduces along the trajectories. Nevertheless, the problem of determining such Lyapunov functions (positive definite and decreasing along the trajectories) for an equilibrium lying on the switching manifold of non-smooth system, in most cases, turns out to be infeasible [16]. Consequently, establishing a unified approach centered on asymptotic stability in Lyapunov sense to tackle the stability in the afore-mentioned scenarios has been found to be much less plausible than focusing on the relatively modern notion of structural stability, specially in bifurcation analysis and classification of non-smooth system. Chapter 4 of this thesis, is dedicated to the proposal of a solution to the problem of structural stability by providing a *Lyapunov framework* where investigating the stability of periodic solution of a *TS fuzzy model representing a non-smooth system*, becomes possible via correlating the concepts of asymptotic and exponential stability with structural stability.

In all bifurcation scenarios that a fixed point of a smooth map can exhibit (saddle, transcritical, pitchfork and Hopf bifurcations), a bifurcation occurs when a multiplier (or identically an eigenvalue of $DP(x^*)$) or a pair of multipliers crosses the imaginary axis under the variation of a system parameter. In a *smooth bifurcation*, the path of multipliers can be defined by a *continuous* function. However, in a DIB, upon variation of parameter μ , the Jacobian of the map becomes *discontinuous* at the switching manifold Σ_{ij} . This means that the multipliers undergo a *jump* when crossing Σ_{ij} . This condition is described by Leine [35] as a unique path of set-valued eigenvalue(s):

$$\overline{DP}(x^*) = \{(1 - \alpha)DP(x_-^*) + \alpha DP(x_+^*), \forall \alpha \mid 0 \leq \alpha \leq 1\}, \quad (2.20)$$

where x^* denotes the unique fixed point which lies on the switching manifold Σ_{ij} for a specific parameter value $\mu = \mu^*$. Then the Jacobian matrix $\overline{DP}(x^*)$ becomes discontinuous

at Σ_{ij} , being dissected into two Jacobin matrices $DP(x_-^*) \in S_i$ before jumping at Σ_{ij} and $DP(x_+^*) \in S_j$ after jumping at Σ_{ij} . $\overline{DP}(x^*)$ in (2.20), also called a *generalized Jacobian*, is defined as the closed convex hull of $DP(x_-^*)$ and $DP(x_+^*)$, which yields the set of values that the eigenvalues of $\overline{DP}(x^*)$ can obtain on Σ_{ij} . Fig. 2.21 illustrates the jump of eigenvalues inducing a non-smooth bifurcation (DIB). The condition can be equivalently described by the multipliers of $\overline{\Phi}(T, x^*)$ for the DIBs of periodic solutions. One or more multipliers of $\overline{\Phi}(T, x^*)$ should undergo a jump over the unit circle at the parameter value $\mu = \mu^*$ when the switching manifold is crossed. This discontinuous path can then be represented by a set-valued function (fundamental solution matrix) of the form similar to (2.20) for the fundamental solution matrix before crossing the switching manifold $\overline{\Phi}(T, x_-^*)$ and the fundamental solution matrix after crossing the switching manifold $\overline{\Phi}(T, x_+^*)$ [72]. The jump itself is described by a *saltation matrix* S , which maps $\overline{\Phi}(T, x_-^*)$ to $\overline{\Phi}(T, x_+^*)$ as

$$\overline{\Phi}(T, x^*) = \overline{\Phi}(T, x_+^*) \cdot S \cdot \overline{\Phi}(T, x_-^*).$$

The saltation matrix is obtained by relating the dynamics of perturbed periodic solutions before crossing the switching manifold Σ_{ij} to those after crossing Σ_{ij} [11, 35, 73].

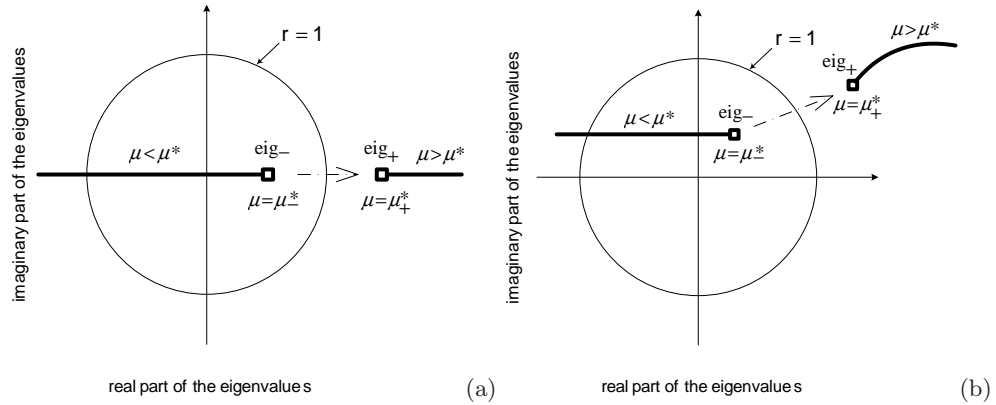


Figure 2.21: On the onset of a DIB, the eigenvalues of the Poincaré map undergo a jump (a) through the real axis (b) through the imaginary axis.

Therefore, the necessary conditions for *structural instability*, of a periodic solution of non-smooth system in a non-topological sense (not in the sense of Definition 2.2) is the jump of the multipliers $\lambda_i, i = 2, \dots, n$ (or a pair of them) through the circle with a radius of unity.

It should be noted that deriving the Poincaré map in non-smooth systems when their switching manifold Σ_{ij} is crossed transversally is not as straightforward as it is in smooth systems. The dynamics local to Σ_{ij} should be examined carefully as the time taken for close trajectories to reach Σ_{ij} is, in general, different. This fact is envisaged in Fig. 2.22 where there is a time lag in crossing Σ_{ij} between a slightly-perturbed trajectory $\Phi(t, x_0 + \delta)$ and the one before perturbation $\Phi(t, x_0)$. If this dynamic is ignored in constructing a Poincaré map to examine a periodic solution on the onset of a DIB, a false map will be derived, leading to wrong conclusions about its Floquet multipliers.

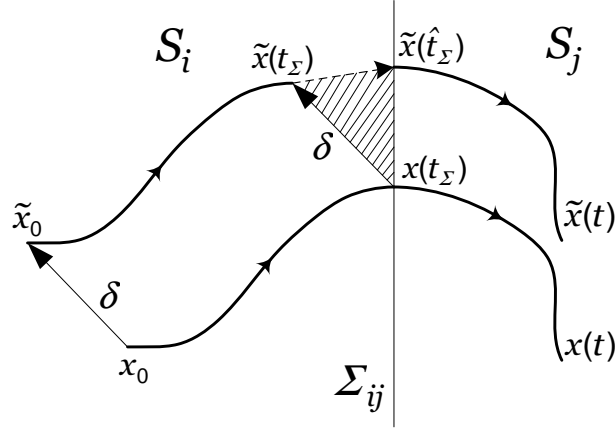


Figure 2.22: The fate of the orbit $\Phi(t, x_0)$ when a perturbation δ is added to its initial conditions to become $\tilde{x}_0 = x_0 + \delta$. $\tilde{x}(t)$ is assumed to cross the switching manifold Σ_{ij} at the point $\tilde{x}(t_\Sigma)$ but it actually crosses Σ_{ij} at the point $\tilde{x}(\hat{t}_\Sigma)$ where there is a small time lag $\delta t = \tilde{x}(\hat{t}_\Sigma) - \tilde{x}(t_\Sigma)$, producing an error in the derivation of the Poincaré map.

2.2.5 Discontinuity map: a prevailing tool to study impacting dynamics

A conventional analytical tool to correct the error (i.e. cross-hatched area in Fig. 2.22) in the derivation of a Poincaré map close to the structurally unstable event is the *discontinuity map* (DM) [41]. The effect of the discontinuity map is to introduce the saltation matrix in the linearization of the map around the periodic orbit in question. The necessity of DM becomes clearer in the special case of a grazing event when the periodic orbit becomes tangent to or grazes the switching manifold (this event can lead to a bifurcation as shown in case study II and Fig. 2.9). In this case, the orbits initiating with some initial condition $x_0 \in \Xi$ close to x^* (Fig. 2.23) just grazes the switching manifold with zero velocity (the velocity vector normal to switching manifold is zero). As a result, the Poincaré map $P(x) = \Phi(T, x)$ is derived as if the intersection with Σ_{ij} is non-existent and the orbit lies wholly inside the region S_i (Fig. 2.23a). To adjust this wrong conjecture, a DM should be defined for the grazing orbit as a local correction to the initial conditions as if the orbit intersects the switching manifold. Then, the map $P(x)$ can be correctly applied as if Σ_{ij} were not there.

To study the grazing bifurcation of a periodic orbit in impacting systems, a special kind of discontinuity map, namely zero-discontinuity map (ZDM), is employed to obtain the Poincaré map near the grazing orbit [41, 74]. The ZDM is established near the grazing point $x(t_\Sigma)$ (Fig. 2.23b) which takes zero time (the detailed definition can be found in [7]). Essentially ZDM represents a saltation matrix associated with the switching event close to the grazing condition. Consider the case of grazing illustrated in Fig. 2.23b more closely (Fig. 2.24). To construct a ZDM, it is required to investigate the fate of two types of trajectories with initial conditions close to $x^* \in \Xi$. Therefore, if the grazing orbit $\Phi(t, x_0)$ grazes Σ_{ij} at the point x_G at time t^* , under the small perturbation of initial condition $x_0 + \delta$, it passes through the point x_1 at time t_1 close to the switching manifold and crosses

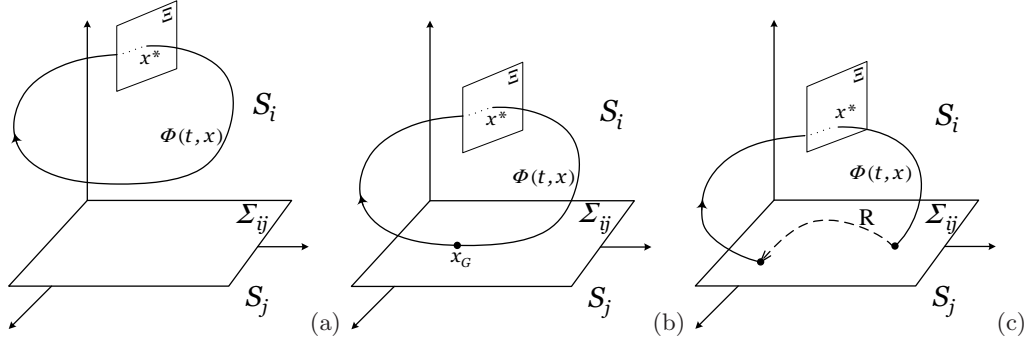


Figure 2.23: Behaviour of the periodic orbit $\Phi(t, x)$ close to the switching manifold Σ_{ij} for the impacting system in case study II: (a) the periodic orbit initiating at some initial condition $x_0 \in \Xi$ close to x^* do not intersect Σ_{ij} meaning the impact has not occurred yet, (b) the periodic orbit grazes Σ_{ij} , and (c) the periodic orbit intersect Σ_{ij} twice, meaning the impact has occurred. In this case a smooth reset map $R : x \mapsto R(x)$ applies to explain the discontinuous jump of the state to a new position.

it at the point x_2 at time $t_2 = t^* + \delta$. Then the reset map R maps the instantaneous jump of x_2 to x_3 and the trajectory becomes continuous in S_i from this point. If we follow the real flow according to the smooth differential equation of the system between the impacts (equation (2.5)), it should rest at the point x_4 . Therefore, the time taken for the point x_1 to reach x_3 , should be the same as would have been taken for the point x_4 to reach x_3 . Therefore, a ZDM can be defined as the mapping $x_1 \mapsto x_4$, which appears as the correction or saltation matrix in the derivation of the Poincaré map as

$$P_s = \Phi(x_0, t_0) \circ S_{ZDM} \circ \Phi(x_4, T - t_0), \quad (2.21)$$

where P_s is the stroboscopic Poincaré map (see Remark of Definition 2.5), $\Phi(x_0, t_0)$ represents the perturbed flow with the initial condition $x_0 \in \Xi$ evolving through time t_1 and $\Phi(x_4, T - t_0)$ represents the flow evolving through time $T - t_1$ with T being the period of the forcing function, i.e the sinusoidal forcing function $g(t)$ as defined in case study II [2, 7]. ZDM is preferred for studying the grazing bifurcation of the impacting system with periodic forcing function (as defined in case study II). For autonomous systems a similar kind of discontinuity mapping, defined with respect to a local Poincaré section or so-called Poincaré section discontinuity mapping (PDM) was found more suitable to study the dynamics near the grazing limit cycle [41, 75]. However, deriving a ZDM for studying grazing bifurcation is problematic as it coincides with an infinite stretching of the phase space in the neighborhood of the grazing orbit, resulting in the well-known problem of the square-root singularity of the Jacobian of a ZDM. As an example, for the case of hard-impact oscillator presented in case study IIs, the Jacobian of the zero-discontinuity map can be derived as [2, 7, 74]:

$$J_{ZDM}^4 = I + \sqrt{2a(x^*)} \frac{W(x^*)H_x}{2\sqrt{-H_{min}}}, \quad (2.22)$$

⁴The letter J in this equation stands for the Jacobian of the stroboscopic map and shall not be confused with matrix J as presented in chapter 3 and 4 to describe the discontinuous (jump) states in a non-smooth TS fuzzy model.

where $H(x)$ is a smooth function representing the switching manifold, H_{min} is the minimum value of $H(\Phi(x))$ at the grazing point, $H_x = \frac{\partial H(x)}{\partial x}$ and $a(x^*)$ is the acceleration of the flow $\Phi(t, x)$ at the grazing point (Fig. 2.23b). As the term $\sqrt{-H_{min}}$ obtains zero value near the grazing orbit, J_{ZDM} obtains an infinite value, which clearly explains the square-root singularity problem.

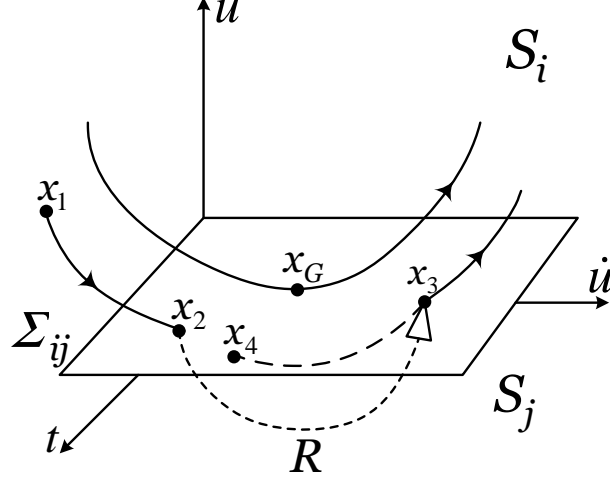


Figure 2.24: Zero-time discontinuity mapping close to grazing in an impacting system. The solid line represents the actual trajectory while the dashed line represents the extended ones. The ZDM is the map $x_1 \mapsto x_4$.

2.2.6 Sliding motions in Filippov-type systems

As can be noticed from Table 2.1, Filippov-type systems (systems with DoS of one) are carefully divided into two types mainly due to the fact that, for instance, in systems like dry-friction oscillators, there is always a strong possibility of a sliding motion. Therefore, the sliding dynamics must be properly defined as the solution trajectories undergo sliding. In fact, if the system is defined as a Filippov system with a single switching manifold Σ , the sliding condition occurs if the switching manifold fulfills the condition

$$\left(\frac{\partial H(x)}{\partial x} F_1\right) \cdot \left(\frac{\partial H(x)}{\partial x} F_2\right) < 0, \quad (2.23)$$

where $H(x)$ is a smooth function whose zero set $H(x) = 0$ represents a switching manifold Σ (i.e. $H = 1 - \dot{u} = 0$ in the case study III). The condition (2.23) implies that Σ should include a *sliding region*, which attracts⁵ trajectories on both sides (i.e. the condition illustrated in Fig. 2.12 in the case study III).

Looking closely at the dynamics near the discontinuity surface $\dot{x} = 0$ illustrated in Fig. 2.12, the trajectories in the close neighborhood of $\dot{x} = 0$ (switching manifold) are attracted towards the manifold from both directions, implying that the trajectory will never leave $\dot{x} = 0$, and an immediate problem of an appropriate description of the motion at $\dot{x} = 0$ arises. A fixed value of the function $P(\dot{x})$ will not solve the problem since $|x| \leq P_0/k$ is a set of equilibrium points feasible only when $P(\dot{x}) + kx = 0$. The motion of trajectories is

⁵The condition (2.23) also implies the trajectories may be generally repelled by a sliding region. However, in cases when the system flow is forward in time, A repelling sliding region is unrealizable [10]

not intrinsic in the set of discontinuities; however, as mentioned earlier, the vector fields form a motion called a sliding motion. Imposing additional assumptions on the stated model or using a more accurate model may lead to the deduction of the dynamics of the sliding motion. For instance, if Coulomb friction is substituted by viscous friction in equation (2.10), $P(\dot{x})$ can be more accurately described by

$$P(\dot{x}) = \begin{cases} P_0 & \text{if } \dot{x} > \epsilon, \\ \frac{P_0}{\epsilon} \dot{x} & \text{if } -\epsilon \leq \dot{x} \leq \epsilon, \\ -P_0 & \text{if } \dot{x} < -\epsilon, \end{cases} \quad (2.24)$$

implying that the solution tends to zero, see [11, 51].

In some cases, sliding motions can be intentionally triggered by a discontinuous control law [10]. By letting a function $s(x) = 0$, $s : \mathbb{R}^n \rightarrow \mathbb{R}$ represents a hypersurface in \mathbb{R}^n and a continuous vector field $\dot{x} = f(x, u)$ with respect to x and u , the sliding mode control law can be defined as:

$$u(x) = \begin{cases} u^+(x), & \text{if } s(x) > 0, \\ u^-(x), & \text{if } s(x) < 0, \end{cases} \quad (2.25)$$

where u^+ and u^- are continuous functions designed in such a way as to drive the vector fields to hypersurface $s(x) = 0$, resulting in a non-smooth system of the form (1.3) with the switching manifold $s(x) = 0$ where the sliding motion takes place. Resulting systems with this kind of sliding mode control strategy are generally called *variable structure systems* [51, 76]. The advantage of sliding mode control is designing a variable structure system which is insensitive to variations in unmodeled process dynamics and robust to external disturbances [10]. At the same time, this type of control can produce unwanted *chattering* phenomena, which occurs if the control law switches very fast between different values on the switching manifold. Normally, introducing hysteresis in the close neighborhood of the switching manifold can prohibit chattering by employing discrete actuators combined with an equivalent continuous control such that the vector field remains in the sliding mode. Nonetheless, chattering is not always undesirable. The performance is improved in some cases by building electric inertialess actuators operating in switching mode only. Hence, the control signal can be designed as a high-frequency discontinuous signal whose mean value is equal to the desired continuous control. This approach is applicable even in continuous control algorithms and the resulting actuators are eligible candidates when using discontinuous controls.

Another formal definition that can describe Filippov-type NSDS in a rigorous way is that of *differential inclusions* [11]. In this definition, we allow the right-hand side of an ODE $\dot{x} = f(x)$ in (2.16) to be not strictly a function, but to be a set-valued function, similar to the form defined for the unique set of eigenvalues in (2.20). Filippov [11] discusses several possible definitions of the set $f(x)$ and dynamics of sliding motions at the switching manifold where the vector field F becomes discontinuous. In Filippov's method, the dynamics at the switching manifold is described by the convex combination of continuous vector fields. Accordingly, the dynamics of sliding motions can be obtained, using *Filippov's convex combination method*, when there is rapid switching between continuous vector fields around the switching manifold [11]. Therefore, in a formal definition, the

set $f(x)$ is given by the smallest convex closed set containing all the limit values of the function f

$$\lim_{\substack{\tilde{x} \rightarrow x \\ \tilde{x} \notin \Sigma \\ x \in \Sigma}} f(\tilde{x}) \quad (2.26)$$

where Σ is a set with zero measure representing the discontinuity set of the vector field F in (1.3), usually given by a number of switching manifolds. At points of continuity, the set $f(x)$ includes one point as mentioned above; but in the case of discontinuities, the set $f(x)$ includes several elements forming for instance segments, polygons or polyhedrons. Therefore if we let the manifold Σ dissecting the vector field F into two regions S^- and S^+ and \tilde{x} be a point approaching the value $x \in \Sigma$ from the regions S^- and S^+ and hence define

$$F_1(x) = \lim_{\substack{\tilde{x} \rightarrow x \\ \tilde{x} \notin S^-}} f(\tilde{x}), \quad F_2(x) = \lim_{\substack{\tilde{x} \rightarrow x \\ \tilde{x} \notin S^+}} f(\tilde{x}),$$

then the set $f(x)$ describes the linear segment joining the endpoints of the vector fields F_1 and F_2 . Let P be the plane tangent to the manifold Σ at the point x . The intersection point of the segment and the plane P determines the *sliding vector field* F_{12} which describes the sliding motion along the manifold Σ ; cf. Figure 2.25. Therefore, the vector field F_{12} is defined by

$$F_{12} = \alpha F_2 + (1 - \alpha) F_1, \quad \alpha = \frac{F_1^n}{F_1^n + F_2^n}, \quad 0 \leq \alpha \leq 1, \quad (2.27)$$

where F_1^n and F_2^n are the projections of the vectors F_1 and F_2 onto the normal vector of the manifold Σ at the point x . Now if Σ is defined by a smooth function $H(x) = 0$ as $\Sigma = \{x : H(x) = 0\}$ and $\nabla H(x) = \frac{\partial H}{\partial x} \neq 0$, then

$$F_1^n = \frac{\nabla H \cdot F_1}{|\nabla H|}, \quad F_2^n = \frac{\nabla H \cdot F_2}{|\nabla H|}, \quad \alpha = \frac{\nabla H \cdot F_1}{\nabla H \cdot F_1 + \nabla H \cdot F_2} \quad (2.28)$$

If the convex definition above applies on the manifold $\dot{x} = 0$ describing the sliding surface for $|x| \leq P_0/k$ in case study III (equation (2.11)), it results in the dynamics $\dot{x} = 0$.

Another way to define a solution for sliding dynamics at the points of discontinuity is by *Utkin's equivalent control method* [10, 51]. The equivalent control method implies a replacement of undefined discontinuous dynamics on the switching manifold with continuous dynamics causing the vector field to follow a straight course along the switching manifold intersection. Even though the term *equivalent control* was originally coined for systems with continuous control inputs as defined in (2.25), the method can be applied to the system without control inputs in such a way that the sliding vector field F_{12} is defined as the average of vector fields F_1 and F_2 in addition to the equivalent control U^{eq} in the direction of difference between F_1 and F_2 :

$$F_{12} = \frac{F_1 + F_2}{2} + \frac{F_2 - F_1}{2} U^{eq}, \quad (2.29)$$

where U^{eq} is

$$U^{eq} = -\frac{\nabla H \cdot F_1 + \nabla H \cdot F_2}{\nabla H \cdot F_1 - \nabla H \cdot F_2}, \quad -1 \leq U^{eq} \leq 1. \quad (2.30)$$

Therefore, U^{eq} is the control that pulls F_{12} in a direction tangent to the switching manifold Σ ; cf. Fig. 2.26.

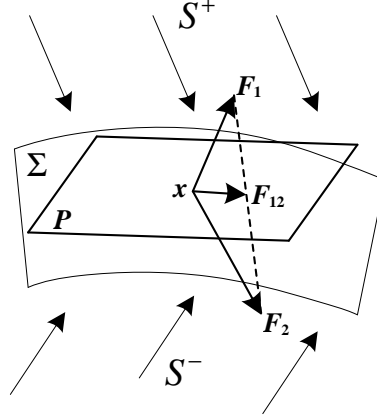


Figure 2.25: Illustration of sliding motion using Filippov's convex combination method.

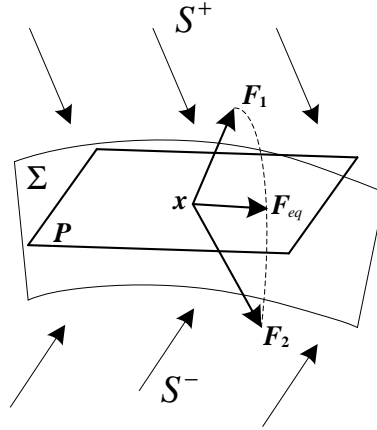


Figure 2.26: Illustration of Utkin's equivalent control method where $F^{eq} := F_{12}$.

2.3 Summary

Non-smooth electrical and mechanical systems representative of three significant groups of NSDS, non-sliding, sliding Filippov-type systems and impacting systems have been introduced and their observed complex dynamics have been illustrated in the form of different case studies. It has been pointed out that the degree of smoothness (DoS) is used as a yardstick in the classification of non-smooth systems. The essential concepts for NSDS have been highlighted in the form of different definitions. Most of these concepts are adopted from those of smooth dynamical systems; nonetheless, the new notion of structural stability, delineating the stability of periodic solutions, was redefined to explain numerous topologically non-equivalent scenarios that can occur with respect to the switching manifold of a non-smooth system. Accordingly, comparing a smooth bifurcation with a non-smooth bifurcation or what is referred to as *discontinuity-induced bifurcation* (DIB), reveals that when a DIB occurs, a stable local orbit abruptly loses its stability to a chaotic orbit, a unique phenomena which is not observable in smooth systems. A literature review of this kind of bifurcation has been presented.

Existing qualitative theory and analytical tools for non-smooth bifurcation analysis, known as the discontinuity mapping approach, has also been briefly reviewed. Despite the sophistication of the rigorous analysis, it has been seen that using the current approach to study the codimension-one grazing bifurcation is still problematic due to the infinite stretching of phase space near the grazing event.

It has been outlined that two major methods exist in the literature for formulating the equation of sliding dynamics in Filippov-type systems, Utkin's equivalent control method and Filippov's convex method, when the solution of a non-smooth system is formalized in the conventional form of differential inclusion.

Chapter 3

Takagi-Sugeno fuzzy modeling

The distinguishing feature of fuzzy logic is that in fuzzy logic everything is - or allowed to be - a matter of degree. The principal tool that may lead to a generalized theory of uncertainty ...

LOTFI A. ZADEH
Information Sciences (2005)

This chapter presents in detail a Takagi-Sugeno (TS) fuzzy modeling structure able to represent non-smooth dynamical systems. It commences with a discussion of TS fuzzy modeling originally designed for smooth nonlinear systems in Section 3.1, which gives an overview on the contemporary structure and different approaches of obtaining such models. The inability of the current TS fuzzy model structure to represent any sort of NSDS will be shown and discussed through a stimulating example in Section 3.1.3. Then, a TS fuzzy model structure capable of modeling all NSDS classified in Table 2.1, is formally proposed in Section 3.2.2. The essential properties of such a modeling structure including state evolution, sliding dynamics, and specially existence (and uniqueness) of the solution will be discussed in the succeeding sections. After suggesting two approaches for constructing the proposed model structure, hence forward called *non-smooth TS fuzzy model structure*, it is shown, through a number of examples, that the new structure can accurately represent NSDS and all their complex dynamics.

3.1 Models for smooth dynamical systems

3.1.1 TS fuzzy model structure

The structure for fuzzy system identification was initially proposed in Takagi and Sugeno's pioneering work [27]. The purpose of the proposed structure was to identify and accurately construct models of the control problems with uncertainties and inaccuracies in their model parameters. Basically, the idea of fuzzy modeling, later referred to as Takagi-Sugeno

(abbreviated as TS) fuzzy modeling, is to develop a nonlinear model of a smooth dynamical system, composing of a number of sub-models which are responsible for respective sub-domains. Although the idea of multi-model approach is well-known in the nonlinear control literature, TS fuzzy modeling based on the concept of fuzzy set theory [5] offered a novel technique to build multi-models of a process using input/output data or the original mathematical model of a system. This model structure is composed of a fuzzy IF-THEN rule base partitioning of a space - usually called the universe of discourse - into fuzzy regions described by rule antecedents. The consequent of each rule j is usually a simple functional expression ($y^j = f^j(x)$). A common format of a rule j can be described as follows:

$$\text{Rule } j : \text{IF } \theta_1 \text{ is } \Gamma_1^j \text{ AND } \theta_2 \text{ is } \Gamma_2^j \text{ AND...AND } \theta_q \text{ is } \Gamma_q^j \text{ THEN } y^j = f^j(x).$$

The vector $\theta \in \mathbb{R}^q$ contains the premise variables and may be a subset of the independent variables $x \in \mathbb{R}^n$. Each premise variable θ_i has its own universe of discourse that is partitioned into fuzzy regions by the fuzzy sets describing linguistic variables Γ_{ik} . The premise variable θ_i belongs to a fuzzy set k with a *truth value* given by a *membership function* $\mu_{ik}(\theta_i) : \mathbb{R} \rightarrow [0, 1]$ for $k = 1, 2, \dots, s_i$ where s_i is the number of fuzzy sets for premise variable i . The notation Γ_i^j and μ_i^j are referred to as linguistic variables and their membership function, respectively, correspond to the premise variable θ_i in rule j . That is, $\Gamma_{ik}^j \in \{\Gamma_{i1}^j, \Gamma_{i2}^j, \dots, \Gamma_{is_i}^j\}$ and $\mu_{ik}^j(\theta_i) \in \{\mu_{i1}^j(\theta_i), \mu_{i2}^j(\theta_i), \dots, \mu_{is_i}^j(\theta_i)\}$.

A truth value (or activation degree) h^j for the complete rule j is computed using the aggregation operator AND, also called a *t-norm*, often denoted by $\otimes : [0, 1] \times [0, 1] \rightarrow [0, 1]$, as:

$$h^j(\theta) = \mu_1^j(\theta_1) \otimes \mu_2^j(\theta_2) \otimes \dots \otimes \mu_q^j(\theta_q) = h^j(\theta) = \prod_{i=1}^q \mu_i^j(\theta_i) \quad (3.1)$$

There are different kind of t-norms. However, \otimes means the simple algebraic product in (3.1). The activation degree for rule j is then normalized as

$$\sum_{j=1}^l w^j(\theta) = 1, \quad w^j(\theta) = \frac{h^j(\theta)}{\sum_{r=1}^l h^r(\theta)}, \quad (3.2)$$

where l is the number of rules. Therefore, the output of a TS model, for a given x and θ , is a *weighted sum of the consequent functions*, f_j , which reads

$$y = \sum_{j=1}^l w^j(\theta) f^j(x). \quad (3.3)$$

The weighting functions are then denoted *interpolation functions* because they are used to interpolate local (sub-) models.

For TS fuzzy model (3.3) to represent a smooth dynamical system, the general form of a smooth system (initially defined in (1.2)) is redefined here as:

$$\begin{cases} \dot{x} = f(x, u, \rho) \\ y = g(x, u, \rho), \end{cases} \quad (3.4)$$

where $f : \mathbb{R}^n \times \mathbb{R}^m \times \mathbb{R}^s \rightarrow \mathbb{R}^n$ and $g : \mathbb{R}^n \times \mathbb{R}^m \times \mathbb{R}^s \rightarrow \mathbb{R}^p$ and $\rho \in \mathbb{R}^s$ is a vector of time varying parameters. If we let $\theta \subset x$, $\theta \subset u$ and $\theta \subset \rho$, the fuzzy model rule base j can be constructed as:

$$\begin{aligned} \text{Rule } j & : \text{ IF } \theta_1 \text{ is } \Gamma_1^j \text{ AND } \theta_2 \text{ is } \Gamma_2^j \text{ AND...AND } \theta_q \text{ is } \Gamma_q^j \\ & \text{ THEN } \begin{cases} \dot{x} = \hat{f}^j(x, u, \rho) \\ y = \hat{g}^j(x, u, \rho) \end{cases} \end{aligned}$$

where $\hat{f}_j : \mathbb{R}^n \times \mathbb{R}^m \times \mathbb{R}^s \rightarrow \mathbb{R}^n$ and $\hat{g}_j : \mathbb{R}^n \times \mathbb{R}^m \times \mathbb{R}^s \rightarrow \mathbb{R}^p$. Then a TS fuzzy model (or system) can be described as:

$$\begin{cases} \dot{x} = \sum_{j=1}^l w^j(\theta) \hat{f}^j(x, u, \rho) \\ y = \sum_{j=1}^l w^j(\theta) \hat{g}^j(x, u, \rho), \end{cases} \quad (3.5)$$

where the weight normalization (3.2) applies on weights $w^j(\theta)$. If the consequent functions \hat{f}_j and \hat{g}_j are to represent local linear sub-models or *fuzzy sub-systems*, the TS fuzzy model structure becomes:

$$\begin{aligned} \dot{x} &= \sum_{j=1}^l w^j(\theta) (A^j x + B^j u) = A(\theta)x + B(\theta)u \\ y &= \sum_{j=1}^l w^j(\theta) C^j x = C(\theta)x, \end{aligned} \quad (3.6)$$

where $A^j \in \mathbb{R}^{n \times n}$, $B^j \in \mathbb{R}^{n \times m}$ and $C^j \in \mathbb{R}^{p \times n}$.

The following theorem addresses the existing universal approximation property of fuzzy logic systems [77, 78]:

Theorem 3.1 (Universal approximation of TS fuzzy systems [77]). For any given real smooth function $\psi(x)$ defined on a compact set $U \subset \mathbb{R}^n$ and an arbitrary $\epsilon > 0$, a TS fuzzy system $f(x)$ exists in the form of (3.6) such that

$$\sup_{x \in U} |f(x) - \psi(x)| < \epsilon.$$

Theorem 3.1 implies that a TS model of the form (3.6) is able to approximate *any smooth dynamical system* (3.4) and its first order derivative [28, 79] to arbitrary accuracy. To enhance the approximation accuracy of model structure (3.6), adding fixed terms, i.e. a^j , $j = 1, \dots, l$ to fuzzy sub-systems is also suggested [80, 81]. In this case, the model structure above can be replaced by an *affine* TS model as introduced by (1.4). It has been shown that an affine TS model structure further possesses the universal approximation capability in modeling any smooth dynamical system, its first order and its second order derivative [80]. Therefore, in this thesis, we henceforward refer to the homogenous model structure (3.6) or the affine model structure (1.4) as a *smooth TS fuzzy model*.

Even though Theorem 3.1 can guarantee that a TS fuzzy model exists to uniformly

approximate any smooth dynamical system (3.4) to arbitrary accuracy, in some cases constructing such models is not straightforward.

3.1.2 Constructing smooth TS fuzzy models

Generally, there are two major approaches to construct a smooth TS fuzzy model: *non-linear identification using experimental input-output data* and *derivation (linearization) from given nonlinear system equations*. Synthesizing a fuzzy model based on input-output data was introduced by Takagi and Sugeno [27] and later elaborated by Kang [82,83]. An exhaustive literature exists on different methods for TS fuzzy identification [84]. Identifying a system using TS fuzzy approach normally involves two major steps of structure identification and parameter identification. In control problems, the TS identification approach is found advantageous for the plants whose direct mathematical models (or part of their model) are difficult to obtain [84]. In this respect, automatic identification to facilitate trial-and-error identification procedure of modeling is even suggested (see [85] and the references therein).

The second approach of derivation from a given nonlinear system is suitable for mechanical or electrical systems whose physical models are readily available. Thereby, this section intends to give an outline in constructing smooth TS fuzzy models from a given smooth dynamical system (3.5) and not to discourse the first approach. Regardless, interested readers can refer to the afore-mentioned references for more details on the subject. The second approach of TS fuzzy modeling can, in turn, be obtained through the two ideas of *sector nonlinearity* and *off-equilibrium linearization* [28,86]. The former is based on building local fuzzy sub-systems through linearizing a nonlinear system by its Taylor expansion for a selection of points far from the system's equilibrium point. The latter is about finding an accurate representation of the original mathematical function by a TS fuzzy model over a domain of interest.

3.1.2.1 Off-equilibrium linearization

Using the off-equilibrium linearization approach, fuzzy sub-systems of a smooth TS fuzzy model are constructed via expanding the 1st-order Taylor series in a chosen set of linearization points θ_j excluding any equilibrium point of the original system. The whole dynamics can then be formed by allowing the rule base to define the degree of validity (or activation degree) of the resulting linear (or affine) fuzzy sub-systems. As a first step, one has to determine which variables in x , u and ρ , i.e. the premise variables θ , participate as nonlinear term in (3.5). The consequent local sub-systems are then obtained by derivation of the functions f and g of a smooth system (1.2) with respect to the vector of x , u and ρ :

$$A^j = \frac{\partial f}{\partial x} \bigg|_{x_j, u_j, \rho_j}, \quad B^j = \frac{\partial f}{\partial u} \bigg|_{x_j, u_j, \rho_j}, \quad C^j = \frac{\partial g}{\partial x} \bigg|_{x_j, u_j, \rho_j}, \quad (3.7)$$

where the set of linearization points $\{x_j\}$, $\{u_j\}$ and $\{\rho_j\}$, $j = 1, 2, \dots, l$ together with a partition of the universe of discourse are carefully chosen to cover the approximation area. With the above matrices and the corresponding membership functions, a smooth

TS fuzzy model can be practically constructed. If an affine TS fuzzy model is to be obtained, fixed terms can be further derived as $a^j = f(x_j, u_j, \rho_j) - A^j x_j - B^j u_j$ and $c^j = g(x_j, u_j, \rho_j) - C^j x_j$.

The idea behind this approach is inspired by classical gain scheduling methods where a nonlinear system is approximated with several linear systems obtained through linearization at the equilibrium manifold of the system (3.4) [87]. If the approximation area needs to be expanded around the equilibrium manifold, fixed affine terms like a^j and c^j should be also taken into account [88].

Example 3.1: Consider the following smooth nonlinear system originally adopted from [88]:

$$\begin{cases} \dot{x}_1 = x_2, \\ \dot{x}_2 = x_1^2 + x_2^2, \end{cases} \quad (3.8)$$

where the input function u is intentionally dropped for modeling purposes. The goal is to derive a TS fuzzy model to represent the nonlinear system (3.8). The model is constructed using the off-equilibrium linearization approach over the chosen set of linearization points $x_1 \in \{0.5, 1.5, 2.5, 3.5\}$ and $x_2 \in \{-1, 0, 1, 4\}$, with selected membership functions illustrated in Fig. 3.1. Checking the approximation accuracy of the resulting model, Fig. 3.2 shows the generated surface of the original nonlinear function \dot{x}_2 in (3.8) compared with that of the obtained TS fuzzy model. Although the approximation accuracy of the TS fuzzy model is acceptable over the chosen linearization points, beyond the range of these points, the accuracy is gradually becoming poorer. To increase the accuracy of modeling using this approach, more linearization points may be added over a wider range or different forms of membership functions should be selected, i.e. sigmoid or gaussian instead of trapezoidal ones used in Fig. 3.1. For a very complex (smooth) nonlinear systems, the selection of the set of linearization points and respective membership functions can be almost infinitely large.

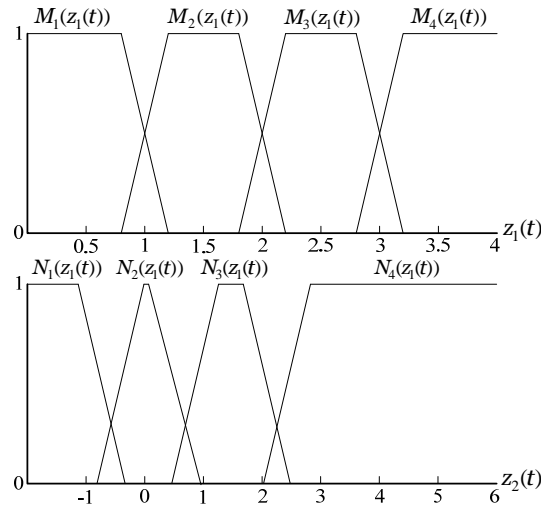


Figure 3.1: Membership functions for the off-equilibrium linearization method. Variables z_1 and z_2 represent the equivalent fuzzy variables for system states x_1 and x_2 , respectively.

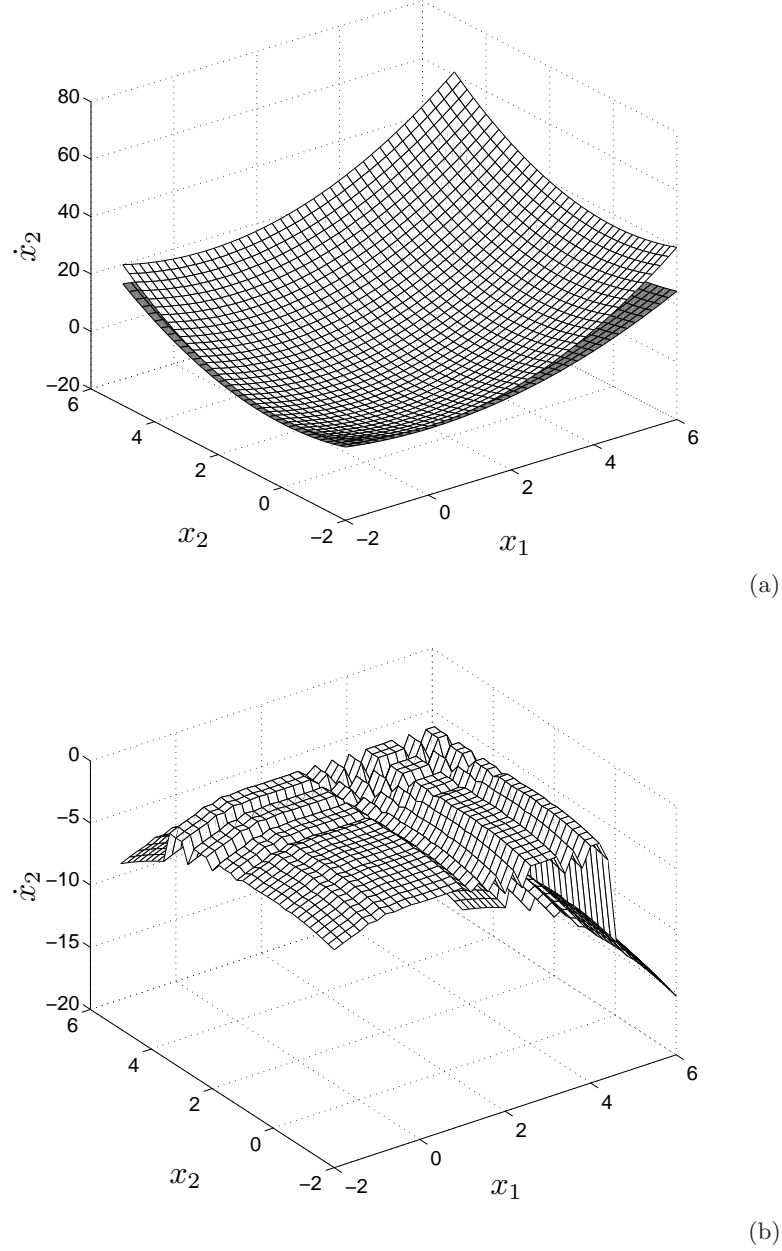


Figure 3.2: The surface function of (a) the original system (3.8) (white mesh) and its TS fuzzy model (grey mesh underneath), (b) the error between the original system and its TS fuzzy model.

In this respect, few methods have been also suggested in the literature to automate the problem of selecting an appropriate set of linearization points and the corresponding membership functions by employing classical optimization algorithms (see for instance [89]) or AI optimization methods like genetic algorithms [90,91]. Both types of algorithms have been shown to be disadvantageous specifically when the number of parameters grow within the algorithm or the dimension of system states are increased.

3.1.2.2 Sector nonlinearity

This approach, initially suggested by Kawamoto et al. [92] and later generalized by Tanaka et al. [28, 93], is about exactly representing a smooth nonlinear system (3.4) by a TS fuzzy model in some specific sector boundaries instead of approximating over a chosen set of linearization points. Therefore, the target of modeling is to find an exact TS fuzzy representation of an original nonlinear function $\dot{x} = f(x(t))$, $f(0) = 0$ in a bounded sector $[\alpha_1 \ \alpha_2]$, or so-called global sector, such that $\dot{x} = f(x(t)) \in [\alpha_1 \ \alpha_2]x(t)$. However, since constructing a TS fuzzy model over global sector is usually found difficult, system states can be further bounded to local sectors as $x(t) \in [-d, d]$ to achieve the highest approximation accuracy possible [28].

The rationale behind this method can be expressed by showing a nonlinear system in matrix form as

$$\begin{aligned} \dot{\mathbf{X}} &= \mathbf{A}_{\mathbf{n} \times \mathbf{n}} \mathbf{X} \\ \begin{bmatrix} \dot{x}_1 \\ \dot{x}_2 \\ \vdots \\ \dot{x}_n \end{bmatrix} &= \begin{bmatrix} a_{11}(x) & \cdots & a_{1n}(x) \\ a_{21}(x) & \cdots & a_{2n}(x) \\ \vdots & \ddots & \vdots \\ a_{n1}(x) & \cdots & a_{nn}(x) \end{bmatrix} \begin{bmatrix} x_1 \\ x_2 \\ \vdots \\ x_n \end{bmatrix}, \end{aligned} \quad (3.9)$$

where any nonlinear term in the matrix $\mathbf{A}_{\mathbf{n} \times \mathbf{n}}$ describes a fuzzy variable $a_{ij} = z_i$, and z_i is bounded as $a_{ij} \in [\min_x a_{ij}(x) \ \max_x a_{ij}(x)]$ for x belongs to the universe of discourse. Therefore each fuzzy variable z_i can be formulated as the convex combination of membership functions

$$z_i(x) = M(z_i(x)) \cdot \min_x a_{ij}(x) + (1 - M(z_i(x))) \cdot \max_x a_{ij}(x).$$

The sector boundaries of a fuzzy variable z_i are determined as $\max_{z_i \in M} z_i$ and $\min_{z_i \in M} z_i$, which in turn, are substituted by the nonlinear terms in (3.9) to form the fuzzy sub-system matrices of a smooth TS fuzzy model.

Example 3.2: Assume the same nonlinear system in Example 3.1. The original system (3.8) is again intended to be represented by a smooth TS fuzzy model using the sector nonlinearity approach over the local sector boundary of $x_1 \in [0.5, 3.5]$ and $x_2 \in [-1, 4]$ with the derived membership functions as shown in Fig. 3.3. For the sake of brevity, detailed steps of constructing this model are omitted here since it is treated in the article [94] written by the author. A full description of the general procedure can also be found in [28]. The surface of the original nonlinear function \dot{x}_2 in (3.8) along with that of its TS fuzzy approximation are depicted in Fig. 3.4. As noticed, this approach is more powerful than the former one as it can exactly represent the system dynamics in the sector boundaries. However, a disadvantage appears in control applications where (should we consider the control input function $u(t)$), the resulting fuzzy sub-systems may turn out to be not controllable or observable using Parallel Distributed Control (PDC) design or the other fuzzy state feedback control approaches [28, 86]. This is mainly because the relationship between system states and control inputs may not be explicitly incorporated

in the fuzzy sub-systems.

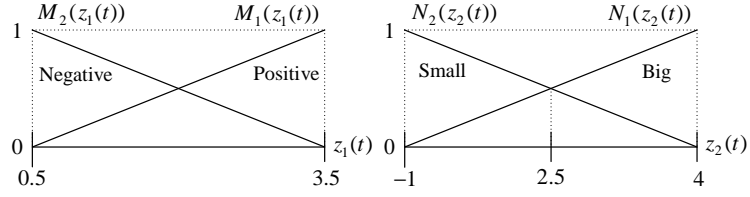


Figure 3.3: Membership functions for the sector nonlinearity method.

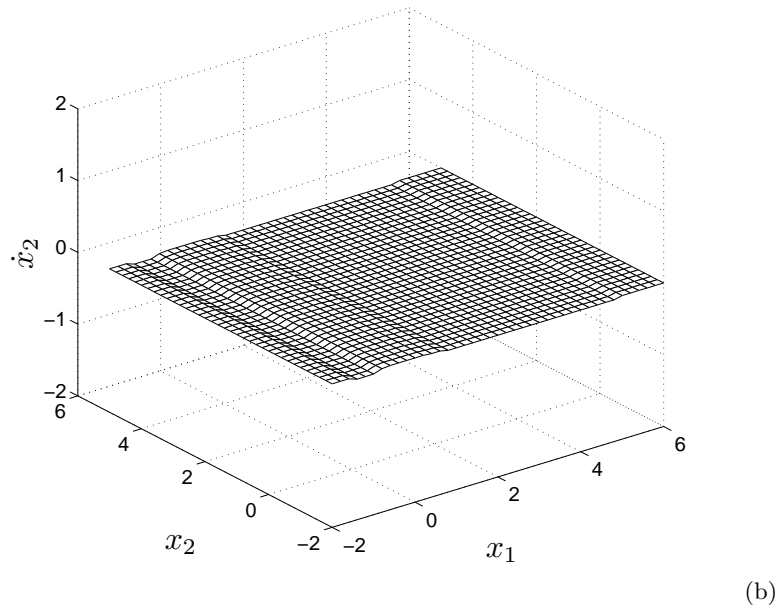
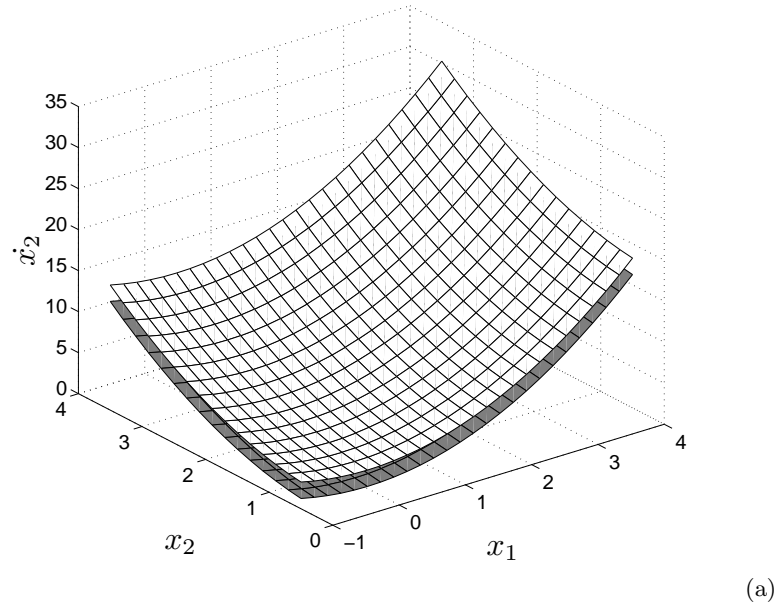


Figure 3.4: The surface function of (a) the original system (3.8) (white mesh) and its TS fuzzy model (grey mesh underneath), (b) the error between the original system and its TS fuzzy model.

3.1.3 The stimulating example

To explore the universal approximation capability (Theorem 3.1) of the existing smooth TS fuzzy modeling approaches in representing a non-smooth system, let's bring up a simple but revealing example, first presented in the book chapter [95]:

Example 3.3: Consider the following non-smooth system:

$$\dot{x} = \begin{cases} \sin(x), & x \in S_1; \\ \cos(x), & x \in S_2, \end{cases} \quad (3.10)$$

where, $S_1 = \{x : H(x) < \pi\}$, $S_2 = \{x : H(x) > \pi\}$ and the switching manifold is defined as $\Sigma_{12} = \{x : H(x) = \pi\}$. To construct a TS fuzzy representation (of the non-smooth system (3.10)), the off-equilibrium approach is preferred here. This is due to the fact that despite the higher approximation accuracy of the sector nonlinearity approach, the resulting fuzzy sub-systems, using off-equilibrium approach, represent local system dynamics explicitly, not merely the sector boundaries. This is important here, assuming that in any accurate model of NSDS, the dynamics close to the switching manifold where system's behaviour is about to be drastically changed, should be carefully captured. As a first attempt, the set of linearization points is carefully chosen as $\{-2.94, -1.54, 1.56, 2.96, 4.54, 6.16, 7.64\}$ to achieve the desired accuracy. Following the procedure outlined in Section 3.1.2, with the chosen membership functions in Fig. 3.6a, the resulting TS fuzzy approximation of the system (3.10) is visible in Fig. 3.5a where the solid line and the dashed line respectively show the trajectory of the original system and its TS fuzzy approximation.

As expected, the flow of $F_1 \in S_1$ represents the generated flow of the original function $\dot{x} = \sin(x)$ in the region S_1 with an acceptable accuracy. However, after passing through Σ_{12} , the flow of F_2 unexpectedly bypasses the linearization point *6.16* to generate a smooth flow through the next linearization point *7.64*. On the second attempt, this erratic behaviour of the simulated fuzzy trajectory is repeated as the generated flow of F_3 in the region S_2 ignores the last linearization point *7.64* to form a smooth flow through the linearization point *6.16*. Changing the loci of linearization points such that they can be closer to the switching manifold Σ_{12} or adding a number of points will result in revisiting the similar or facing even worst scenarios. For instance, on the third attempt, a large number of linearization points, having much shorter distances between each other, is chosen in order to see whether approximation accuracy would be improved. The chosen set is composed of the following linearization points

$$\begin{aligned} x \in \{ & -2.94, -1.54, 1.56, 2.96, 3.544, 3.744, 3.944, 4.242, 4.442, 4.644, 4.944, 5.244, 5.642, \\ & 5.742, 5.942, 6.242, 6.444, 6.744, 6.944, 7.144, 7.444, 7.644, 7.844, 8.044, 8.244, 8.544, \\ & 8.744, 9.044, 9.244 \} \end{aligned}$$

with the selected membership functions depicted in Fig. 3.6b. This time when passing through Σ_{12} , the generated flow of the TS fuzzy model (F_4) becomes a random-like signal in the state-space region S_2 (see Fig. 3.5b), which obviously bypasses a few chosen linearization points. This apparent confusion shows not only that the smooth TS fuzzy model

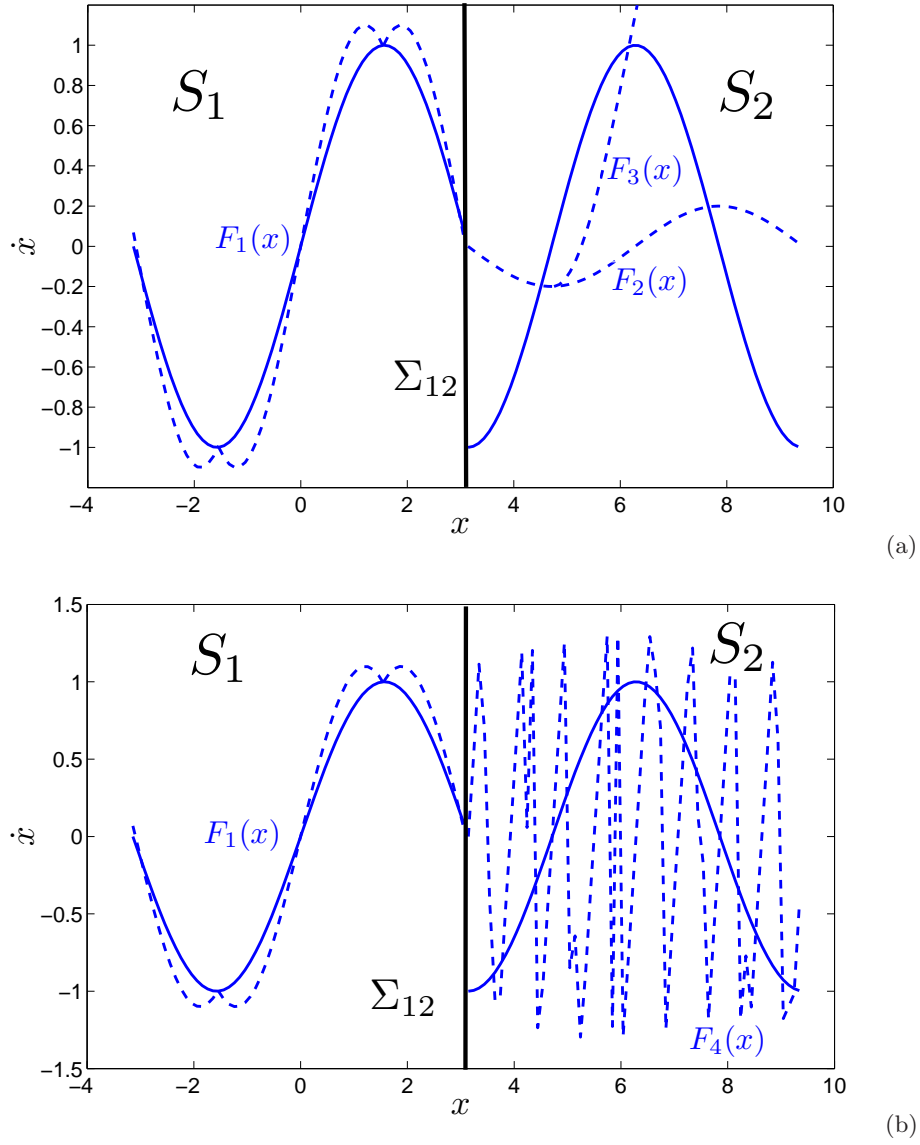


Figure 3.5: Vector fields of the original system (3.10) along with its TS fuzzy approximation obtained using off-equilibrium linearization, (a) with the first set of linearization points, (b) with the more granular set of linearization points.

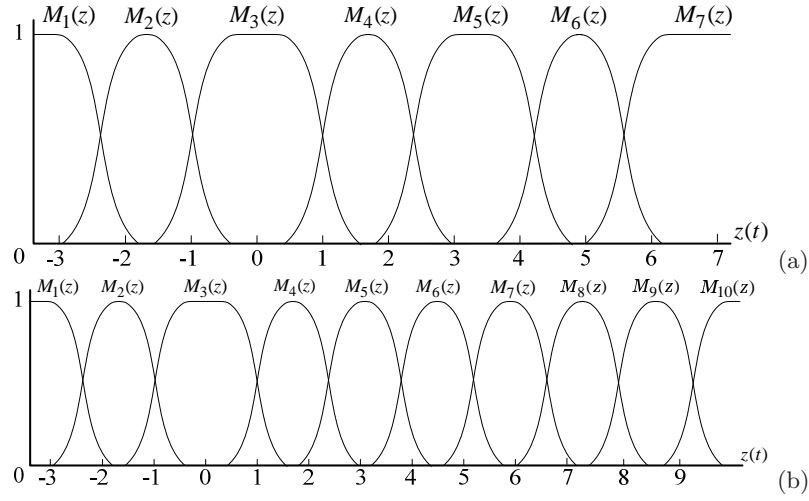


Figure 3.6: Suitable membership functions defined for (a) first set of linearization points, (b) the more granular set of linearization points.

cannot approximate the original vector field (in the region S_2) as desired, but that it also loses its uniqueness through intersection with the switching manifold Σ_{12} . Consequently, three important implications can be enumerated as follows:

1. The current structure of smooth TS fuzzy models (3.6), has a fundamental flaw in representing a simple non-smooth system, i.e. nonlinear system (3.10).
2. It is well-understood, in any non-smooth system, that each vector field F_i is basically smooth in each region S_i . However, an undesired result will come about when one tries to approximate the overall flow $\Phi(x, t)$ of the original system (3.10) passing through Σ_{12} from region S_1 to a completely different dynamics in region S_2 . Therefore, a *discrete map* must also be defined and incorporated in the structure of a smooth TS fuzzy model to describe this abrupt transition with respect to the switching manifold by capturing the exact dynamics just before Σ_{12} to just after Σ_{12} .
3. For a TS fuzzy model to represent a non-smooth system, a switching hypersurface (or hyperplane) must also be properly defined to describe the exact time and location of any switching event in the same way the original switching manifold Σ_{12} is specified.

Considering the above implications, the approximation property of Theorem 3.1, based on the current structure (3.6), is fundamentally questionable for modeling non-smooth dynamical systems. Therefore, the approximation capability of a TS fuzzy model must be extended to include NSDS as will be expounded in the following sections. The important properties of existence and uniqueness will be formally discussed in the context of the proposed structure and why the existing structure cannot hold this important property in case of non-smooth systems.

3.2 Models for non-smooth dynamical systems

This section is dedicated to propose a TS fuzzy model structure able to represent a non-smooth system as defined in (1.3) and classified in Table 2.1. The purpose of the proposed structure is to overcome the fundamental issues of the existing TS model structure, pointed out in Section 3.1.3. It will be shown that the new structure, which we refer to as a *non-smooth TS fuzzy model*, well represents the behaviour of any original non-smooth function at the point of discontinuity while holding the uniqueness (and existence) of the approximative solution. Different conditions for the uniqueness (and existence) of the solution to a non-smooth TS fuzzy system are discussed. The model structure is synthesized in such a way that the special case of sliding and impacting dynamics can be also taken into account as illustrated in Table 2.1 and detailed in Section 2.1.

3.2.1 Discrete-event dynamical systems

Discrete-event dynamical¹ systems have been extensively used in modeling highly complex asynchronous-type systems. Their problems have also been the subject of interest in computer science disciplines specially in the context of Petri nets [96, 97]. The dynamics of these system can be described by discrete events occurring asynchronously over time responsible only for generating state transitions. Naturally, between two events, the states of such systems remain unaffected. This asynchronous behaviour is so familiar in many automated or intelligent control systems where the operation is largely regulated by a digitally-encoded, human-made rules for initiating or terminating activities and scheduling the use of resources through controlled events [12]. Their mathematical models can be expressed by

$$m^+(t) = \xi(m(t), e(t)), \quad (3.11)$$

where m is a discrete state variable, e is a discrete input and ξ is a function describing the change of m . The input $e \in \mathcal{E}$, where $\mathcal{E} = \{e_1, e_2, \dots, e_n\}$ is a finite set including the values e_i or so-called events. For instance an event can be defined by 'hitting a keyboard key', 'turning a switch on' etc. The notation m^+ describes the next state of m . If an underlying countable set \mathcal{T} represents the discrete times associated with each discrete event, then $m^+ = m(t_{k+1})$ should be the event which occurs immediately after a past event occurring at time $m(t) = m(t_k)$, where $t_{k+1} \in \mathcal{T}$ is the discrete time immediately after $t_k \in \mathcal{T}$. Since the dynamic evolution of a discrete event system is actually defined by asynchronous events rather than time, it is common to describe each event by $m(k)$ instead of $m(t_k)$ in (3.11); cf. Fig. 3.7.

Now, the discrete map, addressed in implication No. 2 in Section 3.1.3, can be implemented by defining a discrete event function. This idea is based on the fact that a non-smooth system is essentially composed of smooth and discrete event dynamics which interact with each other. For instance, assume for some reason that it is desirable to study the dynamics of the non-smooth system (3.10) in the region S_1 where the flow of $\sin(x)$

¹It should be pointed out that the word "dynamical" is normally used to emphasize that it is the dynamics of such systems that render them particularly interesting. Nonetheless, these systems can be simply called *discrete event systems* [12].

is a smooth function.

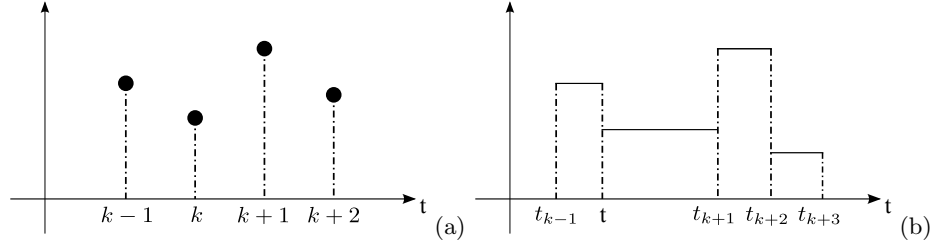


Figure 3.7: The evolution of the state variables of a discrete-event system (a) by events at time k , and (b) in real time t_k .

Then, for representing the flow of $\cos(x)$ defined in region S_2 a discrete event system can be designed (i.e., a switch) such that by changing the discrete states, the continuous states become the states of the new smooth function; that is, $\cos(x)$. In this case, the transitional dynamics close to the switching manifold can be fully understood by studying the interaction of discrete events in a discrete event system, where the time and the location of asynchronous events are exactly defined to form a separate discontinuity set (to address implication No. 3). Therefore, it is possible by synthesizing smooth TS fuzzy models and discrete event systems of the form (3.11) to define an inclusive structure of TS fuzzy models capable of modeling non-smooth systems as well as smooth systems. This structure is formally defined in the following section.

3.2.2 Non-smooth TS fuzzy model structure

A TS fuzzy model structure suitable for modeling non-smooth dynamical systems as defined by (1.3) and classified by Table 2.1, and henceforward, referred to as a *non-smooth TS fuzzy model* is given by the following definitions:

Definition 3.1 A non-autonomous TS fuzzy system $\hat{F} = (\mathbb{R}^n \times M, \mathbb{R}^p \times \mathcal{E}, F_m, \xi)$ can be described as:

$$\begin{aligned} \text{Rule } j : \quad & \text{IF } \theta_1 \text{ is } \Gamma_1^j \text{ AND } \theta_2 \text{ is } \Gamma_2^j \text{ AND } \dots \text{ AND } \theta_q \text{ is } \Gamma_q^j \\ & \begin{cases} \dot{x} = F_m = \sum_{j=1}^l w^j(\theta, m)(A^j(m)x + B^j(m)u) \\ m^+ = \xi(x, m), \end{cases} \end{aligned} \quad (3.12)$$

where $\mathcal{F} = \mathbb{R}^n \times M$ is a fuzzy state space of the system \hat{F} , $\mathbb{R}^p \times \mathcal{E}$ is an external input of the system \hat{F} , $F_m : D_{F_m} \rightarrow \mathbb{R}^n$ represents a smooth dynamical function, and $\xi : D_\xi \rightarrow M$ represents a discrete event function.

Each element of the state vector $x \in \mathbb{R}^n$ in the fuzzy system \hat{F} is referred to as a continuous fuzzy state and each element of the state vector $m \in M$ is referred to as a discrete fuzzy state. The countable set M includes discrete state values m_i , $i \in I_N = \{1, 2, \dots, N\}$ where N can be possibly infinite. Also, $u \in \mathbb{R}^n$ is an input vector of continuous fuzzy states.

Each discrete state $m_i \in M$ is associated with a specific set of fuzzy subsystems:

$$\sum_{j \in \{1, 2, \dots\}} w^j(x, m_i)(A^j(m_i)x + B^j(m_i)u), \quad i \in I_N, \quad j \in I_{l_m}, \quad (3.13)$$

which henceforward we refer to as a *fuzzy sub-vector field* since it represents a smooth vector field, which we denote as F_{m_i} , $F_{m_i} : D_{F_{m_i}} \rightarrow \mathbb{R}^n$, in the fuzzy state space \mathcal{F} (or equivalently, a fuzzy sub-vector field approximates a vector field F_i of non-smooth system (2.13) defined in the region S_i). In each fuzzy sub-vector field, $A^j(m_i) \in \mathbb{R}^{n \times n}$, $B^j(m_i) \in \mathbb{R}^n$ and $w^j : \mathbb{R}^n \times M \rightarrow [0, 1]$ are continuous weighting functions satisfying

$$\sum_{j=1}^{l_m} w^j(\theta, m) = 1, \quad j \in I_{l_m},$$

where l_m is the number of fuzzy rules for that specific fuzzy sub-vector field.

The notation m^+ is interpreted as the next state of $m \in M$. Changing to the next value of m results in a switching to another fuzzy sub-vector field

$$F_{m_k} = \sum_{j \in \{1, 2, \dots\}} w^j(x, m_k)(A^j(m_k)x + B^j(m_k)u), \quad k \in I_N$$

Therefore, *Rule j* in (3.12) can not only describe the interpolation between the local sub-systems of a fuzzy sub-vector field F_{m_i} (with determining the weighting functions w^j) but also can describe the interpolation between the different fuzzy sub-vector fields F_{m_k} , $k \in I_N$ associated with different discrete states m_k .

Note: The notation $F(m_i, x, u)$ is formally correct for a fuzzy sub-vector field defined in (3.13). However, the short notation of F_{m_i} is intentionally employed instead of the former notation, to explicitly emphasize the association of a discrete state m_i with corresponding fuzzy sub-vector field F_{m_i} . If we allow the set M to be a countable set of natural numbers as $M \subseteq \mathbb{N}$, then each fuzzy sub-vector field can also be referred to as $F_1, F_2 \dots$, which is more synonymous with the original definition of NSDS in (2.13).

Definition 3.2 A non-autonomous output TS fuzzy system $\hat{\mathcal{O}} = (\mathbb{R}^n \times M, \mathbb{R}^p \times \mathcal{E}, G_{\tilde{m}}, \varsigma)$ can be described as the system (3.12) along with:

$$\begin{cases} y = G_{\tilde{m}} = \sum_{j=1}^{l_{\tilde{m}}} w^j(\theta, \tilde{m})(C^j(\tilde{m})x), \\ \tilde{m}^+ = \varsigma(x, \tilde{m}), \end{cases} \quad (3.14)$$

where $\mathbb{R}^q \times \hat{\mathcal{O}}$ is an output fuzzy space of the system $\hat{\mathcal{F}}$. $G_{\tilde{m}} : D_{G_{\tilde{m}}} \rightarrow \mathbb{R}^q$ represents a smooth dynamical function and $\varsigma : D_{\varsigma} \rightarrow \hat{\mathcal{O}}$ represents a discrete event function. Each element of y is referred to as continuous fuzzy output and each element of \tilde{m} is referred to as a discrete fuzzy output.

A TS fuzzy system (3.12) as described in Definition 3.1 will be considered as a non-smooth TS fuzzy model in this thesis. However, depending on the context where the output fuzzy space is taken into account, Definition 3.2 can be additionally considered.

Remark 3.1 The discrete fuzzy state variables $m \in M$ as defined in Definition 3.1, is essentially different from continuous fuzzy state variables $x \in \mathfrak{R}$. Even though in some cases discrete fuzzy states may be defined as, $m_i \in \mathfrak{R}$, $i \in I_N$ where $I_N = \{1, 2, \dots, N\}$, there is strictly no relation between the elements of the set M while there is always a relation between the continuous fuzzy state variables in the set \mathfrak{R} as defined in metric spaces. A metric space is a set in which a distance function is defined with specific properties [98]. The distance function implies that the elements in the set, i.e. \mathfrak{R} , have a certain relation to each other. For instance, in the case of electronic dc-dc converters (case study I), the switch "on" and "off" can be modelled with the discrete state variables $m_1 = 1$ and $m_2 = 0$, which are binary variables without any relation with each other.

Remark 3.2 Whether changing the value of a discrete state m in function ξ is affected by an external (or internal) event, which mainly depends on the physical system of interest, the function ξ can be alternatively expressed by a number of switch sets $S_{i,k}$ as

$$S_{i,k} = \{x \in R^n \mid m_k = \xi(x, m_i)\}, \quad i, k \in I_N, \quad (3.15)$$

where $I_N = \{1, 2, \dots, N\}$ (N is possibly infinite as the number of elements in set M ; cf. [99]). Switch sets normally define the change of a discrete state m_i to m_k or change of a fuzzy sub-vector field associated with m_i to another fuzzy sub-vector field associated with m_k in the continuous fuzzy state space R^n where $m_i \neq m_k$. Switch sets are used together with a non-smooth TS fuzzy model (3.12) to define a switching manifold in a more explicit manner.

Remark 3.3 To represent complex impacting dynamics where there are discontinuities (or jumps) in continuous states after intersection with a switching manifold, a function $\chi : D_\chi \rightarrow \mathfrak{R}^n$ describing the state discontinuities should be further incorporated in the model as:

$$x^+ = \chi(x, m), \quad (3.16)$$

where $D_\chi \subseteq \mathfrak{R}^n \times M \times \mathfrak{R}^p \times \mathcal{E}$ and the notation x^+ means the next discontinuous state of x . The related dynamics is illustrated in Table 2.1 under the category of impacting systems with a DoS of zero, describing a considerable class of non-smooth mechanical systems (see [7, 35] and the references therein). However, in electronic switching systems like dc-dc converters this behaviour has not been observed yet [1].

The function χ in (3.16) can be alternatively described by jump sets \mathcal{D}_i as:

$$\mathcal{D}_i = \{x \in \mathfrak{R}^n \mid x^+ = \chi(x, m_i)\}, \quad i \in I_N. \quad (3.17)$$

As switch sets (3.15) and jump sets (3.17) can coexist in the fuzzy state space \mathcal{F} , the relation between two successive continuous fuzzy states can be defined by the matrix J as

$$x^+ = J(m_i)x. \quad (3.18)$$

Remark 3.4 The incorporation of discrete event dynamics in the non-smooth TS fuzzy system \hat{F} , is inspired by the modeling of Petri nets by discrete event dynamical systems where discrete states are commonly defined as a vector value [12, 13, 96]. However, in the sense of Definition 3.1, there is no difference for a discrete state m to be defined as a vector or a scalar value. There is always a possibility to define another set \hat{M} where each of its scalar elements is related to each of the scalar elements of the existing countable set M . In this case, a discrete event function $\hat{\xi}$ can be defined as

$$\hat{m}^+ = \hat{\xi}(x, \hat{m}),$$

where $\hat{m}^+ \in \hat{M}$ and $\hat{m} \in \hat{M}$ are related to $m^+ \in M$.

Remark 3.5 All physical systems whose dynamics are classified in Table 2.1 have a unique path of discontinuous (switching) behaviour with respect to the switching manifold. Nevertheless, the function ξ in (3.12) (or the function ς in (3.14)) can be defined as a multiple-valued function to model possible non-deterministic discrete event behaviours that arise in many control problems [100, 101].

Remark 3.6 All function elements in the non-smooth TS fuzzy system \hat{F} , i.e. $F_m, \xi, \varsigma, G_{\bar{m}}$ (and χ if applicable), can be dependent on t to represent the dynamics of time-varying systems.

Remark 3.7 If the time set \mathcal{T} , cf. Section 3.2.1, is defined as a countable set, it is possible to discretize the continuous-time, non-smooth TS fuzzy system \hat{F} to obtain a discrete-time, non-smooth TS fuzzy model as:

$$\begin{aligned} \text{Rule } j : \quad & \text{IF } \theta_1 \text{ is } \Gamma_1^j \text{ AND } \theta_2 \text{ is } \Gamma_2^j \text{ AND } \dots \text{ AND } \theta_q \text{ is } \Gamma_q^j \\ & \begin{cases} x(t+1) = \sum_{j=1}^l w^j(\theta, m)(G^j(m)x + H^j(m)u) \\ m^+ = \xi(x, m), \end{cases} \end{aligned} \quad (3.19)$$

where $t = kh \in \mathcal{T}$, $k \in N$ and $h > 0$ is the sampling rate. However direct discretization of the continuous-time, non-smooth TS fuzzy model to a discrete-time, non-smooth TS fuzzy model of the form (3.19) would be not plausible unless using digital redesign methods through state matching for each fuzzy sub-vector field and the corresponding sub-systems. Any state matching approach, in turn, impose some forms of state transition matrices to the consequent linear sub-matrices A^j and B^j in (3.12) by multiplying the terms e^{At} and $\int_0^t e^{-A\tau}$ to preserve the necessary information of the continuous, non-smooth TS fuzzy model which may be lost during the sampling interval (see the similar approaches applied on smooth TS fuzzy models [102–104] and see also Section 5.2 on the literature of fuzzy-chaos control methods). For example to have a discrete model, each affine sub-system of a fuzzy sub-vector field F_{m_i} should be transformed to

$$e^{A^j(m_i)t}x(0) + e^{A^j(m_i)t} \int_0^t e^{-A^j(m_i)\tau} B^j(m_i)u(\tau)d\tau, \quad (3.20)$$

where $t = kh$ ($k = 0, 1, 2, \dots$). Letting two consecutive sampling interval to be $t = kh$ and $t = (k+1)h$, each discretized sub-system of F_{m_i} can be expressed by

$$e^{A^j(m_i)h}x(kh) + e^{A^j(m_i)(k+1)h} \int_{kh}^{(k+1)h} e^{-A^j(m_i)\tau} B(m_i)u(\tau)d\tau.$$

Then the continuous states $x(t)$ and inputs $u(t)$ can be matched with the digitally sampled $\hat{x}(kh)$ and $\hat{u}(kh)$ to represent the discrete-time system (3.19) as a close representation of the original continuous-time, non-smooth TS fuzzy model (3.12), if the sampling period is chosen sufficiently small. The discretization process of the model (3.12) would be at best difficult, since as it is apparent from (3.20), the parameters of the consequent function in (3.19) can be no longer time invariant but *time varying* functions, i.e. $G^j(m) = e^{A^j(m_i)h}$, $H^j(m) = e^{A^j(m_i)(k+1)h} \int_{kh}^{(k+1)h} e^{-A^j(m_i)\tau} B(m_i)u(\tau)d\tau$, $t = kh$. There are methods for the accurate discretization of smooth TS fuzzy models (3.6) via proposing different state transition matrices, some of which have been proved effective (see for instance [105] and the references therein) and can be applied on a continuous-time, non-smooth TS fuzzy model by discretizing each (continuous-time) fuzzy sub-vector field F_{m_i} (each F_{m_i} can essentially represent a smooth TS fuzzy model, cf. Remark 3.9). Nevertheless, the main focus of this thesis is on continuous-time fuzzy systems.

It is important to note that non-smooth transitions are already described by discrete event function ξ in (3.19) so there is no need for discretization to capture the switching events between different fuzzy sub-vector fields.

Remark 3.8 If discrete event functions ξ and ς , defined in (3.12) and (3.14), are defined to be explicitly dependent on the input u , then the input signal u can effect the discrete state m too. From the control point of view, this can be advantageous in switching-type controllers when continuous inputs are able to change the discrete states.

Remark 3.9 Each fuzzy sub-vector field F_{m_i} as defined in (3.13) is associated with a specific discrete state $m_i \in M$. Continuous fuzzy states can evolve by $\dot{x} = F_{m_i} = \sum_{j=1}^{l_m} w^j(\theta, m_i)(A^j(m_i)x + B^j(m_i)u)$ when the discrete state $m = m_i$. By changing the discrete state to, say, $m = m_k$, evolution of \dot{x} continues with switching to another fuzzy sub-vector field F_{m_k} , which is smooth until m_k is active. In this way any sudden transition of dynamics with respect to the switching manifold in terms of discontinuities in states (systems with a DoS of zero) or in flows (systems with a DoS of one or higher) can be accurately captured.

Remark 3.10 An invariant set of NSDS (Definition 2.1) can be redefined for a solution to the non-smooth TS fuzzy system \hat{F} in terms of equilibrium points and periodic solutions.

An equilibrium point to the non-smooth TS fuzzy system \hat{F} is the fuzzy state $(x^{eq}, m^{eq}) \in \mathcal{F}$ where the system initiates and fulfills all fuzzy sub-vector fields as $F_{m_i}(x^{eq}, t) = F_{m_i}(x^{eq}, 0)$, $m_i \in M, i \in I_N$ where I_N is the number of discrete states in the set M . Therefore, it will remain in the fuzzy state $(x^{eq}, m^{eq}) \in \mathcal{F}$ for all future times $t \in T$.

A limit cycle is a non-trivial periodic solution to the non-smooth TS fuzzy system \hat{F} when $F_{m_i}(x^p, T) = x^p$, $m_i \in M$, $i \in I_N$. Therefore the continuous fuzzy states fulfill $x(t+T) = x(t)$ and the discrete fuzzy states fulfill $m(t+T) = m(t)$ for $T > 0$.

3.2.3 Evolution of states in a non-smooth TS fuzzy model

Even though the evolution of system states in a non-smooth TS fuzzy model is formally stated in Remark 3.9, loosely speaking the system evolution can be explained as follows. Approximated trajectories starts at an initial condition $(x_0, m_0) \in \mathcal{F}_0$, where \mathcal{F}_0 is referred to as an initial set of fuzzy states for the system \hat{F} , and the initial states are $x_0 = x(t_0)$ and $m_0 = m(t_0)$. The trajectory continues to evolve based on the fuzzy sub-vector field $F_{m_0} = \sum_{j=1}^{l_{m_0}} w^j(x, m_0)(A^j(m_0)x + B^j(m_0)u)$ until the discrete state m changes its value to $m = m_1$ due to the condition of switch set $S_{0,1}$ (the intersection with switching manifold Σ or in general due to an event). Then, the system enters a new set of states $(x_1, m_1) \in \mathcal{F}$, $x_1 = x(t_1)$, $m_1 = m(t_1)$, where the trajectories restart their evolution based on the fuzzy sub-vector field F_{m_1} and maintain their progress until the next change of discrete state m_1 to m_2 induced by the next discrete event as dictated by switch set $S_{1,2}$ and so on. This evolution is illustrated in Fig. 3.8.

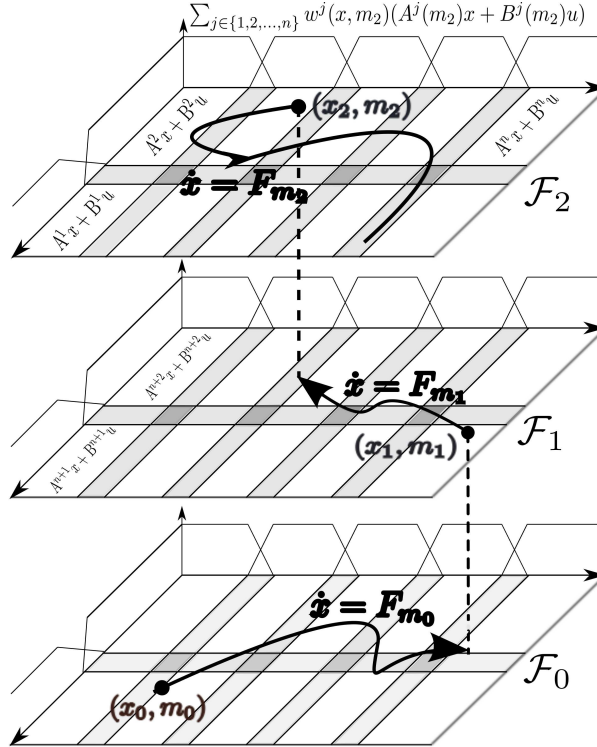


Figure 3.8: Trajectories evolve in a non-smooth TS fuzzy model based on different fuzzy sub-vector fields whose global state spaces (or regions) are separated from each other. Changing of the discrete state m will result in moving from one state space to another state space containing a smooth flow, represented by a fuzzy sub-vector field F_{m_i} , $i = 0, 1, 2, \dots, N$. Each fuzzy state space region \mathcal{F}_i , $i = 0, 1, 2, \dots$, can also be locally divided to different operating regions resulting from the piece-wise linear structure of the membership functions.

3.2.4 The possibility of representing sliding dynamics

Following the discussion in Section 2.2.6 regarding the possible formulation of sliding dynamics for sliding Filippov-type systems, equivalent sliding dynamics can further be represented by a non-smooth TS fuzzy model of the form (3.12). One possible scenario is that a sliding manifold can be formed as a result the coincidence of two (or possibly several) switch sets (see Remark 3.2) at certain continuous fuzzy states. More specifically, a *sliding (measure-zero) manifold* S can be formed by two coinciding switch sets $S_{i,k}$ and $S_{k,i}$, representing a switching manifold. In this case, if the two fuzzy sub-vector fields F_{m_i} and F_{m_k} represent flows with opposite directions in the close vicinity of a sliding manifold S , the flows will slide along S . The possible outcome will be an infinite number of rapid switches between sub-vector fields F_{m_i} and F_{m_k} and consequently between the discrete states m_i and m_k . This scenario is illustrated in Fig. 3.9.

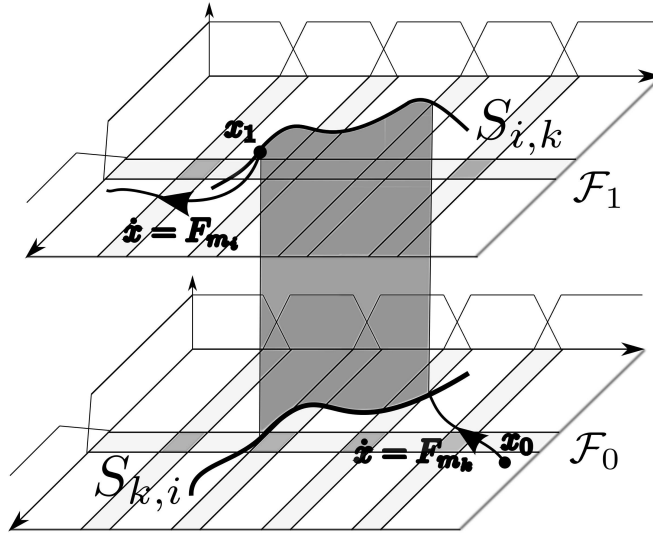


Figure 3.9: The shaded surface depicts the (measure-zero) sliding manifold S , formed by coinciding $S_{i,k}$ and $S_{k,i}$ at certain fuzzy states and the opposite direction of the flows of F_{m_i} and F_{m_k} . In this case an infinite number of rapid switches between the two discrete states m_i and m_k associated with the fuzzy sub-vector fields F_{m_i} and F_{m_k} can occur.

When an infinite number of rapid switching between fuzzy sub-vector fields occur, it is, at best, very difficult to ascertain the value of discrete states at any time in the sliding mode with the initial states $(x_0, m_0) \in \mathcal{F}_0$. To resolve this uncertainty, new discrete states representing the possible sliding modes can be introduced by function ξ to define the sliding dynamics in question. For instance, sliding motions (Fig. 3.9) can be defined by a new discrete state, say m_z , representing the same dynamics as the infinite number of switching between F_{m_i} and F_{m_k} . As a result, a sliding manifold in Fig. 3.9 can be readily represented by switch sets $S_{i,z}$ and $S_{z,k}$ and the equations for sliding flows that slide along S can be formulated in the way described in Section 2.2.6.

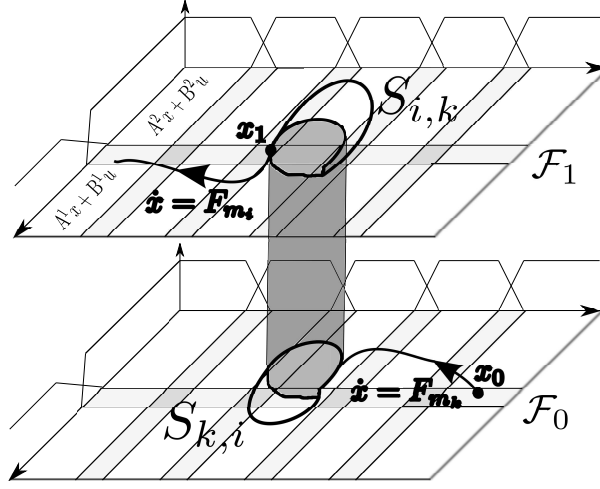


Figure 3.10: Another Possible scenario of coinciding switch sets $S_{i,k}$ and $S_{k,i}$ in a non-smooth TS fuzzy system would result the formation of a non-measure-zero sliding region.

Another possible scenario of sliding dynamics in a non-smooth TS fuzzy model occurs when switch sets coincide and form a sliding region instead of a sliding manifold (see Fig. 3.10). Likewise, the sliding dynamics are definable with the available formulation methods discussed in Section 2.2.6 if we substitute the vector fields F_1 and F_2 of a non-smooth system (2.13) with the fuzzy sub-vector fields F_{m_i} and F_{m_k} to formulate the resulting sliding dynamics.

3.2.5 Sufficient conditions for existence and uniqueness

As mentioned before, the existing universal approximation theorem for fuzzy systems (Theorem 3.1) guaranteed that a TS fuzzy model is able to uniformly approximate any given (smooth) nonlinear function to arbitrary accuracy. Generally, a TS fuzzy model represents an approximative solution of a physical plant based on its mathematical model. Knowing that there is a certain degree of approximation in any model, including TS fuzzy models, it should be first examined if a solution exists (according to the real plant). Guaranteeing the existence, the uniqueness of the solution should then be investigated.

Smooth TS fuzzy models: The *existence of a solution* for a smooth TS fuzzy model structure (3.6) can be defined if the system flow $\Phi(x, t)$, evolving from the initial condition $x_0 = x(t_0)$, it can fulfill the system dynamics for any given inputs *everywhere*. Several sufficient conditions can be enumerated for the existence and uniqueness of a solution to smooth dynamical systems or ODEs that can also be applied to a smooth TS fuzzy system to prove the existence of its approximative solution, cf. Cauchy's existence theorem [106]. If a nonlinear system holds the Lipschitz condition in any given domain, the sufficient condition for existence and uniqueness can be guaranteed [9, 10]. This condition is stated as follows:

Definition 3.3: A nonlinear function $f(x, t)$, which is continuous in x but can be piecewise continuous in t , holds a Lipschitz condition in $\Omega \subseteq \mathbb{R}^n \times \mathbb{R}$ if a constant (called the

Lipschitz constant) L exists such that

$$\|f(x, t) - f(z, t)\| \leq L\|x - z\| \quad \text{when } (x, t) \in \Omega, (z, t) \in \Omega \quad (3.21)$$

It is known that the Lipschitz property is stronger than continuity (for instance, $f(x) = x^{2/3}$ is continuous but not locally Lipschitz at $x = 0$) but weaker than continuous differentiability [9] (for instance, $f(x) = |x|$ is locally Lipschitz but not continuously differentiable at $x = 0$). The Lipschitz condition can hold globally or locally, depending on the domain where the condition of Definition 3.3 applies [9]. The local Lipschitz property of a function is basically a smoothness requirement and it is implied by continuous differentiability [9]. For instance the nonlinear system:

$$\begin{cases} \dot{x}_1 = -x_1 + x_1x_2 \\ \dot{x}_2 = x_2 - x_1x_2, \end{cases}$$

is continuously differentiable in \mathbb{R}^2 ; hence, it is locally Lipschitz on \mathbb{R}^2 [9].

The very useful property of Definition 3.3 is that the existence together with the uniqueness of any approximative solution or flow $\Phi(x, t)$ (with the initial condition $x_0 = x(t_0)$) can be guaranteed over a local domain or interval $[t_0, t_0 + T]$ where $T > 0$ may be very small (Local Lipschitz condition). Then, the interval $[t_0, t_0 + T]$ can be (theoretically) expanded to another local domain or interval $[t_0 + T, t_0 + 2T]$ by repeatedly applying Definition 3.3 over the interval in question until the existence and uniqueness are guaranteed over the whole domain where the flow $\Phi(x, t)$ is defined (global Lipschitz condition). However, in case of a non-smooth system, it is not possible to indefinitely expand the domain of locally Lipschitz flow, since the conditions guaranteeing existence and uniqueness may cease to hold at the point of discontinuity [11]. The *existence and uniqueness of a solution* for the flow $\Phi(x, t)$, $x_0 = x(t_0)$ of a non-smooth system of the form (1.3) must be defined such that if the flow must fulfill the system dynamics for any given inputs *almost everywhere*.

For a smooth nonlinear system, having locally Lipschitz vector fields, the sufficient conditions for global existence and uniqueness can be guaranteed if it is known that the solution will remain in a compact subset of the domain where the Local Lipschitz condition holds. In this case, a unique solution exists and evolves globally for all times after passing the initial time [9]. At the same time, global existence and uniqueness can be concluded from the global Lipschitz condition, the property that only linear systems acquire [9]. Revisiting the consequent (defuzzified) function of a smooth TS fuzzy model (3.6):

$$\begin{aligned} \dot{x} &= \sum_{j=1}^l w^j(\theta)(A^j x + B^j u) = A(\theta)x + B(\theta)u \\ y &= \sum_{j=1}^l w^j(\theta)C^j x = C(\theta)x, \end{aligned}$$

the \dot{x} (and, y) is a convex combination of local linear sub-systems (or affine sub-systems as in (1.4)). Global existence and uniqueness of an approximative solution of the above TS fuzzy model, representing a smooth nonlinear system, can be easily guaranteed by

locally Lipschitz conditions. This due to the fact that fuzzy sub-systems (representing a continuous vector fields) will always remain in the compact subset (convex combination) of its operating region (domain where the locally Lipschitz condition holds). The operating regions of a smooth TS fuzzy system are where only one model rule and the corresponding affine dynamics is active (see Fig 3.8), and the interpolation regions between them are where several dynamics are present [107,108]. However, a smooth TS fuzzy model structure is just a special case of a non-smooth TS fuzzy model, where there exists only one discrete state $m = m_0$ assuming the solution starts at the initial condition (x_0, m_0) . Therefore, in modeling a non-smooth system, an approximative flow $\Phi(x, t)$ of a smooth TS fuzzy model cannot hold the Local Lipschitz property at any switching manifold Σ (which can be considered as instantaneous interval where the vector field itself is not defined in the view of a continuous function), since the flow can no longer remain in the compact subset of its operating region. Consequently, the flow $\Phi(x, t)$ does not fulfill the original system dynamics *everywhere*, where the generated flow of a TS fuzzy model cease to exist at a switching manifold Σ . This is shown in the example of Section 3.1.3, where the generated flow of a smooth TS fuzzy does not follow the original dynamics in region S_2 . It is also evident that the approximative solution cannot be unique (see Fig. 3.5).

Non-smooth TS fuzzy models: Lipschitz continuity does not hold at the discontinuity set Σ in the sense of Definition 3.3. For non-smooth Filippov-type systems, the sufficient conditions for existence and uniqueness is treated in Filippov's book [11], where a non-smooth system is defined as a set-valued function or in the form of differential inclusion as outlined in Filippov's convex combination method (Section 2.2.6). According to Filippov, if a set-valued function $f(x)$ is nonempty, bounded, closed, convex and upper semi-continuous ², then there exist a unique solution $x(t)$ to the differential inclusion [11]. As discussed in Section 2.2.6, the sliding dynamics can also be formulated in the form of differential inclusions; hence, the existence and uniqueness can be investigated. Furthermore, in the sense of differential inclusion, Lipschitz property can be relaxed at the point of discontinuity or switching manifold Σ [11,109].

Sufficient conditions for the existence (and uniqueness) of a solution to the non-smooth TS fuzzy model (3.12) can be guaranteed by the following assumptions.

Assumption 1: Fuzzy sub-vector fields as defined in (3.13) hold the local Lipschitz property in their operating region in the sense of Definition 3.3.

Assumption 2: The number of switchings between fuzzy sub-vector fields (or the discrete states associated with them) belongs to the countable set M defined in finite time.

Assumption 3: Any transition of a discrete state should be uniquely defined. This requires that for any pair of switch sets $S_{i,k} \cap S_{i,z} = \emptyset$, $i \neq k \neq z$.

Each fuzzy sub-vector field F_m can be modeled with a smooth TS fuzzy model structure (3.6) which is active only in one discrete state, i.e. $m = m_0$. A smooth TS fuzzy

²A set-valued function $F(x)$ is called upper semi-continuous at the point x if $\sup_{\hat{x} \in F(\hat{x})} \|\hat{x} - x\| \rightarrow 0$ as $\hat{x} \rightarrow x$.

model (3.6), as discussed before, is locally Lipschitz in its operating region. Therefore, Assumption 1 is a valid assumption. Furthermore, as noticed in the case studies presented in Section 2.1 and in general for the physical model of all electrical and mechanical systems classified in Table 2.1, the state space is partitioned into a finite number of regions S_i where the flows Φ_i are defined as smooth functions (see equation (2.13)). Therefore, Assumption 2 is also a valid assumption. Assumption 3, actually overrides Remark 3.5 of Definition 3.1. This is also acceptable, since non-determinism of discrete events can be hardly realized in the non-smooth systems classified in Table 2.1.

Therefore, with the above assumptions, sufficient condition for global existence and uniqueness of the approximative solution to a non-smooth TS fuzzy model can be provided by the following theorem:

Theorem 3.2 Suppose a smooth solution $x(t)$ is defined on a compact set $U \subseteq \mathbb{R}^n$, $x_0 \in U$ for every solution of a non-smooth TS fuzzy model (3.12) with the initial condition $(x_0, m_0) \in \mathcal{F}_0$. Then there is a solution to the non-smooth TS fuzzy model which is defined for all time t .

Proof: According to Assumption 2, the number of discrete states associated with fuzzy sub-vector fields, belong to a countable set. The solution also remains in the compact set U . Existence and uniqueness of a solution can be guaranteed for the time interval between the switching of discrete states associated with the corresponding fuzzy sub-vector fields. Therefore, a unique solution of the non-smooth TS fuzzy model exists for all time $t > 0$.

Theorem 3.2 provides a supplement to Theorem 3.1 to enhance the universal approximation capability of fuzzy systems by including non-smooth TS fuzzy models in the sense of Definition 3.1. The universal approximation theorem of fuzzy systems, with the new notion of universality, can now be expressed as follows:

Theorem 3.3 (Universal approximation of TS fuzzy systems revisited) For any given real (smooth or non-smooth) dynamical function $\psi(x)$ and an arbitrary $\epsilon > 0$, there exist a TS fuzzy system \hat{F} in the form of (3.12) such that

$$\sup_{x \in U} |\hat{F} - \psi(x)| < \epsilon.$$

Theorem 3.3 states that the non-smooth TS fuzzy system \hat{F} can uniformly approximate any given (smooth or non-smooth) nonlinear function to arbitrary accuracy. In case of approximation of a smooth system, as mentioned before, a non-smooth TS fuzzy model with only one fuzzy sub-vector field associated with one discrete state m_0 can provide the equivalent structure as for a smooth TS fuzzy model.

Example 3.4 (A simple periodic behaviour of an invariant set).

In order to show the simple periodic behaviour of an invariant set in a non-smooth

system, we intend to define an exemplary hypothetical non-smooth TS fuzzy system of the form (3.12). Consider a non-smooth model represented by a TS fuzzy system of the form (3.12), which is described by the following model rules:

Model Rule 1: IF $x_1(t)$ is "Positive" and $x_2(t)$ is "Big," THEN $\begin{cases} \dot{x}(t) = A^1(m_1)x(t) \\ m_1 = \xi(x, m_2), \end{cases}$

Model Rule 2: IF $x_1(t)$ is "Positive" and $x_2(t)$ is "Small," THEN $\begin{cases} \dot{x}(t) = A^2(m_1)x(t) \\ m_1 = \xi(x, m_2), \end{cases}$

Model Rule 3: IF $x_1(t)$ is "Negative" and $x_2(t)$ is "Big," THEN $\begin{cases} \dot{x}(t) = A^3(m_1)x(t) \\ m_1 = \xi(x, m_2), \end{cases}$

Model Rule 4: IF $x_1(t)$ is "Negative" and $x_2(t)$ is "Small," THEN $\begin{cases} \dot{x}(t) = A^4(m_1)x(t) \\ m_1 = \xi(x, m_2), \end{cases}$

which are defined for the first fuzzy sub-vector field according to the membership functions illustrated in Fig. 3.11.

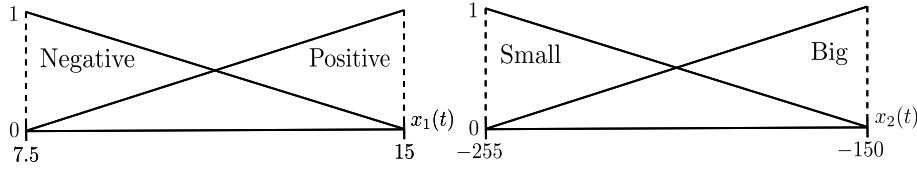


Figure 3.11: Membership functions defined for Example 3.4

The model rules for the second fuzzy sub-vector field can be defined as the above but with exchanging two fuzzy variables x_1 and x_2 and the two discrete variables m_1 and m_2 . Therefore there exist two fuzzy sub-vector fields associated with two switch sets m_1 and m_2 as follows:

$$F_{m_1} = \sum_{j=1}^{l_{m_1}} w^j(x, m_1)(A^j(m_1)x), \text{ and } l_m = 4,$$

$$F_{m_2} = \sum_{j=1}^{l_{m_2}} w^j(x, m_2)(A^j(m_2)x), \text{ and } l_m = 4,$$

where the linear fuzzy sub-systems for F_{m_1} and F_{m_2} are:

$$A^1(m_1) = \begin{bmatrix} 3 & -150 \\ 7.5 & 3 \end{bmatrix}, A^2(m_1) = \begin{bmatrix} 3 & -150 \\ 15 & 3 \end{bmatrix}, A^3(m_1) = \begin{bmatrix} 3 & -225 \\ 15 & 3 \end{bmatrix}, A^4(m_1) = \begin{bmatrix} 3 & -225 \\ 7.5 & 3 \end{bmatrix},$$

$$A^1(m_2) = \begin{bmatrix} 3 & 7.5 \\ -150 & 3 \end{bmatrix}, A^2(m_2) = \begin{bmatrix} 3 & 15 \\ -150 & 3 \end{bmatrix}, A^3(m_2) = \begin{bmatrix} 3 & 15 \\ -225 & 3 \end{bmatrix}, A^4(m_2) = \begin{bmatrix} 3 & 7.5 \\ -225 & 3 \end{bmatrix}.$$

Assume the above linear matrices for each fuzzy sub-vector field, are obtained via some approaches (approaches for constructing a non-smooth TS fuzzy model will be proposed

later in this chapter). Function ξ is defined by the following switch sets (see Remark 3.2):

$$S_{1,2} = \{x \in \mathbb{R}^2 \mid x_2 = kx_1\}, \quad S_{2,1} = \{x \in \mathbb{R}^2 \mid x_2 = -\frac{1}{k}x_1\}.$$

As noticed, the largest linear sub-system member of F_{m_1} and F_{m_2} can be respectively recognized as $A^2(m_1)$ and $A^2(m_2)$, where the value of fuzzy variables lie on the boundary of $[7.5, 15]$ and $[-255, -150]$ as defined for the fuzzy sets (see Fig. 3.11). The eigenvalues of sub-systems $A^2(m_1)$ and $A^2(m_2)$ are calculated as $\lambda = 3 \pm j\omega_0$, where $\omega_0 = 47.43$. Therefore, if k is chosen according to

$$k = \sqrt{\frac{10 - e^{-\pi/\omega_0}}{10e^{-\pi/\omega_0} - 1}} = 1.0413,$$

the response of the model is a periodic oscillatory solution with a period of $T = \pi/\omega_0$ as seen in Figure 3.12a. The switching time between F_{m_1} and F_{m_2} , independent from initial conditions, can be also derived by

$$\pi - \frac{1}{\omega_0} \arctan\left(\frac{\omega_0}{90}\left(k + \frac{1}{k}\right)\right).$$

In an initial investigation for stability of an invariant set, the eigenvalues of all fuzzy sub-systems $A^j(m_i)$, $j = I_{l_m}$, $i = I_N$ have positive real part of 3, meaning that all of them are unstable. However, if the location of the switch sets (effectively the switching manifold) is altered to:

$$S_{1,2} = \{x \in \mathbb{R}^2 \mid x_2 + x_1 = 0\}, \quad S_{2,1} = \{x \in \mathbb{R}^2 \mid x_2 = 0\},$$

the system trajectories converges to a stable solution (stable equilibrium point) as depicted in Fig. 3.12b, where all fuzzy sub-systems are unstable. Now assume that F_{m_1} and F_{m_2} are changed to sub-vector fields with the following sub-systems:

$$\begin{aligned} A^1(m_1) &= \begin{bmatrix} -3 & -150 \\ 7.5 & -3 \end{bmatrix}, \quad A^2(m_1) = \begin{bmatrix} -3 & -150 \\ 15 & -3 \end{bmatrix}, \quad A^3(m_1) = \begin{bmatrix} -3 & -225 \\ 15 & -3 \end{bmatrix}, \quad A^4(m_1) = \begin{bmatrix} -3 & -225 \\ 7.5 & -3 \end{bmatrix}, \\ A^1(m_2) &= \begin{bmatrix} -3 & 7.5 \\ -150 & -3 \end{bmatrix}, \quad A^2(m_2) = \begin{bmatrix} -3 & 15 \\ -150 & -3 \end{bmatrix}, \quad A^3(m_2) = \begin{bmatrix} -3 & 15 \\ -225 & -3 \end{bmatrix}, \quad A^4(m_2) = \begin{bmatrix} -3 & 7.5 \\ -225 & -3 \end{bmatrix}. \end{aligned}$$

The switch sets are also changed to:

$$S_{1,2} = \{x \in \mathbb{R}^2 \mid x_2 = -0.4x_1\} \quad S_{2,1} = \{x \in \mathbb{R}^2 \mid x_2 = 2.5x_1\}$$

Both fuzzy sub-vector fields F_{m_1} and F_{m_2} includes stable sub-systems with the eigenvalues of $-3 \pm \omega_0$. However, as illustrated in Figure 3.13, the system is unstable as the solution trajectories diverge from the equilibrium point.

Although this example shows the trajectory behaviour in the vicinity of a simple form of an invariant set such as equilibrium points, it clarifies that the stability analysis of an invariant set (in the sense of definition of Remark 3.9), in general, demands different

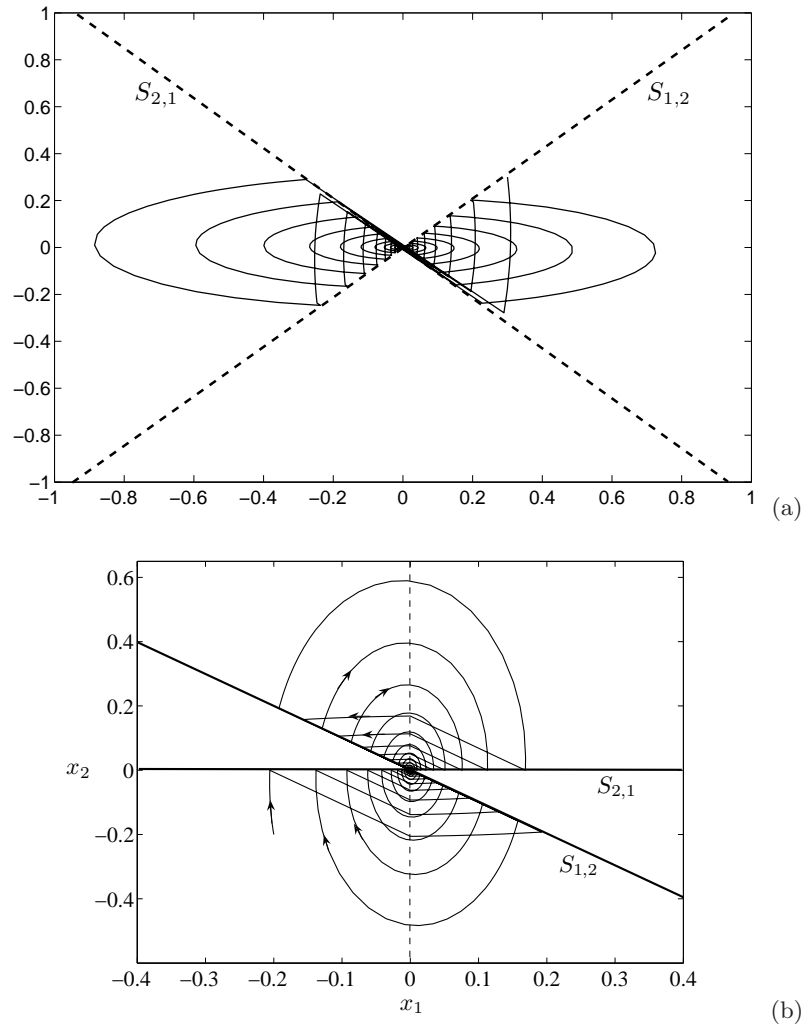


Figure 3.12: (a) The response of a non-smooth TS fuzzy system as a oscillatory closed orbit. (b) Changing the location of switching manifolds can result in a stable TS fuzzy system.

formulations taking into account the dynamics in the close neighborhood of a switching manifold. These formulations will be treated in Chapter 4, where the stability of the complex form of invariant sets like periodic solutions is analyzed. In a non-smooth TS fuzzy model, when compared with its smooth counterpart, there exist a number of crucial issues that need to be addressed. For instance, how can the stability of a non-smooth TS fuzzy system be guaranteed regardless of the switching between discrete states and their corresponding subsystems or sub-vector fields. How can it be shown that a system is stable if the exact locations of switching sets are unknown or if there is an approximation error in representing such manifolds? These comparatively unique kind of robustness issues will be further discussed in Chapter 4.

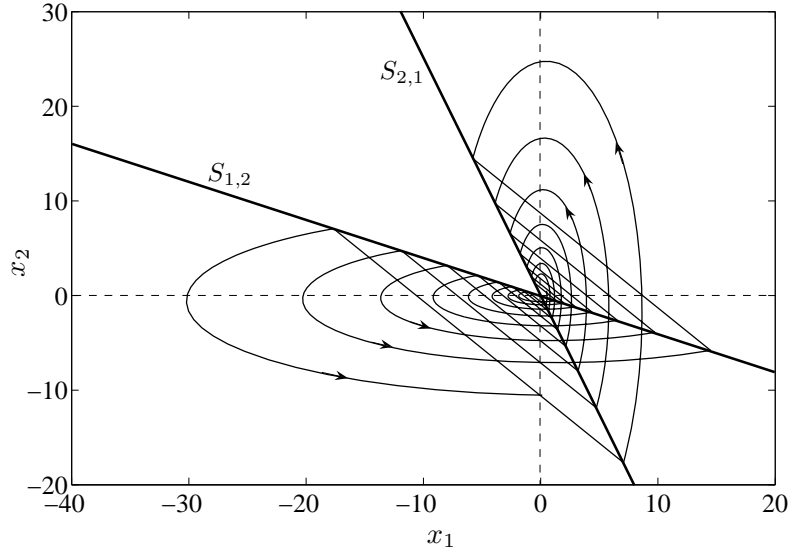


Figure 3.13: Switchings between stable fuzzy subsystems may lead to an unstable system.

3.2.6 Constructing non-smooth TS fuzzy models

In this section, two methods for constructing a non-smooth TS fuzzy model will be presented. The first method is employed for the modeling of non-smooth systems with affine structure in each region of validity, e.g. dc-dc electronic converters. The second proposed method is suitable for non-smooth systems having nonlinear vector fields in each region of validity S_i .

3.2.6.1 Fuzzy sub-vector fields by linearizing transformation

As mentioned in the introductory chapter (Section 1.4), a smooth TS fuzzy model can be considered as a polytopic LPV system. This comes from the fact that fuzzy sets $\Gamma \in \mathcal{F}^n$, $\Gamma : \mathbb{R}^n \rightarrow [0, 1]$ fulfill the following conditions [110] (see also [111] for the original definition):

- Γ is normal, i.e., there exists an $x_0 \in \mathbb{R}^n$ such that $\Gamma(x_0) = 1$,
- Γ is fuzzy-convex, i.e., for any $x, y \in \mathbb{R}^n$ and $0 \leq w \leq 1$

$$\Gamma(wx + (1 - w)y) \geq \min\{\Gamma(x), \Gamma(y)\},$$

- Γ is upper semi-continuous,
- the closure of the set $\{x \in \mathbb{R}^n; \Gamma(x) > 0\}$ is compact.

Then, for $0 < \alpha < 1$, there is a non-empty compact convex subset of \mathbb{R}^n called an α -level set $[\Gamma]^\alpha$, defined as

$$[\Gamma]^\alpha = \{x \in \mathbb{R}^n; \Gamma(x) \geq \alpha\}. \quad (3.22)$$

The set $[\Gamma]^0$ is also called the support of Γ .

According to the above conditions, fuzzy sets Γ^j should describe weighting functions w^j , which are positive scalar functions of parameter-variable states and indicate to what degree each affine sub-model belongs to the overall smooth dynamics. Employing this property, Theorem 3.2 also proves that a non-empty compact convex subset of \mathbb{R}^n can be provided for the fuzzy sets Γ^j of a non-smooth TS fuzzy system where weighting functions determine to what degree each fuzzy sub-vector field (and the corresponding sub-systems) form the overall dynamics. Therefore, a fuzzy sub-vector field can be represented as a weighted sum of affine sub-systems:

$$F_{m_i} = \sum_{j=1}^{l_{m_i}} w^j(\theta, m_i) (A^j(m_i)x + B^j(m_i)u + a^j(m_i)) \quad (3.23)$$

where $w^j : \mathbb{R}^n \times M \rightarrow \mathbb{R}^+$, $j \in I_{l_{m_i}}$. However, with the approach proposed here, the operating region of a sub-system in (3.23) is replaced with flexible regions, defined as $\mathcal{F}_q^{x, m_i, j} \subset \mathcal{F}$. This provides the possibility of representing a fuzzy sub-vector field in q flexible regions. In this way, the regions can be defined as a support set of continuous fuzzy states:

$$[w]^0 = \{x \in \Omega_q^{x, m_i} \mid w^j(x, m_i) > 0\}, \quad (3.24)$$

where each region $\mathcal{F}_q^{x, m_i, j}$ is designated to $[w]^0$ and defines to what degree the affine terms $A^j(m_i)x + B^j(m_i)u + a^j(m_i)$ are a part of (3.23) and hence, the overall dynamics. Having flexible regions instead of fixed regions in the fuzzy state space \mathcal{F} , plays an important role in avoiding the conservative formulation for structural stability analysis using Lyapunov's approach, presented in the next chapter, where the candidate non-smooth Lyapunov functions can be flexibly defined for each fuzzy sub-vector field and its sub-systems.

With the support $[w]^0$ as defined in (3.24), a non-smooth TS fuzzy model can be obtained if fuzzy variables $z_i(x)$ are defined as a convex combination of flexible region boundaries as

$$z_i(x) = M(z_i(x)) \cdot \min_x [w]^0 + (1 - M(z_i(x))) \cdot \max_x [w]^0,$$

where $\min_x [w]^0$ and $\max_x [w]^0$ are respectively the lower boundary and the upper boundary of flexible regions $\mathcal{F}_q^{x, m_i, j}$. As implied, the idea of sector nonlinearity is extended here by substituting the sectors with flexible regions $\mathcal{F}_q^{x, m_i, j}$ for a fuzzy sub-vector field F_{m_i} . From this point on, the rest of the procedure for obtaining the TS model is similar to that of smooth TS fuzzy systems (see Section 3.1.2).

3.2.6.2 Fuzzy sub-vector fields by Taylor expansion

The idea here is to linearized fuzzy sub-vector fields via their 1st-order Taylor expansion around chosen linearization points x_q . Like the former approach, an affine fuzzy sub-vector field (3.23) can be defined in q flexible fuzzy state-space regions $\mathcal{F}_q^{x, m_i, j}$. Therefore, a reasonable number of linearization points can be chosen in flexible partitions of the universe of discourse. As in a non-smooth system of the form (2.13), each vector field F_i actually represents a smooth function in an open region of the phase space S_i . System

parameters for a fuzzy sub-vector field (3.23) can then be constructed as:

$$A_q(m_i) = \frac{\partial F_i}{\partial x} \Big|_{x_q}, \quad B_q(m_i) = F_i(x_q) - \frac{\partial F_i}{\partial x} \Big|_{x_q} (x - x_q) - \frac{\partial F_i}{\partial u} \Big|_{u_q}, \quad (3.25)$$

with an affine term

$$a_q = F_i(x_q, u_q) - A_q(m_i)x_q - B_q(m_i)u_q. \quad (3.26)$$

This method is realizable based on the valid assumption that a fuzzy sub-vector field F_{m_i} in (3.23) represents an approximated smooth function of the original vector field F_i , defined in the region $\mathcal{F}_q^{x, m_i, j}$. Therefore a Taylor expansion of the original vector field F_i around a linearization point x_q in the state-space partition $\mathcal{F}_q^{x, m_i, j}$ yields:

$$F_{m_i} = F_i(x_q) + \frac{\partial F_i}{\partial x} \Big|_{x_q} (x - x_q) + O(F_i^2(x_q)),$$

where the higher-order term $O(F_i^2(x_q))$ is smooth and fulfills

$$\frac{\|O(F_i^2(x_q))\|}{\|x - x_q\|} \rightarrow 0 \quad \text{when} \quad \|x - x_q\| \rightarrow 0.$$

or in an equivalent term, for any $\tilde{R}_q(m_i) > 0$ there exist an $\tilde{r}_q(m_i) > 0$ such that

$$\|O(F_i^2(x_q))\| \leq \tilde{R}_q(m_i)\|x - x_q\|, \quad x \in B_{\tilde{r}_q(m_i)}(x_q).$$

As can be deduced from the above, the higher-order term $O(F_i^2(x_q))$ in the close vicinity of linearization points $x_q \in \mathcal{F}_q^{x, m_i, j}$, will be small and can be neglected.

Obtaining the consequent system parameters as (3.25) and (3.26) and selecting appropriate membership functions for each linearization point, each fuzzy sub-vector field can be constructed as (3.23) to represent the smooth flow of F_i of a non-smooth system. Hence, according to Theorem 3.3, the non-smooth TS fuzzy system can approximate the whole flow of F_i , $i = 1, 2, \dots, n$ belonging to a non-smooth system.

Example 3.5 (Case study I continued, the boost converter). The accuracy of the proposed TS fuzzy modeling approaches can be well examined in this example by applying it to dc-dc boost converters, introduced in case study I, which as already mentioned, are considered as non-smooth Filippov-type systems (see Table 2.1). There have been several attempts in the literature on the application of a TS fuzzy model-based approach to dc-dc electronic converters, mainly in order to control and boost the transient response of the circuit in the presence of disturbances; see for instance [112–115]. In all of these attempts, the given averaged model of the converter is represented by a smooth TS fuzzy model. Due to the fact that averaging technique provides a simplified and mathematically smooth model of a circuit, which neglects the dynamics occurring at fast-scale switching [1], i.e. the period-1 operation shown in Fig. 2.2, and all the ensuing bifurcation scenarios (Fig. 3.17). The purpose of employing the averaging technique is to focus on the central components of power processing and control functions of the

circuit. The averaged (or smooth) model of the converter, however, is not capable of giving any insight or information about fast-scale instabilities and all the ensuing bifurcations including DIBs, arise at the clock frequency. The intention here, as first proposed in [116], is to obtain a non-smooth TS fuzzy model of a dc-dc boost converter, which is able to capture all the fast-scale nonlinearities occurring at clock instants.

Considering the equations (2.1) and (2.2), where state variables are defined as $x_1(t) = i_L(t)$ and $x_2(t) = v_C(t)$ and using the method of linearizing transformation, a non-smooth TS fuzzy model for the boost converter can be obtained with the following model rules:

$$\begin{aligned} \textbf{Model Rule 1:} \quad & \text{IF } x_1(t) \text{ is } \Gamma^1 \text{ THEN } \begin{cases} \dot{x}(t) = A^j(m_1)x(t) + B^j(m_1)u(t), \\ m_1 = \xi(x, m_2), \quad j = 1, 2. \end{cases} \\ \textbf{Model Rule 2:} \quad & \text{IF } x_1(t) \text{ is } \Gamma^2 \text{ THEN } \begin{cases} \dot{x}(t) = A^j(m_2)x(t) + B^j(m_2)u(t), \\ m_2 = \xi(x, m_1), \quad j = 1, 2. \end{cases} \end{aligned} \quad (3.27)$$

where fuzzy sub-vector field matrices with consideration of parasitic variables can be defined as:

$$\begin{aligned} A^1(m_1) = A^2(m_1) &= \begin{bmatrix} -\frac{1}{L}(r_L + r_{SW}) & 0 \\ 0 & -\frac{1}{C(R+r_C)} \end{bmatrix}, \quad B^1(m_1) = B^2(m_1) = \begin{bmatrix} \frac{V_{in}}{L} \\ 0 \end{bmatrix} \\ A^1(m_2) = A^2(m_2) &= \begin{bmatrix} -\frac{1}{L}(r_L + r_{VD} + \frac{Rr_C}{R+r_C}) & -\frac{R}{L(R+r_C)} \\ \frac{R}{C(R+r_C)} & -\frac{1}{C(R+r_C)} \end{bmatrix}, \quad B^1(m_2) = B^2(m_2) = \begin{bmatrix} \frac{V_{in}}{L} \\ 0 \end{bmatrix} \end{aligned}$$

for the two discrete states $M = \{m_1, m_2\}$, which are actually designated for the states of the ON and OFF switches of the circuit under current-mode PWM control. The switching manifold Σ can be represented by two switch sets as

$$\begin{aligned} S_{1,2} &= \{x \in R^n \mid i_L(dT) - I_{ref} > 0\}, \\ S_{2,1} &= \{x \in R^n \mid i_L(dT) - I_{ref} < 0\}, \end{aligned} \quad (3.28)$$

where d stands for duty ratio, calculated from the PWM control action in the n^{th} clock cycle when the circuit is operating in normal period-1 mode [117]:

$$d(n) = \frac{L}{T(r_L + r_{SW})} \ln\left(\frac{V_{in} - (r_L + r_{SW})x_1(n)}{V_{in} - (r_L + r_{SW})I_{ref}}\right). \quad (3.29)$$

In the above relation, $x_1(n)$ denotes the n^{th} sampled input current and the duty cycle $d(n)$ is the n^{th} "on" time expressed as a fraction of the clock period $T = 1 \times 10^{-4}$ s.

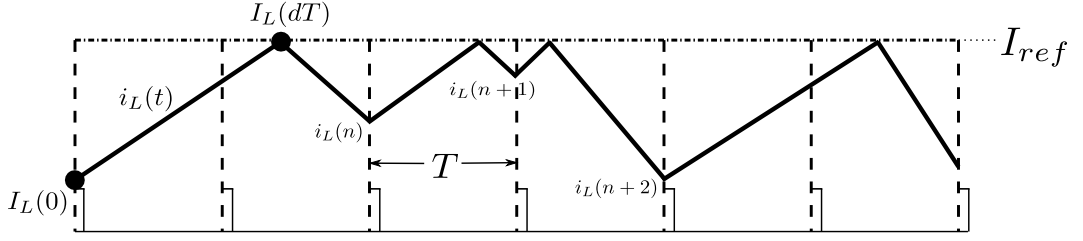
The lower and upper boundary of the assigned fuzzy set support are chosen as

$$-3.3286 < [w]^0 < 11.2314,$$

which means that the fuzzy sets can be formulated as the convex combination:

$$x_1(x) = \Gamma^1(x_1(t)) \cdot (-3.3286) + \Gamma^2(x_1(t)) \cdot (11.2314),$$

where the fuzzy variable is $z_1(t) = x_1(t)$ and $\Gamma^1(x_1(t)) = 1 - \Gamma^2(x_1(t))$. By solving the

Figure 3.14: Waveform of the inductor current $i_L(t)$ in the boost converter.

above, the following membership functions are obtained:

$$\Gamma^1(x_1(t)) = \frac{1}{2} + \frac{x_1(t) - 3.9514}{2l}, \quad \Gamma^2(x_1(t)) = 1 - \Gamma^1(x_1(t)). \quad (3.30)$$

The rationale behind setting the boundaries of $[w]^0$ is that a switching boundary for the inductor current can be defined as $i_L(t) = I_L(0) \pm l$, where $I_L(0) = 3.9514$ is the fixed point of the stroboscopic Poincaré map (see Definition 2.5) when the limit cycle of the original system is period-1 stable. As envisaged in the schematic diagram of Fig. 3.14, the value $l = 7.28 = 2 \times 3.64$ is considered as a deviation which may be created from the perturbation of the inductor current when it does not reach I_{ref} until the next observation of the clock instants³. This deviation error may become much larger in the fuzzy approximation. Therefore, the delay at the switching instants; that is, the delay resulting from the high switching frequency (10MHz) between the two fuzzy sub-vector fields in (3.27), should be avoided by covering a boundary as intentionally considered in the membership functions (3.30).

The accuracy of the obtained TS fuzzy model is easily verifiable when comparing the time responses of the model (3.27) with that of the original circuit under current-mode control in terms of output current i_L (Fig. 3.15) and output voltage v_C (Fig. 3.16) for different values of input voltage V_{in} , where the circuit exhibits different qualitative behaviours ranging from stable period-1 operation to chaos. The qualitative verification of the TS fuzzy model (3.27) in terms of bifurcation diagram (the long-term behaviour when a system's parameter is varied) is also shown in Fig. 3.17.

³Interested readers are referred to [1] for a detailed discussion on piece-wise smooth maps for boost converters, where the fixed point of the map can be derived using Newton-Raphson methods.

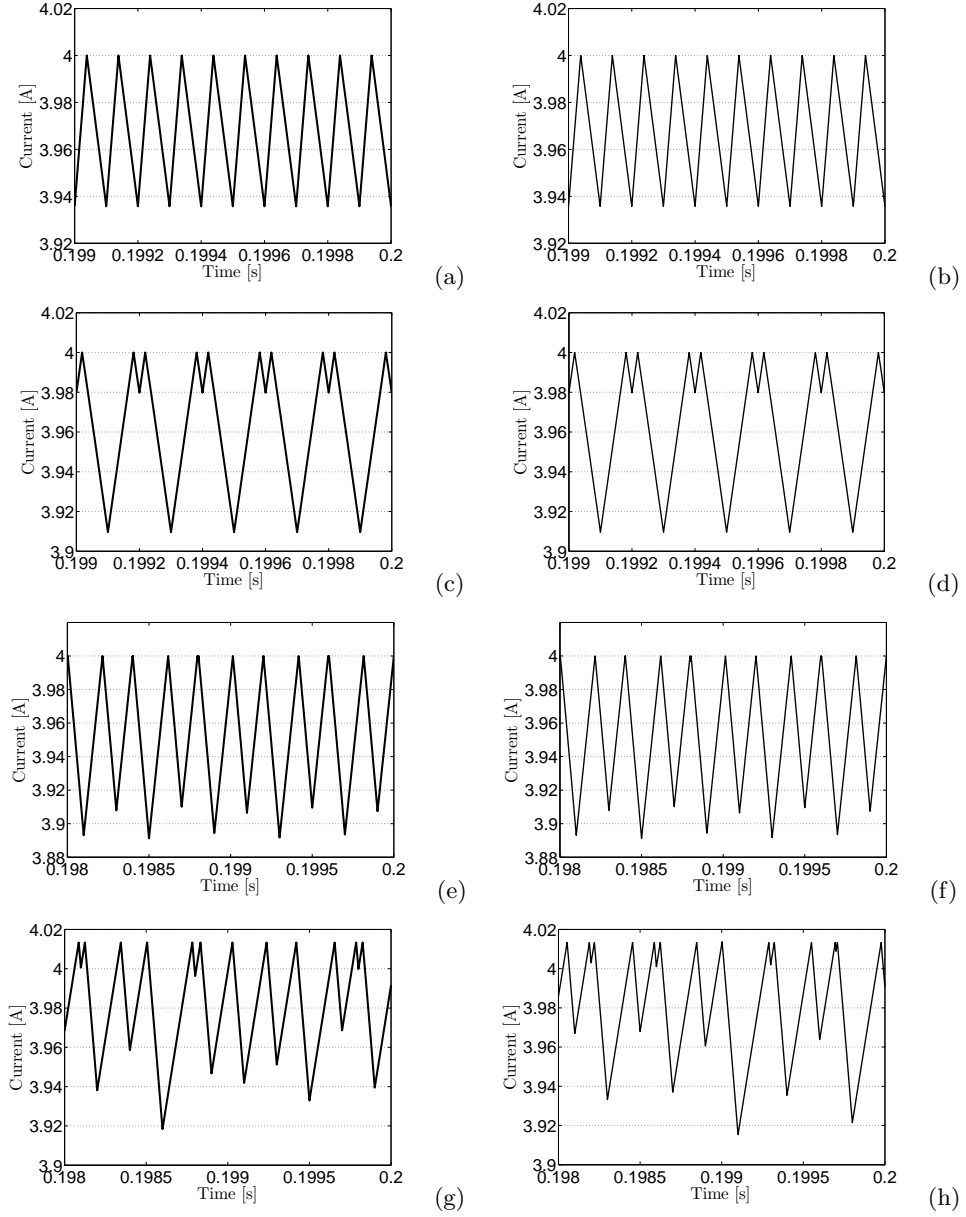


Figure 3.15: Output current time responses of the boost converter: (a) the original system in period-1 operation ($V_{in} = 45V$), (b) its TS Fuzzy model in period-1 operation ($V_{in} = 45V$), (c) the original system in an unstable period-2 operation ($V_{in} = 36V$), (d) its TS Fuzzy model in period-2 operation ($V_{in} = 36V$) (e) the original system in an unstable period-4 operation ($V_{in} = 34V$), (f) its TS Fuzzy model in period-4 operation ($V_{in} = 34V$) (g) the original system operating in chaos ($V_{in} = 20V$), and (h) its TS Fuzzy model ($V_{in} = 20V$).

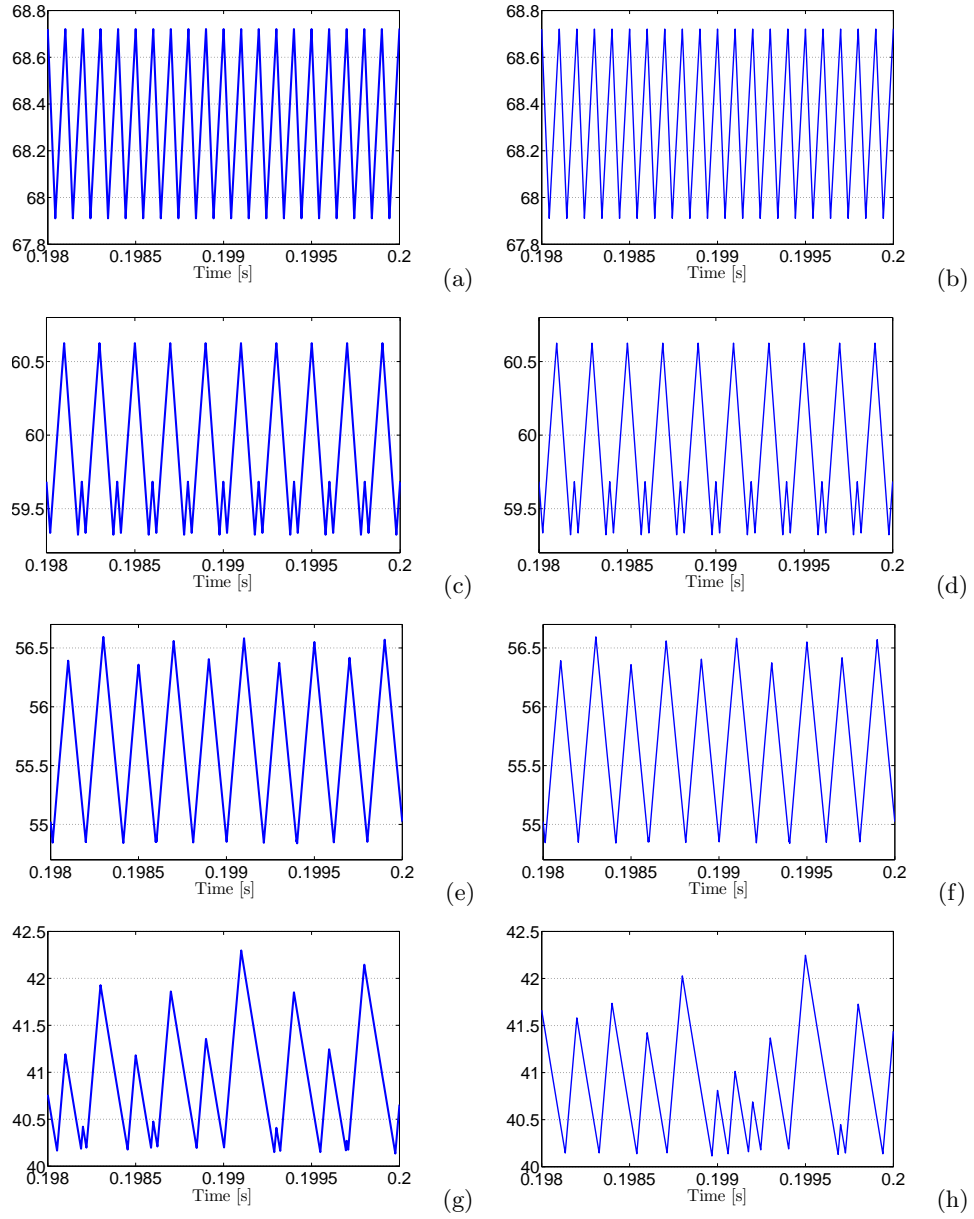


Figure 3.16: Output voltage time responses of the boost converter: (a) the original system in period-1 operation ($V_{in} = 45V$), (b) its TS Fuzzy model in period-1 operation ($V_{in} = 45V$), (c) the original system in an unstable period-2 operation ($V_{in} = 36V$), (d) its TS Fuzzy model in period-2 operation ($V_{in} = 36V$) (e) the original system in an unstable period-4 operation ($V_{in} = 34V$), (f) its TS Fuzzy model in period-4 operation ($V_{in} = 34V$) (g) the original system operating in chaos ($V_{in} = 20V$), and (h) its TS Fuzzy model ($V_{in} = 20V$).

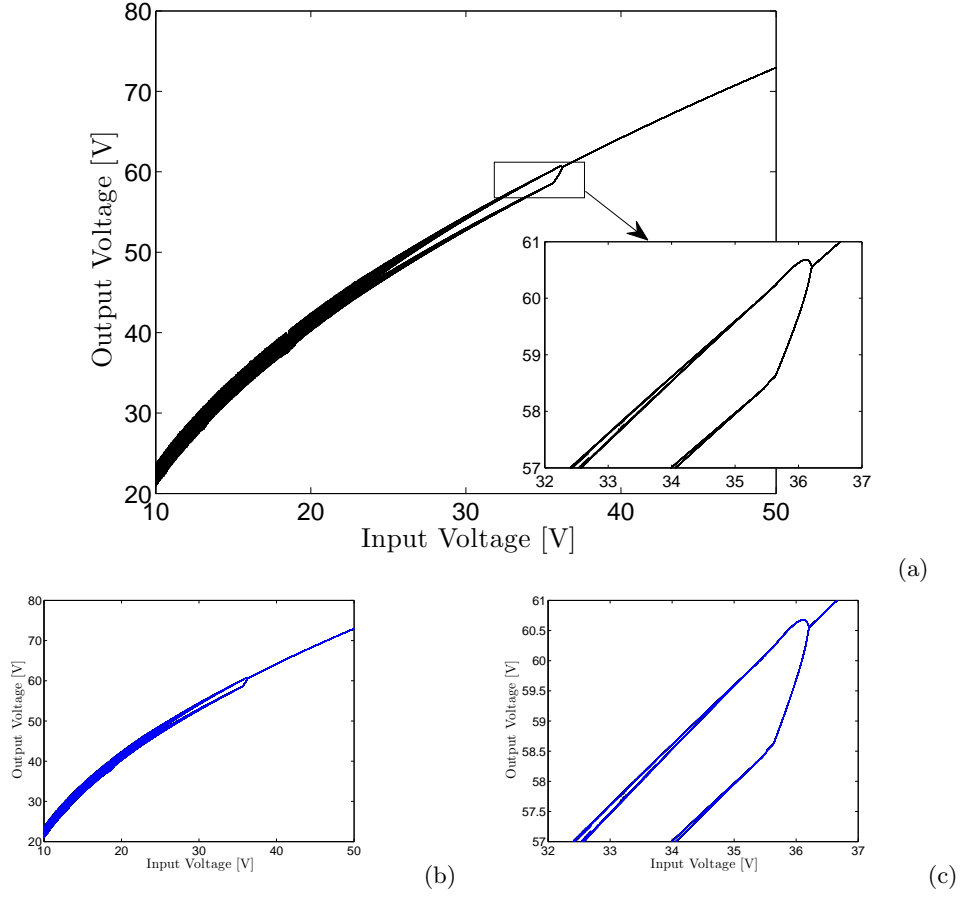


Figure 3.17: The long term behaviour of the boost converter for $V_{in} \in (10, 50)$ is shown via bifurcation diagrams (using switch-on sampling) in (a) the original system, (b) and (c) its TS fuzzy model.

Example 3.6 (Case study I continued, the buck converter). Following the same approach a non-smooth TS fuzzy model of the voltage-mode controlled buck converter circuit (see Fig. 2.1) can be constructed as follows [118]:

$$\textbf{Model Rule } j: \text{ IF } x_2(t) \text{ is } \Gamma^j \text{ THEN } \begin{cases} \dot{x}(t) = A^j(m_i)x(t) + B^j(m_i)u(t) \\ m^+ = \xi(x, m), \quad j = 1, 2, \quad i = 1, 2. \end{cases}$$

where the state variables are defined as $x_1(t) = i_L(t)$, $x_2(t) = v_C(t)$, and fuzzy sub-vector field matrices (excluding the converter parasitic variables) are composed of the sub-systems:

$$\begin{aligned} A^1(m_1) &= A^2(m_1) = \begin{bmatrix} -1/RC & 1/C \\ -1/L & 0 \end{bmatrix}, & B^1(m_1) &= B^2(m_1) = \begin{bmatrix} 0 \\ 1/L \end{bmatrix} V_{in} \\ A^1(m_2) &= A^2(m_2) = \begin{bmatrix} -1/RC & 1/C \\ -1/L & 0 \end{bmatrix}, & B^1(m_2) &= B^2(m_2) = \begin{bmatrix} 0 \\ 0 \end{bmatrix}, \end{aligned} \quad (3.31)$$

for the two discrete states $M = \{m_1, m_2\}$, defined for the *on/off* switch states of the converter under voltage-mode PWM control. Function ξ in (3.31) can be described by two switch sets:

$$\begin{aligned} S_{1,2} &= \{x \in R^n | x_1(dT) - V_{\text{ref}} < \frac{v_{\text{ramp}}}{A}\}, \\ S_{2,1} &= \{x \in R^n | x_1(dT) - V_{\text{ref}} > \frac{v_{\text{ramp}}}{A}\}, \end{aligned} \quad (3.32)$$

where d is the duty ratio and the periodic sawtooth waveform v_{ramp} is given by [119]:

$$v_{\text{ramp}}(t) = V_L + (V_U - V_L) \left(\frac{t}{T} \bmod 1 \right), \quad (3.33)$$

where the ramp signal varies from $V_L = 3.8\text{V}$ to $V_U = 8.2\text{V}$. The same rationale explained in Example 3.5 applies here in choosing fuzzy set support boundaries as $[w]^0 \in [0.7747, 23.3747]$, obtained by the fine tuning around the derived stable fixed point $X(0) = [0.6220, 12.0747]^T$ of the stroboscopic Poincaré map. The following membership functions can then be obtained:

$$\Gamma^1(x_2(t)) = \frac{1}{2} + \frac{x_2(t) - 12.0747}{2l}, \quad \Gamma^2(x_2(t)) = 1 - \Gamma^1(x_2(t)), \quad (3.34)$$

where $v_C(t) = X_2(0) \pm l$ and $l = 11.3$ is chosen as the covering interval for the deviation error.

The reason of selecting such precise numbers for fuzzy set support boundaries in this example is to remove any delay in high frequency switchings, e.g. 10KHz, in electronic converters as pointed out in the previous example of boost converter. Since the conventional dc-dc converters operate with lower frequencies than we select here, in the presence of any parametric noise or model uncertainties, the precise boundaries for fuzzy set support $[w]^0$ can be relaxed to prevent any modeling error, i.e. switching delays. Any existing small modeling error, nevertheless, can be compensated by the robust control strategy which will be proposed in Chapter 5 (see also Section 4.6.1 for the robustness analysis of model uncertainties in switch sets).

As noticed from the bifurcation diagram in Fig. 3.18, the qualitative behaviour of the non-smooth TS fuzzy model (3.31) is well matched with that of the original circuit under voltage-mode control scheme (see Fig. 2.6). The comparison is also made in terms of the time responses in Fig. 3.19. It is visible that the model (3.31) is able to further preserve the invisible asymptotic behaviour of the original circuit, where the unstable period-1 orbit coexists with the stable period-2 orbit for $V_{\text{in}} = 25$ as shown in Fig. 3.20.

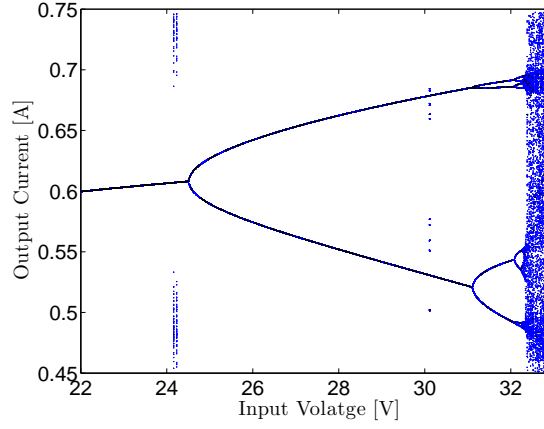


Figure 3.18: The bifurcation diagram for $V_{in} \in (22, 33)$ shows the long-time behaviour of the TS fuzzy model of the buck converter.

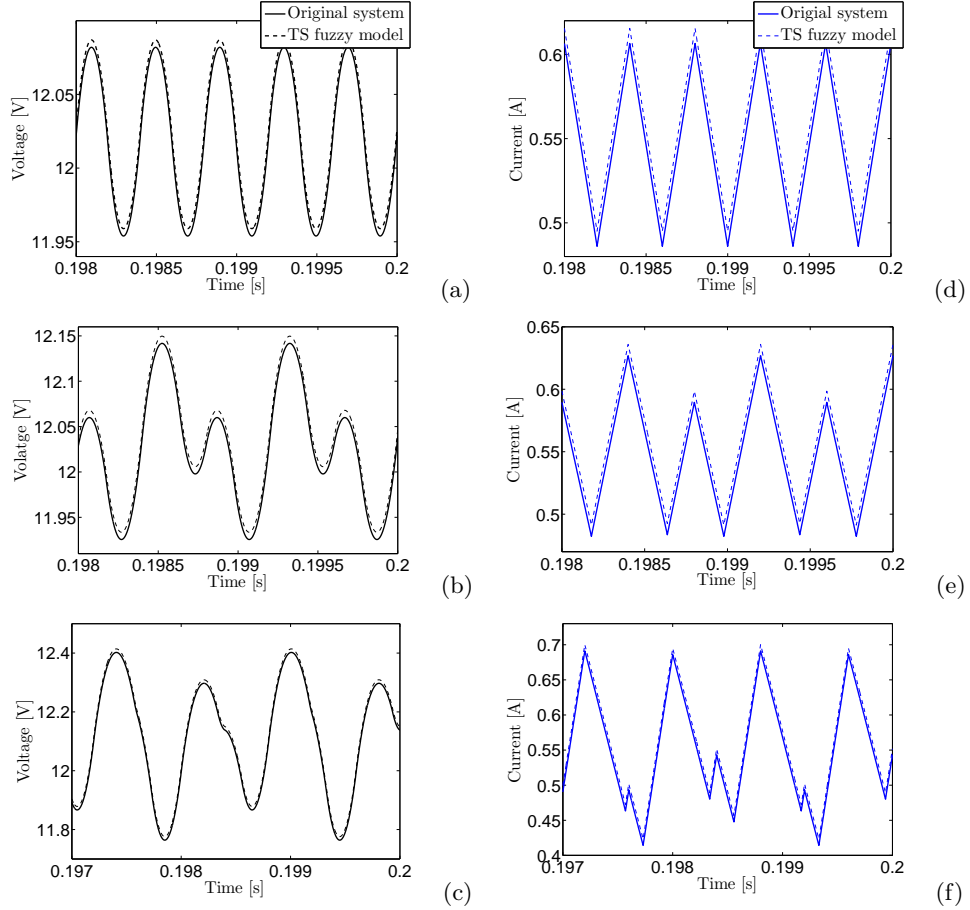


Figure 3.19: Output voltage and current time responses of the buck converter when (a) operating in stable period-1 ($V_{in} = 24V$), (b) operating in period-2 ($V_{in} = 25V$), (c) operating in period-4 ($V_{in} = 32V$). Small differences between the original system's output (solid line) and its TS fuzzy model (dashed line) were intentionally introduced for the sake of visibility, otherwise there exists no error in modeling.

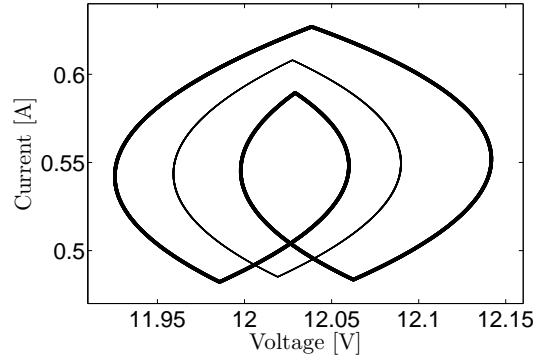


Figure 3.20: The coexisting stable (thick line) and unstable (narrow line) periodic orbit of the TS fuzzy model of the buck converter for $V_{in} = 25V$.

Example 3.7 (Case study II continued, the hard impact oscillator). Compared with examples 3.5 and 3.6, the model of an hard-impact oscillator cannot be easily constructed using the exact structure of Definition 3.1, mainly due to the complexity of the additional discontinuous (jump) states in impacting dynamics after intersection with a switching manifold (notice the dynamics in Table 2.1 and also in Fig. 2.23). As explained in Remark 3.3, discontinuous states can be represented by a non-smooth TS fuzzy model, by further incorporating the function χ describing the mapping of discontinuous states with respect to the switching manifold Σ . Then, as first proposed in [120], the resulting non-smooth TS fuzzy model with the structure (3.12) along with (3.16) is able to represent all the essential nonlinearities as illustrated in Section 2.1.2. In order to obtain the TS fuzzy model, let's describe the original equation (2.5) in canonical form as follows:

$$\begin{cases} \dot{x}_1 = x_2, \\ \dot{x}_2 = -\omega_n^2 x_1 - 2\zeta\omega_n x_2 - F\cos(\omega t), \end{cases} \quad (3.35)$$

where $u(t) = x_1(t)$ and $\dot{u}(t) = v(t) = x_2(t)$. The TS fuzzy model rules for representing (3.35) together with the zero-time mapping equation (2.6), can be described as follows:

Model Rule j : IF $x_2(t)$ is Γ^j THEN

$$\begin{cases} \dot{x}(t) = A^j(m_i)x(t) + B^j(m_i)u(t), & j = 1, 2, 3, 4, & i = 1, 2, \\ m^+ = \xi(x, m), \\ x^+ = \chi(x, m), \end{cases} \quad (3.36)$$

where the state variables $x(t) = [x_1(t) \ x_2(t)]$ are defined as above and $u(t)$ is an input to the model⁴. The method of linearizing transformation is preferred here to determine the boundaries of fuzzy set support. Therefore, for constructing the first fuzzy sub-vector field F_{m_1} , the fuzzy set supports for the state variables x_1 and x_2 are respectively chosen

⁴Note that the input signal $u(t)$ of the TS fuzzy model should not be confused with the state $u(t)$ denoting the position of the mass M with respect to the hard wall in the original equation of the hard-impact oscillator.

as $[w1]^0 \in [-0.5, 0.5]$ and $[w2]^0 \in [2\hat{l}_1, 2\hat{l}_2]$, where $\hat{l}_1 = 4.13$ and $\hat{l}_2 = -3.72$ are respectively the maximum and minimum initial amplitudes of the state x_2 when the system is structurally stable, i.e. $F = 1.4975\text{N}$, $m = 1$. If we assume two fuzzy variables $z_1 = x_1$ and $z_2 = x_2$, they can be described by fuzzy sets as follows:

$$\begin{aligned} z_1 &= 0.5 \cdot \Gamma^1(z_1) + (-0.5) \cdot \Gamma^2(z_1), \\ z_2 &= 8.26 \cdot \Gamma^3(z_2) + (-7.44) \cdot \Gamma^4(z_2). \end{aligned}$$

Since $\Gamma^1(z_1) + \Gamma^2(z_1) = 1$ and $\Gamma^3(z_2) + \Gamma^4(z_2) = 1$, the membership functions are derived as:

$$\begin{aligned} \Gamma^1(z_1) &= \frac{1}{2} + z_1, \quad \Gamma^2(z_1) = 1 - \Gamma^1(z_1), \\ \Gamma^3(z_2) &= \frac{1}{2} + \frac{z_2 - 0.4}{15.7}, \quad \Gamma^4(z_2) = 1 - \Gamma^3(z_2). \end{aligned}$$

According to the above membership functions, the sub-system matrices for F_{m_1} can be constructed as follows:

$$\begin{aligned} A_1(m_1) &= \begin{bmatrix} 0 & 1 \\ \max_{z_1 \in \Gamma^1} z_1 \cdot (-\omega_n^2) & \max_{z_2 \in \Gamma^3} z_2 \cdot (-2\zeta\omega_n) \end{bmatrix}, & A_2(m_1) &= \begin{bmatrix} 0 & 1 \\ \max_{z_1 \in \Gamma^1} z_1 \cdot (-\omega_n^2) & \max_{z_2 \in \Gamma^4} z_2 \cdot (-2\zeta\omega_n) \end{bmatrix}, \\ A_3(m_1) &= \begin{bmatrix} 0 & 1 \\ \max_{z_1 \in \Gamma^2} z_1 \cdot (-\omega_n^2) & \max_{z_2 \in \Gamma^3} z_2 \cdot (-2\zeta\omega_n) \end{bmatrix}, & A_4(m_1) &= \begin{bmatrix} 0 & 1 \\ \max_{z_1 \in \Gamma^2} z_1 \cdot (-\omega_n^2) & \max_{z_2 \in \Gamma^4} z_2 \cdot (-2\zeta\omega_n) \end{bmatrix}, \\ B^1(m_1) &= B^2(m_1) = B^3(m_1) = B^4(m_1) = \begin{bmatrix} 0 \\ -F \end{bmatrix}, \end{aligned}$$

where after plugging the respective number, the fuzzy sub-vector field F_{m_1} can be described by the following matrices:

$$\begin{aligned} A^1(m_1) &= \begin{bmatrix} 0 & 1 \\ -0.5\omega_n^2 & -(2 \cdot 8.26)\zeta\omega_n \end{bmatrix}, & A^2(m_1) &= \begin{bmatrix} 0 & 1 \\ -0.5\omega_n^2 & (2 \cdot 7.44)\zeta\omega_n \end{bmatrix}, \\ A^3(m_1) &= \begin{bmatrix} 0 & 1 \\ 0.5\omega_n^2 & -(2 \cdot 8.26)\zeta\omega_n \end{bmatrix}, & A^4(m_1) &= \begin{bmatrix} 0 & 1 \\ 0.5\omega_n^2 & (2 \cdot 7.44)\zeta\omega_n \end{bmatrix}, \\ B^1(m_1) &= B^2(m_1) = B^3(m_1) = B^4(m_1) = \begin{bmatrix} 0 \\ -F \end{bmatrix}, \end{aligned}$$

where the input signal in (3.36) is $u(t) = \cos(wt)$. To construct the second fuzzy sub-vector field, the fuzzy set supports for the state variables x_1 and x_2 are respectively chosen as $[w3]^0 \in [-4, 0.5]$ and $[w4]^0 \in [-7.32, 8.086]$. Similarly, F_{m_2} is described by the following sub-system matrices:

$$A^1(m_2) = \begin{bmatrix} 0 & 1 \\ -0.5\omega_n^2 & -(2 \cdot 8.086)\zeta\omega_n \end{bmatrix}, \quad A^2(m_2) = \begin{bmatrix} 0 & 1 \\ -0.5\omega_n^2 & (2 \cdot 7.32)\zeta\omega_n \end{bmatrix},$$

$$A^3(m_2) = \begin{bmatrix} 0 & 1 \\ 4\omega_n^2 & -(2 \cdot 8.086)\zeta\omega_n \end{bmatrix}, \quad A^4(m_2) = \begin{bmatrix} 0 & 1 \\ 4\omega_n^2 & (2 \cdot 7.32)\zeta\omega_n \end{bmatrix},$$

$$B^1(m_2) = B^2(m_2) = B^3(m_2) = B^4(m_2) = \begin{bmatrix} 0 \\ 1 \end{bmatrix}.$$

Therefore, the fuzzy sub-vector fields F_{m_1} and F_{m_2} are constructed for the two discrete states $M = \{m_1, m_2\}$ with the parameters w_n , ζ defined in (2.5) for the forcing function period of $T = \frac{\pi\varpi}{w_n\sqrt{1-\zeta^2}} = 9.342s$. Function ξ in (3.36) is alternatively described by two switch sets:

$$\begin{aligned} S_{1,2} &= \{x \in R^n \mid x_1(t) - \sigma > 0\}, \\ S_{2,1} &= \{x \in R^n \mid x_1(t) - \sigma < 0\}, \end{aligned} \quad (3.37)$$

and the function χ in (3.36) is described by jump matrices as defined in (3.18) (see Remark 3.3):

$$J(m_1) = \begin{bmatrix} 1 & 0 \\ 0 & -r \end{bmatrix}, \quad J(m_2) = \begin{bmatrix} 1 & 0 \\ 0 & -1/r \end{bmatrix}, \quad (3.38)$$

The above matrices are determined based on zero-velocity mapping (2.6) when impact occurs with a coefficient of restitution $r = 0.9$.

Time responses of the original impacting system together with its TS fuzzy model is shown in Fig. 3.21 for different forcing function amplitudes (F) when the frequency ratio is chosen as the fixed value of $\varpi = 2.97$.

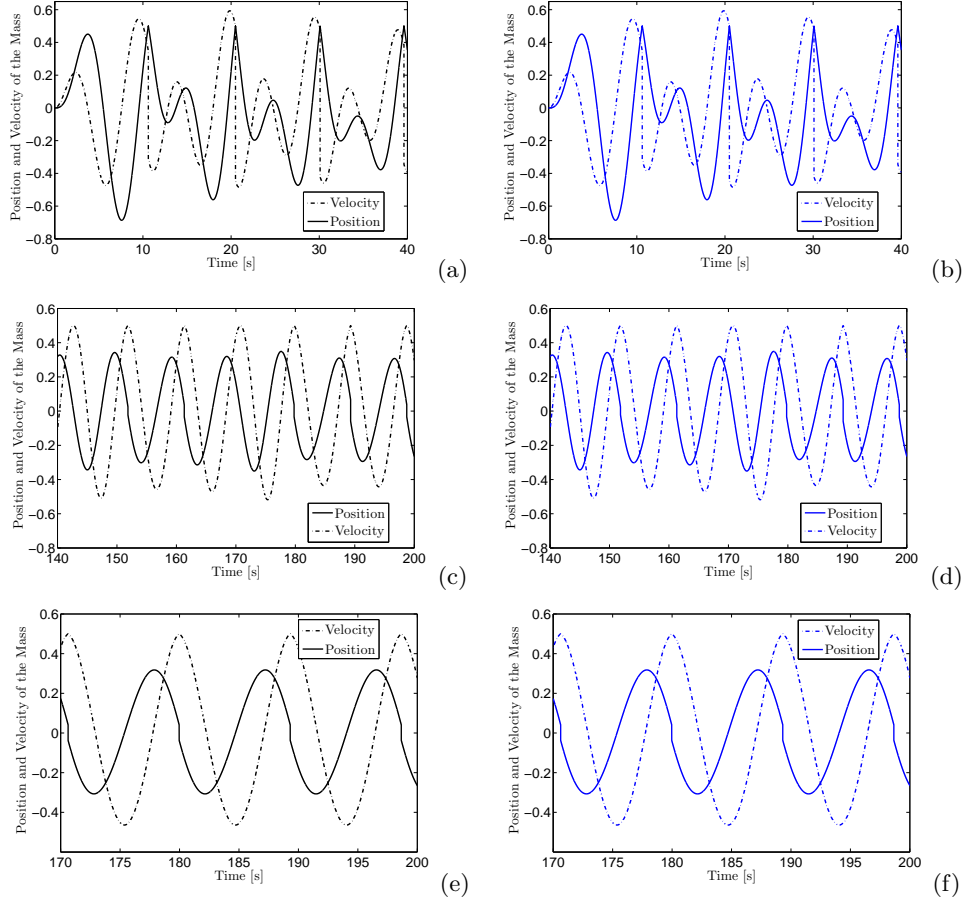


Figure 3.21: Time responses, produced from (a) the original impacting system ($\varpi = 2.97, F = 0.275N$) when the system is stable, (b) its TS fuzzy model ($\varpi = 2.97, F = 0.275N$), (c) the original impacting system ($\varpi = 2.97, F = 0.2759N$) when the system becomes chaotic, (d) its TS fuzzy model ($\varpi = 2.97, F = 0.276N$), (e) the original impacting system ($\varpi = 2.97, F = 0.277N$) when the system becomes stable again, and (f) its TS fuzzy model ($\varpi = 2.97, F = 0.277N$).

As pointed out in Section 2.1.2, and later in Section 2.2.5, it is well known that close to a grazing incident in an impact oscillator, there is an abrupt instability of the local orbit to a much larger chaotic orbit due to the infinite stretching of the phase space. The TS fuzzy model (3.36) can well preserve this typical DIB known as the grazing bifurcation as shown in Fig. 3.23a and 3.23b. The other grazing scenarios are shown in the bifurcation diagrams of Fig. 3.22, which shows that the TS fuzzy model can well represent the dynamics close to the grazing for different values of frequency ratio ϖ .

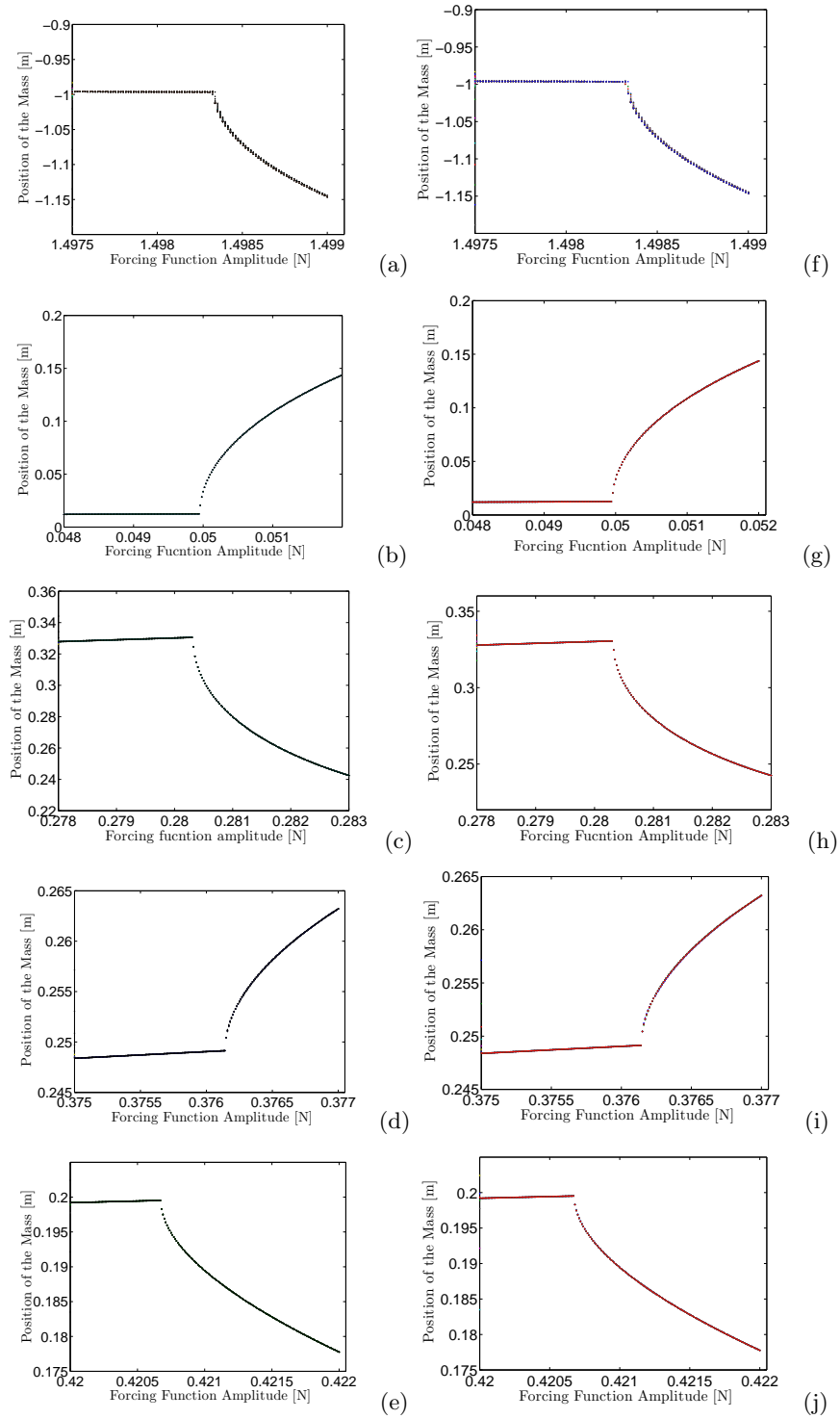


Figure 3.22: The bifurcation diagrams (b-f) shows the dynamics close to grazing in the original impact oscillator when (b) $\varpi = 1$, (c) $\varpi = 2$, (d) $\varpi = 3$, (e) $\varpi = 4$, and (f) $\varpi = 5$. The diagrams (g-j) show the corresponding TS fuzzy model figures.

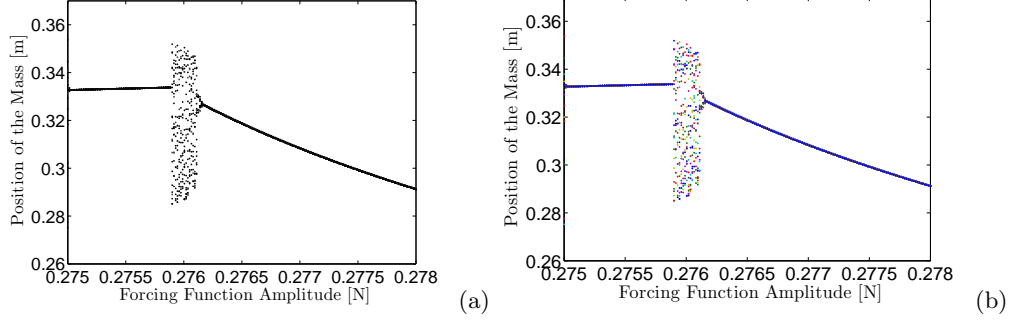


Figure 3.23: The grazing bifurcation in (a) the impact oscillator, and (b) its TS fuzzy model when $\varpi = 2.97$.

Example 3.8 (Case study III continued, dry-friction oscillator). To investigate the accuracy of TS fuzzy modeling for sliding Filippov's systems, we recall the dry-friction oscillator, a mechanical system presented in Section 2.1.3 with the equation of motion (2.7) together with the nonlinear Coulomb friction law (2.8). As mentioned before, in this system, an important DIB occurs by a sliding-grazing event, where the limit cycle instantly loses its stability to a chaotic orbit when touching the boundary of the sliding region.

To construct a non-smooth TS fuzzy model using the linearizing transformation approach, we start by defining the system states as $x_1 = u$ and $x_2 = \dot{u}$, and two fuzzy set supports $[w1]^0$ and $[w2]^0$ for the state variable x_2 , assuming the respective boundaries for the state variable x_2 as $x_2 \in [-0.5, 1]$ and $x_2 \in [1.001, 2.5]$. Therefore, two fuzzy variable z_1 and z_2 can be defined for the nonlinear term $\alpha_1 + 2\alpha_2 + \alpha_2(x_2^2 + 2x_2)$, respectively, based on the supports $[w1]^0$ and $[w2]^0$, as expressed below:

$$\begin{aligned} z_1(t) &= \Gamma_1(z_1(t)) \cdot \min_{x_2} [w1]^0 + (1 - \Gamma_1(z_1(t))) \cdot \max_{x_2} [w1]^0, \\ z_2(t) &= \Gamma_2(z_2(t)) \cdot \min_{x_2} [w1]^0 + (1 - \Gamma_2(z_2(t))) \cdot \max_{x_2} [w1]^0, \end{aligned}$$

which is calculated as

$$\begin{aligned} z_1(t) &= \Gamma^1(z_1(t)) \cdot 2.9625 + \Gamma^2(z_1(t)) \cdot 3.7500, \\ z_2(t) &= \Gamma^3(z_2(t)) \cdot 3.7518 + \Gamma^4(z_2(t)) \cdot 7.4625, \end{aligned}$$

where $\Gamma_1, \Gamma_2, \Gamma_3$ and Γ_4 are fuzzy sets or membership functions, which are obtained as

$$\begin{aligned} \Gamma^1(z_1(t)) &= (z_1(t) - 3.7500)/0.7875, \\ \Gamma^2(z_1(t)) &= (2.9625 - z_1(t))/0.7875, \\ \Gamma^3(z_2(t)) &= (z_2(t) - 7.4625)/3.7107, \\ \Gamma^4(z_2(t)) &= (3.7518 - z_2(t))/3.7107. \end{aligned}$$

The following switch sets describe the function ξ :

$$\begin{aligned} S_{1,2} &= \{x \in R^n \mid 1 - x_2(t) > 0\}, \\ S_{2,1} &= \{x \in R^n \mid 1 - x_2(t) < 0\}, \end{aligned} \quad (3.39)$$

which explains the interaction between the fuzzy sub-vector field F_{m_1} , associated with the discrete state m_1 and composed of the sub-systems

$$\begin{aligned} A^1(m_1) &= \begin{bmatrix} 0 & 1 \\ -1 & 2.9625 \end{bmatrix}, \quad A^2(m_1) = \begin{bmatrix} 0 & 1 \\ -1 & 3.7500 \end{bmatrix}, \quad A^3(m_1) = \begin{bmatrix} 0 & 1 \\ -1 & 3.7518 \end{bmatrix}, \\ A^4(m_1) &= \begin{bmatrix} 0 & 1 \\ -1 & 7.4625 \end{bmatrix}, \quad B^1(m_1) = B^2(m_1) = B^3(m_1) = B^4(m_1) = \begin{bmatrix} 0 \\ \alpha_0 - \alpha_1 + \alpha_2 + F \cos(\omega t) \end{bmatrix}, \end{aligned} \quad (3.40)$$

and the fuzzy sub-vector field F_{m_2} , associated with the discrete state m_2 and composed of the sub-systems

$$\begin{aligned} A^1(m_1) &= \begin{bmatrix} 0 & 1 \\ -1 & 2.9625 \end{bmatrix}, \quad A^2(m_1) = \begin{bmatrix} 0 & 1 \\ -1 & 3.7500 \end{bmatrix}, \quad A^3(m_1) = \begin{bmatrix} 0 & 1 \\ -1 & 3.7518 \end{bmatrix}, \\ A^4(m_1) &= \begin{bmatrix} 0 & 1 \\ -1 & 7.4625 \end{bmatrix}, \quad B^1(m_1) = B^2(m_1) = B^3(m_1) = B^4(m_1) = \begin{bmatrix} 0 \\ -\alpha_0 - \alpha_1 + \alpha_2 + F \cos(\omega t) \end{bmatrix}. \end{aligned} \quad (3.41)$$

Hence, the model rules for dry-friction oscillator are expressed as follows:

Model Rule j : IF $x_2(t)$ is Γ^j THEN

$$\begin{cases} \dot{x}(t) = A^j(m_i)x(t) + B^j(m_i)u(t), & j = 1, 2, 3, 4, \quad i = 1, 2, \\ m^+ = \xi(x, m), \end{cases} \quad (3.42)$$

Comparing the time responses in Fig. 3.25 and the phase portrait of the TS fuzzy model (3.42) for different values of forcing frequency (Fig. 3.24) with that of the original system (Fig. 2.13), confirms the approximation capability of the TS fuzzy model (3.42) in representing 4-dimensional sliding Filippov's systems like the dry-friction oscillator with nonlinear vector fields.

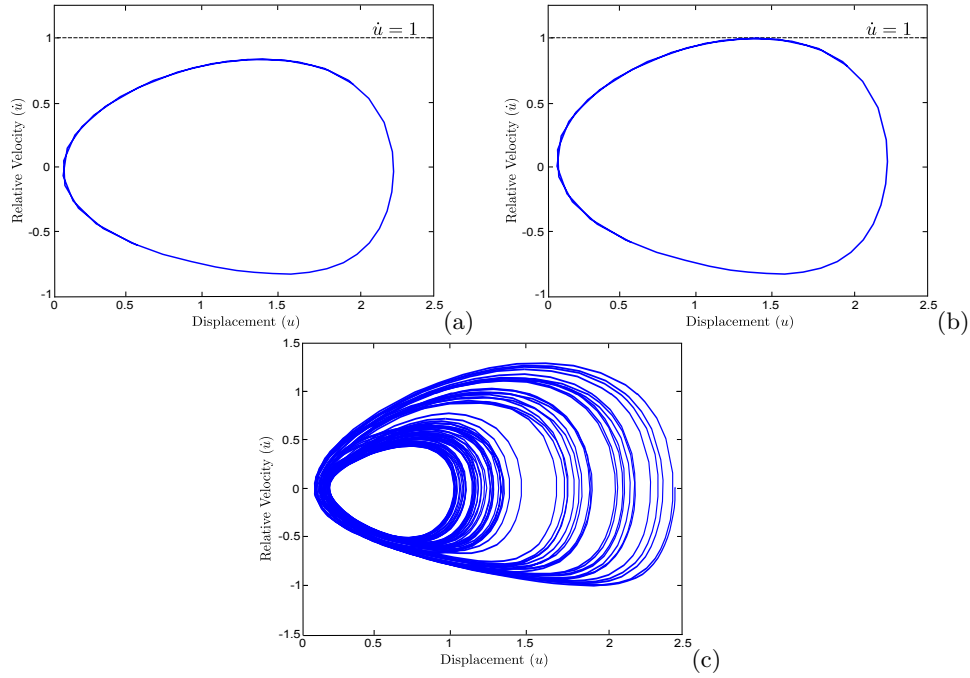


Figure 3.24: $4T$ -periodic ($8\pi/\omega$) orbit of the non-smooth TS fuzzy model (3.42) when (a) it's stable and grazing does not take place, (b) grazes the switching manifold where a sliding region is formed, (c) becomes chaotic due to the grazing-sliding DIB.

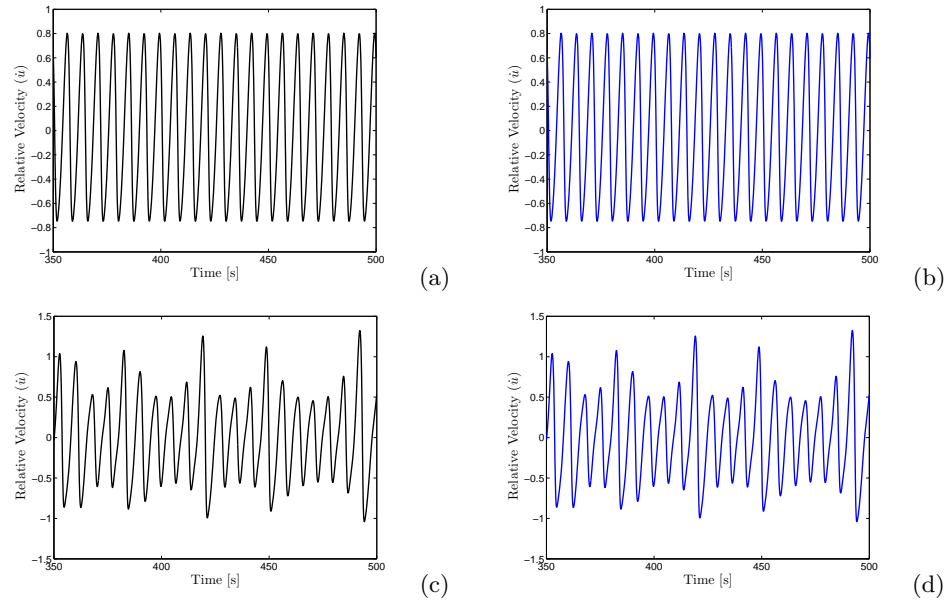


Figure 3.25: Time responses, produced from (a) the original dry-friction oscillator, and (b) its TS fuzzy model, when the system is stable at the forcing frequency $\omega = 1.70781$. The time responses when (c) the original dry-friction oscillator and (d) its TS fuzzy model, becomes chaotic at the frequency $\omega = 1.70779$.

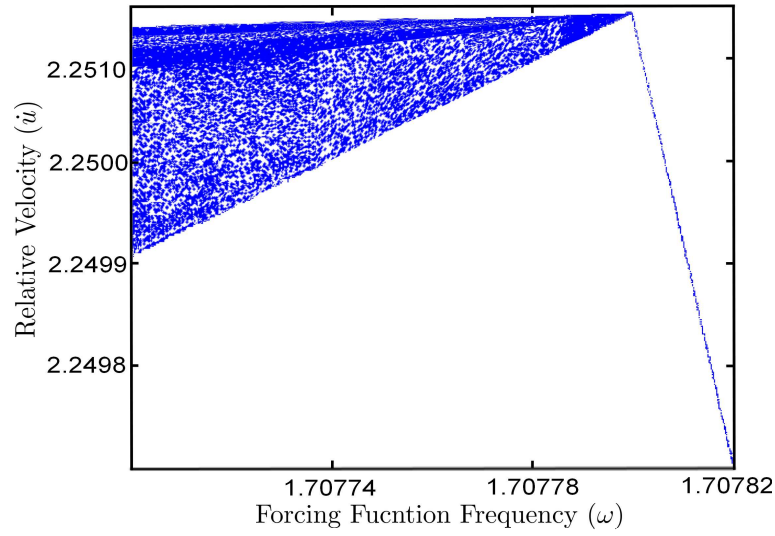


Figure 3.26: Bifurcation diagram obtained from the direct simulation of the TS fuzzy model (3.42) shows the grazing-sliding DIB at the frequency $\omega = 1.70778$.

Compared with that of the original system (Fig. 2.14), the bifurcation diagram in Fig. 3.26 shows that the TS fuzzy model (3.42) accurately exhibit the expected qualitative behaviour near the grazing-sliding event leading to a grazing-sliding DIB.

Example 3.9 (A Filippov system with two switching manifolds). Consider the following non-smooth autonomous system:

$$\dot{x} = \begin{cases} F_1(x), & \text{if } H_1(x) > 0 \\ F_2(x), & \text{if } H_2(x) < 0 \end{cases} \quad (3.43)$$

where there are two switching manifolds defined as zero-sets of smooth functions $H_1(x)$ and $H_2(x)$:

$$\begin{aligned} \Sigma_1 &:= \{x \in \mathbb{R}^2 : H_1(x) := x_2 + x_1 = 0\} \\ \Sigma_2 &:= \{x \in \mathbb{R}^2 : H_2(x) := x_2 = 0\} \end{aligned}$$

and the system dynamics when $H_1(x) \neq 0$, $H_2(x) \neq 0$, is governed by

$$\begin{aligned} F_1(x) &= \begin{pmatrix} -x_1 - 100x_2 - 0.5 |x_1| x_1 + u \\ 10x_1 - x_2 \end{pmatrix}, \\ F_2(x) &= \begin{pmatrix} -x_1 + 10x_2 + u \\ -100x_1 - x_2 - e^{\sin(x_1)} x_1^2 x_2 \end{pmatrix}, \end{aligned}$$

where $u \in \mathbb{R}^2$ is defined as a continuous input. We assume that the system (3.43) has a DoS of unity, meaning this non-smooth system is a Filippov-type system for which $F_1(x) \neq F_2(x)$, $\forall x \in \Sigma_1$, $\forall x \in \Sigma_2$. As apparent, the vector fields $F_1(x)$ and $F_2(x)$ are chosen to be the nonlinear functions of their arguments. To construct a non-smooth TS fuzzy model, the approach of representing fuzzy sub-vector fields by Taylor expansion,

explained in Section 3.2.6, can be employed. Ten linearization points are chosen for the system states x_1 and x_2 to achieve an acceptable accuracy. There chosen points are as follows:

$$\begin{aligned} x_1 &\in \{-15.5, -13.5, -10.5, -7.5, -3.5, -1.5, 0.5, 1.5, 3.5, 5.5\}, \\ x_2 &\in \{-10, -8, -5, -2, -1, 1, 2, 3, 4, 6\}, \end{aligned} \quad (3.44)$$

The respective membership functions are illustrated for both states in Fig. 3.27. The original vector fields F_1 and F_2 are then approximated by Taylor expansion on the above linearization points, as expounded in Section 3.2.6, and the following sub-systems are obtained for the fuzzy sub-vector field F_{m_1} :

$$\begin{aligned} A^1(m_1) &= \begin{bmatrix} 0.5 & -100 \\ 10 & -1 \end{bmatrix} = A^2(m_1) = A^3(m_1) = A^4(m_1) = A^5(m_1) = A^6(m_1), \\ A^7(m_1) &= \begin{bmatrix} -0.5 & -100 \\ 10 & -1 \end{bmatrix} = A^8(m_1) = A^9(m_1) = A^{10}(m_1), \quad B^j(m_1) = \begin{bmatrix} 1 \\ 0 \end{bmatrix}, \quad j = 1, 2, \dots, 10, \end{aligned}$$

and for the fuzzy sub-vector field F_{m_2} :

$$\begin{aligned} A^1(m_2) &= \begin{bmatrix} -1 & 10 \\ 131.5030 & -1 \end{bmatrix}, \quad A^2(m_2) = \begin{bmatrix} -1 & 10 \\ -25.1799 & -1 \end{bmatrix}, \quad A^3(m_2) = \begin{bmatrix} -1 & 10 \\ 72.2223 & -1 \end{bmatrix}, \\ A^4(m_2) &= \begin{bmatrix} -1 & 10 \\ -1.2523 & -1 \end{bmatrix}, \quad A^5(m_2) = \begin{bmatrix} -1 & 10 \\ 6.0750 & -1 \end{bmatrix}, \quad A^6(m_2) = \begin{bmatrix} -1 & 10 \\ -0.3297 & -1 \end{bmatrix}, \\ A^7(m_2) &= \begin{bmatrix} -1 & 10 \\ -4.6477 & -1 \end{bmatrix}, \quad A^8(m_2) = \begin{bmatrix} -1 & 10 \\ -8.9976 & -1 \end{bmatrix}, \quad A^9(m_2) = \begin{bmatrix} -1 & 10 \\ 6.4150 & -1 \end{bmatrix}, \\ A^{10}(m_2) &= \begin{bmatrix} -1 & 10 \\ -14.5121 & -1 \end{bmatrix}, \quad B^j(m_2) = \begin{bmatrix} 1 \\ 0 \end{bmatrix}, \quad j = 1, 2, \dots, 10. \end{aligned}$$

Considering the above sub-systems for F_{m_1} and F_{m_2} , a non-smooth TS fuzzy model of the system (3.43) can be constructed with the following model rules:

$$\begin{aligned} \textbf{Model Rule } j: \quad &\text{IF } x_1 \text{ is } \Gamma^1 \text{ and } x_2 \text{ is } \Gamma^2 \text{ THEN} \\ &\begin{cases} \dot{x} = A^j(m_i)x + B^j(m_i)u, \quad j = 1, 2, \dots, 10, \quad i = 1, 2, \\ m^+ = \xi(x, m), \end{cases} \end{aligned} \quad (3.45)$$

where two discrete states m_1 and m_2 are defined, and the function ξ describes their interaction with the following switch sets:

$$\begin{aligned} S_{1,2} &= \{x \in R^2 \mid x_1 = -x_2\}, \\ S_{2,1} &= \{x \in R^2 \mid x_2 = 0\}, \end{aligned} \quad (3.46)$$

By looking at the evolution of system states in Fig. 3.28b, it can be seen that the behaviour of the original system (Fig. 3.28a) is accurately approximated by TS fuzzy model (3.45), where the solution trajectories through switching between $S_{1,2}$ and $S_{2,1}$, eventually resides in an equilibrium point $(0, 0)$.

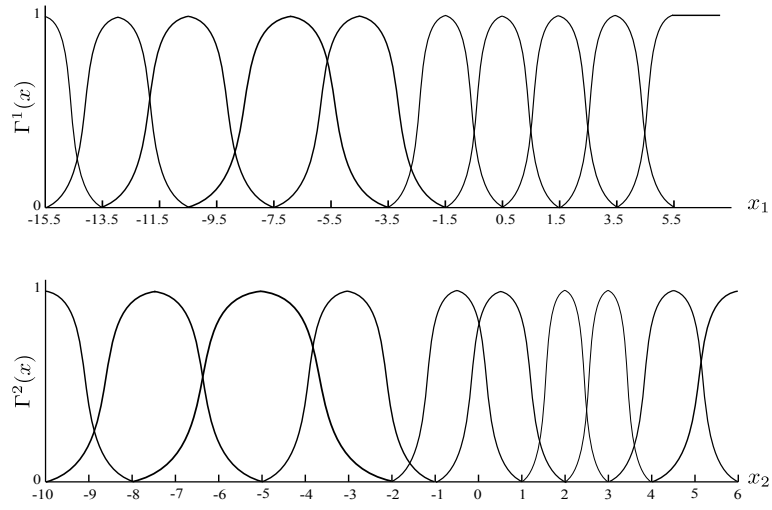
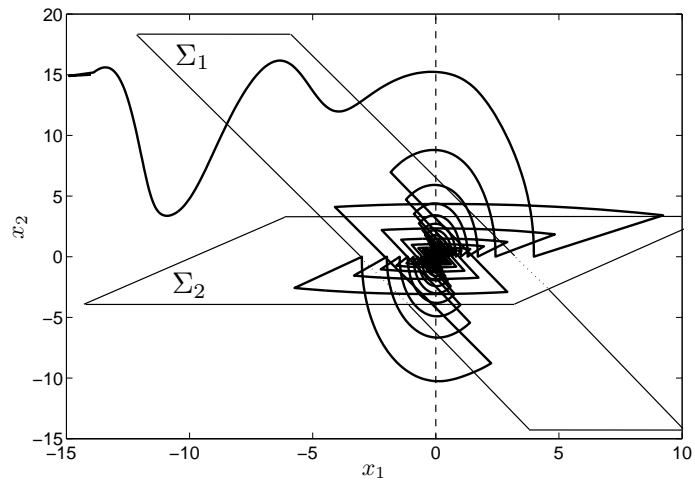
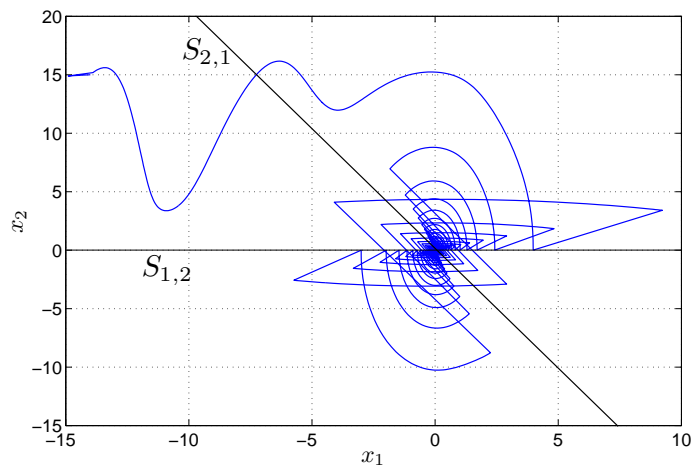


Figure 3.27: Membership functions for Example 3.9



(a)



(b)

Figure 3.28: Comparing (a) the original system and (b) the TS fuzzy model using the approach of Taylor Expansion for constructing non-smooth TS fuzzy models.

Indeed, the accuracy of the Taylor expansion approach depends on the chosen set of linearization points, as determined in (3.44), and the suitable membership functions, as chosen in Fig. 3.27. Furthermore, choosing an appropriate domain where the dynamics of the original function is intended to be approximated by the Taylor expansion approach is an essential step in constructing a non-smooth TS fuzzy model in terms of concentrating on the area needed to be analyzed. For instance, if assessing the stability of a system near a specific invariant set (equilibrium point or limit cycle) is desired, the domain of linearization points should be chosen such that the system trajectories are accurately represented in the neighborhood of the invariant set of interest, i.e. as performed for $x_1 \in [-15.5, 5.5]$ and $x_2 \in [-10, 6]$ in (3.44).

3.2.7 Numerical simulation

As briefly pointed out in the introductory chapter, a comprehensive theory to tackle numerical analysis and design of NSDS demands a solid formalism to include all combinations of discontinuity boundaries and accurate description of non-smooth transitions. To a large extent, this theory, has not yet been established in contrast to their smooth counterparts. More specifically, the direct implementation of numerical solutions to NSDS is impossible using widely-used numerical integration routines designed for smooth systems, since these are incapable of capturing the non-smooth transitions that normally occur in NSDS. Numerical routines for the direct simulation of NSDS have been dominantly developed based on two major approaches: *time stepping* routines and *event driven* routines.

Time stepping is the method employed when combining complementarity systems, describing a non-smooth problem with the set of differential algebraic equations together with inequality constraints [7, 121, 122]. Complementarity formalism, originally used to study rigid body dynamics and mechanical impacting systems, was later found suitable for the development of a specialized platform for modeling, analysis and design of different classes of non-smooth systems [123]. To formulate a non-smooth dynamic, a complementary problem needs a large number of constraints and the corresponding slack variables. Therefore, capturing non-smooth transitions (or events) is very time-consuming for the numerical integration routines using variable time intervals. The time stepping approach becomes an advantage in this respect as it considerably reduces the computational time when checking complementarily constraints at fixed time intervals. However, the drawback of this method is that several non-smooth events may be ignored or not accurately detected [121, 124].

To remedy this problem, event driven methods have been successfully employed in many software algorithms for low-dimensional non-smooth problems. These however have been mainly developed for academic curiosity. The great advantage of event-driven methods is their implementability on existing software platforms originally designed for smooth applications. This makes the development of a specialized and not to mention, costly platform like SICONOS unnecessary. For instance, Piironen and Kuznetsov have implemented the idea of *monitor functions* for the numerical integration routines in MATLAB/SIMULINK to accurately detect switching events of sliding Filippov's systems [125]. Similar routines have been developed by Nordmark and Piironen for the numerical simulation of

chattering phenomena in impacting system [126]. These algorithms can also be efficiently implemented in other commercial modeling and simulation packages like SCILAB, DSTOOL and AUTO'97. Tools such as SLIDECONT, developed as a driver for AUTO'97 by Dercole et al. [127], have been found to be very useful in locating unstable periodic orbits as well as stable ones and the ensuing bifurcation phenomena in sliding Filippov's systems. Its enhanced version, TC-HAT, developed by Thota and Dankowicz [128,129], is further able to analyze NSDS with discontinuous (state) jumps. Basically event driven methods are described as a continuation of trajectories in each phase space region S_i of a non-smooth system, which in turn, can be efficiently solved with well-established numerical integration routines for solving smooth dynamical systems [130]. Non-smooth transitions can be actually implemented with reinitializing the problem as a switching event occurs. Each switching manifold should be carefully defined as a zero set of smooth function $H_{ij} = 0$ for the numerical routine to detect the exact time of an event, and the set of transitional rules to indicate to which trajectory the problem should switch and be reinitialized. The advantages of event driven method can be briefly pointed out as:

1. Non-smooth events are detected accurately so the onset of a bifurcation, specifically a DIB, can be efficiently solved and pinpointed.
2. Reduces the computational time due to the use of variable time-step integration routines
3. Computation of bifurcation diagrams for the set of attracting solutions can be carried out directly using existing numerical routines, specially in the case of Monte Carlo bifurcation diagrams, where a set of initial conditions is chosen randomly to capture all competing attractors, e.g. period-3 attractor around $V_{in} = 24V$ in Fig. 2.6.

Nonetheless, high-dimensional non-smooth problems are the biggest concern for this method since very stiff approximation law for solving their numerical integration practically makes their simulation infeasible. TS fuzzy modeling discussed in this chapter employs event-driven methods to simulate the solution trajectories of a non-smooth system. Non-smooth TS fuzzy models can even formulate a high-dimensional non-smooth problem without the need for stiff solvers. This is owing to the fact that, each vector field within the phase-space region S_i of a non-smooth system can be approximated with a fuzzy sub-vector field F_{m_k} . Then, x^{k+1} , the next value of continuous fuzzy state x^k , can be derived using the simple formulation:

$$x^{k+1} = x^k + hF_{m_k} = x^k + h \sum_{j=1}^{l_{m_k}} w^j(x^k, m_k)(A^j(m_k)x^k + B^j(m_k)u^k + a^j(m_k)),$$

where h is the step length. The above formulation, essentially composed of affine sub-systems, can be solved using the simplest numerical routines available for solving ODEs, e.g. MATLAB `ode45` solver using explicit Runge-Kutta (4,5) formula or `ode23` solver using Runge-Kutta (2,3) formula in the case of mild stiffness. Switching to the next fuzzy sub-vector field is implemented by a collection of switch sets $S_{i,j}$ each describing an inequality condition. It is then monitored when the limit of the inequality, specified in a switch set

$S_{i,j}$ is *asymptotically* reached. If this is the case, the discrete state $m_k = m_i$ is changed to $m_{k+1} = m_j$. This routine can also be expressed by the pseudo code below:

$$\begin{aligned} &\text{IF } m_k = m_i \text{ AND } x^{k+1} \in S_{i,j} \text{ AND } x^k \notin S_{i,j} \\ &\text{THEN } m_{k+1} = m_j \quad \text{ELSE } m_{k+1} = m_i \end{aligned}$$

Although the degree of smoothness of a solution, using fuzzy formulation as above, may be actually higher than a formulation such as complementarity system, all the enumerated advantageous of the event driven method can be met. Most importantly, TS fuzzy formalism using the proposed structure of (3.12) is implemented entirely in a commercially-standard package such as MATLAB/SIMULINK. A few other simple examples in this thesis, avail from the Stateflow software tool in MATLAB/SIMULINK, originally designed for event-driven systems as a model of finite-state automata. In this case, a non-smooth TS fuzzy model can be composed of a portable C code generated from Stateflow chart, acting as switching sets, and SIMULINK models of fuzzy sub-vector fields. To examine the accuracy of the proposed formalism, all Filippov-type systems (sliding and non-sliding) have been additionally simulated using SLIDECONT driver for AUTO'97 in order to be compared with the developed TS fuzzy models in this thesis.

3.3 Summary

The existing structure for TS fuzzy modeling and its construction methods have been reviewed in the first part of this chapter. Through an example in Section 3.1.3 and later emphasizing the existence and uniqueness issues in Section 3.2.5, it has been shown that the current structure for smooth TS fuzzy modeling is incapable of representing the discontinuous nature and the ensuing nonlinearities observed in a non-smooth system. A TS fuzzy modeling structure, capable of representing NSDS, has been formally proposed (Definition 3.1 in Section 3.2.2) such that approximating models, which incorporates discrete event dynamics. Despite the simplicity of the proposed TS fuzzy formalism for NSDS, its powerful enough to accurately represent non-smooth systems with different DoS (as classified in Table 2.1). It has been discussed (Remark 3.3) that it is also possible for a non-smooth TS fuzzy model to represent discontinuous (jump) states to capture different resulting complex dynamics normally observed in impacting systems (with a DoS of zero). Two approaches for constructing such non-smooth TS fuzzy models have been proposed in Section 3.2.6.

It has been discussed in Section 3.2.7 that the proposed non-smooth TS fuzzy models, compared to other formalisms such as complementarity systems, are not so complicated to require special software platforms. In fact, non-smooth TS fuzzy models can take advantage of well-established solvers designed for smooth differential equations. Although formalisms like complementarity systems may be practically successful in bifurcation analysis (for instance, see the work of Santos [131] and the discussion of Brogliato et. al. in [132]), it cannot be guaranteed that such models lead to existence (or uniqueness) of a solution in all circumstances. As detailed in Section 3.2.5, existence and uniqueness results

have been extended, using the familiar existence theorem for Lipschitz continuity, to include non-smooth TS fuzzy formalism. As a result, the universal approximation theorem of fuzzy systems has been redefined to be inclusive of NSDS.

Non-smooth TS fuzzy models are originally designed to render bifurcation analysis (structural stability problems) and control design problems, which will be discussed in the subsequent chapters. It is advantageous for the proposed formalism to be used in a feedback structure forming a closed-loop TS fuzzy system. Without this capability, the non-smooth TS fuzzy structure cannot put to good use for control engineering applications where the overall models are mainly composed of local models connected in various configurations.

Chapter 4

Stability Analysis

As far as the laws of mathematics refer to reality, they are not certain, as far as they are certain, they do not refer to reality...

ALBERT EINSTEIN (1879-1955)

One of the most important, yet complicated subjects, in control theory as well as dynamical system theory is the stability of a nonlinear system. In the fundamental view of Lyapunov (asymptotic) stability, if the trajectory of a nonlinear system starts from an invariant set, to be stable, it must stay in the close neighborhood of that invariant set for all future times. As discussed in Chapter 3, the extension of well-established stability properties of smooth nonlinear systems to non-smooth systems is a demanding task specially in providing necessary and sufficient conditions to guarantee the stability of an invariant set that resides on a switching manifold or somehow loses its (structural) stability by crossing a discontinuity boundary. The main thrust of this chapter is to find a solution to these problems by providing a Lyapunov framework composed of stability conditions to assess (structural) stability of a non-smooth TS fuzzy systems based on the modeling structure of Definition 3.1. It is also explained how the stability conditions can be recast on Linear Matrix Inequalities (LMIs). By solving the resulting LMI problem for (non-smooth) TS fuzzy chaotic systems, the onset of bifurcation phenomenon can be accurately indicated.

4.1 Lyapunov's stability for smooth TS fuzzy systems

Studying the stability of smooth TS fuzzy systems of the form (3.6) in its classical notion has been, to date, dominantly characterized by use of the stability theorems originally developed by Lyapunov, a Russian mathematician and engineer who introduced the foundation of the theory of stability of motions in the late 19th century. His pioneering work on stability of nonlinear systems received the attention of control theorists only after the translations of his major publications in the western hemisphere in early 1960s [133, 134].

Numerous refinements have been proposed thereafter, based on Lyapunov's theory on the stability of motion for nonlinear systems, which carry his name. It was initially suggested by Lyapunov that the stability of a nonlinear system can be drawn by studying the behavior of a *linear system* obtained from linearizing around an equilibrium point, later referred to as Lyapunov's linearization method. This method, nonetheless, has not become popular for smooth nonlinear systems, due to the fact that the analysis only implies local stability properties and unlike Lipschitz continuity methods is not easily extendable for studying global properties. Instead, another Lyapunov's method, i.e. *Lyapunov's direct method*, has been found applicable in studying nonlinear systems (including TS fuzzy systems). This method, by assuming scalar auxiliary functions known as Lyapunov functions, can conclude the global stability of a system if certain formulated conditions based on those functions, are fulfilled. As highlighted in Section 2.2.4, the Lyapunov direct method is advantageous even in the case of non-smooth systems when the stability of an invariant set extending across or residing on the switching manifold, is to be investigated. Therefore, this chapter attempts to employ Lyapunov's direct method for studying the stability of non-smooth TS fuzzy systems. The stability of the complex form of invariant sets like periodic solutions is proven through finding a candidate Lyapunov function, which measures the energy of the perturbation of the invariant set of question. However, in this section, some fundamental definitions are first given to provide a general concept of stability in the Lyapunov's sense for a smooth TS fuzzy model (3.6). These definitions will be later extended to cover the novel notion of structural stability of invariant set (in the sense of Definition 3.1).

Definition 4.1 (Stability in the Lyapunov sense, cf. [9]) The continuous invariant set $x = 0$ of a smooth TS fuzzy model is

- stable if, for each $R > 0$, there exist $r = r(R) > 0$ such that

$$\|x_0\| < r \Rightarrow \|x(t)\| < R, \forall t \geq 0,$$

- asymptotically stable if it is stable and r can be chosen such that

$$\|x_0\| < r \Rightarrow \lim_{t \rightarrow \infty} \|x(t)\| = 0,$$

- exponentially stable if, for each $R > 0$, there exist $r = r(R) > 0$ and two scalars $k_1 = k_1(R) > 0$ and $k_2 = k_2(R) > 0$ such that

$$\|x_0\| < r \Rightarrow \|x(t)\| \leq k_1 e^{-k_2 t} \|x_0\|, \forall t \geq 0,$$

- unstable if non of the options above are satisfied.

The general notion of $B_\delta(x_i)$ is defined as

$$B_\delta(x_i) = \{x \in \mathbb{R}^n \mid \|x - x_i\| \leq \delta\},$$

to describe a spherical region or ball of continuous states with its center in x_i and radius δ . Therefore, a stabilization problem can be stated by the following condition

$$x(0) \in B_r(0) \Rightarrow x(t) \in B_R(0), \forall t \geq 0.$$

State convergence in asymptotic stability does not necessarily convey Lyapunov stability [10, 106] so the stability requirement in the definition of asymptotic stability is inevitable. However, it can be implied from the exponential state convergence to an invariant set, that a nonlinear system is Lyapunov stable, since r can be chosen such that $0 < r < \frac{R}{k_1}$ implying that $\|x(t)\| = k_1 e^{-k_2 t} \|x(0)\| \leq k_1 \|x(0)\| \leq k_1 r \leq R$.

Since $\|x(t)\| \rightarrow 0$ when $t \rightarrow \infty$ for an exponentially stable equilibrium point, exponential stability implies asymptotic stability. However, the converse is not true, as examples can be found which are stable but converge slower than any exponential function $e^{-k_2 t}$, cf. [10].

Figure 4.1 illustrates the geometrical notion of stability in the Lyapunov sense. The center of two spheres with the radius of B_r and B_R is assumed to be an invariant set, e.g. an equilibrium point resides at the origin. The system is Lyapunov stable, if all solution trajectories initiating in the sphere $B_r(0)$ will remain in sphere $B_R(0)$ for all $t \geq 0$. If a system is stable and all solution trajectories converge to an invariant set, then the invariant set is *asymptotically* stable. If an invariant set is asymptotically stable and all solution trajectories converge exponentially to that invariant set, then the invariant set is exponentially stable. As mentioned, exponential stability ($\|x(t)\| \rightarrow 0$ when $t \rightarrow \infty$) conveys asymptotic stability of invariant set but the converse is not always true, cf. [54, 106]. An invariant set will become unstable, if there exist some solution trajectories initiating inside the sphere $B_r(0)$ with an infinitesimal radius of $r > 0$, and exiting the sphere $B_R(0)$ for all $t \geq 0$.

If there is a small perturbation in the solution trajectories to deviate them from the asymptotically stable invariant set, the solution trajectories will eventually converge back to that invariant set when $t \rightarrow +\infty$. Although asymptotical stability carries the more general notion of stability, it does not disclose any information about how fast the solution trajectories can converge to the invariant set in question. Instead, exponential stability can give an estimate of convergence rate to a stable invariant set by imposing a boundary on the solution states at any time. In this manner, the magnitude of the state vector is reduced to $e^{-\tau} \|x(0)\|$ after a time of $\frac{\ln k_1 + \tau}{k_2}$.

Definition 4.2 (Global stability) Definition 4.1 explains the local behavior of solution trajectories (of a smooth TS fuzzy system) when initiating close to an invariant set. Global stability explains the global behavior of solution trajectories when initiated at a distance from the invariant set of question. Therefore, if the continuous invariant set of a smooth TS fuzzy system is asymptotically (or exponentially) stable for any initial fuzzy state then that invariant set is globally asymptotically (or exponentially) stable. In this sense, the globally stable invariant set must be unique. Assuming another globally stable invariant set, e.g. equilibrium point at the origin, would imply that all the solution trajectories would converge to that invariant set instead of the first one for all $t \geq 0$, which

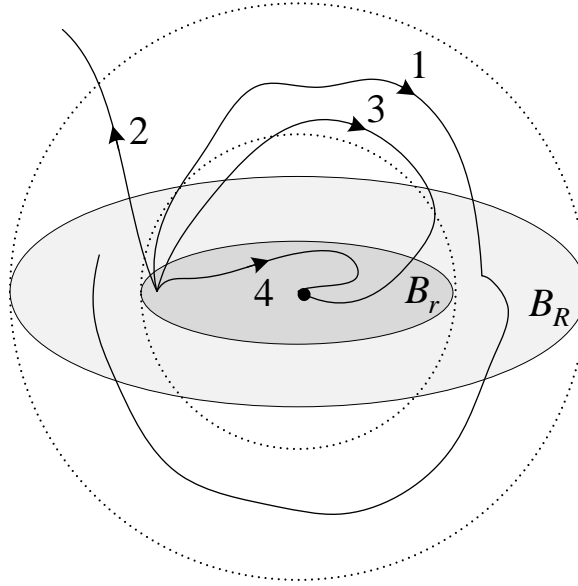


Figure 4.1: Geometrical notion of Lyapunov stability where solution trajectory **1** is stable, solution trajectory **2** is unstable, solution trajectory **3** is asymptotically stable and solution trajectory **4** is exponentially stable.

clearly contradicts our initial assumption. Accordingly, examining global exponential (or asymptotic) stability for a TS fuzzy system with multiple invariant sets is implausible. The global stability of a unique solution nonetheless may result in the need to study more complex scenarios of periodic solutions than mere equilibria.

Definition 4.3 (Region of attraction) An asymptotically stable invariant set means that if a solution initiates close to that set, it will converge and remain there for all future times. The boundary of those initial states is called a *region of attraction* which is an open, connected, invariant set by itself [9]. In the same sense, the set of all initial states of a smooth TS fuzzy system that eventually converge to an asymptotically stable invariant set is called the region of attraction and denoted as RoA . Analytical derivation of RoA for any non-globally stable invariant set is, at best, a daunting task. There are a few methods, which employ geometrical theory of dynamical systems [135], and are not easily applicable. Nevertheless, the estimate of RoA can be calculated via Lyapunov's direct method, which also applies to TS fuzzy systems.

Definition 4.4 (Exponential region of attraction) The region of exponential attraction of a smooth TS fuzzy system (3.6) (or (1.4)), denoted by $R(k_1, k_2)$, is the set of initial fuzzy states $x_0 \in \mathcal{F}_0$ such that the continuous solution trajectories converge exponentially to the invariant set. This can be described as

$$R(k_1, k_2) = \{x_0 \in \mathcal{F}_0 \mid x(t) \rightarrow 0 \text{ as } t \rightarrow \infty \\ \text{and } \|x(t)\| \leq k_1 e^{-k_2 t} \|x_0\|, t \geq 0, k_1 \geq 0, k_2 \geq 0\} \quad (4.1)$$

Since exponential attraction conveys asymptotic attraction, $R(k_1, k_2)$ is a subset of RoA for all positive values of constants k_1 and k_2 . By (4.1), the estimate of the region of exponential attraction can be calculated via Lyapunov's direct method.

4.1.1 Existing formulations for stability analysis

In terms of Lyapunov's direct method, sufficient conditions for the stability of a smooth linear TS fuzzy system (if the term $B^j u$ is dropped) is guaranteed based on the following basic theorem:

Theorem 4.1. (Basic stability for smooth TS fuzzy systems [136]) Assume a TS fuzzy system $\dot{x} = \sum_{j=1}^l w^j(\theta) A^j x$ with the associated fuzzy rules as defined for (3.6). The asymptotic stability of this system can be guaranteed if there is a symmetric positive definite matrix $P = P^T$ such that the following conditions are fulfilled:

$$(A^j)^T P + P A^j < 0, \quad \forall j = 1, 2, \dots, l. \quad (4.2)$$

If we consider a *common* quadratic Lyapunov function candidate $V(x) = x^T P x$, the condition above can be easily proven based on the asymptotic stability of polytypic systems [136]. Sufficient conditions for basic exponential stability can also be guaranteed via the Rayleigh-Ritz theorem [137] as:

$$\dot{V}(x) \leq -\min_j \lambda_{max}((A^j)^T P + P A^j) \|x\|^2. \quad (4.3)$$

The search for the common Lyapunov function $V(x) = x^T P x$ can be formulated as a Linear Matrix Inequality problem, which is solved for a matrix $P > 0$ in the whole state space, using interior-point convex optimization algorithms [136, 138].

Theorem 4.1 only provides basic stability conditions. However, the stability of a smooth TS fuzzy model becomes important when the control input u is considered for each affine sub-system in (3.6). By introducing a state-feedback controller for each sub-system, and substituting in (3.6), the model is converted into the following TS fuzzy system:

$$\dot{x} = \sum_{j=1}^l \sum_{i=1}^l w^j(\theta) w^i(\theta) (A^j + B^j K^i) x, \quad (4.4)$$

where the control rules are $u^j = \sum_{j=1}^l w^j(\theta) K^j x$ with the identical rule base as the model rules. The constant gain matrices K^j , $j = 1, \dots, q$ need to be designed by some bounding conditions. The structure of (4.4) is famously referred as parallel-distributed compensation (PDC) in the literature as a controller is actually designed for each affine local sub-system [28, 139–141]. The asymptotic stability condition of Theorem 4.1, can then be redefined for the TS fuzzy control system (4.4) with the following theorem:

Theorem 4.2. (Asymptotic stability for PDC structure of smooth (continuous-time) TS fuzzy systems [142]) Asymptotic stability of the TS fuzzy system (4.4) is guaranteed if a common positive-definite matrix P exists such that the following conditions are fulfilled:

$$(A^j + B^j K^j)^T P + P(A^j + B^j K^j) < 0, \quad \forall j = 1, 2, \dots, l \quad (4.5)$$

and

$$\left\{ \frac{(A^j + B^j K^i) + (A^i + B^i K^j)}{2} \right\}^T P + P \left\{ \frac{(A^j + B^j K^i) + (A^i + B^i K^j)}{2} \right\} < 0$$

for $i < j$, except the pairs (i, j) such that $w^j(\theta)w^i(\theta) = 0$. (4.6)

A similar stability theorem exists for the asymptotic stability of discrete-time TS fuzzy systems [28, 139].

Theorem 4.2 provides sufficient conditions for global asymptotic stability of smooth TS fuzzy models via PDC design, since it attempts to find common Lyapunov function candidates $V(x) = x^T P x$ decreasing in the whole state space. Several extended stability conditions, based on Theorem 4.1 and Theorem 4.2, have been proposed to stabilize and control smooth nonlinear systems including typical chaotic systems such as Lorenz system, Chua's circuit, or the flexible-joint robot arm model [139, 140, 143] (also see [28] and the references therein). In all of the stability conditions, the search for Lyapunov functions are formulated as convex quadratic linear matrix inequality (LMI) problems. For instance, if robust stability is desired, some parametric uncertainties resulting from unmodeled dynamics, modeling errors or external disturbances, can be introduced in the close-loop structure (4.4) as:

$$\dot{x} = \sum_{j=1}^l \sum_{i=1}^l w^j(\theta)w^i(\theta)((A^j + \Delta A^j) + (B^j + \Delta B^j)K^i)x, \quad (4.7)$$

where ΔA^j and ΔB^j are time-varying matrices representing parametric uncertainties in the plant model. Furthermore it is assumed that matrices ΔA^j and ΔB^j are norm-bounded and structured according to the following assumption:

Assumption 4.1. The parametric uncertainties considered for the closed-loop TS fuzzy system (4.7) are norm-bounded matrices in the form:

$$[\Delta A^j \ \Delta B^j] = D^j F^j [E^{1j} \ E^{2j}],$$

where $D^j \in \mathbb{R}^{n \times n}$, $E^{1j} \in \mathbb{R}^{n \times n}$ and $E^{2j} \in \mathbb{R}^{n \times n}$ are known matrices, and $F^j(m) \in \mathbb{R}^{n \times n}$ is an unknown matrix function with *Lebesgue*-measurable elements such that $(F^j(m))^T F^j(m) \leq I_{n \times n}$.

Therefore, verifying global stability in Lyapunov's sense, can be formulated as the LMI problem below:

Theorem 4.3. (Robust stability for PDC structure of smooth (continuous-time) TS fuzzy systems) The continuous-time TS fuzzy system (4.7) is asymptotically stable if there exist a common matrix $P^T = P > 0$, some gain matrices K^j , and some scalars ϵ^{ji} , ($j, i = 1, \dots, l$), such that the LMI conditions below are fulfilled:

$$\begin{bmatrix} \Psi^{jj} & * & * \\ E^{1j}Q + E^{2j}M^j & -\epsilon^{jj}I & * \\ (D^j)^T & 0 & (-\epsilon^{jj})^{-1}I \end{bmatrix} < 0, \quad 1 \leq j \leq l, \quad (4.8)$$

$$\begin{bmatrix} \Upsilon^{jj} & * & * & * & * \\ E^{1j}Q + E^{2j}M^i & -\epsilon^{jj}I & * & * & * \\ E^{1i}Q + E^{2i}M^j & 0 & -\epsilon^{jj}I & * & * \\ (D^j)^T & 0 & 0 & (-\epsilon^{jj})^{-1}I & * \\ (D^i)^T & 0 & 0 & 0 & (-\epsilon^{jj})^{-1}I \end{bmatrix} < 0, \quad 1 \leq j < i \leq l, \quad (4.9)$$

where

$$\begin{aligned} \Psi^{jj} &= Q(A^j)^T + A^jQ + (M^j)^T(B^j)^T + B^jM^j, \\ \Upsilon^{jj} &= Q(A^j)^T + A^jQ + Q(A^i)^T + A^iQ + (M^i)^T(B^j)^T + B^jM^i + (M^j)^T(B^i)^T + B^iM^j, \\ Q &= P^{-1}, \\ M^j &= K^jP^{-1}, \end{aligned}$$

where $'*'$ stands for the transposed elements in the symmetric positions.

The proof of Theorem 4.3 can be established if we allow the common Lyapunov function to be represented by a positive definite matrix as $V = x^T Px$ [28, 79]. The common Lyapunov function approach may result in formulations such as (4.8) and (4.9) easily guaranteeing global stability. However, in many cases, it may lead to conservative formulations. These conservative formulations cannot be numerically solved using existing convex optimization methods. Therefore they are found misleadingly infeasible whereas the system may be actually stable. In the realm of smooth model-based TS fuzzy systems, there have been suggestions to relax this conservativeness. Early attempts were largely focused on adding additional semi-definite terms to the LMI formulations (4.5) and (4.6) of Theorem 4.2 [142, 144–147]. These approaches, nonetheless, have not proposed effective solutions to the issue of conservativeness when dealing with complex smooth nonlinear systems. In a quest for an effective solution to conservative LMI problems, Lyapunov approaches have been proposed in terms of fuzzy stabilization problems where Lyapunov function candidates are defined as a piecewise or switched Lyapunov functions [148–153]. In the switched Lyapunov function (SLF) approach, the candidate function is essentially composed of switching positive semi-definite matrices P_i , $i = 1, 2, \dots, N$ as:

$$V(t, x(t)) = x(t)^T \left(\sum_{i=1}^N \alpha_i(t) P_i \right) x(t),$$

where $\alpha : Z^+ \rightarrow \{0, 1\}$, $\sum_{i=1}^N \alpha_i(t) = 1$, and $\alpha_i(t_1) = 1$ means that the matrix P_i is activated along with the local affine sub-systems (A_i, B_i) at time t_1 . Normally the

structure of SLF should be similar to that of the system description, representing the dynamics of a smooth nonlinear system as a switching fuzzy system. In this case, the equilibrium point is asymptotically stable if such a Lyapunov function $V(t, x(t))$ exists and decreasing along the solution of a fuzzy system as described by:

$$\Delta V(t, x(t)) = V(t+1, x(t+1)) - V(t, x(t)) < 0, \text{ for all } t$$

In the piecewise Lyapunov function approach, normally Lyapunov function candidates are composed of different symmetric matrices P_i , $i = 1, 2, \dots, N$ as:

$$V(x) = \{x^T P_i x\}, \quad (4.10)$$

where each P_i is allocated to a separated region of state space, e.g. operating region in smooth TS fuzzy model (3.6), (see Fig. 3.8 and also the discussion on the existence and uniqueness of solution to smooth TS fuzzy models in Section 3.2.5). For less conservative LMI formulations, each P_i can be further parameterized as $P_i = F_i P F_i$ where F_i are known matrices for each operating region and P is an unknown matrix. LMI formulations for the (operating) regions can also be parameterized as $E_i R E_i$, where each given matrix E_i is allocated to an (operating) region and $R = R^T$ are the unknown matrices to be solved. The sufficient condition for asymptotic stability of equilibria is verified if the continuous piecewise Lyapunov functions (4.10) exist and decreasing along the solution of a smooth TS fuzzy system. This means if for the positive definite matrices P_i , $i = 1, 2, \dots, N$, the following term:

$$\sum_{k=1}^N \delta_{jik} (P_i - P_k), \quad \delta_{jik} \geq 0$$

is added to any of the LMI stability conditions of Theorems 4.1, 4.2 and 4.3, the resulting conditions must be negative definite. One of the main obstacles to this approach is that, in some cases, the stabilization problem based on the candidate Lyapunov functions (4.10) should be recast as Bilinear Matrix Inequalities (BMI) conditions, not LMI conditions [154, 155]. In general, BMIs are very complicated optimization problems for which a rigorous solution algorithm has not yet been discovered [156, 157] (see also Appendix B). As a consequence, BMI conditions should be transformed to LMI conditions via techniques such as completing squares [158] or additional parametrization [159], to be solvable by current optimization methods. Nevertheless, the transformed LMI conditions may still end up in a conservative formulation.

Another approach that have recently received some attention is the fuzzy Lyapunov function approach where the function candidates can be defined as convex combination of symmetric matrices P_j , $i = 1, 2, \dots, l$ [155, 158, 160, 161]:

$$V(x) = x^T \left\{ \sum_{j=1}^l w^j(\theta) P_j \right\} x, \quad (4.11)$$

where l is the number of rules as described in the smooth TS fuzzy model (3.6). In this approach, a Lyapunov function (positive semi-definite matrix P_j) is associated with

each model rule and the asymptotic stability can be guaranteed if the derivative of (4.11) is negative definite along the trajectory of a smooth TS fuzzy system. Tanaka et al. showed that using fuzzy Lyapunov functions, BMIs can be avoided by directly formulating stability conditions as LMI problems via descriptor representations of TS fuzzy close-loop systems [155]. In this respect, the LMI problem, which is less conservative comparing to common Lyapunov function approaches, assess the asymptotic stability of equilibria if the symmetric positive semi-definite matrices P_j , $i = 1, 2, \dots, l$ exist and if by incorporating the term like

$$\sum_{k=1}^{l-1} \delta_k (P_k - P_l), \quad k = 1, 2, \dots, l-1$$

in the LMIs of Theorem 4.2, the overall condition becomes negative definite.

4.2 Structural stability analysis

In this section, stability conditions are formulated for structural stability of non-smooth TS fuzzy systems as described in Definition 3.1. The concept of structural stability of an invariant set (in the sense of Definition 2.1) for non-smooth systems has already been discussed in Section 2.2.4. The advantage of the proposed stability results is that structural stability of a periodic solution can be verified using the (non-smooth) Lyapunov approach, instead of the existing yet complicated discontinuity mapping approach outlined in Chapter 2. In this approach, the search for Lyapunov function candidates can be automated by recasting on LMI problems. However, the resulting LMI stabilization problems provide formulations for bifurcation analysis able to predict the edge of DIBs. This is important since the existing stability results for smooth TS fuzzy models are centered on the classical notion of stability (stability of equilibria).

The fuzzy model considered for the stability (bifurcation) analysis in this chapter is the non-smooth TS fuzzy model, recalled here as:

$$\begin{cases} \dot{x} = \sum_{j=1}^l w^j(\theta, m_i) (A^j(m_i)x + B^j(m_i)u) \\ m^+ = \xi(x, m) \end{cases} \quad (4.12)$$

where $x \in \mathbb{R}^n$ is a continuous fuzzy state, $m_i \in M$, $i \in I_N = \{1, 2, \dots, N\}$ is a discrete fuzzy state, $A^j(m_i) \in \mathbb{R}^{n \times n}$, $B^j(m_i) \in \mathbb{R}^n$, $w^j: \mathbb{R}^n \times M \rightarrow [0, 1]$, $j \in I_l$, are continuous weighting functions satisfying $\sum_{j=1}^l w^j(\theta, m) = 1$ and l is the overall number of fuzzy rules. Each discrete state $m_i \in M$ is associated with a specific *fuzzy sub-vector field* F_{m_i} as defined by (3.13). The fuzzy state space \mathcal{F} is the Cartesian product $\mathbb{R}^n \times M$. Discrete state switchings are described by switch sets (Remark 3.2):

$$S_{i,k} = \{x \in \mathbb{R}^n \mid m_k = \xi(x, m_i)\}, \quad i \in I_N, \quad k \in I_N, \quad (4.13)$$

All the remarks (Remarks 3.1 to 3.9) of Definition 3.1 (and Definition 3.2 when applicable) is considered to be valid for the model-based stability analysis in this Chapter along with all of the assumptions made (Assumptions 3.1, 3.2 and 3.3).

4.2.1 Non-smooth Lyapunov functions

The Lyapunov approach employed for model-based stability analysis here is the non-smooth (piecewise in time) Lyapunov function approach. Therefore, searching for Lyapunov functions can be formulated in a part of the fuzzy state space and not in the whole space such as when using the common Lyapunov function approach. There are two main reasons behind choosing this approach.

- First, proving asymptotic stability for a non-smooth system, as pointed out in Chapter 2, based on common Lyapunov functions in simple scenarios such as an equilibrium point lying on the switching manifold is implausible [7]. With the same rationale, studying the stability of more complex scenarios of limit cycles with respect to the switching manifold would be even more difficult. Therefore selecting the non-smooth Lyapunov approach for studying non-smooth systems seems inevitable [109, 162] and even synonymous in the case of non-smooth TS fuzzy formalism proposed in this thesis.
- Second, as pointed out in Section 4.1.1, although the formulations for stability results based on common Lyapunov functions are straightforward, in a considerable number of attempts (even in the case of smooth TS fuzzy systems) this leads to conservative results. That's why alternative Lyapunov approaches, outlined in Section 4.1.1, have been suggested in the literature (for smooth TS fuzzy systems) to find remedies for problems. Therefore, for the formulations proposed in this thesis, the non-smooth Lyapunov function approach is selected to achieve less conservative LMI formulations.

The partitioning of the fuzzy state space \mathcal{F} (\mathcal{F} in the sense of Definition 3.1 where both continuous fuzzy states and discrete fuzzy states exist in a system) into Δ detached but flexible regions is a milestone in constructing non-smooth Lyapunov function candidates. Therefore, we let the regions $\Omega \subseteq \mathcal{F}$ be partitioned such that $\Omega_1 \cup \dots \cup \Omega_\Delta = \Omega$, $\Omega_q \cap \Omega_r = \emptyset$, $q \neq r$, $q, r \in I_\Delta$. It is assumed that if a solution trajectory initiates in the region Ω , t_k , $k = 1, 2, \dots$, it can pass through to another region on the condition that $t_k < t_{k+1}$. Note that with this assumption even in the case of infinite partitioning (for instance if a partition is allocated to each solution trajectory of a non-smooth TS fuzzy system with different initial conditions), the trajectory never passes through another region unless it fulfills the requirement $t_k < t_{k+1}$. Therefore, if we assume a solution trajectory passes through to region Ω_q at time t_{k-1} , and then passes through to region Ω_r at time t_k and then passes through another region, we can show this evolution by $(x, m) \in \Omega_q$, $t \in \langle t_{k-1} \ t_k \rangle$ and for the next $(x, m) \in \Omega_r$, $t \in \langle t_k \ t_{k+1} \rangle$.

Let region Ω be a fuzzy set, the following subsets can then be defined:

$$\begin{aligned} \Omega^x &= \{x \in \mathbb{R}^2 \mid (x, m) \in \Omega\}, \text{ including continuous fuzzy states,} \\ \Omega^{x, m_i} &= \{x \in \mathbb{R}^2 \mid (x, m) \in \Omega\}, \text{ including continuous fuzzy states,} \\ \Omega^m &= \{m \in M \mid (x, m) \in \Omega\}, \text{ including discrete fuzzy states.} \end{aligned}$$

Let Λ_{qr} be a set of fuzzy states for which the solution trajectory satisfies (4.12), with initial states $(x_0, m_0) \in \mathcal{F}_0$, and passes from Ω_q to Ω_r , i.e.:

$$\Lambda_{qr} = \{(x, m) \in \Omega \mid \exists t < t_0, \text{ such that } (x(t^-), m(t^-)) \in \Omega_q, (x(t), m(t)) \in \Omega_r\} \quad (4.14)$$

Therefore Λ_{qr} , $q, r \in I_\Delta$, $q \neq r$ can represent boundary regions, which are normally given by the hyperplanes of a region, or the switching manifold of a non-smooth model. If the regions Ω_q^x and Ω_r^x share the same boundary, then $\Lambda_{qr} \neq \emptyset$, implying $\partial\Omega_q^x \cap \partial\Omega_r^x \neq \emptyset$. This is a sufficient condition, nonetheless, due to the fact that the solution trajectory must also move through from one region to another. Therefore if we allow

$$I_\Lambda = \{(q, r) \mid \Lambda_{qr} \neq \emptyset\}, \quad (4.15)$$

which is a set of tuples indicating at least one point for which the solution trajectory moves through from Ω_q to Ω_r . As mentioned before, the state-space partitioning in our approach is flexible. This means that the regions are not necessarily detached by switch sets (4.13) (describing switching manifolds) and a fuzzy sub-vector field can be partitioned to a number of regions (see also Section 3.2.6 for approaches of constructing fuzzy sub-vector fields). Furthermore, two neighboring fuzzy sub-vector fields F_{m_i} and F_{m_k} can share a region disregarding $S_{i,k}$. Nevertheless, in most cases, the regions are detached when the switching occurs by switch sets (intersecting the switching manifold); hence, (as above) the set Λ_{qr}^x represents the region where $S_{i,k} \cap \Lambda_{qr}^x \neq \emptyset$.

The non-smooth Lyapunov function candidates can be defined as

$$V(x) = V_q(x) \text{ when } (x, m) \in \Omega_q \quad (4.16)$$

where $V(x)$ is a non-smooth Lyapunov function at the neighboring regions Λ_{qr} , $(q, r) \in I_\Lambda$. $V(x)$ is composed of local smooth Lyapunov functions $V_q : \text{cl}\Omega_q^x \rightarrow \mathbb{R}$, $q \in I_\Delta$, representing the system's (abstract) energy in each region Ω_q (cl. denotes the closure of a set, which is the smallest closed set containing the set). Considering the assumption of $t_k < t_{k+1}$ for every solution trajectory initiating from Ω , $V(x)$ is also considered *piecewise continuous* as a function of time (see Fig. 4.2). As $V_q(x)$ is assumed to be continuously differentiable on $\text{cl}\Omega_q^x$, $q \in I_\Delta$, using (4.12) the time derivative of $V_q(x)$ is:

$$\dot{V}_q(x) = \sum_{j=1}^l w^j(\theta, m) \frac{\partial V_q(x)}{\partial t} (A^j(m)x + B^j(m)), \quad (x, m) \in \Omega_q \quad (4.17)$$

which, as can be seen, depends on the discrete state m . It is obvious that if we consider the whole \mathcal{F} as one region $\Omega = \mathcal{F}$, the non-smooth Lyapunov function (4.16) becomes a common (and smooth) Lyapunov function when the region $\Lambda_{qr} = \emptyset$ since the switch sets $S_{i,k} = \emptyset$ (no switching occurs). This simply implies that for a stable system, a common Lyapunov function must be decreasing along the trajectories regardless of the switching of fuzzy sub-vector fields. However, as illustrated by Example 3.4, even in the simple case of equilibria, a non-smooth TS fuzzy system can be stable with possessing all or a few individual unstable sub-systems belong to its sub-vector fields. Therefore, the common

Lyapunov function approach will be unable to verify the actual stability.

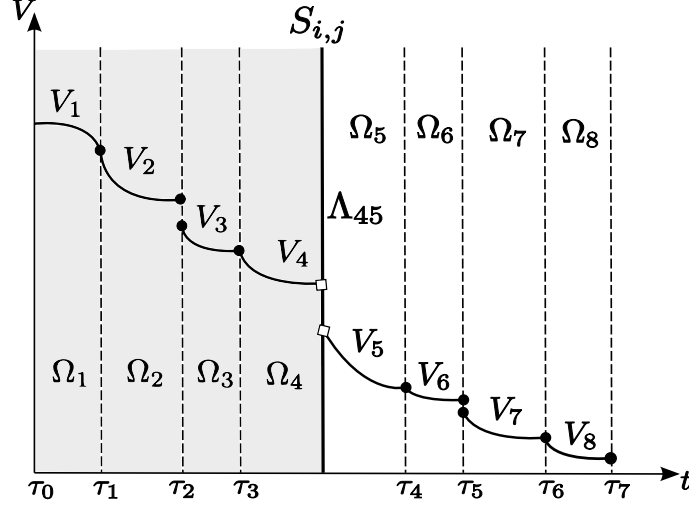


Figure 4.2: The non-smooth Lyapunov function candidate is non-smooth at region Λ_{45} (where the switching $S_{i,j}$ occurs) and piecewise-continuous with respect to time in every region Ω_q where the local functions V_q should be reduced to prove stability.

The theorems for structural stability of non-smooth TS fuzzy models, presented in the following sections, are developed as LMI stabilization problems searching for non-smooth Lyapunov functions of the form (4.16). To formulate LMI problems, non-smooth Lyapunov function candidate (4.16) is first defined as piecewise quadratic matrices with the structure:

$$(x, m) \in \Omega_q, \quad V_q(x) = \pi_q + 2p_q^T x + x^T P_q x, \quad (4.18)$$

where a local Lyapunov function $V_q(x)$ is defined as in (4.16), allocated to a local region Ω_q , $q \in I_\Delta$, and $\pi_q \in \mathbb{R}$, $p_q \in \mathbb{R}^n$ and $P_q = P_q^T \in \mathbb{R}^n \times \mathbb{R}^n$, $q \in I_\Delta$. (4.18) can also be written as

$$(x, m) \in \Omega_q, \quad V_q(x) = \tilde{x}^T \tilde{P}_q \tilde{x} \quad (4.19)$$

by defining

$$\tilde{x} = \begin{bmatrix} x \\ 1 \end{bmatrix}, \quad \tilde{P}_q = \begin{bmatrix} P_q & p_q \\ p_q^T & \pi_q \end{bmatrix}. \quad (4.20)$$

4.3 Stability theorems for Filippov-type systems

All the theorems, presented here, actually link the idea of asymptotic (exponential) Lyapunov stability with the novel notion of structural stability. The LMI stabilization theorems are based on TS fuzzy formalism originally proposed for the stability analysis of DC-DC converters (non-sliding Filippov-type systems discussed in case study I) in [116, 118, 163] and later extended for the analysis of impacting systems (case study II) in [120]. The bifurcation analysis for sliding Filippov's system (dry-friction oscillator in the case study III) can also exert the proposed theorem, which will be shown later in this chapter.

Linear Matrix Inequalities, their concepts and theories which need to be known for the

material of the subsequent chapters, are explained in Appendix B.

Now, if we define

$$\tilde{I} = \begin{bmatrix} I & 0 \\ 0 & 0 \end{bmatrix}$$

where $\tilde{I} \in \mathbb{R}^{n+1} \times \mathbb{R}^{n+1}$, $I \in \mathbb{R}^{n+1} \times \mathbb{R}^{n+1}$ is the identity matrix, and $\tilde{x} = \begin{bmatrix} x \\ 1 \end{bmatrix}$. The first LMI stabilization problem, based on non-smooth Lyapunov function candidates (4.18), is stated by the following theorem:

Theorem 4.4: If there exist piecewise quadratic matrices $\tilde{P}_q, q \in I_\Delta$ as defined by (4.20) such that:

1. $\alpha > 0, \beta > 0, \gamma > 0$
2. $x \in \Omega_q, \alpha \tilde{x}^T \tilde{I} \tilde{x} \leq \tilde{x}^T \tilde{P}_q \tilde{x} \leq \beta \tilde{x}^T \tilde{I} \tilde{x}, q \in I_\Delta$
3. $(x, m) \in \Omega_q, \tilde{x}^T \begin{bmatrix} (A^j(m))^T P_q + P_q A^j(m) & P_q B^j(m) + (A^j(m))^T p_q \\ (B^j(m))^T P_q + p_q^T A^j(m) & (B^j(m))^T p_q + p_q^T B^j(m) \end{bmatrix} \tilde{x} \leq -\gamma \tilde{x}^T \tilde{I} \tilde{x}, m_i \in \Omega_q^m, q \in I_\Delta$
4. $x \in \Omega_{qr}, \tilde{x}^T \tilde{P}_r \tilde{x} \leq \tilde{x}^T \tilde{P}_q \tilde{x}, (q, r) \in I_\Delta$

then the invariant set (limit cycle) is structurally stable in the sense of Lyapunov or the periodic solution exponentially converges to the stable fixed point.

Proof: First we must assume that $\alpha : \mathbb{R}^+ \rightarrow \mathbb{R}^+$ and $\beta : \mathbb{R}^+ \rightarrow \mathbb{R}^+$ are class \mathcal{K} functions. A class \mathcal{K} function is a smooth function $\alpha(0) = 0, \alpha(z) > 0, z > 0$, which should satisfy the condition $\alpha(z_1) \leq \alpha(z_2)$ for $z_1 < z_2$ [9]. Second, we assume that for proving the stability of periodic solutions, the system states (x, m) must converge to the stable fixed point, which is the intersection of the stable limit cycle of interest with the Poincaré section (see Definition 2.5). In this proof and without the loss of generality, the fixed point is considered to be an origin. In this way, structural stability of a periodic solution can be verified by the exponential (asymptotic) stability of the fixed point in the sense of Lyapunov.

To prove stability, it must be first shown that for any $R > 0$ (any $R > 0$ such that $B_R(0)$ is included in Ω_x) there exists $r(R) > 0$ such that $\|x_0\| < r$, which means that $\|x(t)\| < R$ for all $t \geq 0$. Due to the continuity of class \mathcal{K} functions, it can be deduced from the second condition that for any $R > 0$ there exists $r(R) > 0$ such that $\beta(r) > \alpha(R)$. If we let the initial fuzzy state $(x_0, m_0) \in \mathcal{F}_0$ be chosen such that $\|x_0\| < r$ and also let t_k be the consecutive times when the solution trajectory moves through from one region to another, the third condition requires that the candidate Lyapunov function (4.16) reduces along the solution trajectories in every region, and the fourth condition requires that the candidate Lyapunov function (4.16) reduces along the solution trajectories at every discrete state switching (crossing the switching manifold Σ). Accordingly, $V(x(t)) \leq V(x_0)$ for all $t \geq 0$, which can be proved for the asymptotic and exponential stability shown below. Thus,

$$\alpha(\|x(t)\|) \leq V(x(t)) \leq V(x_0) \leq \beta(\|x_0\|) \leq \beta(r) < \alpha(R) \quad (4.21)$$

implying that $\|x(t)\| < R$ for all $t \geq 0$.

To establish the asymptotic stability with regards to the above, it suffices to prove the convergence to the fixed point; hence, for every $\mu > 0$, there is $T > 0$ such that $\|x(t)\| < \mu$ for all $t > T$. Therefore, let $0 < \mu < \|x_0\| < r$ with r obtained as above. Another positive constant $\delta(\mu) > 0$ can be found such that $\beta(\delta) < \alpha(\mu)$, as α and β are essentially class \mathcal{K} functions. To prove that $\beta(\delta) < \alpha(\mu)$, first we should verify:

$$V(x(t)) < V(x(T)) - \int_T^t \gamma(\|x(\tau)\|)d\tau \quad \text{for all } t > T, \quad (4.22)$$

which will be proven by *induction*. If the solution trajectory resides in region Ω_p for $t \in [T, t_1]$, then $V(x(t)) < V_p(x(t))$, $t \in [T, t_1]$ is true. By integrating the third condition, it follows that

$$V(x(t)) < V(x(T)) - \int_T^t \gamma(\|x(\tau)\|)d\tau, \quad t \in [T, t_1].$$

If t_1 is infinite, the solution trajectory remains in the region, and (4.22) is held. In another scenario, assume that the solution trajectory passes through different fuzzy state-space regions and stays in Ω_q for $t \in \langle t_k, t_{k+1} \rangle$. In addition, assume that $V(x(t)) < V(x(T)) - \int_T^t \gamma(\|x(\tau)\|)d\tau$, $t \in \langle t_k, t_{k+1} \rangle$. Now if the trajectory crosses the switching manifold represented by the region $\Lambda_{q,r}$ at time $t_{k+1} > t_k$ and stays in the region Ω_r for $t \in \langle t_{k+1}, t_{k+2} \rangle$, where t_{k+2} may be infinite, likewise as above, it can be shown that:

$$V(x(t)) < V(x(t_{k+1})) - \int_{t_{k+1}}^t \gamma(\|x(\tau)\|)d\tau, \quad t \in \langle t_{k+1}, t_{k+2} \rangle.$$

It can be implied from the fourth condition of the Theorem that

$$V_r(x(t_{k+1} + \varepsilon)) \leq V_q(x(t_{k+1} + \varepsilon)), \quad \text{where } \varepsilon > 0, \varepsilon \rightarrow \infty.$$

Hence

$$\begin{aligned} V(x(t)) &\leq V(x(t_{k+1})) - \int_{t_{k+1}}^t \gamma(\|x(\tau)\|)d\tau \leq \\ &\leq V(x(T)) - \int_T^{t_{k+1}} \gamma(\|x(\tau)\|)d\tau - \int_{t_{k+1}}^t \gamma(\|x(\tau)\|)d\tau \\ &= V(x(T)) - \int_T^t \gamma(\|x(\tau)\|)d\tau, \quad t \in \langle t_{k+1}, t_{k+2} \rangle. \end{aligned}$$

Because $V(x(t)) \leq V(x(T)) - \int_T^t \gamma(\|x(\tau)\|)d\tau$ holds for $t \in [T, t_1]$, and $V(x(t)) \leq V(x(T)) - \int_T^t \gamma(\|x(\tau)\|)d\tau$, $t \in \langle t_k, t_{k+1} \rangle$, means that $V(x(t)) \leq V(x(T)) - \int_T^t \gamma(\|x(\tau)\|)d\tau$, $t \in \langle t_k, t_{k+2} \rangle$, therefore by *induction*, (4.22) holds.

Second, we should show that there is a $T > 0$ such that $\|x(t)\| \leq \delta$ for all $t > T$, which will be proven by *contradiction*.

Assume that $\|x(t)\| > \delta$ for all $t \geq 0$. As (4.22) holds and α , β and γ are defined as

class \mathcal{K} functions, we can show that:

$$\begin{aligned} V(x_0) - t\gamma(\delta) &\geq V(x_0) - \int_0^t \gamma(\delta) d\tau \geq V(x_0) - \int_0^t \gamma(\|x(\tau)\|) d\tau \\ &\geq V(x(t)) \geq \alpha(\|x(t)\|) \geq \alpha(\delta) > 0. \end{aligned}$$

Since the left-hand side obtains a negative value at the end, the above *contradicts* the first assumption that $\|x(t)\| > \delta$ for all $t \geq 0$. Therefore, there is a $T > 0$ such that $\|x(t)\| \leq \delta$ for all $t > T$.

Considering all the above, if $R_c = \{(x, m) \in \mathcal{F} \mid V(x) \leq c\}$ and $R_c \subseteq \Omega$ then every solution trajectory initiating in R_c will stay in R_c for all $t \geq 0$. Therefore, the asymptotic stability of the fixed point is concluded by $R_c \subseteq RoA$.

Being asymptotically stable, the exponential convergence of the periodic solution to the stable fixed point should be proven. To establish exponential stability, it has to be shown that the scalars, $k_1 > 0$ and $k_2 > 0$ exist such that

$$\|x(t)\| \leq k_1 e^{-k_2 t} \|x_0\|, \quad t \geq 0. \quad (4.23)$$

Let define $k_1 = \sqrt{\beta/\alpha}$ and $k_2 = \gamma/2\beta$. If

$$V(x(t)) \leq V(x_0) e^{-2k_2 t}, \quad t \geq 0, \quad (4.24)$$

holds then (4.23) is deduced from the second condition of the Theorem. Hence, it needs to be shown that (4.24) is true, which will be proven by *induction*. Assume the solution trajectory resides in the region Ω_p for the time interval $t \in [0 \ t_1]$. Therefore $V(x(t)) = V_p(x(t))$, $t \in [0 \ t_1]$. According to the second and third conditions, we have:

$$\dot{V}(x) \leq -\gamma\|x\|^2 \leq -\frac{\gamma}{\beta} V(x).$$

Thus

$$V(x(t)) \leq V(x_0) e^{-\frac{\gamma}{\beta} t} = V(x_0) e^{-2k_2 t}, \quad t \in [0 \ t_1].$$

If t_1 is infinite, then the solution trajectory remains in the region and (4.24) holds. In another scenario, assume that the trajectory passes through different fuzzy state-space (local) regions and remains in Ω_q for $t \in \langle t_k \ t_{k+1} \rangle$. In addition, assume that $V(x(t)) < V(x_0) e^{-2k_2 t}$, $t \in \langle t_k \ t_{k+1} \rangle$. Now, if the solution trajectory crosses the switching manifold represented by the region $\Lambda_{q,r}$ at time $t_{k+1} > t_k$ and remains in the region Ω_r for $t \in \langle t_{k+1} \ t_{k+2} \rangle$, where t_{k+2} may be infinite, then likewise as above, it can be shown that

$$V(x(t)) \leq V(x(t_{k+1})) e^{-2k_2(t-t_{k+1})}, \quad t \in \langle t_{k+1} \ t_{k+2} \rangle.$$

It can be further implied from the fourth condition of the Theorem that $V_r(x(t_{k+1} + \varepsilon)) \leq$

$V_q(x(t_{k+1} + \varepsilon))$, where $\varepsilon > 0$, $\varepsilon \rightarrow \infty$. Hence

$$\begin{aligned} V(x(t)) &\leq V(x(t_{k+1}))e^{-2k_2(t-t_{k+1})} \\ &\leq V(x_0)e^{-2k_2t_{k+1}}e^{-2k_2(t-t_{k+1})} \\ &= V(x_0)e^{-2k_2t}, \quad t \in \langle t_{k+1} \ t_{k+2} \rangle. \end{aligned}$$

As $V(x(t)) \leq V(x_0)e^{-2k_2t}$ holds for $t \in [0 \ t_1]$, and $V(x(t)) \leq V(x_0)e^{-2k_2t}$, $t \in \langle t_k \ t_{k+1} \rangle$ means that $V(x(t)) \leq V(x_0)e^{-2k_2t}$, $t \in \langle t_k \ t_{k+2} \rangle$, therefore (4.24) holds by induction.

Considering all the above, if $R_c = \{(x, m) \in \mathcal{F} \mid V(x) \leq c\}$ and $R_c \subseteq \Omega$ then every solution trajectory initiating in R_c will stay in R_c for all $t \geq 0$. Therefore, the exponential convergence to the stable fixed point is concluded for Theorem 4.4 by $R_c \subseteq R(k_1, k_2)$, where the exponential region of attraction is redefined here (cf. Definition 4.4) to apply in our case as:

$$\begin{aligned} R(k_1, k_2) &= \{(x_0, m_0) \in \mathcal{F}_0 \mid x(t) \rightarrow 0 \text{ as } t \rightarrow \infty \\ &\text{and } \|x(t)\| \leq k_1 e^{-k_2 t} \|x_0\|, \ t \geq 0, \ k_1 \geq 0, \ k_2 \geq 0\}, \end{aligned} \quad (4.25)$$

with $x(t) \rightarrow 0$ means convergence of a periodic solution to the stable fixed point of Poincaré map as time goes to infinity. Q.E.D.

Remark 4.1: The only requirement enforced on the non-smooth Lyapunov function (4.16) is that $V(x) \leq V(x_0)$, which means that, moving through each region Ω_q , it should be reduced compared to its initial value. This brings more relaxed stability conditions as it makes the calculation of the solution trajectories of a non-smooth TS fuzzy model (4.12) unnecessary. Similar requirements on the Lyapunov functions have been suggested in the literature for the classical stability of general switched systems [164, 165], which disadvantageously necessitates the calculation of solution trajectories.

Remark 4.2: As α is defined as a class \mathcal{K} function, it can be said that there exists a δ fulfilling $0 < \delta < R$ such that $\alpha(\delta) < \alpha(R)$. Therefore, the created region $U = \{x \in B_R(0) \mid V(x) \leq \alpha(\delta)\}$ is a compact (closed and bounded) subset of $B_R(0)$ (see [9] for an analogous rationalization in terms of classical notion of stability). Every solution trajectory initiated in the region U will then remain in U for all future times as $V(x(t)) \leq V(x_0) \leq \alpha(\delta)$ for all future times. Therefore, according to Theorem 3.2, it can be concluded that a solution exists for a non-smooth fuzzy model of the form (4.12).

Remark 4.3: The notation $\|\cdot\|$ stands for an arbitrary norm in \mathbb{R}^n [166]. Therefore, it includes the notation of the *Euclidean* norm $\|x\| = \sqrt{\sum_{i=1}^n |x_i|^2}$ or the *sup* norm $\|x\| = \max\{|x_1|, \dots, |x_n|\}$. Both are equivalent as they define the same convergence in a finite-dimensional vector space (like \mathbb{R}^n) [166]. Note that one special class \mathcal{K} function is $c \times \|\cdot\|^2$ where c is a positive constant, which is employed in the proof of Theorem 4.4.

Remark 4.4: In the third condition of the theorem, individual sub-systems $(A^j(m), B^j(m))$ of the fuzzy sub-vector fields F_m , as defined by (3.13), explicitly depend on discrete states

m through the time derivative of \dot{V}_q in (4.17). As the local regions can be derived with $\Omega_q = \{(x, m) \in \Omega_q^{x, m_i} \times \{m_i\}, m_i \in \Omega_q^m\}$, where Ω_q^{x, m_i} and Ω_q^m are defined in Section 4.2.1, the third condition can be identically formulated to be satisfied for the states $x \in \Omega_q^{x, m_i}$, $m_i \in \Omega_q^m$, where m is explicitly substituted by m_i in the theorem.

Remark 4.5: In terms of exponential convergence, we let the norms $\|\cdot\|^2$ be with the maximum power of two, which can be formulated to LMI conditions as $x^T x$. This is necessary for formulating quadratic function elements in the LMI conditions of the theorem.

Remark 4.6: In the LMI stabilization problem of the theorem, we are concerned with finding the optimized solution to LMI conditions when multiplied by $1/\gamma$. However, it is possible to multiply each condition by a positive constant without violating the proof of the theorem.

4.3.1 Substitution of confined regions with LMI quadratic forms

As noticed in the former theorem, all stability conditions are confined to be effective in a part of the fuzzy state space \mathcal{F} in the way explained in Section 4.3. The second, third and fourth conditions are limited to regions Ω_q^x , Ω_q^{x, m_i} for all discrete states $m_i \in \Omega_q^m$ and the boundary regions $\Lambda_{q,r}^x$ respectively. In order to fully formulate all of the stability conditions into LMI conditions, a route should be explored to recast the region confinements to LMIs. This is possible by first redefining the regions as quadratic functions and then transforming the confined conditions to unconfined conditions using the well-known \mathcal{S} -procedure technique (see Appendix B). In this section, this procedure is first outlined in general terms and then applied to the confined conditions in the stability theorems.

Assume that $Q^0(x) : \mathbb{R}^n \rightarrow \mathbb{R}$ is a function with unknown variables to be determined, and fulfills the inequality:

$$Q^0(x) \geq 0 \text{ for all } x \text{ in the region } \Omega. \quad (4.26)$$

Additionally let's define known functions $Q^k(x) : \mathbb{R}^n \rightarrow \mathbb{R}$, $k \in I_s$, which fulfills the condition

$$Q^k(x) \geq 0, \quad k \in I_s, \text{ for all } x \text{ in the region } \Omega.$$

Allow (4.26) to be substituted by a stronger constraint as:

$$Q^0(x) \geq 0 \text{ for all } x \text{ satisfying } Q^k(x) \geq 0, \quad k \in I_s \quad (4.27)$$

In this manner, the region Ω in (4.26) has been substituted by inequalities $Q^k(x) \geq 0$, $k \in I_s$.

To substitute the confined condition (4.27) by an unconfined condition, a technique called \mathcal{S} -procedure can be employed. In this respect, additional variables $\lambda^k \geq 0$, $k \in I_s$ should be introduced by employing the following lemma:

Lemma 4.1 [136]: If there exist $\lambda^k \geq 0$, $k \in I_s$, such that:

$$\forall x \in \mathbb{R}^n, Q^0(x) \geq \sum_{k=1}^s \lambda^k Q^k(x), \quad (4.28)$$

then (4.27) is true.

Since it is already known that $\lambda^k \geq 0$, $k \in I_s$, the proof of the above lemma can be directly followed. Therefore for all states x fulfilling the inequality $Q^k(x) \geq 0$, $k \in I_s$, it is also true that $\sum_{k=1}^s \lambda^k Q^k(x) \geq 0$.

According to Lemma 4.1, the confined condition (4.26) can be substituted by an unconfined condition (4.28). If the quadratic forms are defined as follows:

$$Q^k(x) = x^T Z^k x + 2(c^k)^T x + d^k = \tilde{x}^T \tilde{Z}^k \tilde{x}, \quad k = 0, \dots, s, \quad (4.29)$$

where $\tilde{x} = \begin{bmatrix} x \\ 1 \end{bmatrix}$ and $\tilde{Z}^k = \begin{bmatrix} Z^k & c^k \\ (c^k)^T & d^k \end{bmatrix}$, where $Z^k = (Z^k)^T \in \mathbb{R}^n \times \mathbb{R}^n$, $c^k \in \mathbb{R}^n$ and $d^k \in \mathbb{R}$, then (4.28) can be formulated as an LMI:

$$\tilde{Z}^0 \geq \sum_{k=1}^s \lambda^k \tilde{Z}^k, \quad \lambda^k \geq 0, \quad k \in I_s. \quad (4.30)$$

The advantage of formulating the LMI condition as above instead of only $\tilde{Z}^0 \geq 0$ is that the condition does not have to be satisfied in the whole of \mathcal{F} , implying that the inequality $\tilde{Z}^0 \geq 0$ should be satisfied for a part of \mathcal{F} where at least all $\tilde{x}^T \tilde{Z}^k \tilde{x} \geq 0$ are fulfilled. Then, by solving (4.30), the matrix \tilde{Z}^0 and the different λ^k can be determined.

Remark 4.7: It is preferable not to substitute a region Ω with the quadratic forms $Q^k(x) \geq 0$ such that the states satisfying all these inequalities are much larger than the region itself. This is due to the fact that the stronger condition of (4.27) may result in a conservative formulation implying no feasible solution while the condition (4.26) actually has a solution. In some cases, less conservative conditions are crucial for a solution to exist, e.g. when all individual sub-systems of a fuzzy sub-vector field are unstable. The determination of the parameters in (4.29) such that the region Ω is substituted by quadratic forms $Q^k(x) \geq 0$ with less conservative formulation will be discussed in detail in Section 4.3.1. It will be shown that determination of the parameters in (4.29) in a less conservative formulation, i.e. feasible condition of (4.27), will result in substituting a region Ω with the quadratic forms $Q^k(x) \geq 0$ such that the states satisfying all these inequalities are the *smallest possible region* covering Ω .

Remark 4.8: The substitution of (4.27) by Lemma 4.1 may result in a conservative LMI formulation as well. It can be shown, nonetheless, that the converse is true only in the case of $s = 1$, cf. [136], contingent on the existence of some states x such that $Q^1(x) > 0$.

Remark 4.9 If the boundary regions Λ_{qr} , representing switching manifolds, is substituted by quadratic forms $Q^k(x) = 0$, $k \in I_s$, it will not be necessary to impose constraints

on parameters such as $\lambda^k \geq 0$, $k \in I_s$ in Lemma 4.1, due to the fact that the lemma is true regardless of the sign of these parameters. In this manner, matrices \tilde{Z}^k substituting the regions Λ_{qr} can be denoted as $\tilde{Z}_{q,r}^k$.

All of the afore-explained general procedures can be applied to the stability conditions of Theorem 4.4 to formulate the confined regions as unconfined LMI conditions. This can be achieved by expressing all of the conditions in Theorem 4.4 by quadratic inequalities $Q^k(x) \geq 0$, where $Q^k(x)$ is defined as (4.29). Therefore, Theorem 4.4 can be reformulated as follows:

Theorem 4.5: If there exist piecewise quadratic matrices $\tilde{P}_q, q \in I_\Delta$ as defined by (4.20), constants η_k^{qr} and if there is a solution to min β subject to

1. $\alpha > 0$, $\mu_q^k \geq 0$, $\hat{\mu}_q^k \geq 0$, $\nu_{qij}^k > 0$,
2. $\begin{bmatrix} \alpha & 0 \\ 0 & 0 \end{bmatrix} + \sum_{k=1}^{s_q} \mu_q^k \begin{bmatrix} Z_q^k & c_q^k \\ (c_q^k)^T & d_q^k \end{bmatrix} \leq \tilde{P}_q$,
3. $\tilde{P}_q \leq \begin{bmatrix} \beta & 0 \\ 0 & 0 \end{bmatrix} + \sum_{k=1}^{s_q} \hat{\mu}_q^k \begin{bmatrix} Z_q^k & c_q^k \\ (c_q^k)^T & d_q^k \end{bmatrix}$, $q \in I_\Delta$,
4. $\begin{bmatrix} (A^j(m_i))^T P_q + P_q A^j(m_i) & P_q B^j(m_i) + (A^j(m_i))^T p_q \\ (B^j(m_i))^T P_q + p_q^T A^j(m_i) & (B^j(m_i))^T p_q + p_q^T B^j(m_i) \end{bmatrix} + \sum_{k=1}^{s_{qij}} \nu_{qij}^k \begin{bmatrix} Z_q^k & c_q^k \\ (c_q^k)^T & d_q^k \end{bmatrix} \leq -\tilde{I}$, $q \in I_\Delta$, $m_i \in \Omega_q^m$,
5. $\tilde{P}_r \leq \tilde{P}_q - \sum_{k=1}^{s_{qr}} \eta_k^{qr} \begin{bmatrix} Z_{qr}^k & c_{qr}^k \\ (c_{qr}^k)^T & d_{qr}^k \end{bmatrix}$, $(q, r) \in I_\Lambda$,

then the invariant set (limit cycle) is structurally stable in the sense of Lyapunov or the periodic solution exponentially converges to the stable fixed point.

Remark 4.10: As previously mentioned in Remark 4.6, to derive the rate of exponential convergence, the conditions in Theorem 4.4 are scaled by $1/\gamma$ and then the LMI optimization problem can be solved when β is minimized.

Remark 4.11: The search for non-smooth Lyapunov function candidates $V(x)$ is formulated in flexible regions (except for regions Λ_{qr} representing switch sets) as in the theorem. However, the size of the regions Ω_q has a pivotal role in relaxing the conservative LMI formulation. As it will be shown later in this chapter through different examples (also see Appendix A) finer region partitions may be needed in some cases to verify structural stability in the close neighborhood of a bifurcation point. At the same time, if the regions are substituted by quadratic inequalities covering too large a region, the LMI stabilization problem in Theorem 4.5 may be found infeasible and the analysis will fail to predict the bifurcation point.

Remark 4.12 If we search for the maximal value of α when trying to minimize β , the computational effort will be minimized. The maximal value of α is the smallest eigenvalue of all matrices P_q , should all regions contain the origin as an interior point. This is mainly due to $\lambda_q^{min} x^T x \leq x^T P_q x$ [9, 167] where λ_q^{min} is the smallest eigenvalue of P_q .

4.4 Stability theorems for impacting systems

As described in the previous chapter, non-smooth TS fuzzy models are able to represent impacting dynamics by including discontinuity (or jumps) in continuous states by incorporating a specific function χ to describe the state discontinuities as defined by (3.16). The set of fuzzy states (x, m) where the discontinuous states occur can be equivalently described by jump sets \mathcal{D}_i (see Remark 3.3 of Definition 3.1) as:

$$\mathcal{D}_i = \{x \in \mathbb{R}^n \mid x^+ = \chi(x, m_i)\}, \quad i \in I_N, \quad (4.31)$$

where the relationship between two successive continuous fuzzy states can be defined by the matrix J as:

$$x^+ = J(m_i)x. \quad (4.32)$$

As explained in Chapter 2, an impacting system can be analytically expressed (in its conventional way) by assuming a discontinuity boundary Σ (or an hard boundary $H(x)$), a set of the reset map $R(x)$ [7], and the system states as $x = (u, \frac{du}{dt})^T$, cf. Section 2.1.2. Therefore the system can be alternatively described by:

$$\begin{aligned} \dot{x} &= F(x), & \text{if } x \in S^+ \\ x &\mapsto R(x), & \text{if } x \in \Sigma \end{aligned}$$

where, $S^+ = \{x : H(x) > 0\}$ and $\Sigma = \{x : H(x) = 0\}$, and $H(x)$ is a smooth function describing the switching manifold Σ . If we assume the set ∂S_1^+ is defined as $\partial S_1^+ = \{x : \frac{\partial H(x)}{\partial x_1}\}$ and the function $\zeta \in \partial S_1^+$, then, according to zero-time mapping in an hard impact oscillator, we can define $\zeta : x \mapsto rx$.

To prove the stability of a periodic solution, the non-smooth Lyapunov function candidate (4.16) must be reduced or stay at the same energy level from just before the discontinuous jump occurs. This can be realized if we require the last condition of Theorem 4.4 to be:

$$(x, m_i) \in \Lambda_{qr} \quad V_r(\chi(x, m_i)) \leq V_q(x) + V(\zeta(x, m_i)) \quad (q, r) \in I_\Lambda, \quad (4.33)$$

The boundary region Λ_{qr} , as defined by (4.14), represents the switch sets and the set of tuples I_Λ can be defined as (4.15). However, if a discontinuous jump takes place by crossing the switching manifold and the solution trajectories remain in the same region Ω_q as just before crossing the switching manifold, then Λ_{qr} can be represented by Λ_{qq} for such solution states. Moreover, due to the discontinuity in states, if $\Lambda_{qr} \neq \emptyset$, the local region Ω_q must not share a boundary with Ω_r . Obviously, if the solution trajectory passes through Ω_r from Ω_q without any jump when crossing Λ_{qr} , the function $\chi(x, m_i)$ is no longer necessary. For proving stability, it is necessary to assume that there is a finite number of discontinuous states in finite time. This means that the states defined by function χ , cannot undergo consecutive discontinuous jumps in an infinite manner. Except for the condition (4.33) and all the related explanations, the remaining of the proof is similar to that of Theorem 4.4. When applying the general procedure explained in Section

4.3.1, Theorem 4.4 can be fully formulated as the following LMI stabilization problem for studying impacting dynamics:

Theorem 4.6: If there exist piecewise quadratic matrices $\tilde{P}_q, q \in I_\Delta$ as defined by (4.20), constants η_k^{qr} and if there is a solution to min β subject to

1. $\alpha > 0, \mu_q^k \geq 0, \hat{\mu}_q^k \geq 0, \nu_{qij}^k > 0,$
2. $\begin{bmatrix} \alpha & 0 \\ 0 & 0 \end{bmatrix} + \sum_{k=1}^{s_q} \mu_q^k \begin{bmatrix} Z_q^k & c_q^k \\ (c_q^k)^T & d_q^k \end{bmatrix} \leq \tilde{P}_q,$
3. $\tilde{P}_q \leq \begin{bmatrix} \beta & 0 \\ 0 & 0 \end{bmatrix} + \sum_{k=1}^{s_q} \hat{\mu}_q^k \begin{bmatrix} Z_q^k & c_q^k \\ (c_q^k)^T & d_q^k \end{bmatrix}, q \in I_\Delta,$
4. $\begin{bmatrix} (A^j(m_i))^T P_q + P_q A^j(m_i) & P_q B^j(m_i) + (A^j(m_i))^T p_q \\ (B^j(m_i))^T P_q + p_q^T A^j(m_i) & (B^j(m_i))^T p_q + p_q^T B^j(m_i) \end{bmatrix} + \sum_{k=1}^{s_{qij}} \nu_{qij}^k \begin{bmatrix} Z_q^k & c_q^k \\ (c_q^k)^T & d_q^k \end{bmatrix} \leq -\tilde{I}, q \in I_\Delta, m_i \in \Omega_q^m,$
5. $\begin{bmatrix} J(m_i) & 0 \\ 0 & 1 \end{bmatrix}^T \begin{bmatrix} P_r & p_r \\ p_r^T & \pi_r \end{bmatrix} \begin{bmatrix} J(m_i) & 0 \\ 0 & 1 \end{bmatrix} \leq \begin{bmatrix} P_q & p_q \\ p_q^T & \pi_q \end{bmatrix} + \begin{bmatrix} H(m_i) & 0 \\ 0 & 1 \end{bmatrix}^T \begin{bmatrix} P_q & p_q \\ p_q^T & \pi_q \end{bmatrix} \begin{bmatrix} H(m_i) & 0 \\ 0 & 1 \end{bmatrix} - \sum_{k=1}^{s_{qr}} \eta_{qr}^k \begin{bmatrix} Z_{qr}^k & c_{qr}^k \\ (c_{qr}^k)^T & d_{qr}^k \end{bmatrix}, (q, r) \in I_\Lambda$

then the invariant set (limit cycle) is structurally stable in the sense of Lyapunov or the periodic solution exponentially converges to the stable fixed point.

Remark 4.19: The matrix $J(m_i)$, as defined in (4.32), describes a discontinuous state destination map, e.g. the zero-time velocity reversal in an hard-impact oscillator as defined by the map (2.6). According to function ζ , the matrix $H(m_i)$, $i \in I_N$ can be defined as:

$$H(m_i) = \begin{bmatrix} 1 & 0 \\ r \frac{\partial H}{\partial x_1} & 1 \end{bmatrix},$$

for the purpose of setting a limit on the region boundary defined by the set Λ_{qr} .

4.5 Substituting flexible regions by quadratic inequalities

This section intends to describe how by determining additional parameters in (4.29) the fuzzy state space regions $\Omega \subseteq \mathcal{F}$ can be substituted by quadratic inequalities $Q^k(x) \geq 0$ (Section 4.3.1). This means that the non-strict ¹ LMI $Q^0(x) \geq \tilde{x}^T \tilde{Z}^0 \tilde{x}$ should not be satisfied in the entire fuzzy state space but only in the part where all $\tilde{x}^T \tilde{Z}^k \tilde{x}$ should be greater or equal to zero, leading to LMI condition (4.30). For a solution to exist, conservative LMI formulations should be avoided. This essentially means, in substituting the regions Ω with quadratic inequalities $Q^k(x) \geq 0$, we should not allow $Q^k(x) \geq 0$ to

¹Strict and non-strict LMIs refer to the definite and semi-definite LMI conditions, cf. Appendix B

cover a much larger region than Ω . An initial attempt, in this respect, is to let regions $\Omega \subseteq \mathcal{F}$ be partitioned by the switch sets $S_{i,j}$ (which is then represented as regions Λ_{qr}) of a non-smooth TS fuzzy model.

A stepping stone in avoiding the conservatism is to partition the region $\Omega \subseteq \mathcal{F}$ by hyperplanes, e.g. let the switching manifolds partition the state space. Although in our approach, $\Omega \subseteq \mathcal{F}$ can be flexibly selected, it should not be selected in such a way that the region partitions would become so complicated (or coarse) for the LMI stabilization problem to be found numerically unsolvable. Partitioning based on switch sets $S_{i,j}$ (or switching hyperplanes) can be a sensible choice since the resulting regions are simply substituted by quadratic inequalities of the form $Q^k(x) \geq 0$. Nevertheless, in some cases, as will be exemplified later in this chapter, close to an unstable limit cycle, e.g. grazing bifurcation resulting from sinusoidal impacting, regions $\Lambda_{q,r}$ should take an arbitrary form. This means that regions $\Omega \subseteq \mathcal{F}$ are required to be partitioned into finer regions or even arbitrary regions, substituted by quadratic inequalities $Q^k(x) \geq 0$.

4.5.1 Region Ω restricted by hyperplanes

At first, a region $\Omega \subseteq \mathcal{F}$ is assumed to be defined such that it encompass the origin. The quadratic inequality in (4.29) can then be defined as $Q^k(x) = x^T Z^k x \geq 0$. Additionally assume that a solution Z^0 is found for the LMI problem (4.30). Therefore, if x_0 is a state fulfilling $x_0^T Z^0 x_0 \geq 0$, so will $v x_0^T Z^0 x_0 \geq 0$ for any scalar v . In this manner, the inequality $x^T Z^0 x \geq 0$ cannot be restricted at states fulfilling only single half-planes with the form:

$$f^T x \geq 0,$$

since if $x^T Z^0 x \geq 0$ is to be fulfilled for the above, it should also be fulfilled for the states satisfying the other half-plane $-f^T x \geq 0$. This implies that $x^T Z^0 x \geq 0$ should be fulfilled for all states. Consequently, a region encompassing the origin should be at least composed of two half-planes or Z^0 should not be defined as a positive semi-definite in the condition $x^T Z^0 x \geq 0$.

Quadratic inequalities restricted by half-planes: In the first case, a region is given by a set of states limited by two half-planes:

$$(f^a)^T \geq 0 \quad \text{and} \quad (f^b)^T \geq 0. \quad (4.34)$$

Therefore Ω can be represented by quadratic inequalities (see also Fig. 4.5.1):

$$x^T Z^0 x \geq 0, \quad \text{where } Z^0 = f^a (f^b)^T + f^b (f^a)^T. \quad (4.35)$$

A region Ω can be substituted by quadratic inequalities (4.35) represented by only two hyperplanes, if the dimension $n = 2$. However, if the dimensions $n > 2$, (4.35) should be represented by more than two hyperplanes (all the possible combinations of two different half-planes). This results in $\frac{\kappa(\kappa-1)}{2}$ different quadratic inequalities (4.35) and λ^k in (4.28), where κ is the number of half-planes. Since $x^T Z^k x \geq 0$ is true for all states, it

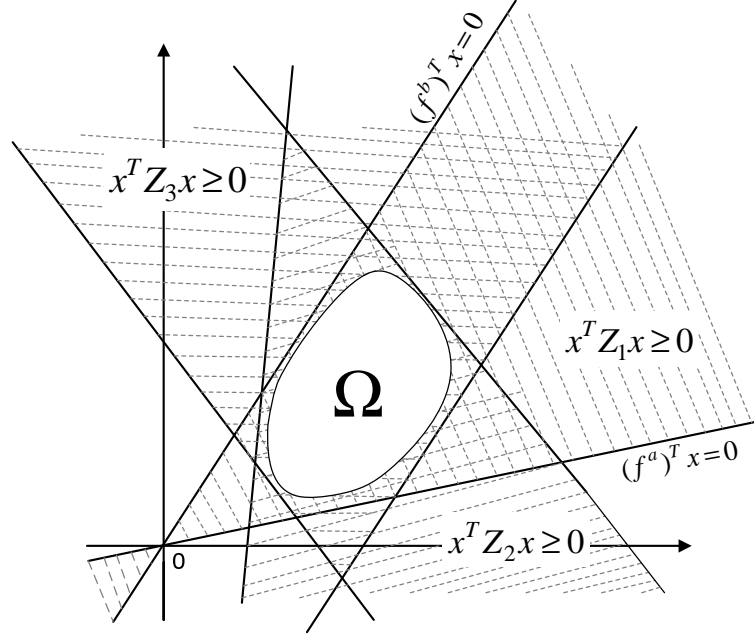


Figure 4.3: The white region Ω is substituted with a region representing semi-definite conditions $x^T Z_1 x \geq 0, x^T Z_2 x \geq 0$ and $x^T Z_3 x \geq 0$, each of which limited by two hyperplanes $(f^a)^T x \geq 0$ and $(f^b)^T x \geq 0$ requiring both set of states x_0 and $-x_0$ to be fulfilled for inequality conditions. The region Ω can be also substituted with semi-definite conditions whose property requires to fulfill just for set of states x_0 .

is justified to eliminate the combination of identical half-planes. If the region Ω is limited by several half-planes, it is not possible to precisely represent the regions by the forms $x^T Z^k x \geq 0$ even in the case of (4.35). As it is difficult to prefer a set of solutions for states fulfilling $x^T Z^1 x \geq 0$ over another set, all plausible combinations should be considered. The additional parameters λ^k can then be derived by solving the resulting LMI problem (4.30), which in turn, indicates the best-fitted quadratic inequality for the substitution of region Ω .

If a region does not encompass the origin, a half-plane must have the affine form

$$f^T x + g \geq 0, \quad (4.36)$$

which can be represented by a quadratic inequality [136]

$$\begin{bmatrix} x \\ 1 \end{bmatrix}^T \tilde{Z}^0 \begin{bmatrix} x \\ 1 \end{bmatrix}, \text{ where } \tilde{Z}^0 = \begin{bmatrix} 0_{n \times n} & f \\ f^T & 2g \end{bmatrix}. \quad (4.37)$$

Similarly, if the region Ω is to be limited by more than two half-planes, all plausible combinations of the two different half-planes in addition to the quadratic inequalities representing a single half-plane should be taken into account. As a result, $\frac{\kappa(\kappa-1)}{2}$ different quadratic inequities and parameters λ^k are to be determined, where κ designates the

number of half-planes. For clarification, if the half-planes are given, say, by:

$$(f^a)^T x + g^a \geq 0 \text{ and } (f^b)^T x + g^b \geq 0,$$

the quadratic inequalities for substitution of the region Ω are then expressed:

$$\begin{bmatrix} x \\ 1 \end{bmatrix}^T \begin{bmatrix} f^a(f^b)^T + f^b(f^a)^T & g^b f^a + g^a f^b \\ g^b(f^a)^T + g^a(f^b)^T & 2g^a g^b \end{bmatrix} \begin{bmatrix} x \\ 1 \end{bmatrix} \geq 0, \quad (4.38)$$

$$\begin{bmatrix} x \\ 1 \end{bmatrix}^T \begin{bmatrix} 0 & f^a \\ (f^a)^T & 2g^a \end{bmatrix} \begin{bmatrix} x \\ 1 \end{bmatrix} \geq 0, \quad (4.39)$$

$$\begin{bmatrix} x \\ 1 \end{bmatrix}^T \begin{bmatrix} 0 & f^b \\ (f^b)^T & 2g^b \end{bmatrix} \begin{bmatrix} x \\ 1 \end{bmatrix} \geq 0. \quad (4.40)$$

Quadratic inequalities restricted by ellipsoids: To avoid a large number of parameters λ^k in (4.28), a region can be substituted by a quadratic inequality $\tilde{x}^T \tilde{Z}^2 \tilde{x} \geq 0$ representing an elliptic cone for regions encompassing the origin, or an ellipsoid for regions not encompassing the origin [168]. To illustrate the ellipsoid, assume that the region Ω representing a cubic region is restricted by $2n$ half-planes (4.36) which fulfills $(f^a)^T f^b = 0$ (cf. Figure 4.4). The region can then be substituted by a quadratic function fulfilling the elliptic equation

$$\left(\frac{x^1 - o^1}{r^1}\right)^2 + \dots + \left(\frac{x^n - o^n}{r^n}\right)^2 \leq 1, \quad (4.41)$$

where o is the center of hypercube. The superscript k of x and o means the k^{th} component of the corresponding vectors. The coefficients r^k , $k \in I_n$, should be chosen such that the region $\Omega \subseteq \mathcal{F}$ fits in the possible smallest hypervolume of the ellipsoid, meaning $r^k = \sqrt{n}a^k$, where a^k is the side of the hypercube in the k^{th} direction.

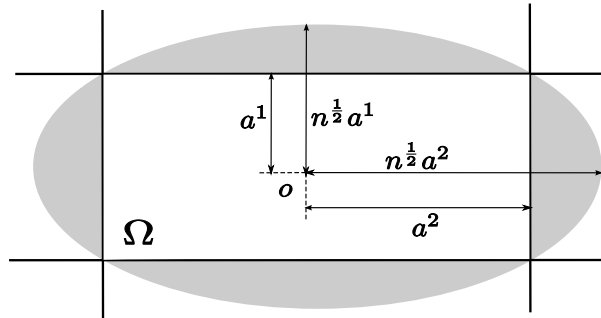


Figure 4.4: Shaded cubic region Ω restricted by two half-planes can also be substituted by an ellipsoid.

The elliptic region (4.41) can be then expressed as a quadratic inequality:

$$\begin{bmatrix} x \\ 1 \end{bmatrix}^T \begin{bmatrix} Z^0 & c^0 \\ (c^0)^T & d^0 \end{bmatrix} \begin{bmatrix} x \\ 1 \end{bmatrix} \geq 0,$$

where

$$\begin{cases} Z^0 = \text{diag}\{\frac{-1}{(r^0)^2}, \dots, \frac{-1}{(r^n)^2}\}, \\ c^0 = [\frac{o^1}{(r^0)^2} \dots \frac{o^n}{(r^n)^2}], \\ d^0 = 1 - \frac{(o^1)^2}{(r^0)^2} - \dots - \frac{(o^n)^2}{(r^n)^2}. \end{cases} \quad (4.42)$$

If a closed region with known vertices are to be formed by general hyperplanes, the best-fitted ellipsoid can be determined by formulating an LMI problem [136]. In comparison to the former approach of restricting by hyperplanes, the ellipsoid representation may result in conservative LMI formulations. This mainly comes from the fact that, searching for the best fitted ellipsoid to cover the region Ω is an *a priori* problem whereas in the former approach, the inequalities substituting the region can be known by obtaining additional parameters λ^k (although there may be a large number of them) via solving the LMI problem. In practice, a specific procedure or rule for selecting the best region representation does not exist. As confirmed by experience, nonetheless, this approach results in less conservative LMI formulations since it deals with less unknown variables.

Quadratic equalities representing hyperplanes: The boundary regions Λ_{qr} can be represented by a set of states fulfilling quadratic equalities of the form:

$$f^T x + g = 0, \quad (4.43)$$

where $f = [f^1 \dots f^n]^T \in \Re^n$ and $g \in \Re$. The quadratic form (4.43) is equivalent to the quadratic equalities

$$2(\lambda^T x + \lambda^{n+1})^T (f^T x + g) = 0, \quad (4.44)$$

where $\lambda = [\lambda^1, \dots, \lambda^n]^T \in \Re^n$ and $\lambda^{n+1} \in \Re$ are arbitrary additional parameters. The equality (4.44) can be rewritten as:

$$\tilde{x}^T \begin{bmatrix} \lambda \\ \lambda^{n+1} \end{bmatrix} [f^T \ g] \tilde{x} + \tilde{x}^T \begin{bmatrix} f \\ g \end{bmatrix} [\lambda^T \ \lambda^{n+1}] \tilde{x} = \sum_{k=1}^{n+1} \lambda^k \tilde{x}^T \tilde{Z}^k \tilde{x} = 0,$$

where

$$\tilde{Z}^k = e^k [f^T \ g] + [f^T \ g]^T (e^k)^T, \quad \tilde{x} = \begin{bmatrix} x \\ 1 \end{bmatrix}, \quad (4.45)$$

and e^k is a column vector with n elements such that

$$e^k(i) = \begin{cases} 1, & i = k, \\ 0, & i \neq k, \end{cases}$$

where i means the i^{th} element of e^k .

These quadratic equalities can be used to express regions Λ_{qr} in the form of LMIs (4.30), solving specifically for the case of equality with parameters λ^k to be determined. Therefore,

$$\begin{cases} \text{the set of states fulfilling (4.43)} \\ \text{the set of states fulfilling (4.44)} \end{cases} \Rightarrow \text{the set of states fulfilling } (\lambda^T x + \lambda^{n+1})^T = 0$$

Note that the quadratic equality given by (4.43) has $n + 1$ additional variables. If (4.43) divides two regions encompassing the origin, the parameter $g = 0$ and the last row and column can be removed in the above quadratic inequalities (see Appendix B). The last quadratic equality can then be omitted to leave n free parameters λ^k in the LMI formulation. If we have a quadratic equality at two hyperplanes

$$2((f^a)^T x + g^a)((f^b)^T x + g^b) = \tilde{x}^T \tilde{Z}^0 \tilde{x} = 0, \quad (4.46)$$

where

$$\tilde{Z}^0 = \begin{bmatrix} f^a(f^b)^T + f^b(f^a)^T & g^b f^a + g^a f^b \\ g^b(f^a)^T + g^a(f^b)^T & 2g^a g^b \end{bmatrix},$$

and the vectors $[(f^a)^T \ g^a]$ and $[(f^b)^T \ g^b]$ are linearly independent, only one unknown parameter remains to be determined in the LMI (4.30). A quadratic equality such as (4.46) cannot be formed at states fulfilling three (linearly independent) hyperplanes, except for the case when the quadratic form equivalently is equal to zero, which implies that $\tilde{x}^T \tilde{Z}^0 \tilde{x}$ must be fulfilled for all states.

4.5.2 Bifurcation analysis of the case studies

In this section, we intend to show how the LMI stabilization problems of Theorems 4.5 and 4.6 can be employed to analytically predict the onset of bifurcations as illustrated in the non-smooth TS fuzzy models of the different case studies introduced in Section 2.1 of Chapter 2. All the LMI solvers used for the following examples are listed in Appendix B.

Example 4.1 (Case study I continued, the boost converter). Recalling Example 3.5 where the non-smooth fuzzy model of the boost converter (3.27) accurately exhibits all nonlinear phenomena resulting from fast-scale instabilities of the circuit (Fig. 3.17). The stable limit cycle (period-1 operation) becomes unstable at the operating point $(V_{in}, I_{ref}) = (36.239V, 4A)$. Therefore, the model becomes structurally unstable at this operating point and the bifurcation occurs leading to a period-2 orbit. As discussed in Section 4.3, Theorem 4.4 and the LMI stabilization problem in Theorem 4.5 (after transforming unconfined conditions to LMIs), can provide an analytical approach for Filippov-type fuzzy models to pinpoint the afore-mentioned unstable operating point. This can be achieved by solving the LMI stabilization problem to discover if the problem is feasible or not. As a first step, we partition the fuzzy state space \mathcal{F} according to the switching hyperplane indicated by switch sets $S_{1,2}$ and $S_{1,2}$. Therefore, the stability can be verified by two regions, associated with two discrete states

$$\begin{aligned} \Omega_1 &= \{(x, m) \in \mathcal{F} \mid x \in \mathbb{R}^n, m = m_1\}, \\ \Omega_2 &= \{(x, m) \in \mathcal{F} \mid x \in \mathbb{R}^n, m = m_2\}. \end{aligned} \quad (4.47)$$

Following the procedure outlined in Section 4.3.1 for region substitution with quadratic inequalities and Section 4.5, the full LMI problem of Theorem 4.6 is solved for the non-smooth TS fuzzy model (3.27) operating under conventional current-mode control for the

operating point of $(V_{\text{in}}, I_{\text{ref}}) = (36.24V, 4A)$. The feasible solution result is:

$$\tilde{\mathbf{P}}_1 = \begin{bmatrix} 1.2397 & 0 & 0.5956 \\ 0 & 1.1200 & 0 \\ 0.5956 & 0 & 2.4795 \end{bmatrix}, \quad \tilde{\mathbf{P}}_2 = \begin{bmatrix} 129.3565 & -2.2224 & 86.9494 \\ -2.2224 & 1.0404 & -1.7740 \\ 86.9494 & -1.7740 & 96.9417 \end{bmatrix},$$

for the optimal value of $\beta = 166.9391$. This means that the system exponentially converges to the stable periodic solution (period-1 orbit), which is confirmed by the bifurcation diagram of Fig. 3.17. Solving the LMI problem for the operating point $(V_{\text{in}}, I_{\text{ref}}) = (36.238V, 4A)$ when the system loses its stability to period-2 operation (see Fig. 3.15d and Fig. 3.16d) results in an infeasible solution and likewise for any input voltage less than $V_{\text{in}} = 36.238V$. In fact, the local properties of the periodic limit cycles are assessed by the LMI problem. The feasibility of the LMI problem indicates the stability of the local period-1 orbit. However, when the period-1 orbit becomes unstable it does not diverge to infinity but it converges to another period-2 and eventually a chaotic orbit. This local loss of structural stability (transition from period-1 to period-2 orbit) is detected when the LMI problem becomes infeasible. Therefore, if for a specific parameter the LMI is feasible then the local period-1 orbit (the fixed point of the Poincaré map) is stable, while if it is not feasible the local period-1 orbit is unstable. So when by changing any system parameter, e.g. the input voltage, we go from a feasible to a non-feasible LMI we can claim that the system has been structurally unstable and hence a bifurcation took place.

This proves that structural stability can be analytically verified and the bifurcation point accurately detected using Theorem 4.5. Finer region partitions do not have any effect on stability results in this case but it does take more computational time for the LMI solver to search for a feasible solution. It should be noted that using a common quadratic Lyapunov function candidate with merging Ω_1 and Ω_2 into $\Omega = \Omega_1 \cup \Omega_2$, results in infeasible solution in all of the operating points. Therefore, non-smooth Lyapunov functions (4.16) have an essential role in the bifurcation analysis.

Example 4.2 (Case study I continued, the buck converter). For the bifurcation analysis of another (non-sliding) Filippov-type system, the dc-dc buck converter, we consider the non-smooth TS fuzzy model (3.31) described in Example 3.6. The fuzzy state space is again partitioned into two detached regions as:

$$\begin{aligned} \Omega_1 &= \{(x, m) \in \mathcal{F} \mid x \in \mathbb{R}^n, m = m_1\}, \\ \Omega_2 &= \{(x, m) \in \mathcal{F} \mid x \in \mathbb{R}^n, m = m_2\}, \end{aligned} \tag{4.48}$$

and the region Λ_{gr} is allocated for the switch sets described in (3.32) with the hyperplane:

$$x_1(dT) - V_{\text{ref}} - \frac{v_{\text{ramp}}}{A} = 0.$$

Solving the LMI stabilization problem of Theorem 4.5 for the operating point $V_{\text{in}} = 24V$ and $V_{\text{ref}} = 11.3V$, results in a feasible solution:

$$\tilde{\mathbf{P}}_1 = \begin{bmatrix} 2.2526 & -12.8865 & -39.1678 \\ -12.8865 & 0.0026 & -103.3283 \\ -39.1678 & -103.3283 & 0.0004 \end{bmatrix}, \quad \tilde{\mathbf{P}}_2 = \begin{bmatrix} 2.2526 & 12.8865 & -39.1678 \\ 12.8865 & 387.3544 & 103.3283 \\ -39.1678 & 103.3283 & 2235.9155 \end{bmatrix},$$

with the optimal value of $\beta = 2.4962$. Therefore, the solution exponentially converges to the stable period-1 orbit. This result is well in agreement with the bifurcation diagram of Fig. 3.18. If we change the operating point to $V_{\text{in}} = 25V$ and $V_{\text{ref}} = 11.3V$, the LMI problem results in an infeasible solution. The operating point $V_{\text{in}} = 25V$ is a special case in that there is coexisting period-1 orbit with a period-2 orbit as shown in Fig. 3.20. However, the period-1 orbit becomes unstable while the period-2 orbit becomes permanent as confirmed by traditional analytical approaches [1, 119] briefly explained in Chapter 2. The LMI stability results confirm that the model of the converter (3.31) under voltage-mode control is unstable when referring to period-1 operation.

Example 4.3 (Case study II continued, the hard impact oscillator). As explained in Example 3.7, the model of an hard-impact oscillator can be converted into the non-smooth TS fuzzy model (3.36), where the incorporated jump matrices (3.38):

$$J(m_1) = \begin{bmatrix} 1 & 0 \\ 0 & -r \end{bmatrix}, \quad J(m_2) = \begin{bmatrix} 1 & 0 \\ 0 & -1/r \end{bmatrix}, \quad (4.49)$$

with a coefficient of restitution $r = 0.9$, can describe the discontinuous states when coinciding with the switch sets $S_{1,2}$ and $S_{2,1}$ in (3.37) (discontinuous states occur when crossing the switching manifold $\Sigma := x_1(t) - \sigma = 0$). As discussed in Section 2.2.5, using an analytical approach like discontinuity mapping, we are faced with an infinite stretching of phase space in the neighborhood of the grazing orbit due to the square-root singularity of the jacobian of the Poincaré map. Therefore, the former approaches are problematic in the bifurcation analysis of a grazing event. Here, we intend to examine if the LMI stabilization problem proposed in Theorem 4.6 (Section 4.4) can solve this problem by detecting the unstable periodic orbit near the grazing event. In this respect, we divide our analysis into two areas: in the close neighborhood of the grazing incident and at the grazing incident.

Stability in the neighborhood of grazing: For this purpose, we first partition the fuzzy state space \mathcal{F} by the hyperplanes of switch sets $S_{1,2}$ and $S_{2,1}$ into two partitions. In this manner, the region Λ_{qr} , as in Section 4.5, can be described by the following quadratic equality:

$$2(\lambda^T x + \lambda^{n+1})^T (f^T x + g) = 2(\lambda^T x + \lambda^{n+1})^T \begin{pmatrix} 1 \\ 0 \end{pmatrix} x - \sigma = 0, \quad (4.50)$$

and the regions Ω_q and Ω_r can be described, respectively, by the inequalities restricted by hyperplanes as:

$$\begin{bmatrix} 1 \\ 0 \end{bmatrix} x - \sigma \geq 0, \quad \begin{bmatrix} -1 \\ 0 \end{bmatrix} x + \sigma \geq 0.$$

We choose the frequency ratio of $m = 2.97$ and a forcing function amplitude $F = 0.2751N$ to solve the LMI stabilization problem in Theorem 4.6. This results in a feasible solution:

$$\tilde{\mathbf{P}}_1 = \begin{bmatrix} -422.546 & 6.7878 & -0.2307 \\ 6.7878 & -335.691 & 0.2655 \\ -0.2307 & 0.2655 & -423.048 \end{bmatrix}, \quad \tilde{\mathbf{P}}_2 = \begin{bmatrix} 7.1287 & 0.1781 & -2.7433 \\ 0.1781 & 7.1287 & -3.3345 \\ -2.7433 & -3.3345 & -706.9402 \end{bmatrix},$$

with an optimum value of $\beta = 193.3704$. Therefore, the non-smooth TS fuzzy model (3.36) is structurally (exponentially) stable as confirmed by the bifurcation diagram of Fig. 3.23b. However, close to the grazing point where the bifurcation occurs, e.g. the operating point ($m = 2.97$, $F = 0.2757N$), solving the LMI problem will result in an infeasible solution although the local orbit is actually stable. To relax this conservative result of LMI formulation, finer partitions are needed. Therefore, we partition further the fuzzy state space into four partitions such that two partitions are formed quite close to Λ_{qr} as described by (4.50). Thus, the partitions can be restricted by the following hyperplanes:

$$\begin{aligned} (f^a)^T x - \sigma - 0.0002 &\geq 0, & (f^b)^T x + \sigma + 0.0002 &\geq 0, \\ (f^a)^T x - \sigma &\geq 0, & (f^b)^T x + \sigma &\geq 0, \\ (f^a)^T x - \sigma + 0.0002 &\geq 0, & (f^b)^T x + \sigma - 0.0002 &\geq 0, \end{aligned} \quad (4.51)$$

where $f^a = [1 \ 0]$ and $f^b = [-1 \ 0]$. With the above partitioning, solving the LMI problem gives the feasible solution:

$$\begin{aligned} \tilde{\mathbf{P}}_1 &= \begin{bmatrix} -422.4312 & 8.7087 & -0.2833 \\ 8.7087 & -335.7263 & 0.3126 \\ -0.2833 & 0.3126 & -422.9401 \end{bmatrix}, & \tilde{\mathbf{P}}_2 &= \begin{bmatrix} 9.2904 & 0.2321 & -4.3017 \\ 0.2321 & 9.2904 & -4.3548 \\ -4.3017 & -4.3548 & -706.8930 \end{bmatrix}, \\ \tilde{\mathbf{P}}_3 &= \begin{bmatrix} 6.7425 & 0.1684 & -3.4002 \\ 0.1684 & 6.7425 & -3.5557 \\ -3.4002 & -0.3557 & -706.9479 \end{bmatrix}, & \tilde{\mathbf{P}}_4 &= \begin{bmatrix} -422.1627 & 8.4460 & -0.2702 \\ 8.4460 & -335.6612 & 0.3301 \\ -0.2702 & 0.3301 & -423.0231 \end{bmatrix}, \end{aligned}$$

with the optimum value of $\beta = 241.29$. These LMI results verify that the local orbit is structurally (exponentially) stable near the grazing point ($m = 2.97$, $F = 0.2757N$). Having more partitions (eight partitions), in which the regions are restricted closer to the hyperplane $(f^a)^T x - \sigma = 0$, we can achieve an accuracy of ($m = 2.97$, $F = 0.275762N$) in the prediction of grazing bifurcation point.

The LMI problem in Theorem 4.6 can also analytically confirm the other conditions of grazing (Figs. 3.22f-j) when the periodic orbit is stable. For instance, for the operating points $m = 2$, $F \in [1.4975N, 1.4990N]$ and $m = 3$, $F \in [0.048N, 0.052N]$, the feasibility problem can be solved with two region partitions and four region partitions of \mathcal{F} as explained above. The large chaotic region, occurring between the operating points

$m = 2.97$, $F \in [0.2760N, 0.2763N]$ (see also Fig. 3.23b), resulting from the grazing bifurcation, can be recognized by the infeasibility of the LMI stabilization problem, with the region partitioning as described by (4.51).

Stability at the grazing point: In the previous section, the problem of the infinite stretching of the phase space near the grazing event was overcome by applying the proposed LMI stability conditions in Theorem 4.6 to provide an analysis of the grazing bifurcation. However, the special case of Theorem 4.6 *at the grazing event* ($\varpi = 2.97$ and $F = 0.2759N$) needs further examination because of the resulting conservative LMI formulations. This problem is analyzed here to show that the resulting formulations are actually quadratic matrix inequalities (QMIs), which are actually not solvable since the local piece-wise quadratic matrices P_q are not invertible at the grazing point. The analysis is presented here in the hope that future LMI solvers will be able to overcome this difficulty.

At the operating point ($m = 2.97$ and $F = 0.2759N$) where the grazing event occurs, solving the feasibility problem of Theorem 4.6 will take an infinite amount of computational time for optimizing the local minima, even if the number of regions for a non-smooth Lyapunov function is increased or the regions are formed arbitrary close to the hyperplane $(f^a)^T x - \sigma = 0$. To investigate this seemingly conservative LMI formulation, we need to delve into the LMI stabilization problem of Theorem 4.6. For this purpose, we define a PDC-like structured close-loop system based on the non-smooth TS fuzzy model of the hard-impact oscillator (3.36). Therefore, by defining a gain matrix for each fuzzy sub-vector field, the local gains can be designed with the following structure:

$$\begin{cases} u(t) = \sum_{j=1}^{l_m} \mu^j(x, m) K^j(m) x(t) \\ m^+ = \xi(x, m), \\ x^+ = \chi(x, m), \end{cases} \quad (4.52)$$

where the gain matrices are reasonably assumed to be bounded as $\sup_{1 \leq j \leq l_m} \|F^j\| \leq 1$. Substituting (4.52) into the model (3.36), the closed-loop TS fuzzy system is represented as

$$\begin{cases} \dot{x} = \sum_{j=1}^{l_m} \sum_{i=1}^{l_m} \mu^j(x, m) \mu^i(x, m) \{A^j(m)x \\ \quad + B^j(m)K^i(m)\}x(t) \\ m^+ = \xi(x, m), \\ x^+ = \chi(x, m). \end{cases} \quad (4.53)$$

Looking at system dynamics just before the impact and at the grazing point x_G (see Figs. 2.23a and 2.23b), it is interesting to know how the solution trajectory reacts just before the impact, under a small perturbation. The perturbation can be defined as parametric uncertainty matrices for the fuzzy sub-vector fields of the model (3.36) with the following assumption, which unlike Assumption 4.1, is defined for the non-smooth structure of TS fuzzy model of impacting system.

Assumption 4.2: The parametric uncertainties considered for the TS fuzzy model

(3.36) are norm-bounded, in the form:

$$\begin{cases} [\Delta A^j(m) \ \Delta B^j(m)] = D^j(m) F^j(m) [E^{1j}(m) \ E^{2j}(m)], \\ m^+ = \xi(x, m), \\ x^+ = \chi(x, m). \end{cases}$$

where $D^j(m) \in \Re^{n \times n}$, $E^{1j}(m) \in \Re^{n \times n}$ and $E^{2j}(m) \in \Re^{n \times n}$ are known matrices, and $K^j(t)(m) \in \Re^{n \times n}$ is an unknown matrix function with *Lebesgue*-measurable elements such that $(F^j(m))^T F^j(m) \leq I_{n \times n}$.

To determine the components of the known matrices in Assumption 4.2, the idea of the variational equations [169] can be used to obtain a solution for the fuzzy sub-vector fields when the system trajectory experiences a small perturbation. Therefore, say, for the parametric uncertainty matrix $\Delta A^j(m_2)$, $j = 1, 2$, we look for a periodic solution to the following variational equation:

$$\frac{d}{dt} \begin{bmatrix} \delta x_1(t) \\ \delta x_2(t) \end{bmatrix} = \begin{bmatrix} 0 & 1 \\ -w_n^2 & -0.2\zeta w_n \end{bmatrix} \begin{bmatrix} \delta x_1(t) \\ \delta x_2(t) \end{bmatrix}, \quad \begin{cases} \delta x_1(0) = \delta x_{10} \\ \delta x_2(0) = \delta x_{20} \end{cases}. \quad (4.54)$$

The solution of the above equation, which can be solved as a first-order differential equations, is obtained for an infinitesimal time of evolution τ , as follows:

$$\begin{bmatrix} \delta x_1(\tau) \\ \delta x_2(\tau) \end{bmatrix} = e^{-0.1\zeta w_n \tau} \begin{bmatrix} C_\tau + \frac{0.1\zeta}{\eta} S_\tau & S_\tau / \omega_0 \\ -\frac{1}{\eta} \omega_0 S_\tau & C_\tau - \frac{0.1\zeta}{\eta} S_\tau \end{bmatrix} \begin{bmatrix} \delta x_{10} \\ \delta x_{20} \end{bmatrix}, \quad (4.55)$$

where $\omega_0 = \omega_n \eta$, $\eta = \sqrt{1 - 0.01\zeta^2}$, $C_\tau = \cos(\omega_0 \tau)$ and $S_\tau = \sin(\omega_0 \tau)$. Now, if we substitute τ with the period T and specify $\Delta B^j(m_2) = [0 \ 0]^T$, $j = 1, 2$, based on Assumption 4.2, the $\Delta A^j(m_2)$, $j = 1, 2$ can be equivalently described by:

$$\begin{aligned} E^{2j}(m_2) &= [0 \ 0]^T, \quad E^{1j}(m_2) = \begin{bmatrix} C_\tau + \frac{0.1\zeta}{\eta} S_\tau & S_\tau / \omega_0 \\ -\frac{1}{\eta} \omega_0 S_\tau & C_\tau - \frac{0.1\zeta}{\eta} S_\tau \end{bmatrix} \\ D^j(m_2) &= e^{-0.1\zeta w_n \tau} \begin{bmatrix} -1 & 0 \\ 0 & 1 \end{bmatrix}, \quad F^j(m_2) = \begin{bmatrix} \delta_1(t) & 0 \\ 0 & \delta_2(t) \end{bmatrix}, \end{aligned}$$

with $j = 1, 2$ for all matrices. The fourth condition of Theorem 4.6 requires that the local Lyapunov function $V_q : \mathbf{cl}\Omega_q^x \rightarrow \Re$ in (4.16) be decreased in its region of validity. In other words, the fourth LMI condition will be fulfilled if the time derivative of $V_q(x)$ is negative for all the fuzzy sub-vector fields in the defined regions. Therefore, the time derivative of $V_q(x)$ based on (4.17) for the perturbed closed-loop TS fuzzy system (4.53), can be derived through parametric uncertainties as:

$$\dot{V}_q(x) = \sum_{j=1}^{l_m} \sum_{i=1}^{l_m} \mu^j(x, m) \mu^i(x, m) \frac{\partial V_q(x)}{\partial x} \{ (A^j(m) + \Delta A^j(m))x + (B^j(m) + \Delta B^j(m))K^i(m) \} x. \quad (4.56)$$

With the knowledge of $\mu^j \mu^i \geq 0$, for $V_q(x)$, $q \in I_\Delta$ to be negative, the following condition

must be fulfilled:

$$\frac{\partial V_q(x)}{\partial x} \{(A^j(m) + \Delta A^j(m))x + (B^j(m) + \Delta B^j(m))K^i(m)\}x \leq 0, \quad x \in \Omega^{x, m_i, j}, \quad m_i \in \Omega_q^m.$$

Based on the quadratic piecewise structure of local Lyapunov functions (4.18), the above can be expanded as follows:

$$\begin{aligned} \dot{x}^T P_q x + \dot{x}^T p_q + x^T P_q \dot{x} + p_q^T \dot{x} &= \sum_{j=1}^{l_m} \sum_{i=1}^{l_m} \mu^j(x, m) \mu^i(x, m) \{ \{ ((A^j(m) + \Delta A^j(m) + (B^j(m) + \Delta B^j(m))K^i(m))x)^T P_q x + x^T P_q (A^j(m) + \Delta A^j(m) \\ &\quad + (B^j(m) + \Delta B^j(m))K^i(m))x \} \{ ((A^j(m) + \Delta A^j(m) + (B^j(m) + \Delta B^j(m))K^i(m))x)^T p_q + p_q^T (A^j(m) + \Delta A^j(m) \\ &\quad + (B^j(m) + \Delta B^j(m))K^i(m))x \} \}. \end{aligned} \quad (4.57)$$

This may be reformulated as:

$$\begin{aligned} \dot{x}^T P_q x + x^T P_q \dot{x} &= \sum_{j=1}^{l_m} (\mu^j(x, m))^2 x^T \{ (A^j(m) + \Delta A^j(m) + (B^j(m) + \Delta B^j(m))K^i(m))^T P_q \\ &\quad + P_q (A^j(m) + \Delta A^j(m) + (B^j(m) + \Delta B^j(m))K^i(m)) \} x(t) \\ &\quad + 2 \sum_{j < i}^{l_m} \mu^j(x, m) \mu^i(x, m) x^T \{ ((A^j(m) + \Delta A^j(m) + (B^j(m) + \Delta B^j(m))K^i(m)) \\ &\quad + A^i(m) + \Delta A^i(m) + (B^i(m) + \Delta B^i(m))K^j(m))/2)^T P_q + P_q ((A^j(m) \\ &\quad + \Delta A^j(m) + (B^j(m) + \Delta B^j(m))K^i(m) + A^i(m) + \Delta A^i(m) + (B^i(m) \\ &\quad + \Delta B^i(m))K^j(m))/2) \} x \end{aligned}$$

To investigate why the LMI formulation becomes too conservative just at grazing point, it suffices to examine if the first sum of the above equation is semi-definite negative. First, we assume that this is the case as follows:

$$\begin{aligned} (A^j(m) + \Delta A^j(m) + (B^j(m) + \Delta B^j(m))K^i(m))^T P_q \\ + P_q (A^j(m) + \Delta A^j(m) + (B^j(m) + \Delta B^j(m))K^i(m)) \leq 0, \quad j \in I_{l_m}, \quad m_i \in \Omega_q^m. \end{aligned} \quad (4.58)$$

Based on the Assumption 4.2, if we seek, for instance, the equivalent of (4.58) for the fuzzy sub-vector field associated with discrete state m_2 , we obtain:

$$\begin{aligned} (A^j(m_2))^T P_q + P_q A^j(m_2) + (K^j(m_2))^T (B^j(m_2))^T P_q + P_q B^j(m_2) K^j(m_2) \\ + P_q D^j(m_2) F^j(m_2) (E^{1j}(m_2) + E^{2j}(m_2) K^j(m_2)) + (E^{1j}(m_2) \\ + E^{2j}(m_2) K^j(m_2))^T (F^j(m_2))^T (D^j(m_2))^T P_q \leq 0. \end{aligned} \quad (4.59)$$

To ease the theoretical difficulties that interior-point algorithms will face when solving the LMI (4.59) with uncertain constraints, the formulation can be transformed using the following Lemma [170]:

Lemma 4.2: The following inequality holds:

$$S + DFE + E^T F^T D^T < 0,$$

where $D \in \mathbb{R}^{n \times n}$, $E \in \mathbb{R}^{n \times n}$ are given as constant matrices, $S \in \mathbb{R}^{n \times n}$ is a symmetric constant matrix and F fulfills the condition $F^T F \leq I_{n \times n}$, if and only if for some $\epsilon > 0$

$$S + \begin{bmatrix} \epsilon^{-1} E^T & \epsilon D \end{bmatrix} \begin{bmatrix} \epsilon^{-1} E \\ \epsilon D^T \end{bmatrix} < 0.$$

Using Lemma 4.2, (4.59) holds for all the gain matrices K^j such that $(K^j)^T K^j \leq I_{n \times n}$, if and only if there exists a constant $(\epsilon^{jj})^{1/2}$ such that

$$\begin{aligned} & (A^j(m_2))^T P_q + P_q A^j(m_2) + (K^j(m_2))^T (B^j(m_2))^T P_q + P_q B^j(m_2) K^j(m_2) \\ & + \begin{bmatrix} (E^{1j}(m_2) + E^{2j}(m_2) K^j(m_2))^T & P_q D^j(m_2) \end{bmatrix} \begin{bmatrix} (\epsilon^{jj})^{-1} I & 0 \\ 0 & (\epsilon^{jj})^{-1} I \end{bmatrix} \\ & \times \begin{bmatrix} E^{1j}(m_2) + E^{2j}(m_2) K^j(m_2) \\ (P_q D^j(m_2))^T \end{bmatrix} \leq 0, \end{aligned} \quad (4.60)$$

and by applying *Schur* complements, (4.60) can be equivalently represented as:

$$\begin{bmatrix} \Xi^{jj} & (\Upsilon^j)^T & P_q^T D^j(m_2) \\ \Upsilon^j & -\epsilon^{jj} I & 0 \\ D^j(m_2))^T P_q & 0 & (-\epsilon^{jj})^{-1} I \end{bmatrix} \leq 0, \quad (4.61)$$

where $\Xi^{jj} = (A^j(m_2))^T P_q + P_q A^j(m_2) + (K^j(m_2))^T (B^j(m_2))^T P_q + P_q B^j(m_2) K^j(m_2)$ and $\Upsilon^j = E^{1j}(m_2) + E^{2j}(m_2) K^j(m_2)$ for $j = 1, 2$.

The matrix inequality (4.61) is a quadratic matrix inequality (QMI), which is part of (4.57) and consequently part of the fourth condition in Theorem 4.6 to be fulfilled for the sub-vector field F_{m_2} . For the formulation (4.61) to be solvable by any available convex optimization technique, it must be transformed to an LMI. This is realizable if we define a transformation matrix with the element of the inverted matrix P_q^{-1} [28, 170] (see Appendix B). However, the problem is identifiable if the last condition of Theorem 4.6 is put under scrutiny. It is realized that the quadratic Lyapunov function candidate $V_q(x) = \pi_q + 2p_q^T x + x^T P_q x$, $q \in I_\Delta$ is not invertible, as otherwise for the given matrix $H(m_i)$, $i \in I_N$, the fifth condition cannot be held on the region boundary Λ_{qr} defined for the switching manifold.

Example 4.4 (Case study III continued, the dry friction oscillator). Recalling the model of dry-friction oscillator (3.42) in Example 3.8, which was found to be accurately representative of the dynamics of a system where a grazing sliding bifurcation causes an abrupt chaotic orbit by varying the frequency of oscillation ω as a bifurcation parameter (see Fig. 3.26).

It has been discussed in Section 3.2.4 that in a non-smooth TS fuzzy model, a sliding

region \hat{S} (one of the possible scenarios) can be formed by coinciding two switch sets $S_{1,2}$ and $S_{2,1}$, as is the case here. In fact, fuzzy sub-vector fields F_{m_1} and F_{m_2} represent the solution trajectories with opposite directions in the close vicinity of the switch sets; hence, they form an attractive sliding region \hat{S} . The sliding dynamics can also be described with classical formulation of sliding dynamics (Section 2.2.6), if we substitute the original vector fields F_1 and F_2 of a non-smooth system of the form (1.3), with the fuzzy sub-vector fields of the model of the dry-friction oscillator (3.42):

$$\begin{aligned} F_{m_1} &= \sum_{j=1}^{l_{m_1}} A^j(m_1)x(t) + B^j(m_1)u(t), \quad l_{m_1} = 4, \\ F_{m_2} &= \sum_{j=1}^{l_{m_2}} A^j(m_2)x(t) + B^j(m_2)u(t), \quad l_{m_2} = 4, \end{aligned}$$

where the corresponding subsystems are derived respectively as (3.40) and (3.41) in Example 3.8. For instance, using Utkin's equivalent control method, if we assume the manifold $S = \{x \in R^n \mid 1 - x_2(t) = 0\}$, resulting from coinciding $S_{1,2}$ and $S_{2,1}$, the sliding dynamics can be formulated by the equivalent control:

$$F_{m_1, m_2} = \frac{F_{m_1} + F_{m_2}}{2} + \frac{F_{m_1} + F_{m_2}}{2} U_{eq},$$

where F_{m_1, m_2} denotes sliding fuzzy sub-vector field and the equivalent control U_{eq} is described by:

$$U_{eq} = -\frac{\nabla S \cdot F_{m_1} + \nabla S \cdot F_{m_2}}{\nabla S \cdot F_{m_2} - \nabla S \cdot F_{m_1}}, \quad U_{eq} \in [-1, 1],$$

where $\nabla S = \partial S / \partial x$. Therefore:

$$U_{eq} = -\frac{F_{m_1} + F_{m_2}}{F_{m_2} - F_{m_1}}, \quad U_{eq} \in [-1, 1],$$

and the sliding region \hat{S} is

$$\hat{S} = \{x \in S : -1 \leq U_{eq} \leq 1\}.$$

For the analysis of the grazing-sliding bifurcation, the LMI stabilization problem of Theorem 4.5 is initially attempted with partitioning the fuzzy state space $\{\Omega \subseteq \mathcal{F}\}$ into two regions Ω_1 and Ω_2 , where the boundary region Λ_{qr} can be represented by the hyperplane (quadratic equalities):

$$2(\lambda^T x + \lambda^{n+1})^T (f^T x + g) = 2(\lambda^T x + \lambda^{n+1})^T \left(\begin{bmatrix} 0 \\ -1 \end{bmatrix} x + 1 \right) = 0. \quad (4.62)$$

For any forcing function frequency ω close to the frequency when grazing occurs, say $\omega = 1.707817$, the LMI results unexpectedly show infeasibility of the solution, when the $4T$ periodic orbit is still stable and grazing has not occurred (as can be seen from the phase portrait in Fig. 3.24a). This conservative result require $\{\Omega \subseteq \mathcal{F}\}$ to be partitioned

by finer regions similar to the previous case of impacting systems. The second attempt is to distribute the regions such that they are formed closer to $S = \{x \in R^n \mid 1 - x_2(t) = 0\}$, where the switch sets $S_{1,2}$ and $S_{2,1}$ coincides and form a sliding region. Hence, we have four detached regions restricted by the boundary regions (represented by hyperplanes):

$$\begin{aligned} 2(\lambda^T x + \lambda^{n+1})^T \{(f^a)^T x + g^a\} &= 0, \\ 2(\lambda^T x + \lambda^{n+1})^T \{(f^b)^T x + g^b\} &= 0, \\ 2(\lambda^T x + \lambda^{n+1})^T \{(f^c)^T x + g^c\} &= 0, \end{aligned}$$

where $f^a = f^b = f^c = [0 \ -1]$, $g^a = 0.9$, $g^b = 1$ and $g^c = 1.1$. Solving the LMI problem, in this case, results in a feasible solution for the former frequency of $\omega = 1.707817$ as:

$$\begin{aligned} \tilde{\mathbf{P}}_1 &= \begin{bmatrix} 63.089 & 8.827 & 7.217 \\ 8.827 & 56.022 & 9.312 \\ 7.217 & 9.312 & 51.619 \end{bmatrix}, \quad \tilde{\mathbf{P}}_2 = \begin{bmatrix} 63.123 & 8.681 & 8.139 \\ 8.381 & 56.402 & 9.017 \\ 8.139 & 9.017 & 51.101 \end{bmatrix}, \\ \tilde{\mathbf{P}}_3 &= \begin{bmatrix} 63.123 & 8.682 & 8.142 \\ 8.682 & 56.402 & 9.017 \\ 8.142 & 9.017 & 51.101 \end{bmatrix}, \quad \tilde{\mathbf{P}}_4 = \begin{bmatrix} 64.448 & 6.592 & 12.537 \\ 6.592 & 57.851 & 7.642 \\ 12.537 & 7.642 & 47.333 \end{bmatrix}, \end{aligned}$$

with the optimum value of $\beta = 32.053$. This means that the sliding orbit is exponentially stable in the sense of Lyapunov. However, the accuracy of feasible LMI results cannot go further than $\omega = 1.70781$, where the bifurcation point of $\omega = 1.70779$ is still not detected. Therefore, as a third attempt, the regions $\{\Omega \subseteq \mathcal{F}\}$ are formed with eight region partitions restricted by the following boundary regions:

$$\begin{aligned} 2(\lambda^T x + \lambda^{n+1})^T \{(f^a)^T x + g^a\} &= 0, \\ 2(\lambda^T x + \lambda^{n+1})^T \{(f^b)^T x + g^b\} &= 0, \\ 2(\lambda^T x + \lambda^{n+1})^T \{(f^c)^T x + g^c\} &= 0, \\ 2(\lambda^T x + \lambda^{n+1})^T \{(f^d)^T x + g^d\} &= 0, \\ 2(\lambda^T x + \lambda^{n+1})^T \{(f^e)^T x + g^e\} &= 0, \end{aligned}$$

where $f^a = f^b = f^c = f^d = f^e = [0 \ -1]$, $g^a = 0.9$, $g^b = 0.999$, $g^c = 1$, $g^d = 1.001$ and $g^e = 1.1$. The above hyperplanes introduce progressively narrower regions close to the first boundary region Λ_{qr} in (4.62) where the additional parameters λ is determined by solving the quadratic inequalities as described in Section 4.5; cf. Fig. 4.5. Moving forward, solving the LMI stabilization problem of Theorem 4.5, results in a feasible solution exactly

at the bifurcation point of $\omega = 1.70779$, with the following piecewise quadratic matrices:

$$\begin{aligned} \tilde{\mathbf{P}}_1 &= \begin{bmatrix} 19.442 & 2.354 & 24.076 \\ 2.354 & 0.631 & 3.336 \\ 24.076 & 3.336 & 999.939 \end{bmatrix}, & \tilde{\mathbf{P}}_2 &= \begin{bmatrix} 9.663 & 2.065 & 51.176 \\ 2.065 & 1.381 & 20.344 \\ 51.176 & 20.334 & 999.939 \end{bmatrix}, \\ \tilde{\mathbf{P}}_3 &= \begin{bmatrix} 11.206 & 2.153 & 67.411 \\ 2.153 & 1.148 & 20.118 \\ 67.411 & 20.118 & 999.939 \end{bmatrix}, & \tilde{\mathbf{P}}_4 &= \begin{bmatrix} 11.209 & 2.153 & 67.448 \\ 2.153 & 1.148 & 20.117 \\ 67.448 & 20.117 & 999.939 \end{bmatrix}, \\ \tilde{\mathbf{P}}_5 &= \begin{bmatrix} 9.663 & 2.065 & 51.176 \\ 2.065 & 1.381 & 20.344 \\ 51.176 & 20.344 & 999.851 \end{bmatrix}, & \tilde{\mathbf{P}}_6 &= \begin{bmatrix} 11.206 & 2.153 & 67.411 \\ 2.153 & 1.148 & 20.118 \\ 67.411 & 20.118 & 999.939 \end{bmatrix}, \\ \tilde{\mathbf{P}}_7 &= \begin{bmatrix} 11.209 & 2.153 & 67.448 \\ 2.153 & 1.148 & 20.117 \\ 67.448 & 20.117 & 999.851 \end{bmatrix}, & \tilde{\mathbf{P}}_8 &= \begin{bmatrix} 19.440 & 2.354 & 141.477 \\ 2.354 & 0.628 & 19.601 \\ 141.477 & 19.601 & 999.939 \end{bmatrix}, \end{aligned}$$

where the exponential convergence is optimized with the value of $\beta = 36.295$. Therefore, analytically the LMI stabilization problem of Theorem 4.5 confirms the stability of $4T$ periodic orbit when grazes the sliding region (see Fig. 3.24b). For any frequency less than $\omega = 1.70779$, grazing-sliding bifurcation results in a sudden chaotic attractor, which is analytically confirmed by the infeasibility of LMI results .

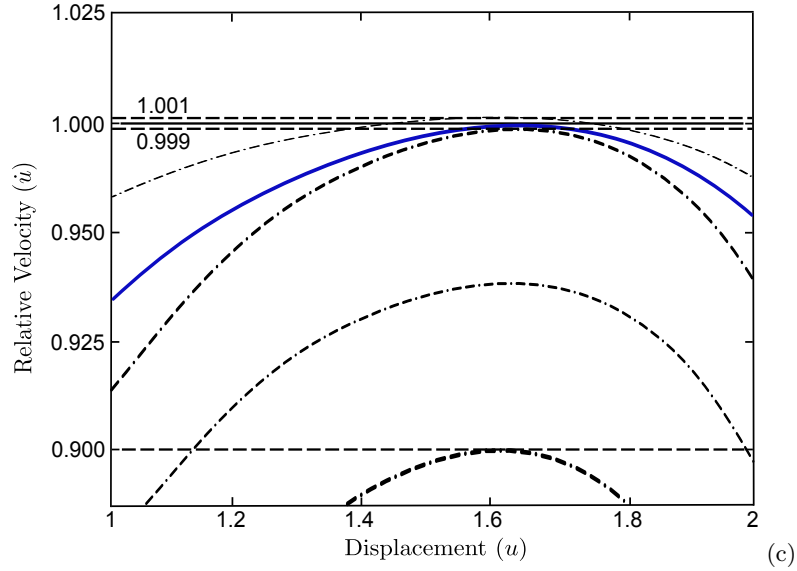


Figure 4.5: An illustration of region partitioning and estimated energy levels of the non-smooth Lyapunov function candidate in the local regions (dot-dashed curves) when sliding (local) orbit grazes the switching manifold.

As noticed, the critical numbers of piecewise quadratic matrices resulted from a feasible solution show that the proposed region partitioning plays an important role here in pinpointing the bifurcation point very close to the grazing-sliding event. The more (finer) region partitions are chosen closer to the sliding region, the more is possible to detect a bifurcation point very close to the grazing-sliding bifurcation point. However, more and finer region partitions will result in more critical piecewise quadratic matrices if the LMI

problem is found feasible, i.e. the case of $\omega = 1.70779$. Although a certain procedure does not exist to identify how many partitions and what size of partitions lead to the desired results, in practice the conservative LMI formulation for discontinuity-induced bifurcation analysis, can be relaxed by selecting finer partitions close to the sliding region. Selecting numerous partitions, nonetheless, may result in a considerable computational burden, leading to an infeasible solution. Therefore, a compromise always exists between the accuracy of the prediction of bifurcation point and the computational burden of the numerical analysis.

4.5.3 Numerical Complexity

For the LMI analysis presented in this chapter, the number of unknown LMI variables is directly proportionate to the number of region partitions of fuzzy state space. For every Ω_q encompassing the origin, there are $\frac{n(n+1)}{2}$ unknown LMI variables for each piecewise matrix \tilde{P}_q and in case of every Ω_q not encompassing the origin, the number of unknown LMI variables is increased to $\frac{(n+1)(n+2)}{2}$. If the energy level of local Lyapunov functions become equal at region boundaries $V_q = V_r$ for the set of states fulfilling $Q^k(x) = 0$, the number of unknown variables can be decreased to n or $n + 1$, cf. Appendix B.

The number of unknown parameters λ^k when substituting a region Ω by quadratic inequalities in (4.28), is directly proportionate to the number of quadratic functions $Q^k(x)$. As explained in Section 4.3.1, all the unconfined regions in LMI stabilization problem of Theorem 4.5 and Theorem 4.6 should be substituted by quadratic inequalities $Q^k(x) \geq 0$. Moreover, to verify exponential convergence, α and β are considered as unknown variables. Therefore, the number of unknown variables in the LMI stabilization problem, is proportional to the number of partitioned fuzzy regions, the number of quadratic inequalities needed for substitution and the number of quadratic equalities needed for region boundaries. How many additional parameters are needed to be specified, is case-dependant as shown by the examples in this chapter, with different dynamics close to the switching manifold. Theoretically, there is no limitation on the number of variables. However, in practice, memory capacity and the efficiency of the algorithms employed by LMI solvers can limit the maximum number of variables (see Appendix B for the LMI solvers employed in this thesis). Nonetheless, it is preferable to substitute region Ω by a lower number of quadratic inequalities as possible. Also for the reduction of unknown variables, the quadratic inequalities describing ellipsoids (Section 4.5) are better substitutions for a flexible-sized region Ω . Moreover, if the fuzzy sub-vector field of a non-smooth TS fuzzy model fulfills the condition

$$\sum_{j \in \{1, 2, \dots\}} w^j(x, m_i)(A^j(m_i)x + B^j(m_i)) = - \sum_{j \in \{1, 2, \dots\}} w^j(-x, m_i)(A^j(m_i)(-x) + B^j(m_i)),$$

and the regions are partitioned such that for every Ω^+ fulfilling positive states, there is a symmetrical Ω^- fulfilling negative states where $x \in \Omega^+ \Rightarrow -x \in \Omega^-$, then the same set of quadratic inequalities can be used for the substitution of both Ω^+ and Ω^- to reduce the number of unknown variables in the LMI problem.

To reduce LMI variables even further, it is possible to set some parameters and variables to pre-determined values. The great disadvantage of reducing the computational burden in this way is that the LMI problem of interest may be found conservative without a feasible solution though, a solution for the LMI problem actually exists before setting the parameters to pre-determined values.

4.6 Robustness

This section is focused on stability robustness issues of non-smooth TS Fuzzy models presented in the preceding sections. A considerable number of attempts in designing robust controllers and robust switching controllers for the stabilization problem (in its classical notion) of TS fuzzy systems can be found in the literature. These attempts mainly take advantage of classical observer methods such as sliding mode, H_∞ criteria, state-feedback and so on [171–176] (also see [28] and the references therein). However, stability robustness becomes a major concern in this thesis, when the possibility of curbing DIBs leading to chaos and preserving the (structurally) stable periodic solution (period-1 orbit) in the presence of model uncertainties are to be investigated. In this respect, the model uncertainties can appear in the location of the switch sets and also the modeled continuous fuzzy sub-vector fields. Specifically it will be shown in the next chapter, that these model uncertainties can play an important role in designing robust controllers for suppressing the chaotic phenomena in non-smooth TS fuzzy models.

4.6.1 Model uncertainties in switch sets

There are different reasons for incorporating uncertainties in modeling of switch sets. Some of these uncertainties arise from the physical system itself. For instance, the location of switch sets may be changed as a result of uncertainties in the parameters of a physical system. Uncertainties in the location of the switch sets may further occur while modeling a dynamical system. For instance, unmodeled dynamics like neglected dead times may result in an unknown location of switch sets. Furthermore, if there is a delay for a real-time system in generating the next instantaneous value of the controller signal, the resulting dead time is normally ignored in the modeling of many systems. Batch processes with a sequence of processing actions [177] can be a good example of this kind of model uncertainties. Delay in generating an instantaneous signal for switchings in high-frequency power electronic converters would be another example. Finally, the location of the switch sets may become uncertain resulting from unforeseen and/or uncontrollable events such as an operator pushing a button.

Using Lyapunov framework presented for structural stability in sections 4.3 and 4.4, these uncertainties arising from any source can be easily incorporated in the non-smooth TS model by extending the nominal switch sets to guarantee stability. To discuss this further, first assume that fuzzy states (x, m_i) and (x, m_k) are both satisfy the second, third and fourth conditions of the theorems proposed in Section 4.3 and 4.4. If the fuzzy states (x, m_i) and (x, m_k) are both in the same region partition Ω_q , then the stability of the TS fuzzy system can be held when switching from the fuzzy sub-vector field F_{m_i} to F_{m_k} .

This can be deduced from the fifth stability condition when the local Lyapunov function V_q is actually the same at both these states, implying that local Lyapunov functions are equal when the switching between two fuzzy sub-vector fields occur. Therefore, at least from a robustness point of view, a common local Lyapunov function for different discrete states is desirable. In case of sliding mode behavior, the infinitely fast switching cannot be allowed, mainly because such behavior may introduce dynamics other than the nominal one. Nevertheless, it can be allowed if the sliding dynamics are defined in a way such that the common Lyapunov function becomes valid for the sliding dynamics as well, cf. Section 3.2.4.

Now assume that the fuzzy states (x, m_i) and (x, m_k) are in different region partitions Ω_q and Ω_r , respectively. As implied from the fifth stability condition in the LMI stabilization problem of Theorem 4.5, when the local Lyapunov function $V_r(x)$ becomes less than or equal to $V_q(x)$, it is possible to switch from F_{m_i} to F_{m_k} at the continuous fuzzy state x . To assure stability in the proposed Lyapunov framework, local Lyapunov functions should be reduced (in the same region and in different regions resulted from switching between F_{m_i} and F_{m_j}). The set of continuous Fuzzy states that fulfill this requirement, are called *admissible switch regions* or *ASR* due to the fact that when switching of fuzzy sub-vector fields occur, the structural stability is not violated. The notation $ASR(m_i, m_k)$ is adopted to indicate the set of continuous fuzzy states when F_{m_i} is allowed to be changed to F_{m_k} . Normally $ASR(m_i, m_k)$ is much larger than the nominal switch set $S_{i,k}$; hence, $S_{i,k} \subseteq ASR(m_i, m_k)$. Also the union of the *ASR* follows:

$$ASR(m_i, m_k) \cup ASR(m_k, m_i) \supseteq \forall x \text{ where } \{\exists m_i, m_k \mid V_q(x) \in \Omega_q, V_r(x) \in \Omega_r\}.$$

Note that normally

$$ASR(m_i, m_k) \cup ASR(m_k, m_i) \supseteq S_{i,k} \cup S_{k,i},$$

which arise from requiring the LMI conditions to be valid in larger regions than necessary. This in turn might result in a conservative LMI formulation when substituting the region partitions by quadratic inequalities (Sections 4.3.1 and 4.5). If m_i and m_k are the discrete states allowed to be in the entire fuzzy state space \mathcal{F} , then

$$ASR(m_i, m_k) \cup ASR(m_i, m_k) = \mathcal{F}.$$

The exponential convergence rate to the stable periodic orbit will be fixed if the switching occurs in the *ASRs* instead of the switch sets originally defined for the model. This is due to fifth condition of the LMI stabilization problems having no direct impact on the $R(k_1, k_2)$ estimate. Even though *ASRs* are actually measured from a given Lyapunov function, it is possible to incorporate uncertainties in the switch sets before solving the feasibility problem. The advantage of such inclusion is that structural stability can still be verified by switching anywhere in the *ASR*. This arises from the fact that the non-smooth Lyapunov function is compelled to reduce in the uncertain regions where there is a possibility for sub-vector field switching. These uncertain switch sets are then substituted

with quadratic inequalities as previously described. There may be a possible scenario when uncertain switch regions $S_{i,k}$ and $S_{k,i}$ overlap in the continuous fuzzy state space, implying that the switching can be bidirectional ($F_{m_i} \rightarrow F_{m_k}$ or $F_{m_k} \rightarrow F_{m_i}$) at the same fuzzy continuous states. It practically requires that the associated local Lyapunov functions must be equal to each other at these states, otherwise the stability can not be verified. In the event of sliding motion in such uncertain regions, the non-smooth Lyapunov function must also be reduced for the region allocated to the sliding dynamics.

Generally, by increasing the degree of uncertainty in the switch sets, producing larger uncertain switch regions, the LMI stability conditions may become conservative. Therefore, there is always a tradeoff between the degree of uncertainty and the possibility of finding a feasible solution to the LMI problem. All the way, if a solution exists, *ASR* can be calculated and the uncertain switch regions can be stretched even more.

4.6.2 Model uncertainties in selecting fuzzy sub-vector fields

The Lyapunov framework proposed in this chapter can be essentially employed for the robustness analysis of existing uncertainties in different fuzzy sub-vector fields and the corresponding subsystems of a non-smooth TS fuzzy system. These uncertainties can be traced between two dichotomies: uncertainties as to which fuzzy state combinations are possible in a fuzzy system, which, in turn, result in uncertain selection of the different sub-vector fields, and uncertainties in the values of the sub-vector fields at different fuzzy states. These types of uncertainties may also arise from uncertainties in parameter identification or unmodeled dynamics in the original mathematical model of the physical system. The second type of uncertainties is the out of the scope of this discussion but there is literature covering this aspect (see for instance [178–181]). When not all of the fuzzy state combinations are realizable in a non-smooth TS fuzzy system, this may lead to uncertainties in selecting the possible sub-vector fields at certain continuous states. This is a major attribute of TS fuzzy systems, which are the convex combination of the weighted affine subsystems and sub-vector fields, or any system of the form of a weighed sum of affine subsystems. The problem arises from the fact that the associated weight of a fuzzy sub-vector field (or in our case support $[w]^0$ as defined in (3.24)) may be quite uncertain as a result of the use of a given identification method.

The conditions in LMI stabilization problems are confined to the nominal regions where the fuzzy states are possible. Nevertheless, as highlighted above, the formulation in the second, third, and fourth stability conditions provides the possibility for the flexible regions to be larger than the nominal specified ones. This can be implemented by the substitution of regions by quadratic inequalities, although this may lead to a conservative formulation as pointed out in Sections 4.3.1 and 4.5. The larger regions allow, for instance, the fuzzy sub-vector fields F_{m_1} and F_{m_3} to switch to F_{m_2} anywhere in the fuzzy state space, even though the Lyapunov function is originally bound to be reduced for F_{m_2} in the region $|x_1| < x_0$. Uncertainties arising from the unknown location of fuzzy sub-vector fields can also be formulated in the LMI stabilization problems by confining the stability conditions to the uncertain regions, in the same format highlighted above.

It is already known that in a non-smooth TS fuzzy model as proposed by Definition

3.1, a fuzzy sub-vector field is the convex hull of affine sub-systems. There might be the case when a local Lyapunov function can be found to verify the stability of all extreme members of the convex hull for different fuzzy sub-vector fields. In this case, the Lyapunov (energy) function can be reduced for such extreme members (sub-systems). However, this might not result in verifying the stability of a non-smooth TS fuzzy system due to two possible scenarios.

- First, when local Lyapunov functions allocated to regions sharing the same boundary, are not equal at some boundary states, the stability is verifiable, if and only if, the solution trajectories evolve in a direction such that the non-smooth Lyapunov function reduces at these states. Therefore, all extreme members of the convex hull must evolve in the same direction.
- Second, if local Lyapunov functions are equal at some boundary states, solution trajectories can evolve bidirectionally. However, verifying stability when sliding motion occurs at the region boundaries will be problematic.

According to our assumptions, all sliding motions (in case of their occurrence) should be substituted by their equivalent dynamics in a TS fuzzy model, cf. Section 3.2.4). Nevertheless, if two sub-vector fields belonging to different fuzzy regions are not equal at the region boundaries there is still a possibility that another sliding motion occurs, which is not considered in the dynamics of TS fuzzy model before verifying the stability. Therefore, the stability of a non-smooth TS fuzzy system depends on the event of the afore-mentioned possible scenarios. If these two scenarios occur, stability cannot be verified. Indeed, in the event of sliding motion, one of the local Lyapunov functions must also be the Lyapunov function defined for the sliding dynamics.

4.7 Summary

Based on the proposed non-smooth TS fuzzy model structure of Definition 3.1, a stability theory is developed in the Lyapunov sense to assess structural stability of the most important classes of non-smooth dynamical system showing different degrees of smoothness. It's been asserted that the existing theory for stability analysis of TS fuzzy systems is fundamentally restricted to the classical notion of stability (stability of equilibria). The proposed stability theorems are formulated as linear matrix inequalities (LMIs) to be solved numerically by efficient interior-point methods. Solving LMI stability conditions as a feasibility problem can analytically predict the edge of discontinuity-induced bifurcation (DIBs), the bifurcation phenomena unique to non-smooth systems, through investigating the stability of periodic solutions. The stability theorems presented in this chapter can be fairly generalized to expand the application of model-based TS fuzzy approach to non-smooth dynamical systems by suggesting a Lyapunov framework for bifurcation analysis and ensuing chaotic dynamics. A number of relevant but archetypal examples were included to support this assertion.

Using the non-smooth Lyapunov function approach is fundamental to the development of stabilization theorems for studying Filippov-type systems (sliding and non-sliding) and

impacting systems, as presented in Sections 4.3 and 4.4. Lyapunov function candidates are defined as non-smooth functions based on the switching manifold, and further piece-wise smooth in time, based on detached but flexible regions of fuzzy state space. In this manner, the stability conditions are confined in different local regions instead of the entire state space. The regions are then expressed as quadratic inequalities. By adopting the \mathcal{S} -procedure technique, the confined stability conditions are substituted by unconfined conditions. A few methods were proposed to substitute fuzzy state-space region partitions with quadratic inequalities. The chain of substitutions will result in LMI problems formulated as numerous quadratic functions with unknown parameters in a non-conservative manner. Therefore, all the stability conditions are fully recast on LMIs.

The flexibility of partitioning the fuzzy state space also plays an important role in LMI formulation of the proposed stability theorems. This flexibility allows identical local Lyapunov functions to be searched for in different fuzzy sub-vector fields or multiple local Lyapunov functions to be searched for in single fuzzy sub-vector field (and the associated discrete state). Therefore, the conservative formulation of bilinear matrix inequalities (BMI), which normally results from the piece-wise structure of quadratic Lyapunov functions, can be avoided. Moreover, region partitions can be constructed arbitrarily close to the switching manifold. It was shown how this approach can relax the conservative LMI formulations in finding a feasible solution, specially in the event of a grazing bifurcation in an impacting system and a sliding-grazing bifurcation in a sliding Filippov-type system.

Model uncertainties and inaccuracies are inevitable in any mathematical modeling attempt when trying to mimic reality. This remains true for the non-smooth TS fuzzy modeling proposed in this thesis. However, this uncertainty can be dealt with very well by the essential discontinuities and uncertainties affiliated with non-smooth dynamical systems. Robustness analysis takes advantage of the proposed Lyapunov structure when uncertainties occur in modeling the discrete states governed by switch sets and in selecting the fuzzy sub-vector fields to achieve robust control strategies and guarantee the stability (of periodic solutions in the sense of Lyapunov), which will be presented in the next chapter.

Chapter 5

Controller design for DC-DC converters

Chaos often breeds life, when order breeds habit...

HENRY ADAMS (1858-1918)

This chapter proposes Lyapunov-based control strategies to suppress nonlinear phenomena and unwanted chaos in electrical Filippov-type system like DC-DC electronic converters. The strategies are applicable to the non-smooth TS fuzzy modeling methods proposed in Chapter 3 and are mainly based on the structural stability theorems discussed in Chapter 4.

5.1 General motive

Consider a simple problem of controlling a swinging pendulum to its upright position. Although the original system is not a non-smooth system, a switching control strategy can be devised to switch between one controller pushing the pendulum up, and another controller maintaining it in its upright position. This switching control strategy can convert the close-loop system in its entirety to a piece-wise smooth system. By doing so, the fundamental problem will be narrowed down to when the switching events should take place to stabilize the pendulum at its upright position. Generally speaking, a controller can be designed in such a way that an algorithm generates switching events, based on some stability criterion, to activate locally designed controllers [182]. A common approach in studying a large class of nonlinear systems is linearization around some local points to break the system down into a number of linear sub-systems (see Definition 2.4 and Theorem 2.1 in Section 2.2.4). In a similar fashion, a nonlinear controller can be composed of a number of linear controllers that can only operate in certain pre-specified areas of state space. At the same time, a scheduling variable can be used to determine which operating

region the system is currently active and to enable the appropriate linear sub-controller. These type of controllers are known as gain-schedulers [183, 184], and are widely-used in industry. However, design of linear controllers and switching algorithms in the control industry are mainly based on engineering experience combined with lengthy simulations. Intrinsically, fuzzy logic imitates human reasoning through approximate information and underlying uncertainty to generate decisions. Non-smooth TS fuzzy models in the sense of Definition 3.1, can be ultimately viewed as an aggregation of certain local affine models. Thus, the complex control task can be distributed into several local task components. In summation, it is sensible to establish a controller design framework such as fuzzy model-based switching/gain-scheduling or fuzzy model-based adaptive control scheme.

In our design, the location of switching events in state space is crucial in terms of curbing the chaotic behavior of a non-smooth model. The design objective for a closed-loop TS fuzzy system, which is normally composed of a number of local controllers in different fuzzy operating regions, is to locate a specific fuzzy sub-vector field or a set of sub-systems such that the closed-loop system, according to the stability conditions proposed in Chapter 4, becomes *structurally* stable. Nevertheless, practically different choices of fuzzy sub-vector fields (and the corresponding sub-systems) are available to ensure close-loop stability. Therefore additional performance criteria must be imposed to satisfy the selection of the right fuzzy sub-vector fields, driving the close-loop system to a stable periodic solution.

5.2 Literature on Fuzzy-chaos control

The first attempt that seemingly utilized the classical feedback control idea and pole-placement method to control unwanted chaos is famously referred to as the OGY (Ott, Grebogi and Yorke) control method [20]. Virtually, the very nature of chaos avail OGY method in the sense of using its structural stability and its basic property of having a dense set of periodic orbits near a saddle point. The control methodology was first found unorthodox for control theorists and engineers who, till then, predominately tried to use "brute force"¹ types of controls to regulate and stabilize unstable dynamics. In fact, the essential property of many chaotic dynamical systems including NSDS asks for non-conventional control methods other than "brute force" to curb the extreme sensitivity of chaos to small variations of system's parameters. In this respect, some newly-developed approaches have been put to use in the field of chaos control, including system parameter tuning, bifurcation monitoring, entropy reduction, state pinning, phase delay, weak oscillation input, disorder input, and some specially-designed feedback and adaptive controls, to list just a few [186, 187]. These chaos control methodologies have a major impact on many

¹In mathematics, brute force technique is to consider a series of possible answers and to test the accuracy of each of them. However, here *brute force* type of control refers to the conventional method in control theory where the goal is often to prove stability of some target state, e.g. equilibrium point, or to design control laws in order to achieve such stability by making some large alterations in system parameters and testing each scenario [185]. In the same way, one approach in controlling chaos, is to make large alteration in the system, which can completely changes its dynamics in such a way as to achieve the desired behaviour (or attractor). However, OGY method by taking advantage of the nature of a chaotic attractor, attempts to make *small* time-dependent perturbations to an accessible system parameter to achieve a desired attracting time-periodic motion [20].

novel, time and energy-critical applications, such as delta-sigma modulators and power electronic converters. Nevertheless, designing nonlinear control systems to effectively suppress the harmful chaos in non-smooth dynamical systems and curb their natural, extreme sensitivity to tiny parameter variations, is an open problem.

A flurry of chaos control results using fuzzy logic approaches appeared in 1990's. Many publications [142, 143, 188–193] showed a focus on different nonlinear system applications rather than scientific curiosity. The interest is justifiable if we understand the fact that fuzzy set theory is designed to mathematically represent uncertainty and vagueness, the essential qualitative property of deterministic nonlinear dynamical systems. Hence, it can provide effective tools to deal with imprecision caused by unstable periodic behavior like bifurcation or aperiodic behaviour like chaos. The design methods for fuzzy control of chaotic systems can be branched out based on two well-known modeling approaches, the Mamdani model and the Takagi-Sugeno model. Fuzzy logic controllers (FLC) based on the Mamdani model, also referred to as model-free controllers, have been applied to systems without a requirement for the exact mathematical model of a process, or when its dynamics are unknown, for example chemical processing applications. In some cases, the mathematical model is hardly definable and the sensors provide noisy and fragmental data. Therefore, expert's knowledge can play an essential role in these types of controllers. The integration of Mamdani-type fuzzy control method with classical chaos control methods have been successful in a few cases [108, 192] to preserve stable orbits and increase the robustness to noise. The application of this method, however, has been quite limited, mainly because of the lack of systematic design procedure and availability of any analytical tool for rigorous stability analysis.

The term *fuzzy model-based control* has become popular after the introduction of the seminal paper on fuzzy system identification by Takagi and Sugeno [27]. With TS-model-based fuzzy control method, it is possible to provide effective tools for systematic design and mathematical stability analysis (taking advantage of LMIs) to stabilize chaotic dynamics with parametric uncertainties. Adopting a TS fuzzy model-based method of control can be justified by knowing that, in most real plants, although a mathematical model exists, the system may be highly nonlinear and in some intervals, uncertain. In terms of the stabilization of equilibria, considerable amounts of work have shown that this control methodology can provide promising solutions for controlling complex nonlinear plants or ill-defined models by uniting qualitative experts' knowledge with a mathematical model for the controller design [81, 172, 174, 176, 183]. The LMI technique provides the possibility of enforcing an assortment of design specifications and constraints, which can be numerically solved using efficient convex optimization algorithm when there is no analytical solution [28, 136].

The Parallel Distributed Compensation (PDC) technique was first introduced to design each local control rule based on the corresponding model rule in a TS fuzzy model [139]. The advantage of this approach is that the locally designed fuzzy controllers share the same fuzzy sets with the fuzzy model in the premise parts. As mentioned in Section 4.1.1, the stability conditions for PDC design, whether model dynamics are chaotic or not, are mainly derived from the Lyapunov direct method, where the system is represented as a

continuous-time (or a discrete-time) TS fuzzy system [171].

Adaptive controls have been merged with fuzzy model-based control to stabilize nonlinear systems showing chaotic dynamics [193–195]. Generally, an adaptive control strategy should compensate nonparametric uncertainties such as unmodeled dynamics, measurement noise, computational round-off errors and in some cases, sampling delays. Adaptive fuzzy control can, however, unite dynamic adaptation to environmental changes in the presence of nonparametric uncertainties with linguistic fuzzy information from human operators [196]. This is specially effectual when there is a high degree of unmodeled dynamics in the plant.

Presently, complex fuzzy control systems are preferably designed as continuous-time analog controllers but implemented digitally to take advantage of high-speed microprocessors such as Digital Signal Processors (DSPs) [197, 198]. Direct digital design methods cannot be employed in this respect, as digital control laws lack the necessary information of continuous-time plant lost because of digital sampling. To preserve this crucial information of analogue-designed control system during discretization, a technique called digital redesign (DR) has been proposed, which is realizable through state-matching [199]. Although the DR technique was originally developed for linear systems, it has been extended and enhanced by many others to be applicable to nonlinear systems linearized by some linearization methods [102, 103, 200, 201]. Intelligent Digital Redesign (IDR) has been introduced for the direct and efficient digital implementation of analogue-based nonlinear fuzzy algorithms [202] and has been improved to control nonlinearity of complex chaotic systems [104, 203–207].

5.3 Design problem

As defined by Definition 3.1, a non-smooth TS fuzzy model structure is basically composed of a number of fuzzy sub-vector fields (with the corresponding sub-systems), representing continuous vector fields and associated with a certain discrete state. If a fuzzy sub-vector field is represented as $F_m = \sum_{j \in \{1, 2, \dots\}} w^j(x, m)(A^j(m)x + B^j(m)u)$, we can define a set of continuous fuzzy states $x \in \mathcal{F}$ denoted by $\tilde{\Omega}_i$, $\tilde{\Omega}_i \subset \mathcal{F}$ which a fuzzy sub-vector field can belong to. In fact, the set specifies the maximum admissible region $A_F(x, m)$ where a fuzzy sub-vector field is selected. Therefore $A_F(x, m)$ can be defined as:

$$A_F(x, m) = \{F_{m_i} \mid \sum_{j \in \{1, 2, \dots\}} A^j(m_i)x + B^j(m_i)u \text{ is admissible to be selected in } \tilde{\Omega}_i\}$$

To have a minimum number of sub-vector fields at each continuous state x , the above set should be assumed "non-empty" in the region $\tilde{\Omega}$, which can be fulfilled by the condition below:

$$\bigcup_{i=1}^N \tilde{\Omega}_i = \tilde{\Omega}.$$

Moreover, in case of non-trivial design problems, it should be assumed that there exist at least two overlapping regions $\tilde{\Omega}_i$ and $\tilde{\Omega}_j$, $i \neq j$, where fuzzy sub-vector fields are unequal. There are different possible reasons for selecting a specific set of fuzzy sub-vector fields over

others. For instance, some criteria must be satisfied for the closed-loop control system, which is not possible through the selection of some specific sub-vector fields at specific states. Or alternatively, a specific set of sub-vector fields can drive the closed-loop system to instability, which can be avoided by removing them from $A_F(x, m)$. More importantly, specific sub-vector fields can be intentionally included in the set $A_F(x, m)$, which is quite advantageous when we have the knowledge of which specific sub-vector fields can best fit the design problem criteria. All told, the *design problem*, for the control strategies proposed in this chapter, can be targeted as selecting a fuzzy sub-vector field from the set $A_F(x, m)$ such that a closed-loop system becomes *structurally stable* by fulfilling specific criteria.

The **design problem** utilizes LMI stabilization problems (proposed in the form of Theorems) in Chapter 4 to design a *stable TS fuzzy closed-loop system*. Since selecting fuzzy sub-vector fields for the closed-loop system to be stable is not a unique procedure, additional criteria needs to be introduced. These additional criteria should be desirably set for faster convergence to a stable periodic solution or the so-called faster *decay rate* to the stable periodic solution, which depends on each case, where the corresponding explanation will be given.

By designing local controllers for different fuzzy sub-vector fields in different regions $\tilde{\Omega}_i$, $i = 1, 2, \dots, N$, the design problem is focused on the location of switch sets. This can be done by designing the function ξ in the non-smooth model (3.12) such that the closed-loop system becomes stable, which is verified by the LMI conditions presented subsequently in this chapter.

5.4 Fuzzy switching (gain-scheduling) strategy

The design method, presented here, is based on fulfilling two objectives. First, to design local controllers for every fuzzy sub-vector field F_m (and its corresponding sub-systems) in every region $\tilde{\Omega}_i$. It is assumed, that based on non-smooth Lyapunov function structure (4.16), a local Lyapunov function exists to measure the energy of each of the fuzzy sub-vector fields in each region $\tilde{\Omega}_i$. Local control-law design based on the *pre-determined local Lyapunov functions* may naturally come along with such local Lyapunov functions associated with each sub-vector field. The second objective is to place the location of the switch sets (or design the function ξ) such that the first, second, third and the fifth LMIs of Theorem 4.5 (see Section 4.3) along with the LMI conditions of the subsequent theorem, presented shortly, are satisfied, guaranteeing the structural stability of the closed-loop TS fuzzy system. Local control-law design exerts gain-scheduling control methodology. Henceforth, the j^{th} rule of the control input can be defined as:

Control Rule j : IF θ_1 is Γ_1^j and ... and θ_q is Γ_q^j THEN

$$\begin{cases} u(t) = -K^j(m)x(t), & j = 1, \dots, l \\ m^+ = \xi(x, m) \end{cases} \quad (5.1)$$

If a local state-feedback controller is to be designed for each fuzzy sub-vector field, the fuzzy controller can be resulted as follows:

$$\begin{cases} u(t) = \sum_{j=1}^{l_m} w^j(\theta, m) K^j(m) x(t) \\ m^+ = \xi(x, m) \end{cases} \quad (5.2)$$

The closed-loop system is a result of substituting (5.2) in a non-smooth TS fuzzy model of the form (3.12):

$$\begin{cases} \dot{x} = \sum_{j=1}^{l_m} \sum_{i=1}^{l_m} w^j(\theta, m) w^i(\theta, m) (A^j(m)x + B^j(m)K^i(m))x(t) \\ m^+ = \xi(x, m). \end{cases} \quad (5.3)$$

Computing the local feedback gains $K^j(m)$ is the first step of the fuzzy regulator design. Considering all of the assumptions mentioned in the previous section, it is assumed that the regions $\tilde{\Omega}_i$ already cover the state space, implying that the second and third conditions in the LMI stabilization problem of Theorem 4.5 are fulfilled. To determine local fuzzy regulator feedback gains $K^j(m)$, the fourth condition of stability is to be reformulated to the closed-loop system by the following Theorem:

Theorem 5.1: Let $X \in \mathbb{R}^n \times \mathbb{R}^n$ be a diagonal positive definite matrix. A non-smooth TS model (3.12) with $u \in \mathbb{R}^n$ as an input vector, can be structurally stabilized via the local controller (5.2) in the region $x \in \Omega_q^{x, m_i}$, where the fourth condition of theorem 4.5 is replaced by:

$$\begin{aligned} x \in \Omega_q^{x, m_i}, \quad \tilde{x}^T ((\bar{A}^j(m))^T + \bar{G}^{ji}(m)^T) \tilde{P}_q + \tilde{P}_q (\bar{A}^j(m) + \bar{G}^{ji}(m)) \\ + \bar{X}(m) \tilde{P}_q \bar{X}(m) \tilde{x} < 0, \quad m_i \in \Omega_q^m, q \in I_\Delta \end{aligned} \quad (5.4)$$

where $\bar{A}^j(m) = \begin{bmatrix} A^j(m) & 0 \\ 0 & 0 \end{bmatrix}$, $\bar{G}^{ij}(m) = \begin{bmatrix} -B^j(m)K^i(m) & 0 \\ 0 & 0 \end{bmatrix}$ and $\bar{X}(m) = \begin{bmatrix} X(m) & 0 \\ 0 & 0 \end{bmatrix}$.

Proof: Choose the non-smooth Lyapunov function in (4.16) and the piecewise quadratic structure for local Lyapunov function V_q as defined by (4.18) valid in each region Ω_q . As $V_q(x)$ is assumed to be continuously differentiable on $\text{cl}\Omega_q^x$, $q \in I_\Delta$, the time derivative of $V_q(x)$, with regards to (4.17), for the closed-loop system (5.3) can be derived as:

$$\dot{V}_q(x) = \sum_{j=1}^{l_m} \sum_{i=1}^{l_m} w^j(\theta, m) w^i(\theta, m) \frac{\partial V_q(x)}{\partial x} (A^j(m)x + B^j(m)K^i(m))x, \quad (x, m) \in \Omega_q \quad (5.5)$$

It follows directly from (5.5) that if:

$$\frac{\partial V_q(x)}{\partial x} (A^j(m)x + B^j(m)K^i(m))x \leq 0, \quad x \in \Omega^{x, m_i, j}, m_i \in \Omega_q^m$$

then $\dot{V}_q(x) \leq 0$, $q \in I_\Delta$ due to the fact that $w^j(\theta, m)w^i(\theta, m) \geq 0$. Using the piecewise quadratic structure (4.18), this condition can be formulated as:

$$\begin{aligned} \dot{x}^T P_q x + \dot{x}^T p_q + x P_q \dot{x} + p_q^T \dot{x} &= \tilde{x}^T (\bar{A}^j(m)^T \tilde{P}_q + \tilde{P}_q \bar{A}^j(m) \\ &= + \bar{G}^{ji}(m)^T \tilde{P}_q + \bar{G}^{ji}(m) \tilde{P}_q) \tilde{x} \end{aligned}$$

where $\bar{A}^j(m) = \begin{bmatrix} A^j(m) & 0 \\ 0 & 0 \end{bmatrix}$, $\bar{G}^{ij}(m) = \begin{bmatrix} -B^j(m)K^i(m) & 0 \\ 0 & 0 \end{bmatrix}$, $\tilde{P}_q = \begin{bmatrix} P_q & p_q \\ p_q^T & \pi_q \end{bmatrix}$, and $\tilde{x} = \begin{bmatrix} x \\ 1 \end{bmatrix}$.

Let $X(m)$ be a diagonal positive definite matrix so we can write:

$$\tilde{x}^T ((\bar{A}^j(m)^T + \bar{G}^{ji}(m)^T) \tilde{P}_q + \tilde{P}_q (\bar{A}^j(m) + \bar{G}^{ji}(m))) + \bar{X}(m) \tilde{P}_q \bar{X}(m) \tilde{x} < 0, \text{ for all } i \in I_{l_m}, j \in I_{l_m}, \quad (5.6)$$

From (5.6), it follows:

$$\dot{V}_q(x(t)) \leq \dot{\tilde{x}}^T(t) \bar{X}(m) \tilde{P}_q \bar{X}(m) \tilde{x}(t) \leq -\beta V(x(t)),$$

where $\beta = -(\lambda_{\min}(\bar{X}(m) \tilde{P}_q \bar{X}(m)) / \lambda_{\max}(P_q))$ and $\lambda_{\min}(\cdot), \lambda_{\max}(\cdot)$ denote the minimal and maximal eigenvalues of the matrix, respectively. Hence:

$$V(x(t)) \leq V(0) e^{-\beta t},$$

assuming '0' is the fixed point of the Poincaré map. Therefore, $\|x(t)\|^2 \leq (V(0) / \lambda_{\min}(\tilde{P}_q)) e^{-\beta t}$ is concluded. Q.E.D.

Remark 5.1: Conventional fuzzy-chaos control methods (see Section 5.2) are primarily designed to suppress chaos thus improving the transient response is not a matter of focus due to the fact that fulfilling these two design criteria is hard to achieve. The intention of introducing diagonal matrices $X \in \mathbb{R}^n \times \mathbb{R}^n$, contrary to the standard control practice able to fulfill only one design criterium, is to achieve a better transient response as well as to guarantee structural stability (period-1 operation) of the converter. A similar approach have been proposed by Lian et al. [112] to achieve the best transient response, however this was for an average (or smooth) model of DC-DC converters, which as discussed before (see case study I in Section 2.1.1) would entirely ignore the fast-scale instabilities such as period-doubling bifurcation and chaos. Here, the diagonal matrix $X(m)$ is introduced to provide a faster decay rate for the trajectory associated with each discrete state m_i ; and therefore, a better transient performance for each controller gain $K^i(m)$ associated with each sub-vector field. If the right numbers are plugged into the diagonal matrices, the close-loop system may converge faster to the stable periodic solution (stable fixed point of the Poincaré map) fulfilling the LMI conditions of Theorem 4.5 and Theorem 5.1.

After designing local controllers, switch sets should be located (if possible) such that a local Lyapunov function associated with a fuzzy sub-vector field decreases at each discrete state according to the fifth condition of stability in Theorem 4.5. The proposed method to locate the switch sets (design function ξ) follows as a result of the LMI stability conditions

formulated in Theorem 4.5 and reformulated in Theorem 5.1. As previously mentioned, local Lyapunov functions are naturally available from local control-law design according to Theorem 5.1. Therefore, if the switch sets are to be located (or the function ξ are to be designed) such that the conditions in Theorem 4.5 along with Theorem 5.1 are fulfilled, then structural stability of the closed-loop fuzzy system can be achieved. The idea can be enlightened by the following example.

Example 5.1. Assume a non-smooth TS fuzzy system of the form (3.12) with two simple linear fuzzy sub-vector fields (without any corresponding sub-systems). The sub-vector fields are described by the matrices:

$$F_{m_1} = \begin{bmatrix} 1 & 3 \\ 0 & 0.1 \end{bmatrix}, \quad F_{m_2} = \begin{bmatrix} 0.1 & 0 \\ -3 & 1 \end{bmatrix}$$

Also assume the system is (structurally) stabilizable by a non-smooth Lyapunov function, composed of local quadratic matrices

$$P_1 = \begin{bmatrix} 1 & -5 \\ -5 & 50 \end{bmatrix}, \quad P_2 = \begin{bmatrix} 50 & 5 \\ 5 & 1 \end{bmatrix}$$

and illustrated respectively as cross-hatched regions in the left and middle picture of Figure 5.2. As apparent, the two regions fulfilled the condition (see Section 5.3)

$$\bigcup_{i=1}^2 \tilde{\Omega}_i = \tilde{\Omega}$$

by covering the whole fuzzy state space and also overlapping each other at specific states where a sub-vector field are to be selected from two possible choices. The weighting function for this non-smooth fuzzy system is given in Fig. 5.1. The regions where the local Lyapunov functions P_1 and P_2 are strictly reducing are depicted in Figure 5.3 as cross-hatched areas. Having known the solution trajectory direction, if the sub-vector fields are chosen in such a way that F_{m_1} is switched to F_{m_2} somewhere in the selected region (first and third quadrants of Figure 5.3 (left)) and remain in that manner until the states in the second and fourth quadrants of Figure 5.3 (right) are reached, the switching direction reverses as F_{m_2} is switched to F_{m_1} and so on; therefore, ensuring stability. The switching between fuzzy sub-vector fields can take place anywhere in the cross-hatched region. One possible scenario is shown in Figure 5.4. Switching anywhere in the interior of the cross-hatched region results in exponential convergence to the stable fixed point according to Theorem 4.5.

With a pre-determined Lyapunov function as in this example (and in general if determined by Theorem 5.1), the assumption of the time when switching between sub-vector fields takes place is essential in ensuring the stability of the closed-loop system. If we let the switching occur when the local Lyapunov functions are equal at region boundaries, the other possibilities of fulfilling the stability conditions are, in practice, eliminated, resulting in an unstable system in some cases. Choosing a sub-vector field associated with

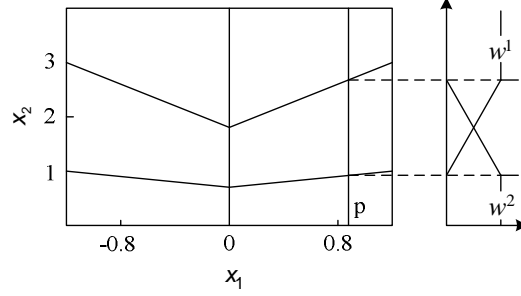


Figure 5.1: Weighting function $w^j(\theta)$ for a specific value p of x_1 . The vertices of the weighting functions for a specific value p of x_1 are given by the intersection of the vertical $x_1 = p$ and the hyperplanes.

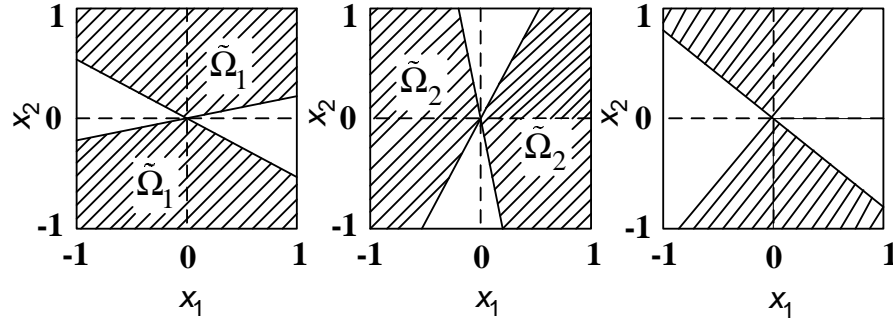


Figure 5.2: The cross-hatched regions are states fulfilling (left) $x^T(F_{m_1}P_1 + P_1F_{m_1})x \leq 0$, (middle) $x^T(F_{m_2}P_2 + P_2F_{m_2})x \leq 0$ and (right) $x^T(P_2 - P_1)x \leq 0$.

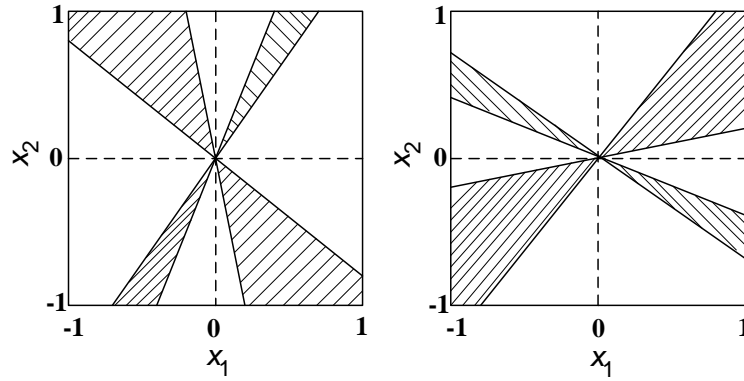


Figure 5.3: The cross-hatched regions indicate states where both local Lyapunov functions decreases and the energy reduces when the switching occurs from $F_{m_1}x$ to $F_{m_2}x$ and $F_{m_2}x$ to $F_{m_1}x$.

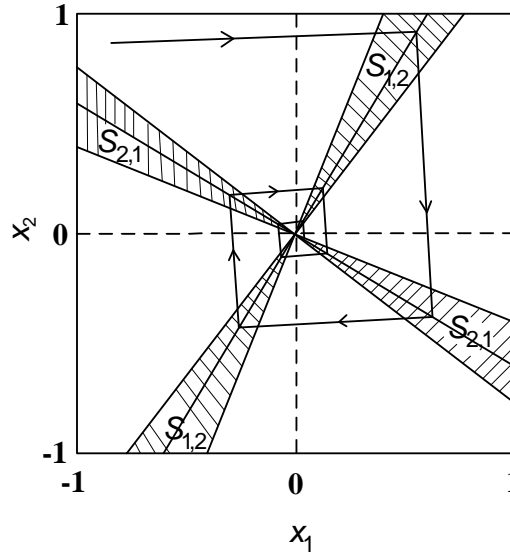


Figure 5.4: Switching anywhere in the cross-hatched regions leads to a stable closed-loop TS fuzzy system, if the sub-vector field switchings take place in the interior of the cross-hatched regions.

the smallest local Lyapunov function induce the system trajectory to reach the boundary of the region where the energy, measured by the local Lyapunov function, is guaranteed to be decreasing. Consequently, a switching must occur to another sub-vector field but the switching will not happen at states where the two local Lyapunov functions are equal, as enforced, for instance, by the assumptions made in some switching strategies for designing local controllers [184, 208]. In these control strategies, local controllers are assumed to have local Lyapunov functions, which are imposed to be equal at every switching between local controllers. Moreover, the local controller associated with the smallest Lyapunov function is on the priority to be chosen at each switching instant to fulfill the stability criteria of a close-loop system. Applying similar strategies in our case where non-smooth models are involved, may lead to an unwanted sliding motion. This is mainly because the chosen sub-vector field should be the function of continuous fuzzy states not discrete states. The direct practical outcome of the proposed switching strategy in this instance, is the design flexibility to achieve robust closed-loop stability. Nevertheless, achieving the best switching strategy depends on the given local Lyapunov functions, which can be, in turn, achieved via designing local fuzzy controllers as proposed by Theorem 5.1. In this case, the success rate of fulfilling the stability conditions is boosted with a large number of local controllers overlapping each other in wide regions. However, having designed a multitude of local controllers cannot always guarantee success of the design, even by calibrating different local Lyapunov functions. Nonetheless, if a sub-vector field (or the corresponding sub-systems) is found to be stable in the whole region of validity (with an associated local Lyapunov function), the switching strategy can always lead to stability by selecting that sub-vector field in the whole region. To ensure robust stability and in some cases, better decay rate, the location of the switching manifold (switch sets) can be manipulated as illustrated in the following example:

Example 5.2. Assume the fuzzy sub-vector fields introduced in Example 5.1 are changed to the following matrices:

$$F_{m_1} = \begin{bmatrix} -1 & -3 \\ 0 & -0.1 \end{bmatrix}, \quad F_{m_2} = \begin{bmatrix} -0.1 & 0 \\ -3 & -1 \end{bmatrix},$$

which are stabilizable by the local Lyapunov functions:

$$P_1 = \begin{bmatrix} 1 & -5 \\ -5 & 50 \end{bmatrix}, \quad P_2 = \begin{bmatrix} 50 & -5 \\ -5 & 1 \end{bmatrix},$$

with the same corresponding weighting function as in Figure 5.1. However, the switching sets are defined as:

$$S_{1,2} = \{x \in \mathbb{R}^2 \mid x_2 = kx_1\}, \quad S_{2,1} = \{x \in \mathbb{R}^2 \mid x_1 = -kx_2\}. \quad (5.7)$$

The cross-hatched region in Figure 5.5 represents the area where $x^T(P_2 - P_1)x \leq 0$. It is apparent that if $S_{1,2}$ and $S_{2,1}$ in (5.7) are initially selected with $k = 1$, switching from the sub-vector field $F_{m_1}x$ to $F_{m_2}x$, anywhere in the cross-hatched region, or in non-cross-hatched region can ensure the system stability. However, if the location of $S_{1,2}$ and $S_{2,1}$ are changed by the value of $k = 0.2$, as seen in Figure 5.5, not only is the structural stability ensured, but the estimate of the convergence rate will be improved.

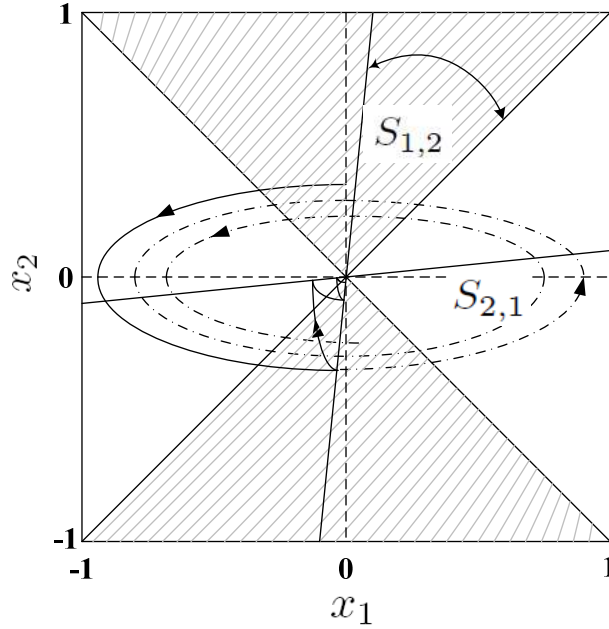


Figure 5.5: Switching from the fuzzy sub-vector field $F_{m_1}x$ to $F_{m_2}x$, at any place in the cross-hatched region, or inversely in the non-cross-hatched region, leads to a stable closed-loop fuzzy system. The solid-line solution trajectory is simulated with the manipulated switch sets ($k = 0.2$) against the dotted-dashed-line trajectory with initial switch sets. It is apparent that the convergence rate of the solid-line trajectory is faster than the dot-dashed trajectory.

Example 5.3 (Case study I continued, Control of chaotic phenomena in the boost converter). In this example, the proposed control strategy expounded in Section 5.4 along with the two simple examples 5.1 and 5.2, is applied to the dc-dc boost converter, to stabilize the resulting close-loop TS fuzzy system and hence by suppressing the chaotic behavior, and regulate the output response of the system to a stable period-1 operation for an acceptable range of parameter variation. First, recall Example 3.5 where the non-smooth TS fuzzy model of the circuit is developed as:

Plant Rule j : IF $x_1(t)$ is Γ^j THEN

$$\dot{x} = \begin{cases} A^j(m_i)x(t) + B^j(m_i)u(t), & j = 1, 2, \quad i = 1, 2, \\ m^+ = \xi(x, m), \end{cases} \quad (5.8)$$

where the continuous state vector is $x(t) = [i_L(t) \ v_C(t)]^T$, discrete states are $M = \{m_1, m_2\}$, sub-vector field matrices $A^j(m_i)$ and $B^j(m_i)$, and the fuzzy sets Γ^j are defined exactly as in Example 3.5. Switching between the ON and OFF states is conducted based on the switch sets:

$$\begin{aligned} S_{1,2} &= \{x \in R^n \mid i_L(dT) - I_{\text{ref}} > 0\}, \\ S_{2,1} &= \{x \in R^n \mid i_L(dT) - I_{\text{ref}} < 0\}, \end{aligned} \quad (5.9)$$

where d is the duty ratio and $T = 1 \times 10^{-4}$ s (the frequency of the switching $f = 10\text{KHz}$). Further, the region partitions defined as (4.47) for the stability analysis in Example 4.1, also applies here.

To design the local controllers (5.2), the diagonal matrices (see Remark 5.1) for discrete states m_1 and m_2 are set as:

$$X(m_1) = \text{diag}([9.6 \ 16 \ 0]), \quad X(m_2) = \text{diag}([8 \ 12.5 \ 0])$$

Using Theorem 5.1, deriving the diagonal matrices by assuming $\bar{X}(m)$ as a matrix variable is at best difficult mainly because the resulting condition (5.4) would be nonlinear matrix inequality (NMIs) not a LMI problem (see Appendix B). Therefore, the diagonal elements of $X(m)$ should be first specified before solving the LMI problem in Theorem 5.1. To achieve the best transient response The numbers for diagonal matrices can be determined after a number of trials. However, to have an initial best guess, the piecewise quadratic matrices \tilde{P}_1 and \tilde{P}_2 resulted from a feasible solution in Example 4.1 can be substituted in the LMI problem of Theorem 5.1 and the problem (including the remaining LMI stability conditions in Theorem 4.5) can be solved with the given piecewise quadratic matrices and $X(m_1)$ and $X(m_2)$, including the gain matrices $K^i(m)$, as unknown matrices (matrices $A^j(m)$ and $B^j(m)$ are already given so the condition (5.4) will not be a nonlinear matrix inequality). If the LMI problem is found feasible, initial diagonal numbers for $X(m_1)$ and $X(m_2)$ can be derived. Nevertheless, the initial matrices may not result in improving the transient responses, hence the numbers should be tuned (by observing the responses) and the LMI problem of Theorem 5.1 should be solved for a number of times to achieve a desirable transient response.

Now by solving the LMI problem in Theorem 5.1 to determine the local control gains

as (5.1) for the closed-loop system, and the remaining conditions in Theorem 4.5, the following gains are obtained:

$$\begin{aligned} K^1(m_1) &= K^2(m_1) = [3.6198, \quad 3.5370] \\ K^1(m_2) &= K^2(m_2) = [3.5037, \quad 0.1179] \end{aligned} \quad (5.10)$$

Therefore the control action $u(t)$ can be defined as:

$$\begin{cases} u(t) = -\Gamma^1(i_L)(K_1^1(m_1)i_L + K_2^1(m_1)v_c) \\ \quad -\Gamma^2(i_L)(K_1^1(m_2)i_L + K_2^1(m_2)v_c) \\ m^+ = \xi(x, m) \end{cases} \quad (5.11)$$

and the duty ratio to fire the control signal can be calculated as (with all the fixed parameters defined as in Appendix C):

$$d(t) = \frac{L}{T(r_L + r_{SW})} \ln\left(\frac{V_{in} - (r_L + r_{SW})u(t)}{V_{in} - (r_L + r_{SW})I_{ref}}\right) \quad (5.12)$$

As discussed in Example 5.1, the location of switch sets should be designed such that the fifth condition of the LMI stabilization problem of theorem 4.5 is specifically satisfied. To achieve such stability robustness, admissible switch regions or *ASR* are defined (Section 4.6). This means that if a switching occurs anywhere in these regions, the stability of the closed-loop system will be ensured. The *ASRs* for this example are given by

$$\begin{aligned} ASR(m_1, m_2) &= \{x \in \mathbb{R}^n | x^T(\tilde{P}_2 - \tilde{P}_1)x \leq 0\} \\ &= \{x \in \mathbb{R}^n | 225.84x_1^2(dT) + 10.24x_1(dT)x_2(dT) \\ &\quad - 330.63x_2^2(dT) \leq 39.68\} \\ ASR(m_2, m_1) &= \{x \in \mathbb{R}^n | x^T(\tilde{P}_2 - \tilde{P}_1)x \geq 0\} \\ &= \{x \in \mathbb{R}^n | 225.84x_1^2(dT) + 10.24x_1(dT)x_2(dT) \\ &\quad - 330.63x_2^2(dT) \geq 39.68\} \end{aligned}$$

Designing the switch sets (or function ξ) such that switching occurs anywhere within the given *ASRs*, guarantees that the local Lyapunov functions reduce at every switching region. Therefore, having designed the local controllers as (5.11), the remaining LMIs in Theorem 4.5 including the fifth condition will be fulfilled, resulting in structurally stable closed-loop systems.

Figs 5.6c, 5.6d, 5.7c, and 5.7d clearly show that the proposed fuzzy control strategy can stabilize the local orbit to a period-1 orbit for a wide range of parameter variation when comparing to the conventional control methods. As discussed in Case study I, the structural stability cannot be dealt with and this consequently leads to a chaotic orbit (Figs. 5.6a, 5.6b, 5.7a, and 5.7b). The time responses for the operating point $(V_{in}, I_{ref}) = (20V, 4A)$ also confirms that by applying the proposed TS fuzzy control scheme, the fast-scale responses can be well regulated to stable period-1 behaviour (Fig. 5.8c and 5.8d) from a chaotic behaviour (Fig. 5.8a and 5.8b).

To check the performance in terms of slow-scale transient (and steady-state) re-

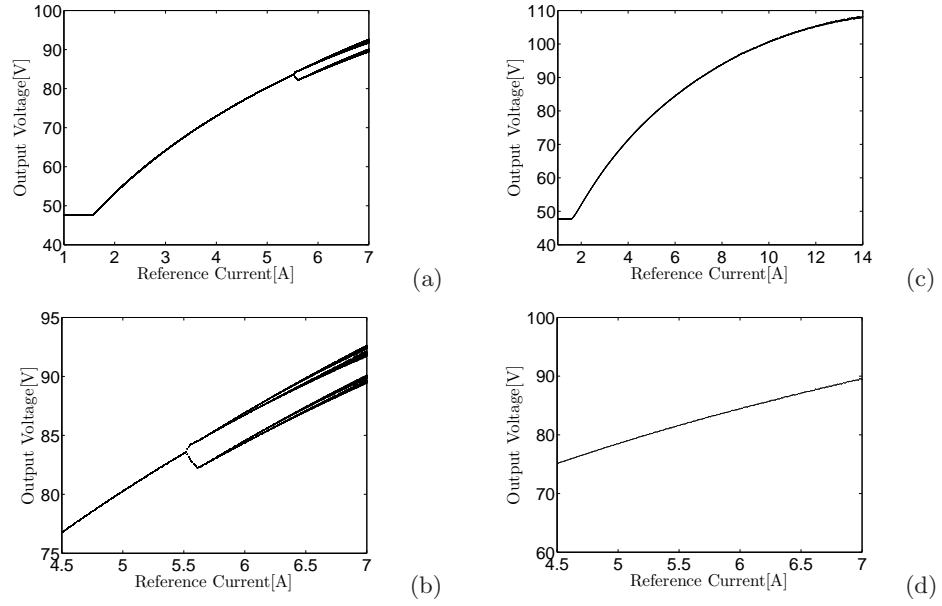


Figure 5.6: Bifurcation diagrams varying reference current using (a),(b) the conventional control scheme, and (c), (d) the proposed TS fuzzy control scheme.

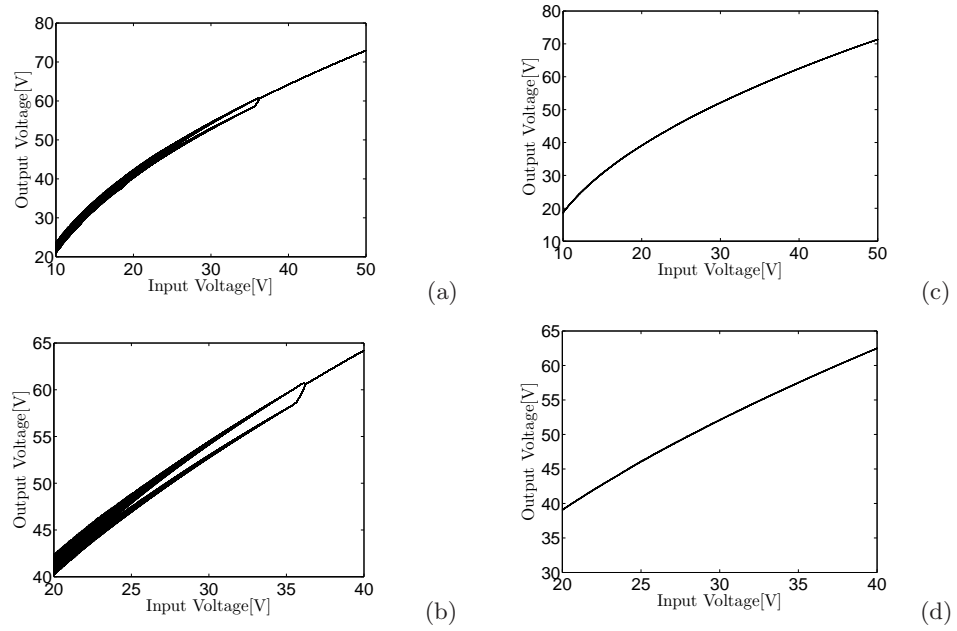


Figure 5.7: Bifurcation diagrams varying supply voltage using (a),(b) the conventional control scheme and (c), (d) the proposed TS fuzzy control scheme.

sponse, the close-loop TS fuzzy system is subject to an abrupt variation of supply voltage ($45V \rightarrow 85V \rightarrow 45V$) and load resistance ($30\Omega \rightarrow 50\Omega \rightarrow 30\Omega$), all with a short step change interval of 0.1s and a reference current ($4A \rightarrow 6A$) at 0.2s when the system responses passed the transient. The improved slow-scale performance under the proposed control strategy is evident in Figs. 5.9c, 5.9d, 5.10c, 5.10d, 5.11c and 5.11d compared to

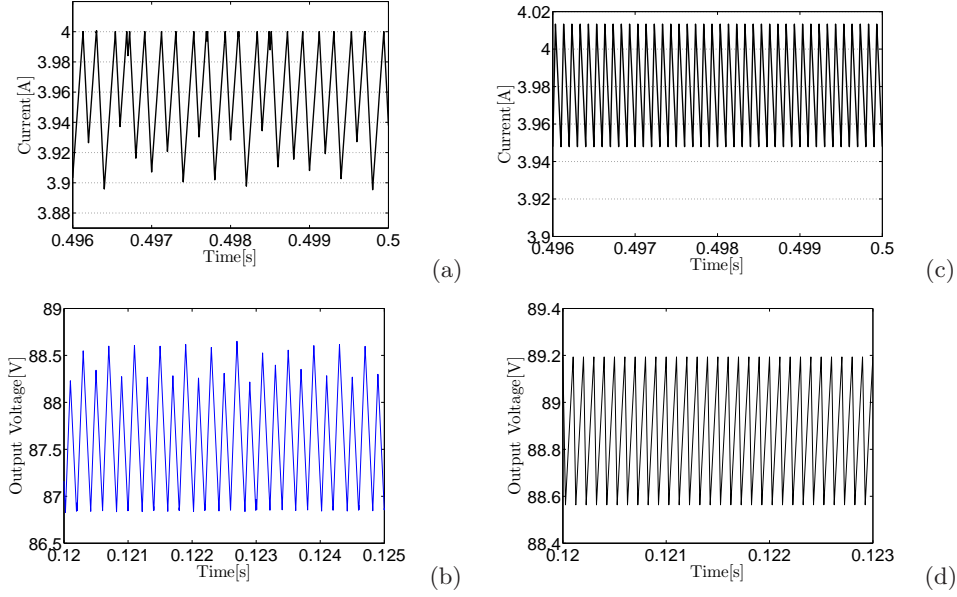


Figure 5.8: System responses is (a),(b) chaotic under the conventional control scheme, and (d), (c) regulated under the proposed TS fuzzy control scheme.

that of the conventional control scheme² (Figs. 5.9a, 5.9b, 5.10a, 5.10b, 5.11a and 5.11b). Therefore, as described by Remark 5.1, it is possible to hold the structural stability of a periodic orbit as well as meeting additional typical design criteria for boosting the (slow-scale) steady-state performance of a TS fuzzy system. It is noticeable from the magnified diagrams in Fig. 5.10d and Fig. 5.11d that while improving the transient response, the TS fuzzy controller regulates the system responses, which would otherwise undergo a destabilizing chaotic behaviour when using a conventional control scheme (the magnified picture in Fig. 5.10a and Fig. 5.11a). These improvements are also visible in Fig. 5.12 for the output voltage responses when subjected to the same abrupt variations.

²The conventional control scheme here means the PWM controllers or PI controllers normally used for controlling dc-dc converters as discussed in Section 2.1.1.

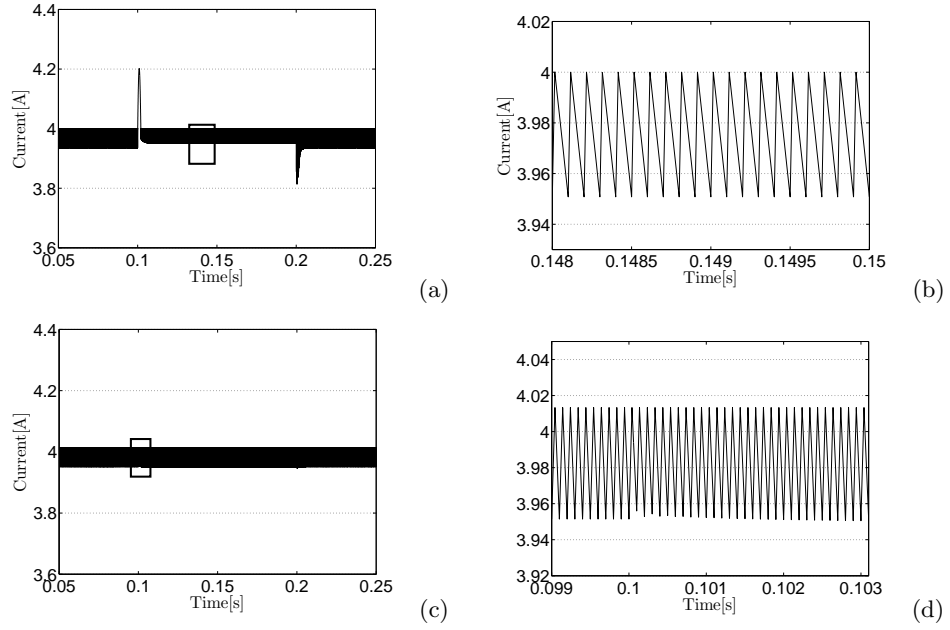


Figure 5.9: Output current response of the close-loop system subject to a sudden supply voltage V_{in} change from 45V to 85V and 85V to 45V at 0.1s and 0.2s, respectively, with the fixed parameter $R = 30\Omega$ under (a),(b) the conventional control scheme, and (c), (d) the proposed TS fuzzy control scheme. (b) and (d) are the magnified rectangle area in (a) and (c), respectively.

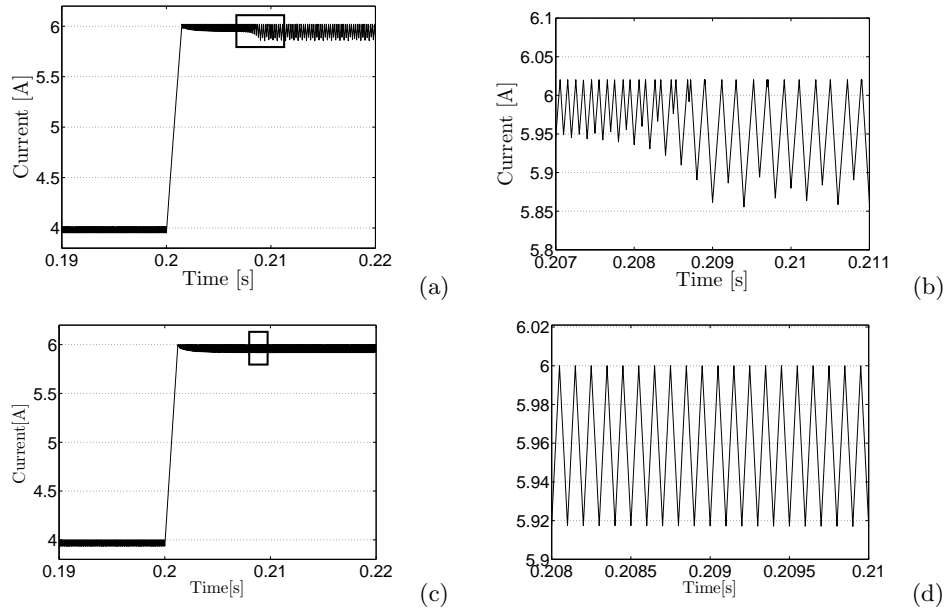


Figure 5.10: Output current response of the close-loop system subject to a large reference current I_{ref} step change from 4A to 6A at 0.2s with the fixed parameter $V_{in} = 45V$ under (a),(b) the conventional control scheme and (c), (d) the proposed TS fuzzy control scheme. (b) and (d) are the magnified rectangle area in (a) and (c), respectively.

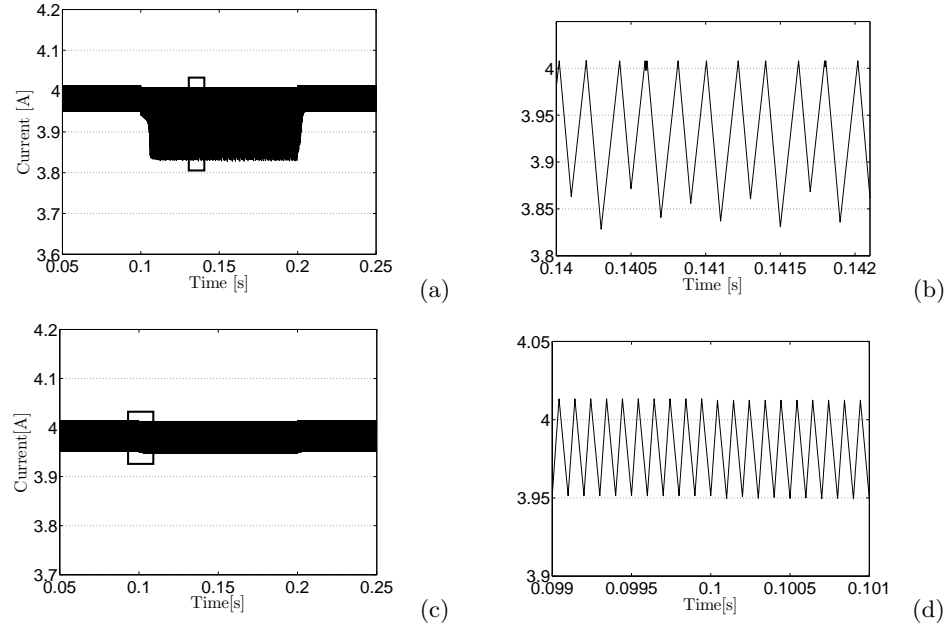


Figure 5.11: Output current response of the close-loop fuzzy system subject to a sudden load resistance R changing from 30Ω to 50Ω and 50Ω back to 30Ω at 0.1s and 0.2s respectively with the fixed parameters $V_{in} = 45V$ and $I_{ref} = 4A$ under (a), (b) the conventional control scheme and (c), (d) the proposed TS fuzzy control scheme. (b) and (d) are the magnified rectangle area in (a) and (c), respectively.

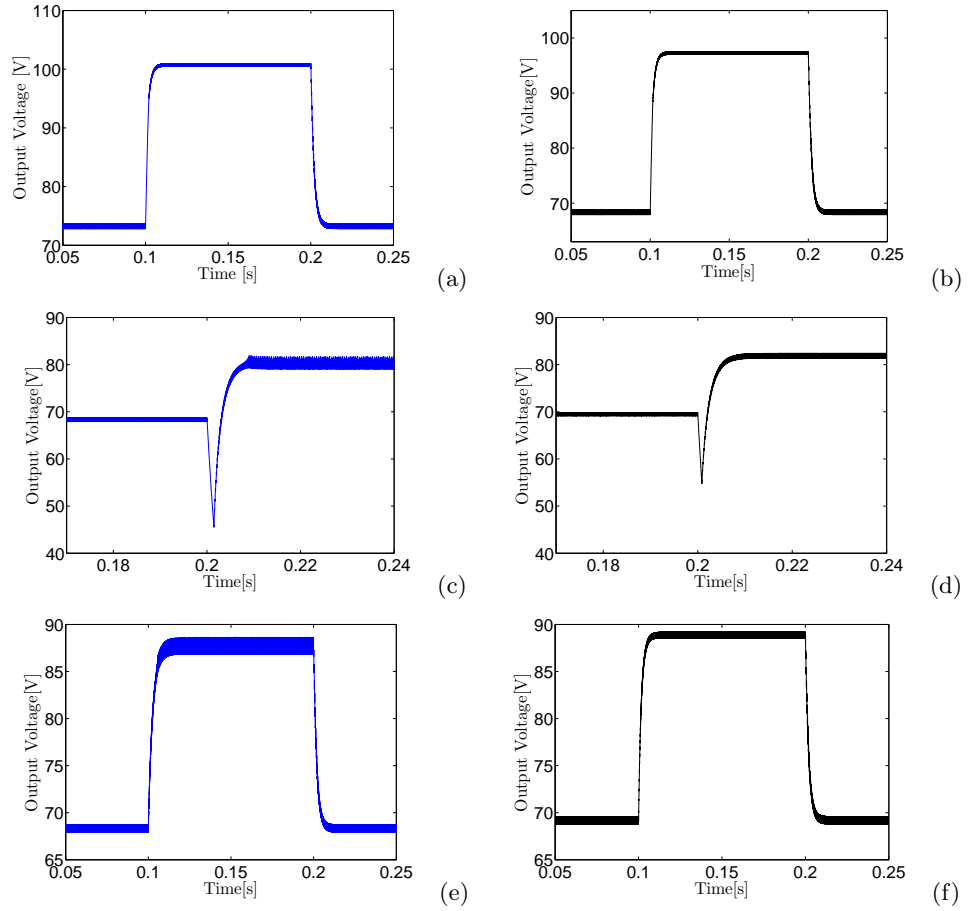


Figure 5.12: Output voltage response of the closed-loop fuzzy system subject to an abrupt variations of (b) supply voltage ($45V \rightarrow 85V \rightarrow 45V$), (d) the reference current ($4A \rightarrow 6A$), (f) load resistance ($30\Omega \rightarrow 50\Omega \rightarrow 30\Omega$), versus that of the conventional control scheme (a, b, and c) under the same abrupt variations.

Example 5.4 (Case study I continued, Control of chaotic phenomena in buck converter). As another example to show the effectiveness of the control strategy proposed in Section 5.4 in suppressing the chaotic phenomena, we recall the non-smooth TS fuzzy model of the buck converter expounded in Example 3.6, along with the stability analysis of the local orbit in Example 4.2. The non-smooth TS fuzzy model (3.31) is described as:

$$\textbf{Model Rule } j: \text{ IF } x_2(t) \text{ is } \Gamma^j \text{ THEN } \begin{cases} \dot{x}(t) = A^j(m_i)x(t) + B^j(m_i)u(t) \\ m^+ = \xi(x, m), \quad j = 1, 2, \quad i = 1, 2. \end{cases}$$

where the continuous state vector is $x(t) = [i_L(t) \ v_C(t)]^T$, discrete states are $M = \{m_1, m_2\}$, sub-vector field matrices $A^j(m_i)$ and $B^j(m_i)$ are defined as (3.31), fuzzy sets

$\Gamma^j(x_2(t))$ are constructed as (3.34), and the switch sets are defined as:

$$\begin{aligned} S_{1,2} &= \{x \in R^n | x_1(dT) - V_{\text{ref}} < \frac{v_{\text{ramp}}}{A}\}, \\ S_{2,1} &= \{x \in R^n | x_1(dT) - V_{\text{ref}} > \frac{v_{\text{ramp}}}{A}\}, \end{aligned}$$

where d is the duty ratio and the periodic sawtooth waveform v_{ramp} defined as in (3.33) varying from 3.8V to 8.2V with a period of $T = 1/2500s$ (see Fig. 2.3). Region partitions as defined by (4.48) in Example 4.2 for dividing fuzzy state space $\Omega \subseteq \mathcal{F}$.

The diagonal matrices for the two discrete states m_1 and m_2 are initially defined as

$$X(m_1) = \text{diag}([167 \ 14 \ 0]), \quad X(m_2) = \text{diag}([136 \ 10.5 \ 0]) \quad (5.13)$$

Assuming the model is operating with an input voltage of $V_{\text{in}} = 24V$, the LMI problem in Theorem 5.1 along with the remaining conditions in Theorem 4.5, is found feasible with the resulting gains:

$$\begin{aligned} K^1(m_1) &= K^2(m_1) = [0.43167, \ 0.43175], \\ K^1(m_2) &= K^2(m_2) = [0.4822, \ 0.03162], \end{aligned} \quad (5.14)$$

for the local controllers 5.1 of the closed-loop system. Therefore, the control input $u(t)$ is defined as:

$$\begin{cases} u(t) = -\Gamma^1(x_1(t))(K_1^1(m_1)x_1(t) + K_2^1(m_1)x_2(t)) \\ \quad -\Gamma^2(i_L)(K_1^1(m_2)x_1(t) + K_2^1(m_2)x_2(t)), \\ m^+ = \xi(x, m), \end{cases} \quad (5.15)$$

with the duty ratio $d = t_{\text{on}}/T$ governed by the switch sets $S_{1,2}$ and $S_{2,1}$ to decide when the model of buck converter should switch based on the voltage across the capacitors $v_C(t)$. The admissible switch region ASR , in this case, can be determined based on the solution matrices \tilde{P}_1 and \tilde{P}_2 in the Example 4.2, given by:

$$\begin{aligned} ASR(m_1, m_2) &= \{x \in \mathbb{R}^n | 387.3518x_2^2(dT) + 51.546x_1(dT)x_2(dT) \leq 0\} \\ ASR(m_2, m_1) &= \{x \in \mathbb{R}^n | 387.3518x_2^2(dT) + 51.546x_1(dT)x_2(dT) \geq 0\}. \end{aligned}$$

Therefore, designing the location of switch sets such that the switching occurs anywhere in the above regions $ASR(m_1, m_2)$ and $ASR(m_2, m_1)$ ensures the structural stability in the Lyapunov sense while fulfilling the fifth condition of the LMI stabilization problem of Theorem 4.5.

As seen in the bifurcation diagram of Fig. 2.6, a period-3 attractor can appear at a supply voltage $V_{\text{in}} = 24.16V$ with a different set of initial conditions. However, the proposed TS fuzzy control strategy can stabilize the local orbit to a stable period-1 orbit with the same initial condition as seen in the time responses of Fig. 5.13. Also, under conventional controller³, a period-2 orbit can appear if the supply voltage is varied to $V_{\text{in}} = 25V$ (see the coexisting attractors in Fig. 3.20) whereas under TS fuzzy controller, the period-1 orbit is stable as seen in the time responses of Fig. 5.14.

³The conventional controller here means the PWM controllers or PI controllers normally used for controlling dc-dc buck converters as discussed in Section 2.1.1.

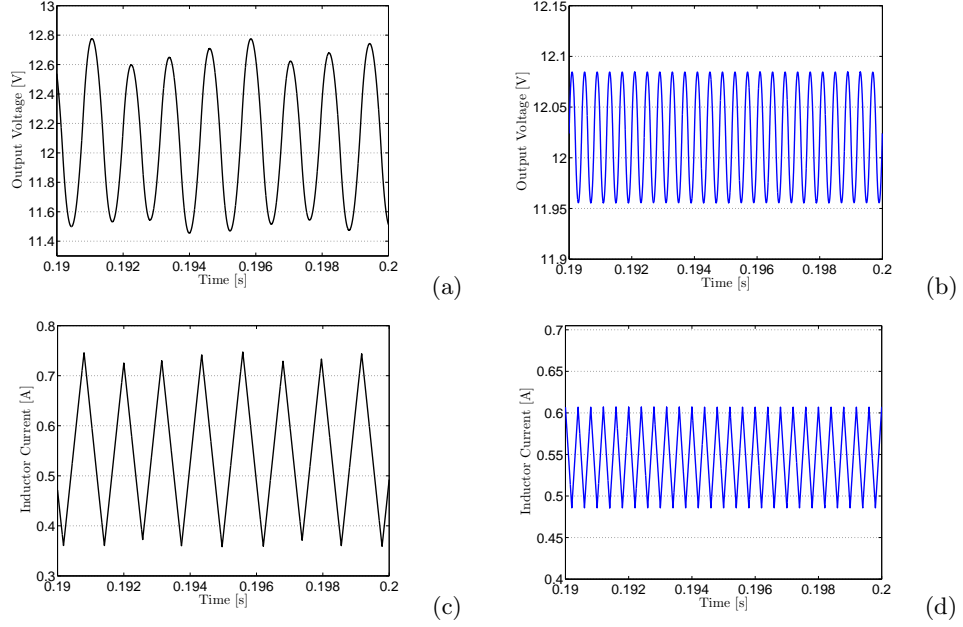


Figure 5.13: System responses at $V_{in} = 24.16V$ is (a),(c) unstable with period-3 attractor under conventional control, (b),(d) regulated to period-1 orbit under the proposed TS fuzzy control.

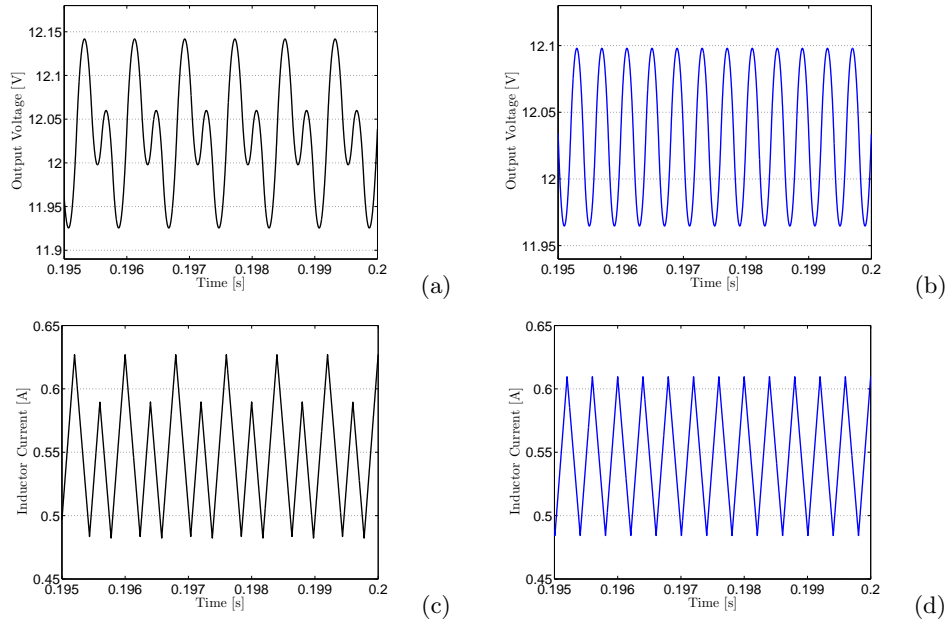


Figure 5.14: System responses at $V_{in} = 25V$ (a),(c) unstable with period-2 attractor under conventional control, (b),(d) regulated to period-1 orbit under the proposed TS fuzzy control.

Stabilizing to period-1 orbit from the higher periodic orbit (where the bifurcation occurs) and chaotic orbit is also evident from Figs. 5.15b and 5.16b where the fuzzy controller suppress the nonlinear phenomena, i.e. discontinuity-induced bifurcation and chaos, for a wide range of parameter variation ($V_{in} \in [24, 36]$) compared to that of the conventional

control scheme (Figs 5.15a and 5.16a). This means that the proposed TS fuzzy control strategy can *structurally* stabilize the local orbit to period-1 orbit and prevent the destabilizing bifurcation leading to chaos normally occurs if we employ conventional controllers.

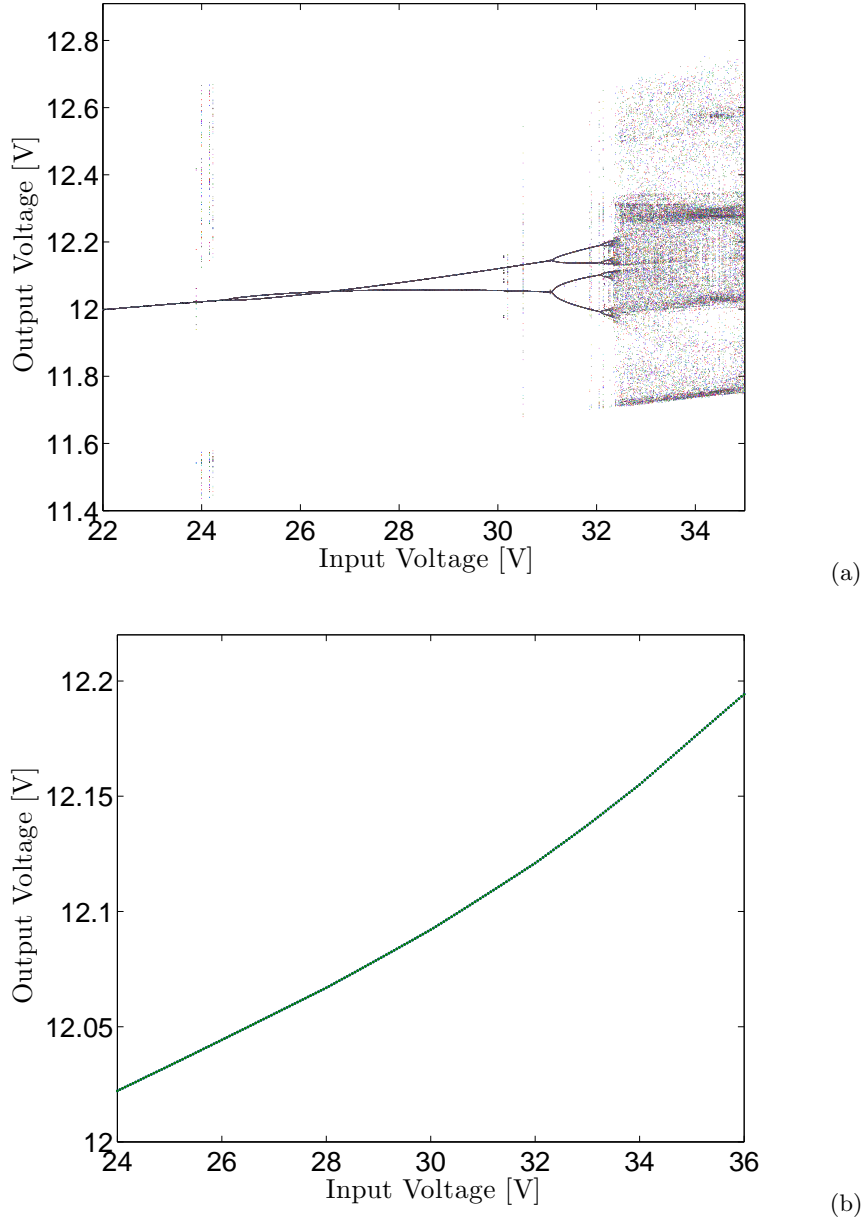


Figure 5.15: Bifurcation diagrams of output voltage v_C with the input voltage V_{in} as the bifurcation parameter for (a) conventional control, (b) proposed TS fuzzy control scheme. Evidently the proposed TS fuzzy control scheme can structurally stabilize the output voltage for a wide range of parameter variation.

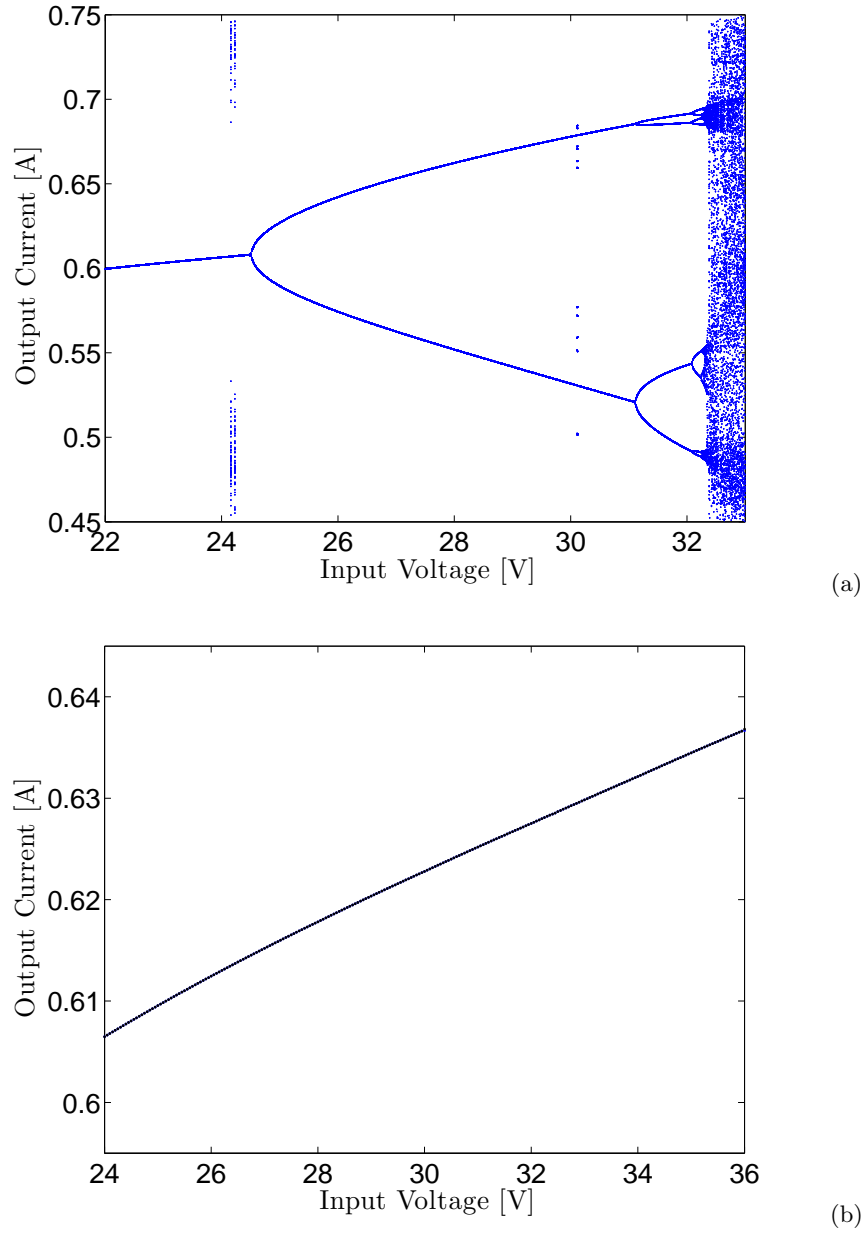


Figure 5.16: Bifurcation diagrams of output current i_L with the input voltage V_{in} as bifurcation parameter for (a) conventional control, (b) proposed TS fuzzy control. Evidently the proposed TS fuzzy control scheme can structurally stabilize the output current for a wide range of parameter variation.

The slow-scale steady-state performance of the close-loop TS fuzzy system without consideration of diagonal matrices in (5.13) under the abrupt variation of supply voltage ($20V \rightarrow 35V \rightarrow 20V$) can be seen in Fig. 5.17b compared to that of the conventional controller. It is clear that although the output voltage is stabilized to a period-1 orbit (see the magnified diagram in Fig. 5.17d), there is no discernible improvement in the transient response. However, involving the diagonal matrices (5.13) as demonstrated in Theorem 5.2 improves the response by reducing the overshoot from 12.8523V to 12.326 (the highest peak of the signal) and settling time from 0.1215s to 0.1052s (period-1 operation) as visible

from Fig. 5.18.

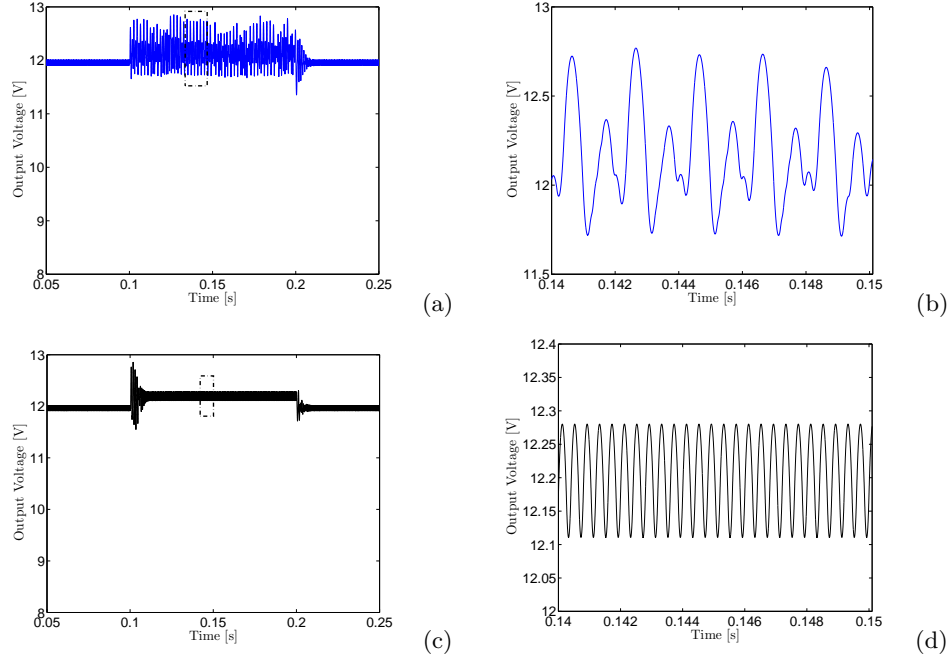


Figure 5.17: Output voltage response of (a), (b) the conventional control scheme subject to an abrupt variations of supply voltage ($20V \rightarrow 35V \rightarrow 20V$) versus (c), (d) the closed-loop TS fuzzy system scheme under the same conditions. (b) and (d) are the magnified rectangle area in (a) and (c), respectively.

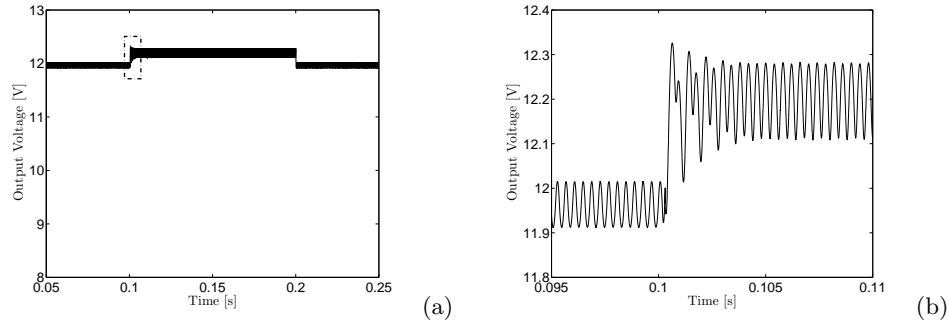


Figure 5.18: Output voltage response of the closed-loop TS fuzzy control system subject to an abrupt variation of supply voltage ($20V \rightarrow 35V \rightarrow 20V$). The transient response is significantly improved using Theorem 5.1. (b) shows the magnified rectangle area in (a).

5.5 Summary

A switching fuzzy control strategy has been proposed in this chapter to structurally stabilize non-smooth electrical Filippov systems like dc-dc electronic converters. Based on the LMI stabilization problems presented in the previous chapter for Filippov's systems (Section 4.3), the design problem has been formulated as LMIs to fulfill different requirements. Structural stability has been achieved by fulfilling two objectives of designing local state-feedback controllers based on pre-determined local Lyapunov functions and locating the switch sets such that the closed-loop TS fuzzy system converges to the stable fixed

point exponentially. The slow scale transient performance can also be boosted by setting some additional requirements in the matrix form for each discrete state. It has been shown that if the LMI design problem is found feasible, the control strategy can be effective in suppressing the unwanted nonlinear phenomena in the example DC-DC electronic converters for a wide range range of parameter variation while boosting the slow-scale transient response. The success of the proposed design problem depends on the existence of local Lyapunov functions in each region of validity, which is a legitimate assumption when the design of the continuous input signal is based on stability theorems presented in Section 4.3 and the Theorem presented in this chapter for designing local controllers.

Robustness of the proposed control strategy has been shown in terms of guaranteeing structural stability despite model uncertainties and the quality of steady-state operations subject to abrupt variation of fixed parameters. If the switch sets (or relocating the switching manifolds) are designed anywhere in the admissible switch regions (*ASRs*), the non-smooth Lyapunov functions would reduce at every switching instants, leading to a stable closed-loop TS fuzzy system.

Chapter 6

Concluding Remarks

I have had in mind solely to expound in this work that which I have arrived at up to the present moment, and which, perhaps, may serve as a point of departure for other researchers of the same kind...

ALEXANDER M. LYAPUNOV

In his treatise: the general problem of the stability of motion (1892)

This chapter gives an overview of the thesis focusing on the proposed solutions for modeling, stability analysis and control design for non-smooth electrical and mechanical systems. Recommendations are also made for the future research.

6.1 Overview and Summary of Contributions

In this section an overview of the thesis is given and the contributions are highlighted.

An overview of the concepts of NSDS and the contemporary analytical tools for studying these systems was presented in Chapter 2. Non-smooth electrical systems (DC-DC electronic converters) and mechanical systems (impact and dry-friction oscillators) were introduced in the form of different case studies and their observed nonlinear phenomena including discontinuity-induced bifurcations (DIBs) and chaos were illustrated. The case studies, representing the significant groups of non-smooth systems, were employed throughout this thesis to validate the theoretical analysis developed in the main chapters of the thesis (Chapters 3, 4 and 5). NSDS were classified based on the degree of smoothness (DoS), a yardstick used to separate different types of rich, complex dynamics normally observed in these systems (see Table 2.1). The emphasis on DIBs as non-smooth bifurcations and their distinct differences compared with smooth bifurcations were highlighted in terms of different definitions including the novel notion of structural stability (piecewise-topological equivalence). Poincaré mapping and nonlinear discontinuity mapping were briefly explained as the contemporary analytical approach for the bifurcation analysis of NSDS. It was further mentioned that using the resulting techniques (ZDM and

PDM), specifically for studying impacting systems, is problematic when investigating a DIB near the grazing point will result in an infinite stretching of phase space.

The first contribution of the thesis was presented in Chapter 3 where a TS fuzzy modeling structure was formalized to represent the non-smoothness and all the essential nonlinearities observed in NSDS. It was initially shown by a simple example (Section 3.1.3) that the current fuzzy modeling structure, or the so-called Takagi-Sugeno model [27], was fundamentally unable to approximate any sort of non-smooth systems. The proposed novel TS fuzzy modeling structure incorporates discrete event dynamics for converting nonlinear, non-smooth differential equations to what we refer to as *non-smooth TS fuzzy models*. In addressing the issue of existence (and uniqueness) (Section 3.2.5), the reasons why the current (smooth) TS fuzzy modeling approaches could not hold the existence (and uniqueness) when approximating non-smooth mathematical models and why the proposed structure could rigourously hold this property were discussed. It was pointed out that the non-smooth TS fuzzy formalism is readily implementable on existing software platforms (Section 3.2.7). Moreover, the proposed formalism is general enough to represent various types of NSDS with different DoS, including impacting systems showing complex dynamics of discontinuous (jump) states with respect to a switching manifold (DoS of zero). Two methods for constructing such models were suggested (Section 3.2.6), which were subsequently corroborated through modeling of the case studies introduced in Chapter 2.

The focus in Chapter 4 was on stability analysis. A Lyapunov framework was developed for structural stability of non-smooth TS fuzzy models. It was shown how the Lyapunov concepts for (asymptotic and exponential) stability can be connected with the new notion of structural stability for verifying the stability of local orbits (or periodic solutions) of a non-smooth model. Two main stability theorems were respectively proposed (Sections 4.3 and 4.4) for the bifurcation analysis of Filippov-type systems and impacting systems. All the theorems were formulated as Linear Matrix inequality (LMI) conditions to be solved numerically as a convex stabilization problem by existing interior-point methods. The validity of the analytical approach was proven via different examples where the onset of DIBs were accurately detected. The special case of grazing was also discussed in detail (Example 4.3), where the stability of a grazing orbit was examined. It was shown that in the vicinity of the grazing orbit, the LMI formulation could successfully pinpoint the onset of the grazing DIB while exactly at the grazing orbit, the stabilization problem was transformed to a QMI problem. The instrumental role of partitioning the fuzzy state space \mathcal{F} into flexible regions was specially highlighted for the case of grazing-sliding bifurcations (Example 4.4) in relaxing the conservative LMI formulation verifying the exponential stability near the bifurcation point. However, it was pointed out that excessive partitioning might lead to a conservative result by increasing the computational burden, meaning that the actual stability could not be verified. Stability robustness was also addressed in terms of model uncertainties in selecting the fuzzy sub-vector fields and the location of the switching instants.

In Chapter 5, A TS model-based control strategy was presented in the form of different theorems to curb the chaotic phenomena in electrical Filippov-type systems. The control strategies, a combination of switching and state feedback control, were founded on the LMI

stabilization theorems proposed in Chapter 4. The design problem was mainly concerned with locating the switch sets and determining the state feedback gains such that structural stability of a closed-loop TS fuzzy system was guaranteed. It was shown that the strategy was successful in stabilizing the chaotic (or non-singular periodic) orbit to a period-1 orbit for a wider range of parameter variation. It was further illustrated that the proposed design could render the robustness (in the view of structural stability) as well as improving the (slow-scale) transient response when subject to an abrupt variation of fixed system parameters.

6.2 Topics for Future Research

Even though this thesis may enhance analytical approaches for TS fuzzy systems, it should be considered as an avenue for additional investigations and questions related to the subject.

Unified theory for bifurcation analysis of TS fuzzy systems. A number of methods have been suggested in the literature for the stability analysis of TS fuzzy systems in terms of Lyapunov direct method; see Section 4.1. However, even in the domain of smooth TS fuzzy systems, almost all of these results have been focused on the classical notion of stability (stability of equilibria) rather than the notion of structural stability (stability of periodic solutions). There have been a number of studies investigating the onset of smooth bifurcations (see Section 2.2.2) in smooth TS fuzzy systems, eventually leading to the adoption of the contemporary approach of the Jacobian of the Poincaré map $DP(x^*)$ (see Section 2.2.4) for studying the periodic solution in question [79, 209, 210]. Therefore the lack of an unified Lyapunov theory for studying structural stability of non-smooth TS fuzzy systems, which embraces the theory for smooth TS fuzzy systems, is certainly an area that needs further effort.

Stability analysis for higher periodic orbits. For structural stability of non-smooth TS fuzzy systems, the onset of the first bifurcation (when for the first time, a branch bifurcates from another branch), or the onset of a DIB, like grazing and sliding bifurcations (when no branching behavior is observed and the local stable orbit instantly loses its stability to a chaotic orbit, can be detected using the Lyapunov framework presented in Chapter 4. However, a Lyapunov analysis is not developed to assess the instability of higher periodic orbits (more than one), e.g. period-2 operation in dc-dc converters. It is known that using the discontinuity mapping approach, the investigation of higher periodic orbits is possible via a complicated analytical formulation. However for the simple case of a boost converter (non-sliding Filippov-type system), the formulation may take such a considerable computational time that the analytical solution becomes implausible for a periodic orbit higher than four. If a Lyapunov-based analysis is developed for such purpose, it would most likely result in some form of non-linear matrix inequalities (see Appendix B). If NMIs are to be solved by any existing optimization algorithms, they must be transformed to LMIs. A major concern arises in these transformations in that the resulting formulation may still be found conservative if the original formulation contains too

many nonlinear matrix elements. Consequently, more powerful optimization algorithms for solving BMIs and QMIs need to be developed in tandem with expanding more complex Lyapunov-based stabilization problems for TS fuzzy systems.

Converse theorems for structural stability. In Sections 4.3 and 4.4, stabilization problems are formulated based on non-smooth Lyapunov functions which are not allowed to be increased at switching manifolds. This requirement is intentionally introduced due to the fact that, otherwise, assessing stability would depend on the difficult task of calculating the fuzzy solution trajectories. This gives rise to an interesting question. Is it *necessary* or simply *limiting* if we let the non-smooth Lyapunov functions be decreased in the entire interval of the trajectory evolution? Answering this, demands the existence of converse theorems for the problems presented in Chapter 4, i.e. if a TS fuzzy system is structurally stable, then non-smooth Lyapunov functions must exist. Following the general approach in establishing converse theorems for smooth dynamical systems, suggests Lyapunov functions should be defined based on the solution trajectories of the system of interest. This implies that Lyapunov functions can essentially acquire similar properties to the solution in terms of smoothness and differentiability. With the same argument, for a stable non-smooth TS fuzzy system, an existence of non-smooth Lyapunov functions (defined locally smooth and continuously differentiable for each fuzzy sub-vector field but non-smooth at points governed by switch sets) should be expected. More specifically, the presence of discontinuous (jump) states in impacting dynamics would require any stabilization problem to be formulated based on non-smooth Lyapunov function candidates. Rigorous converse theorems for stabilization problems presented in this thesis remain to be developed.

Automation of region partitioning. It has been seen in a number of examples in this thesis (Chapter 4) that the success of the proposed methods for verifying the stability of a local orbit depends on defining the appropriate region partitions for fuzzy state space. As these regions can be flexibly defined, the allocation procedure is mainly ad hoc. Therefore, providing general guidelines (or algorithms) to automate the procedure can be a good topic for future investigation. It is imperative for finding a feasible solution to the LMI stabilization problems that finer partitions to be defined progressively close to the switching manifold (Examples 4.3 and 4.4). However, it may take several attempts to correctly determine the size of the partitions since it is not known how many local piecewise Lyapunov function candidates for each region and each (possibly unstable) fuzzy sub-vector fields are needed to show the onset of bifurcation point. Defining the boundary of fuzzy state-space partitions can also affect the estimate of exponential convergence to a stable fixed point. It is important to know how the size of partitions can affect the estimate of exponential convergence. Undoubtedly, this requirement is better considered (if possible) through an automated routine for region partitioning. Forming extra region partitions or finer partitions would result in conservative LMI formulations. Therefore, it would be an important advancement if the size, number and structure of region partitions could be optimized for less computational effort in finding feasible solutions to LMI stabilization problems for predicting the onset of bifurcation phenomena.

The presence of noise. As discussed in stability robustness issues (see Section 4.6), the model uncertainties or unmodeled dynamics in the location of switch sets can be easily incorporated in the non-smooth TS model by extending the nominal switch sets in the proposed LMI framework to guarantee stability. One of the important source to create these type of uncertainties may be the presence of noise, e.g. the measurement noise. In the most of examples in this thesis, by introducing several region partitions of fuzzy state space, verifying structural stability is becoming critical if a feasible solution is found for the LMI problems. Therefore, the presence of noise, even arbitrarily small, may cause in undesired switches between different control laws which could eventually prevent the desired control goal to be achieved. Extending the nominal switch sets by introducing admissible switch regions (ASR), as suggested in Section 4.6.1, can avoid this problem to some degree by allowing the location of switch sets, i.e. switching manifolds, to be adjusted freely in such a way as the structural stability is not violated. However, such robustness, may be archived at the cost of very restrictive hypothesis on the switching control laws as proposed in Chapter 5, depending on the magnitude of measurement noise. Therefore, it is preferable to seek for better approaches to guarantee the structural stability of a non-smooth TS fuzzy system in the presence of noise.

Appendix A

Modeling and analysis of current-mode controlled Ćuk converter

This appendix is dedicated to the TS fuzzy modeling and (structural) stability analysis of the relatively more sophisticated 4-dimensional system like the current-mode controlled Ćuk converter as shown in Fig. A.1.

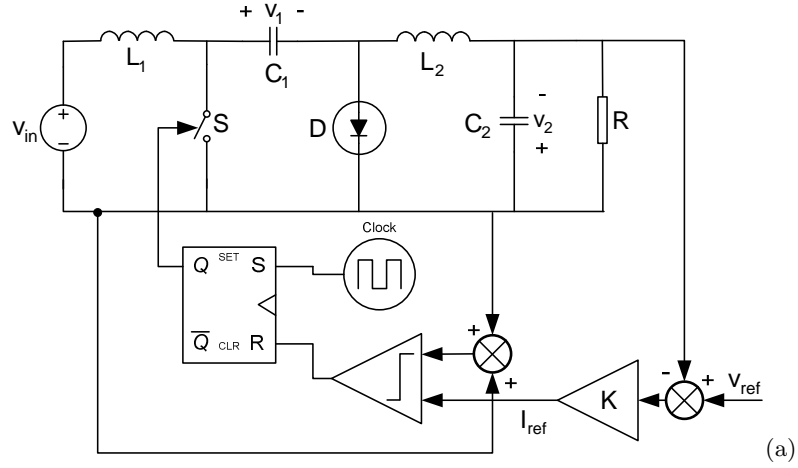


Figure A.1: Current-mode controlled Ćuk converter.

In this circuit, the close-loop control scheme regulates the sum of the inductor currents $i_{L1} + i_{L2}$ by comparing it with the value of the reference current I_{ref} to generate the switching signal (see Fig. A.2). The proportional feedback controller is used to generate the reference current by subtracting the reference voltage V_{ref} from v_1 and amplifying the error with gain K , i.e. $I_{ref} = K(V_{ref} - v_1)$. The switch S is turned ON at the beginning of the cycle $t = nT$ and stays on until $i_{L1} + i_{L2}$ reaches the value of I_{ref} when it is turned

OFF until the next cycle begins. Under this control logic, the duty ratio in each cycle is derived by

$$d_n = \frac{I_{ref} - (i_{L1} + i_{L2})_n}{\left(\frac{E}{L_1} + \frac{v_{C2,n} - v_{C1,n}}{L_2}\right)T}, \quad (\text{A.1})$$

where the subscript n denotes values at $t = nT$ and T is the period. Therefore, the governing dynamics of the Ćuk converter circuit are described by four sets of differential equations:

$$\frac{dv_{C1}}{dt} = \begin{cases} \frac{-1}{RC2}v_{C1} + \frac{1}{C2}i_{L1}, & S \text{ is off} \\ \frac{-1}{RC2}v_{C1} + \frac{1}{C2}i_{L1}, & S \text{ is on} \end{cases} \quad \frac{dv_{C2}}{dt} = \begin{cases} \frac{-1}{C1}i_{L1}, & S \text{ is off} \\ \frac{-1}{C2}i_{L2}, & S \text{ is on} \end{cases} \quad (\text{A.2})$$

$$\frac{di_{L1}}{dt} = \begin{cases} \frac{-1}{L2}v_{C1} + \frac{1}{L2}v_{C2}, & S \text{ is off} \\ \frac{-1}{L2}v_{C1}, & S \text{ is on} \end{cases} \quad \frac{di_{L2}}{dt} = \begin{cases} \frac{1}{L1}V_{in}, & S \text{ is off} \\ \frac{-1}{L1}v_{C2} + \frac{1}{L1}V_{in}, & S \text{ is on} \end{cases} \quad (\text{A.3})$$

where inductor currents i_{L1} , i_{L2} and the output voltages v_{C1} and v_{C2} are the state variables. It can also be seen that in the 4th-ordered Ćuk converter, upon varying a system's parameter like reference current I_{ref} , the circuit's output undergoes a destabilizing bifurcation phenomenon, which eventually leads to chaos [1,211,212]. This scenario is clear from the phase plane diagrams of Fig. A.3 where the sum of the inductor currents ($i_{L1} + i_{L2}$) is plotted against the sum of the voltage across the capacitors ($v_{C1} + v_{C2}$). The long time behaviour of the system is depicted in the form of a bifurcation diagram (Fig. A.4) where the reference current I_{ref} is varied as the bifurcation parameter.

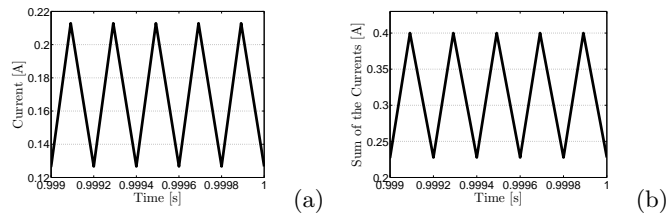


Figure A.2: Nominal stable period-1 operation of the current-mode controlled Ćuk converter. The period of the regulated output signals of (a) first inductor current and (b) sum of the inductor currents of the Ćuk converter are equal to the period of the PWM signal.

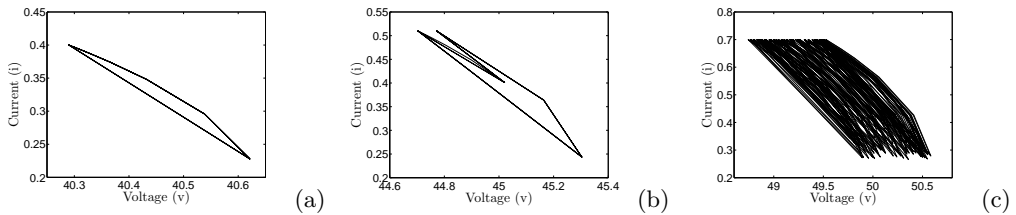


Figure A.3: Periodic orbit of the Ćuk converter: (a) period-1 operation with $I_{ref} = 0.4\text{A}$, (b) period-2 operation with $I_{ref} = 0.51\text{A}$ and (c) chaotic operation with $I_{ref} = 0.7\text{A}$.

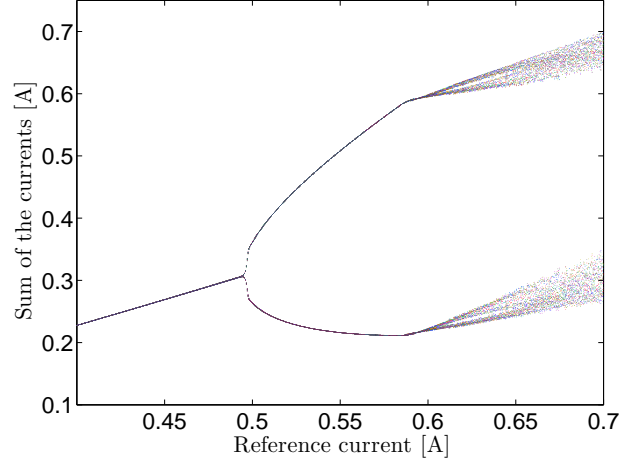


Figure A.4: The Monte Carlo bifurcation diagram of the Ćuk converter shows how the circuit loses its stability to a period-2 and then to a chaotic attractor upon variation of the reference current I_{ref} as a bifurcation parameter.

Using the approach of discrete nonlinear modeling, studying the stability of a fourth-order system like Ćuk converters is difficult compared to single-diode dc-dc converters such as boost and buck, mainly due to the necessity of deriving a complicated fourth-order iterative stroboscopic Poincaré map [211–213]. Using the TS fuzzy model-based approach proposed in Chapters 3 and 4, we can see how effectively the instability of period-1 limit cycle of the circuit, or the onset of the period-doubling bifurcation can be investigated. In this respect, we first convert the original dynamical equation of the system to a non-smooth TS fuzzy model of the form (3.12).

A.1 TS fuzzy model of the Ćuk converter

The non-smooth TS fuzzy model of the Ćuk converter can be described by the following model rules:

$$\begin{aligned} \text{Model Rule } j : & \text{ IF } (x_3 + x_4) \text{ is } \Gamma^j \\ \text{THEN } \dot{x} = & \begin{cases} A^j(m_i)x + B^j(m_i)u \\ m^+ = \xi(x, m), \quad j = 1, 2, \quad i = 1, 2, \end{cases} \end{aligned} \quad (\text{A.4})$$

where the four state variables are defined as $x_1(t) = v_{C1}(t)$, $x_2(t) = v_{C2}(t)$, $x_3(t) = i_{L1}(t)$, $x_4(t) = v_{C2}(t)$ and $u(t)$ is the input voltage V_{in} . According to (A.4), there are two fuzzy sub-vector fields F_{m_1} and F_{m_2} composed of the sub-system matrices:

$$A^1(m_1) = A^2(m_1) = \begin{bmatrix} -1/RC2 & 0 & 1/C2 & 0 \\ 0 & 0 & -1/C1 & 0 \\ -1/L2 & 1/L2 & 0 & 0 \\ 0 & 0 & 0 & 0 \end{bmatrix}, \quad B^1(m_1) = B^2(m_1) = \begin{bmatrix} 0 \\ 0 \\ 0 \\ 1/L1 \end{bmatrix}, \quad (\text{A.5})$$

$$A^1(m_2) = A^2(m_2) = \begin{bmatrix} -1/RC2 & 0 & 1/C2 & 0 \\ 0 & 0 & 0 & 1/C1 \\ -1/L2 & 0 & 0 & 0 \\ 0 & -1/L1 & 0 & 0 \end{bmatrix}, \quad B^1(m_2) = B^2(m_2) = \begin{bmatrix} 0 \\ 0 \\ 0 \\ 1/L1 \end{bmatrix}, \quad (\text{A.6})$$

which are associated with two discrete states $M = \{m_1, m_2\}$, defined for the ON and OFF switching states of the original circuit of the Ćuk converter under current-mode control PWM scheme (see Table 2.1). Function ξ in (A.4) can be described by the following switch sets:

$$\begin{aligned} S_{1,2} &= \{x \in R^n \mid x_3(dT) + x_4(dT) + Kx_1 < KV_{\text{ref}}\}, \\ S_{2,1} &= \{x \in R^n \mid x_3(dT) + x_4(dT) + Kx_1 > KV_{\text{ref}}\}, \end{aligned} \quad (\text{A.7})$$

where d is the duty ratio, T is the period of switching and K is the proportional gain of the outer feedback loop. The membership functions are constructed as

$$\begin{aligned} \Gamma^1(x_3(t) + x_4(t)) &= \frac{1}{2} \left(1 + \frac{X_1(0) - x_3(t) - x_4(t)}{2l} \right), \\ \Gamma^2(x_3(t) + x_4(t)) &= \frac{1}{2} \left(1 + \frac{X_1(0) - x_3(t) - x_4(t)}{2l} \right), \end{aligned}$$

where $l = 0.2$ is a constant chosen for the range of $i_{L1}(t) + i_{L2}(t) \in \{0.4 - l, 0.4 + l\}$ to cover the interval of deviation error (similar to the case of the boost converter in Example 3.5). The fixed point $X(0) = [12.7187, 27.5608, 0.1012, 0.1268]$ explains the transversal intersection of the stable periodic orbit (period-1) with the switching manifold when the switch is on *off* state (Fig. A.5).

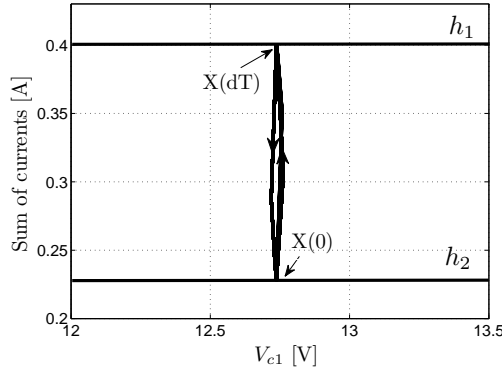


Figure A.5: The phase space diagram shows the transversal intersection of stable period-1 limit cycle.

Looking at the time responses in Fig. A.6, and the bifurcation diagram of Fig. A.7, it is evident that the non-smooth TS fuzzy model (A.4) can well capture the fast-scale switching behaviour and the resulting instabilities leading to chaos.

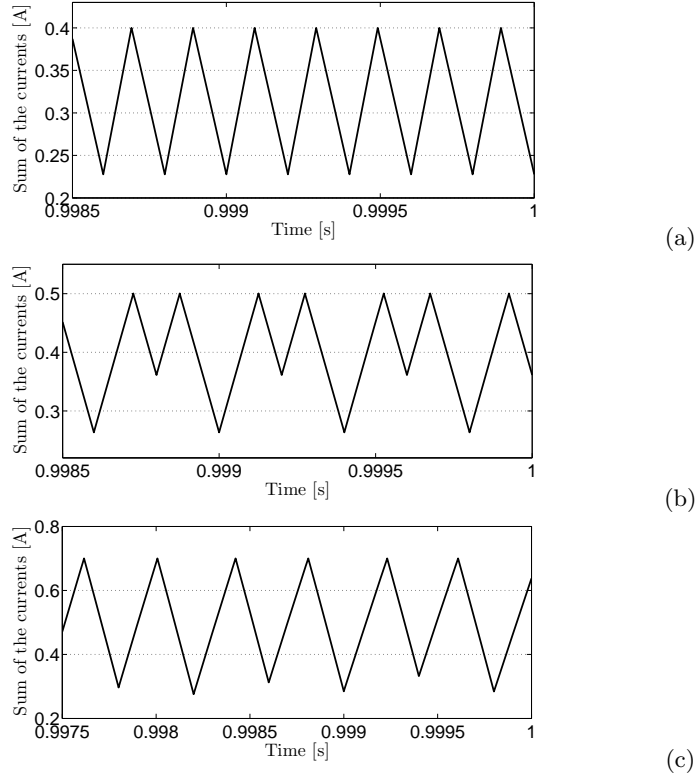


Figure A.6: The non-smooth TS fuzzy model (A.4) operates in (a) stable period-1 orbit when $I_{\text{ref}} = 0.4A$, (b) period-2 orbit when the reference current is varied to $I_{\text{ref}} = 0.5A$, and (c) chaotic orbit when the reference current is varied to $I_{\text{ref}} = 0.7A$.

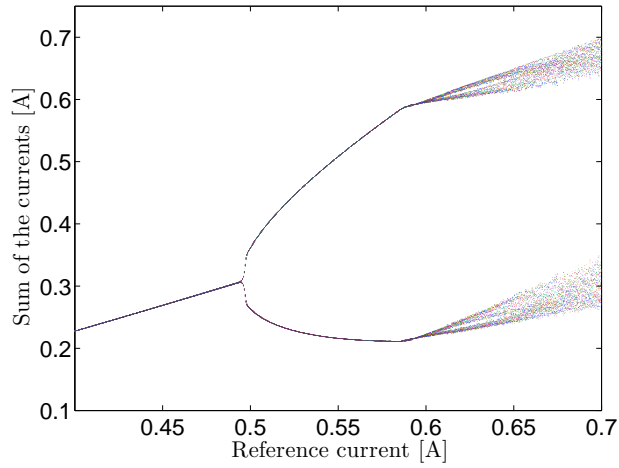


Figure A.7: The Monte-carlo bifurcation diagram of the TS fuzzy model of the Ćuk converter (A.4) when the reference current I_{ref} is varied as a bifurcation parameter.

A.2 Structural stability analysis

To analytically confirm the onset of the bifurcation visible in Fig. A.7, the fuzzy state space $\Omega \in \mathcal{F}$ is initially partitioned according to the switching hyperplane represented by the region Λ_{qr} fulfilling $\Lambda_{qr} \cap S_{1,2} \neq \emptyset$ and $\Lambda_{qr} \cap S_{1,2} \neq \emptyset$. Therefore, region partitions can be defined as

$$\begin{aligned}\Omega_1 &= \{(x, m) \in \mathcal{F} \mid x \in \mathbb{R}^n, m = m_1\} \\ \Omega_2 &= \{(x, m) \in \mathcal{F} \mid x \in \mathbb{R}^n, m = m_2\}\end{aligned}\tag{A.8}$$

After transforming the regions to quadratic inequalities as expounded in Section 4.3.1 and Section 4.5, the LMI stabilization problem of *Theorem 4.5* can be solved for the reference current value of $I_{\text{ref}} = 0.42$. This results in a feasible solution:

$$\begin{aligned}\tilde{\mathbf{P}}_1 &= \begin{bmatrix} 43.8488 & 41.3433 & -93.4600 & 0 & 0 \\ 41.3433 & 42.5052 & -90.0070 & 0 & 0 \\ -93.46 & -90.00 & 810.9474 & 0 & 0 \\ 0 & 0 & 0 & 1.33 & -833.36 \\ 0 & 0 & 0 & -833.36 & 2.08 \end{bmatrix} \\ \tilde{\mathbf{P}}_2 &= \begin{bmatrix} 1.0210 & 0 & -1.8009 & 0 & 0 \\ 0 & 1.6300 & 0 & -0.0050 & -24.44 \\ -1.8009 & 0 & 269.87 & 0 & 0 \\ 0 & -0.0050 & 0 & 554.86 & -0.14 \\ 0 & -24.44 & 0 & -0.147 & 949.35 \end{bmatrix}\end{aligned}$$

with the optimal value of $\beta = 2.43$. This proves that the solution trajectories exponentially converge to the stable periodic solution (fixed point of the Poincaré map) or simply that the system behaves in stable period-1 operation. For the range of parameter variation $I_{\text{ref}} = \{0.3A, 0.495A\}$, the LMI stabilization problem results in a feasible solution as expected (see Fig. A.7). However, at the operating point $I_{\text{ref}} = 0.496A$, solving the LMI stabilization problem results in an infeasible solution, which actually is the operating point where the period-doubling bifurcation occurs as confirmed by the Monte-carlo bifurcation diagram (Fig. A.7).

Table A.1: Different trials of partitioning of $\Omega \in \mathcal{F}$ shows too many region partitions may lead to a conservative result

Number of Partitions in \mathcal{F}	LMI feasibility	Optimum value of β	Numerical complexity
1	not feasible	N/A	low
2	feasible	2.4330	low
4	feasible	2.4340	medium
8	feasible	2.4540	medium
16	feasible	2.4650	high
32	not feasible	N/A	very high

As the LMI conditions of the stabilization problem (*Theorem 4.5*) are not conserva-

tive when the region partitioning (A.8) applies, defining finer region partitions are not necessary. However, if the number of regions exceeds a reasonable number, a conservative formulation may result (see Table A.1), which misleadingly hides a possible feasible solution.

Appendix B

Linear Matrix Inequalities

Looking closely at the TS fuzzy model-based approach for smooth dynamical systems, Linear Matrix inequalities (LMIs) can be considered as the cornerstone of any rigorous stabilization formulation based on Lyapunov analysis. In this thesis, it has been shown how the modern notion of structural stability for NSDS (and hence non-smooth TS fuzzy models) can be efficiently recast as LMI problems to be solved numerically by the existing interior-point optimization algorithms. As well as fuzzy system technology, a vast number of control problems in other areas can also be solved via LMIs as some form of an optimization problem. The aim of this appendix is first to provide some principal knowledge of LMIs and their standard problems, collectively attained from references [136, 214]. Secondly, a discussion of strict LMI problems in general and also in the case of the theorems presented in Chapter 4 is presented. We conclude with a brief discussion of the best optimization toolboxes available for solving LMI problems.

B.1 The formal definition

An LMI is a matrix inequality of the form:

$$J(x) = J_0 + \sum_{i=1}^m x_i J_i > 0, \quad (\text{B.1})$$

where $x = [x_1, x_2, \dots, x_n]^T$ is the variable and symmetric matrices $J_i \in \mathbb{R}^{n \times n}$ are given. The symbol " > 0 " is conventionally called positive definite. A positive definite $J(x) > 0$ in (B.1) is called a strict LMI and a positive semi-definite $J(x) \geq 0$ in (B.1) is called a non-strict LMI.

Multiple LMIs $J^1(x) > 0, \dots, J^n(x) > 0$ can be formulated as single LMI as $\text{diag}(J^1(x) > 0, \dots, J^n(x) > 0)$. LMIs can formulate a variety of convex constraints on x . Nevertheless, LMIs are normally described in such a way that *matrices are variables*, e.g. the basic Lyapunov stability for TS fuzzy system

$$P > 0, \quad (A^j)^T P + P A^j < 0, \quad \forall j = 1, 2, \dots, l \quad (\text{B.2})$$

which is an LMI where matrix A^j , $j = 1, 2, \dots, l$ is given and the matrix P is the variable. Such LMI can be explicitly described as the form above.

B.1.1 Some standard LMI problems

The standard LMI problem is to find a feasible solution x_f fulfilling the LMI $J(x) > 0$ or find the LMI is infeasible by finding no optimized solution. It is possible to find a feasible solution x_f where additionally one parameter or some parameters are minimized. This is referred to as a *generalized eigenvalue problem*, which can be formulated in the general form as

$$\begin{aligned} \text{Min} \quad & \delta \\ \text{Subject to} \quad & \delta B(x) - A(x) > 0, \quad B(x) > 0, \quad C(x) > 0, \end{aligned}$$

If $B(x) = I_{n \times n}$ in the problem above, the LMI problem is called an *eigenvalue problem*. Eigenvalues can be formulated as minimizing a linear function subject to an LMI $J(x) > 0$. In the case when all matrices J_i are diagonal, the problem is transformed to general linear programming problem.

B.1.2 S-procedure

The \mathcal{S} -procedure is a general approach to substitute a confined condition on a function with an unconfined condition. To described this, as used in this thesis (Section 4.3.1), let Q^0, \dots, Q^s be quadratic functions of the variable $x \in \mathbb{R}^n$, which are defined as

$$Q^k(x) = x^T Z^k x + 2(c^k)^T x + d^k, \quad k = 0, \dots, s, \quad (\text{B.3})$$

where $Z^k = (Z^k)^T \in \mathbb{R}^n \times \mathbb{R}^n$, $c^k \in \mathbb{R}^n$ and $d^k \in \mathbb{R}$. The confined condition

$$Q^0(x) \geq 0 \text{ for all } x \text{ satisfying } Q^k(x) \geq 0, \quad k \in I_s, \quad (\text{B.4})$$

can be substituted by an unconfined condition via the following Lemma

Lemma A.1: If there exist $\lambda^k \geq 0$, $k \in I_s$, such that:

$$\forall x \in \mathbb{R}^n, \quad Q^0(x) \geq \sum_{k=1}^s \lambda^k Q^k(x), \quad (\text{B.5})$$

then (B.4) is true \square

By introducing parameters λ^k , $k \in I_s$, condition (B.4) can be formulated as an LMI according to Lemma A.1:

$$\begin{bmatrix} x \\ 1 \end{bmatrix}^T \begin{bmatrix} Z^k & c^k \\ (c^k)^T & d^k \end{bmatrix} \begin{bmatrix} x \\ 1 \end{bmatrix} \geq \sum_{k=1}^s \lambda^k \begin{bmatrix} x \\ 1 \end{bmatrix}^T \begin{bmatrix} Z^k & c^k \\ (c^k)^T & d^k \end{bmatrix} \begin{bmatrix} x \\ 1 \end{bmatrix}, \quad \lambda^k \geq 0, \quad k \in I_s. \quad (\text{B.6})$$

The problem of finding if a quadratic inequality is positive semi-definite while other

quadratic inequalities are positive semi-definite has been subjected to scrutiny of applied mathematician for almost 80 years. The work of Aizerman et al. [215] showed the important application of \mathcal{S} -procedure although it had been used before in some control problems. Several generalizations for \mathcal{S} -procedure have also been introduced during the past 30 years (see [136] and the references therein).

B.2 Nonlinear matrix inequalities

Nonlinear matrix inequalities (NMIs) are inequalities where the matrix variables are formulated as nonlinear terms. The most important type of NMIs are bilinear matrix inequalities and quadratic matrix inequalities, which are implausible to be directly solved by existing LMI solvers unless they are transformed to LMIs.

B.2.1 Bilinear matrix inequalities

Consider the bilinear matrix inequality (BMI)

$$PA^T + AP + BKP + PK^TB^T < 0, \quad (\text{B.7})$$

where $P = P^T > 0$ and K is the matrix variables. The BMI (B.7) can be linearized to an LMI condition using the positive definiteness of matrix P as

$$PA^T + AP + BM + M^TB^T < 0, \quad (\text{B.8})$$

where $M = KP$. This transformation is crucial in designing model-based controllers for TS fuzzy systems.

B.2.2 Quadratic matrix inequalities

Let α and β be index sets. $A(\alpha, \beta)$ is the sub-matrix formed by the rows indexed by α and the columns indexed by β in A . The sub-matrix $A(\hat{\alpha}, \hat{\beta})$ is derived by removing the rows indexed by α and columns indexed by β in A . The special matrix

$$A(\hat{\alpha}, \hat{\alpha}) - A(\hat{\alpha}, \alpha)A(\alpha, \alpha)^{-1}A(\alpha, \hat{\alpha}) \quad (\text{B.9})$$

is called the Schur complement of $A(\alpha, \alpha)$ in A . Let A be symmetric, positive definite and partitioned as

$$A = \begin{bmatrix} A_{11} & A_{12} \\ A_{12}^T & A_{22} \end{bmatrix}. \quad (\text{B.10})$$

It can then be shown that the Schur complements of A_{11} and A_{22} in A have the following properties

$$A_{22} - A_{12}^T A_{11}^{-1} A_{12} > 0 \quad \text{and} \quad A_{11} - A_{12} A_{22}^{-1} A_{12}^T > 0. \quad (\text{B.11})$$

Employing the Schur complement it is possible to transform a quadratic matrix inequalities (QMIs) of the form

$$P(x) - R(x)S(x)^{-1}R(x)^T > 0, \quad (\text{B.12})$$

where $P(x) = P(x)^T > 0$ and $S(x) = S(x)^T > 0$ to an LMI as:

$$\begin{bmatrix} P(x) & R(x) \\ R(x)^T & S(x) \end{bmatrix} > 0, \quad (\text{B.13})$$

where $S(x)$ is indeed an invertible matrix.

B.3 Finding a solution to strict inequalities

LMI problems may be composed of positive-definite (strict) inequalities and positive semi-definite (non-strict) inequalities. If all the conditions like $J^i(x) \geq 0$ are substituted by conditions like $J^i(x) > 0$, the result is an LMI problem with only positive-definite inequalities. If there is a feasible solution x_f to the LMI problem with inequalities like $J^i(x) > 0$, there is definitely a feasible solution to the one with inequalities like $J^i(x) \geq 0$. However, the converse is not true. In some cases, after the substitution, x_f cannot be found, despite the fact that there is a feasible solution x_f for the original LMI problem with the inequalities $J^i(x) \geq 0$. This is due to the fact that inequalities like $J^i(x) \geq 0$ may include an implicit equality like $\text{diag}(P, -P) \geq 0$ which, in turn, may have an implicit equality of $P = 0$. Another possibility is that the LMI is turned out to be singular, shown by $J(P) = \text{diag}(P, 0) \geq 0$ even if $P > 0$. Therefore, substitution of semi-definite conditions with definite conditions will not result in a feasible solution.

LMIs with inequalities like $J^i(x) \geq 0$ can be equivalently transformed to LMI with inequalities like $J^i(x) > 0$ by removing implicit inequalities or nonsingular terms. In this way, the LMI problem can be further simplified by omitting any constant null-spaces. A typical problem that may arise in the transformation is, as mentioned before, the infeasibility of any solution to the resulting LMI problem. At the same time, the best optimization algorithms for LMI solvers cannot deal with most of the inequalities like $J^i(x) \geq 0$ in an LMI problem unless they are transformed to inequalities like $J^i(x) > 0$ (see the next section). If all hidden equality constraints and nonsingular terms are recognized and excluded from an LMI, the solver can find a solution to the LMI problem with strict inequalities in a similar way to the original LMI problem. This section attempts to address this problem by explaining how to recognize implicit equalities and nonsingular terms in the LMI stabilization problems of Theorem 4.5 and Theorem 4.6 to ease the transformation to positive definite inequalities; and hence to find the feasible solution in a similar manner to that of the original LMI problem.

When the fuzzy state-space region Ω_q^x encompasses the origin, it can be deduced that $V_q(0) = 0$ in the second condition of all stability theorems stated (Sections 4.3 and 4.4). $V_q = \tilde{x}^T P_q \tilde{x}$ in the (4.18) also becomes $V_q = x^T P_q x$, meaning that the terms π_q and p_q are equal to zero. Therefore, $\pi_q = 0$ and $p_q = 0$ are the first implicit equalities that should be considered if the transformation to positive-definite inequalities is necessary. Moreover, there are additional implicit inequalities in the parameters associated with regions Ω_q , substituted by semi-definite inequalities $Q^k(x) \geq 0$, where $Q^k(x)$ is defined as (4.29). For clarification, we reformulate the second, third and fourth conditions of the

LMI stabilization problem of Theorem 4.5 when $\pi_q = 0$ and $p_q = 0$ as

$$\begin{aligned}
2. \quad & \begin{bmatrix} \alpha I - P_q + \sum_{k=1}^{s_q} \lambda_q^k Z_q^k & \sum_{k=1}^{s_q} \lambda_q^k c_q^k \\ \sum_{k=1}^{s_q} \lambda_q^k (c_q^k)^T & \sum_{k=1}^{s_q} \lambda_q^k d_q^k \end{bmatrix} \leq 0, \\
3. \quad & \begin{bmatrix} P_q - \beta I + \sum_{k=1}^{s_q} v_q^k Z_q^k & \sum_{k=1}^{s_q} v_q^k c_q^k \\ \sum_{k=1}^{s_q} v_q^k c_q^k T & \sum_{k=1}^{s_q} v_q^k d_q^k \end{bmatrix} \leq 0, \\
4. \quad & \begin{bmatrix} A^T(m_i)P_q + P_q A(m_i) + I + \sum_{k=1}^{s_{q,m_i}} \lambda_{q,m_i}^k Z_{q,m_i}^k & P_q B(m_i) + \sum_{k=1}^{s_{q,m_i}} \lambda_{q,m_i}^k c_{q,m_i}^k \\ B(m_i)^T P_q + \sum_{k=1}^{s_{q,m_i}} \lambda_{q,m_i}^k (c_{q,m_i}^k)^T & \sum_{k=1}^{s_{q,m_i}} \lambda_{q,m_i}^k d_{q,m_i}^k \end{bmatrix} \leq 0,
\end{aligned}$$

where Ω_q^x encompassing the origin enforces that $Q^k(0) \geq 0$, $k \in I_s$ so $d^k \geq 0$ in (4.29). Hence, $\sum_{k=1}^s \lambda^k d^k \geq 0$ since all $\lambda^k \geq 0$. Consequently, all elements in the lower right corner of the above matrices should be positive semi-definite. On the other hand, all the elements in the lower right corner should also be " ≤ 0 " [216]. Therefore the LMI elements $\sum_{k=1}^{s_q} \lambda_q^k d_q^k = 0$, $\sum_{k=1}^{s_q} v_q^k d_q^k = 0$ and $\sum_{k=1}^{s_{q,m_i}} \lambda_{q,m_i}^k d_{q,m_i}^k = 0$. A matrix variable with " 0 " in the lower right corner cannot fulfill a positive-definite inequality [216]. The only way to solve the above inequalities by positive-definite conditions, is transforming the singular matrix to a non-singular one by putting all the matrix elements in the last row and column as $\sum_{k=1}^{s_q} \lambda_q^k c_q^k = 0$, $\sum_{k=1}^{s_q} v_q^k c_q^k = 0$ and $P_q B(m_i) + \sum_{k=1}^{s_{q,m_i}} \lambda_{q,m_i}^k c_{q,m_i}^k = 0$. In this manner, there is a possibility to transform the LMI conditions in Theorem 4.5 and 4.6 to positive-definite inequalities.

There are two ways to assign $\sum_{k=1}^s \lambda^k d^k = 0$ by either $\lambda^k = 0$ or $d^k = 0$. $\lambda^k = 0$ implies that $Q^k(x) \geq 0$ is a redundant condition, which obviously conflicts with its initial purpose. It also means that the other conditions in the LMI problem should be fulfilled in the entire fuzzy state space, which, as already emphasized, is quite conservative and leads to an infeasible solution. Therefore, for regions Ω_q^x defined by the quadratic forms (4.29) and encompassing the origin, parameters $d^k = 0$ should be selected. The same arguments is valid for the elements $\sum_{k=1}^s \lambda^k c^k = 0$.

Similarly, for the fifth condition of the stability theorems, if region Ω_r^x encompasses the origin, then $\pi_r = 0$ and $p_r = 0$. Therefore the condition can be reformulated as

$$5. \quad \begin{bmatrix} P_r - P_q + \sum_{k=1}^{s_{q,r}} \lambda_{q,r}^k Z_{q,r}^k & \sum_{k=1}^{s_{q,r}} \lambda_{q,r}^k c_{q,r}^k \\ \sum_{k=1}^{s_{q,r}} \lambda_{q,r}^k (c_{q,r}^k)^T & \sum_{k=1}^{s_{q,r}} \lambda_{q,r}^k d_{q,r}^k \end{bmatrix} \leq 0,$$

As $Q^k(0) = 0$, $k \in I_s$, the parameters $\lambda_{q,r}^k$ should be assigned to zero in (4.29) and then $\sum_{k=1}^{s_{q,r}} \lambda_{q,r}^k d_{q,r}^k$. Similarly, the singular matrix can be transformed to a non-singular matrix in case of parameters $c_{q,r}^k = 0$ when both regions Ω_q^x and Ω_r^x encompass the origin. In brief, for regions Ω_q^x encompassing the origin, the local Lyapunov function can be defined as $V_q(x) = x^T P_q x$ by letting $\pi_q = 0$ and $p_q = 0$ and all regions can be defined as $Q^k(x) = x^T Z^k x$ by letting $c^k = 0$ and $d^k = 0$, $k \in I_s$. The same applies for region Ω_r^x with the corresponding parameters, if it encompasses the origin.

It may be the case, specially close to the switching manifold (defined by switch sets), that in terms of matrix inequalities, the evolution of a trajectory should be considered

bidirectional between regions Ω_q^x and Ω_r^x at states described by the same parameters in $Q^k(x) = 0$. Therefore, an implicit equality for the local Lyapunov functions $V_q(x)$ and $V_r(x)$, measuring the energy in the regions Ω_q^x and Ω_r^x respectively, can be introduced by explicitly formulating the conditions $V_q(x) \leq V_r(x)$ and $V_r(x) \leq V_q(x)$. In this case, the condition becomes

$$\tilde{P}_r + \sum_{k=1}^{s_{q,r}} \lambda_{q,r}^k \tilde{Z}_{q,r}^k \leq \tilde{P}_q \quad \text{and} \quad \tilde{P}_q + \sum_{k=1}^{s_{r,q}} \lambda_{q,r}^k \tilde{Z}_{r,q}^k \leq \tilde{P}_r,$$

which should be fulfilled for all states. For the states fulfilling the quadratic equality $Q^k(x) = 0$, it is necessary that $\tilde{P}_r \leq \tilde{P}_q$ and $\tilde{P}_q \leq \tilde{P}_r$, meaning that $\tilde{P}_q = \tilde{P}_r$ should hold close to the switching manifold (see Figure below).

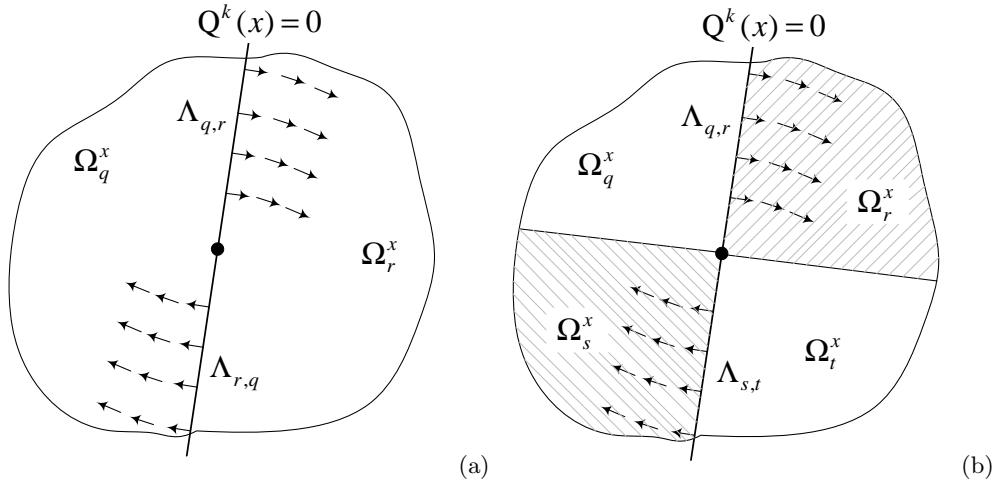


Figure B.1: (a) The vector field is bidirectional between Ω_q^x and Ω_r^x . The circle on the surface show the turning point of the vector fields. (b) Two regions are split into four to avoid an implicit equality like $\tilde{P}_q = \tilde{P}_r$.

For transforming to positive-definite conditions, there are two ways to remove these implicit equalities. The first is to further split the former partitions with respect to Λ_{qr} in such a way that a solution trajectory passes through Ω_q^x to Ω_r^x or unidirectionally if otherwise. The main drawback of this method is the increasing computational burden as a result of the increasing number of unknown LMI variables. Moreover, splitting regions with respect to Λ_{qr} as explained above is not an effortless task.

The second method, which is more practical, is to let $\tilde{P}_q \equiv \tilde{P}_r$. Since this equality condition only have to occur on hyperplanes $Q_{q,r}^k = 0$, a less conservative condition is to allow

$$\tilde{P}_r = \tilde{P}_q + \sum_{k=1}^{s_{q,r}} \lambda_{q,r}^k \tilde{Z}_{q,r}^k \quad (\text{B.14})$$

where, indeed, the special case of $\lambda_{q,r}^k = 0$ result in the equality $\tilde{P}_q \equiv \tilde{P}_r$. This implies that the fifth condition in stability theorems should be substituted by Linear Matrix Equality (LME) conditions. Similarly, if another matrix like \tilde{P}_s should fulfill the condition $\tilde{P}_s \equiv \tilde{P}_r$

on hyperplane $Q_{r,s}^k(x) = 0$, then the condition can be formulated as

$$\tilde{P}_s = \tilde{P}_q + \sum_{k=1}^{s_{q,r}} \lambda_{q,r}^k \tilde{Z}_{q,r}^k + \sum_{k=1}^{s_{r,s}} \lambda_{r,s}^k \tilde{Z}_{r,s}^k$$

and so on.

B.4 LMI solvers

There is a handful of available commercial LMI solvers and open-source software packages that can solve standard LMI problems efficiently. The most familiar of these is the LMI toolbox of MATLAB. Numerical optimization routines for solving LMI problems in this toolbox are **feasp** for standard LMI problems and **gevp** for the generalized eigenvalue minimization problems. Although the LMI toolbox can handle tens or even hundreds of thousands of matrix variables, defining an LMI problem with too many matrix variables (over a million) is difficult to solve. Moreover, LMI convex optimization numerical routines can only deal with strict (positive-definite) inequalities.

There are two other software packages named YALMIP and LMITOOL, which were employed for the LMI problems of this thesis. YALMIP, which can be run on a MATLAB platform, is developed for modeling and solving convex optimization problems [217]. Defining an LMI problem in this toolbox is easy and rather intuitive. Compared to the LMI toolbox, it additionally supports more than 20 (commercial) solvers to solve standard LMI problems more efficiently. For instance, PENBMI is specially designed to solve Bilinear Matrix Inequalities (BMI) or large scale LMI feasibility problems and PENSDP is designed for LMI constraints with linear semi-definite programming problems (non-strict inequalities).

LMITOOL is a part of the open source scientific modeling software named *SCILAB* [218]. The LMITOOL provides an attractive user interface for automating the definition of an LMI problem, which is solved by a routine called **lmisolver**. The optimization algorithms of **lmisolver** have special interior-point routines for equality constraints or linear matrix equalities (LME). However, **lmisolver** is not suitable for handling LMI problems with numerous unknown matrix variables normally expected in a large-scale standard LMI problem.

Appendix C

Parameter Values

C.1 DC-DC Converters

Boost converter:

Resistance (R) = $30\ \Omega$

Inductance (L) = $27\ \text{mH}$

Capacitance (C) = $120\ \mu\text{F}$

Parasitic resistance for inductor (r_L) = $1.2\ \Omega$

Parasitic resistance for diode (r_{VD}) = $0.24\ \Omega$

Parasitic resistance for switch (r_{SW}) = $0.3\ \Omega$

Parasitic resistance for capacitor (r_C) = $0.2\ \Omega$

Period (T) = $1 \times 10^{-4}\ \text{s}$

Buck converter:

Resistance (R) = $22\ \Omega$

Inductance (L) = $20\ \text{mH}$

Capacitance (C) = $47\ \mu\text{F}$

Reference voltage (V_{ref}) = $11.3\ \text{V}$

Upper value for ramp signal (V_U) = $8.2\ \text{V}$ in Section 2.1.1

Lower value for ramp signal (V_L) = $3.8\ \text{V}$ in Section 2.1.1

Proportional gain (A) = 8.4 in Section 2.1.1

Period (T) = $4 \times 10^{-4}\ \text{s}$

Cuk converter:

Resistance (R) = $75\ \Omega$

1st inductance ($L1$) = $1\ \text{mH}$

2nd inductance ($L2$) = $1\ \text{mH}$

Capacitance (C) = $47\ \mu\text{F}$

Input voltage (V_{in}) = $15\ \text{V}$

Period (T) = $4 \times 10^{-4}\ \text{s}$

C.2 Forced hard impact oscillator

Mass (M) = 1 kg

Spring stiffness (k) = 1 N/m

Viscous damping coefficient (c) = 0.5 N/(ms)

Damping factor (ζ) = 0.25 ms/(m.kg)

Natural frequency (ω_n) = 1 N/(m.kg)

The maximum distance of the mass with respect to the hard wall (σ) = 5 m

C.3 Forced dry-friction oscillator

Mass (M) = 1 kg

Viscous damping coefficient (c) = 0 N/(ms)

Spring stiffness (K) = 1 N/m

Constant velocity (V) = 1 m/s

1st coefficient for kinematic friction (α_0) = 1.5 N

2nd coefficient for kinematic friction (α_1) = 1.5 Ns/m

3rd coefficient for kinematic friction (α_2) = 0.45 Ns³/m³

Forcing function amplitude (F) = 1 N

Bibliography

- [1] S. Banerjee and G. Verghese, eds., *Nonlinear Phenomena in Power Electronics: attractors, bifurcation, chaos, and nonlinear control*. New York, NY 10016-5997: IEEE Press, 1 ed., 2001.
- [2] S. Kundu, S. Banerjee, and D. Giaouris, “Vanishing singularity in hard impacting systems,” *AIMS journals, Discrete and Continuous Dynamical Systems, Part B*, vol. Accepted for publication, 2010.
- [3] Y. Yoshitake and A. Sueoka, “Forced self-excited vibration with dry friction,” *Applied nonlinear dynamics and chaos of mechanical systems with discontinuities, World Scientific, Editors Marian Wiercigroch and Bram de Kraker*, 2000.
- [4] E. Loren, “Deterministic non periodic flows,” *Atoms Sci*, vol. 20, pp. 130–141, 1963.
- [5] L. Zadeh, “Fuzzy sets,” *Information and control*, vol. 8, no. 3, pp. 338–353, 1965.
- [6] S. Strogatz, *Nonlinear dynamics and chaos: With applications to physics, biology, chemistry, and engineering*. Westview Pr, 2000.
- [7] M. di Bernardo, C. Budd, A. Champneys, and P. Kowalczyk, *Piecewise-smooth dynamical systems: theory and applications*. London: Springer Verlag, 1st ed., 2008.
- [8] D. Anosov, V. Arnold, S. Aranson, I. Bronshtein, V. Grines, and Y. Il’Yashenko, *Ordinary differential equations and smooth dynamical systems*. Springer Verlag, 1997.
- [9] H. K. Khalil, *Nonlinear Systems*. Upper Saddle River, New Jersey: Prentice-Hall, 2nd ed., 1996.
- [10] J.-J.E. Slotine and W. Li, *Applied Nonlinear Control*. New Jersey: Prentice Hall, 1991.
- [11] A. F. Filippov, *Differential equations with discontinuous righthand sides*. Dortrecht: Kluwer Academic Publishers, 1988.
- [12] E. Chong, “Discrete event systems: Modeling and performance analysis,” *Discrete Event Dynamic Systems*, vol. 4, no. 1, pp. 113–116, 1994.
- [13] R. David and H. Alla, *Petri Nets and Grafcet: Tools for modelling discrete event systems*. Prentice Hall, 1992.

- [14] Y. Tsypkin, *Relay control systems*. Cambridge University Press Cambridge, 1984.
- [15] E. Sontag, *Mathematical control theory: deterministic finite dimensional systems*. Springer Verlag, 1998.
- [16] D. Liberzon, *Switching in systems and control*. Springer, 2003.
- [17] V. Duindam and S. Stramigioli, *Modeling and Control for Efficient Bipedal Walking Robots*, vol. 53 of *Springer Tracts in Advanced Robotics*. Berlin, Heidelberg: Springer, 2009.
- [18] Y. Hurmuzlu, F. Génot, and B. Brogliato, “Modeling, stability and control of biped robots: A general framework,” *Automatica*, vol. 40, no. 10, pp. 1647–1664, 2004.
- [19] G. Tao and F. Lewis, *Adaptive control of nonsmooth dynamic systems*. Springer Verlag, 2001.
- [20] E. Ott, C. Grebogi, and J. Yorke, “Controlling chaos,” *Physical Review Letters*, vol. 64, no. 11, pp. 1196–1199, 1990.
- [21] T. Shinbrot, C. Grebogi, E. Ott, and J. Yorke, “Using small perturbations to control chaos,” *Nature*, vol. 363, pp. 411–417, 1993.
- [22] M. Bleich and J. Socolar, “Stability of periodic orbits controlled by time-delay feedback,” *Physics Letters A*, vol. 210, no. 1-2, pp. 87–94, 1996.
- [23] M. Bleich, D. Hochheiser, J. Moloney, and J. Socolar, “Controlling extended systems with spatially filtered, time-delayed feedback,” *Physical Review E*, vol. 55, no. 3, pp. 2119–2126, 1997.
- [24] G. Chen and X. Dong, *From chaos to order*. World Sci., 1998.
- [25] G. Chen, *Controlling chaos and bifurcations in engineering systems*. CRC Pr I Llc, 1999.
- [26] M. Di Bernardo and G. Chen, “Controlling bifurcations in nonsmooth dynamical systems,” *Controlling Chaos and Bifurcations in Engineering Systems*, pp. 391–412, 2000.
- [27] T. Takagi and M. Sugeno, “Fuzzy identification of systems and its applications to modeling and control,” *IEEE Transaction on Systems, Man and Cybernetics*, vol. 15, no. 1, pp. 116–132, 1985.
- [28] K. Tanaka, *Fuzzy Control Systems Design and Analysis: a Linear Matrix Inequality Approach*. Newark: John Wiley & Sons, 2001.
- [29] J. Deane and D. Hamill, “Analysis, simulation and experimental study of chaos in the buck converter,” in *Power Electronics Specialists Conference, 1990. PESC’90 Record., 21st Annual IEEE*, pp. 491–498, 1990.

- [30] G. Yuan, S. Banerjee, E. Ott, and J. Yorke, "Border-collision bifurcations in the buck converter," *IEEE Transactions on Circuits and Systems-I: Fundamental theory and applications*, vol. 45, no. 7, pp. 707–716, 1998.
- [31] K. Chakrabarty, G. Poddar, and S. Banerjee, "Bifurcation behavior of the buck converter," *IEEE Transactions on Power Electronics*, vol. 11, no. 3, pp. 439–447, 1996.
- [32] E. Fossas and G. Olivar, "Study of chaos in the buck converter," *IEEE Transactions on Circuits and Systems I: Fundamental Theory and Applications*, vol. 43, no. 1, pp. 13–25, 1996.
- [33] D. Hamill and J. Deane, "Modeling of chaotic dc-dc converters by iterated nonlinear mappings," *IEEE Transaction on Power Electronics*, vol. 7, pp. 25–36, January 1992.
- [34] K. Chakrabarty, G. Poddar, and S. Banerjee, "Bifurcation behavior of the buck converter," *IEEE Transactions on Power Electronics*, vol. 11, no. 3, pp. 439–447, 1996.
- [35] R. I. Leine and H. Nijmeijer, *Dynamics and Bifurcations of Non-Smooth Mechanical Systems*. Berlin, Germany: Springer, 2004.
- [36] F. Peterka, "Part 1: Theoretical analysis of n-multiple (1/n)-impact solutions," *CSAV Acta Technica*, vol. 19, no. 4, pp. 462–473, 1974.
- [37] F. Peterka, "Laws of impact motion of mechanical systems with one degree of freedom. II- Results of analogue computer modelling of the motion," *Acta Technica CSAV*, vol. 19, no. 5, pp. 569–580, 1974.
- [38] V. Babitskii, "Theory of Vibroimpact Systems," 1978.
- [39] S. Shaw and P. Holmes, "A periodically forced piecewise linear oscillator," *Journal of Sound and Vibration*, vol. 90, no. 1, pp. 129–155, 1983.
- [40] J. Thompson and R. Ghaffari, "Chaotic dynamics of an impact oscillator," *Physical Review A*, vol. 27, no. 3, pp. 1741–1743, 1983.
- [41] A. Nordmark, "Non-periodic motion caused by grazing incidence in an impact oscillator," *Journal of Sound Vibration*, vol. 145, pp. 279–297, 1991.
- [42] J. de Weger, D. Binks, J. Molenaar, and W. van de Water, "Generic behavior of grazing impact oscillators," *Physical review letters*, vol. 76, no. 21, pp. 3951–3954, 1996.
- [43] S. Bishop, "Impact oscillators," *Philosophical Transactions: Physical Sciences and Engineering*, vol. 347, no. 1683, pp. 347–351, 1994.
- [44] D. Wagg and S. Bishop, "Application of non-smooth modelling techniques to the dynamics of a flexible impacting beam," *Journal of Sound and Vibration*, vol. 256, no. 5, pp. 803–820, 2002.

- [45] N. Hinrichs, M. Oestreich, and K. Popp, “Experiments, modelling and analysis of friction and impact oscillators,” *Zeitschrift für angewandte Mathematik und Mechanik*, vol. 79, 1999.
- [46] M. Oestreich, N. Hinrichs, and K. Popp, “Bifurcation and stability analysis for a non-smooth friction oscillator,” *Archive of Applied Mechanics*, vol. 66, no. 5, pp. 301–314, 1996.
- [47] K. Popp and P. Stelzer, “Stick-slip vibrations and chaos,” *Philosophical Transactions: Physical Sciences and Engineering*, vol. 332, no. 1624, pp. 89–105, 1990.
- [48] N. Hinrichs, M. Oestreich, and K. Popp, “On the modelling of friction oscillators,” *Journal of Sound and Vibration*, vol. 216, no. 3, pp. 435–459, 1998.
- [49] U. Galvanetto, “Nonlinear dynamics of multiple friction oscillators,” *Computer methods in applied mechanics and engineering*, vol. 178, no. 3-4, pp. 291–306, 1999.
- [50] U. Galvanetto, “Some discontinuous bifurcations in a two-block stick-slip system,” *Journal of Sound and vibration*, vol. 248, no. 4, pp. 653–669, 2001.
- [51] V. I. Utkin, *Sliding Modes in Control and Optimisation*. Springer-Verlog, 1992.
- [52] M. Di Bernardo, P. Kowalczyk, and A. Nordmark, “Sliding bifurcations: a novel mechanism for the sudden onset of chaos in dry-friction oscillators,” *International Journal of Bifurcation and Chaos*, vol. 13, no. 10, pp. 2935–2948, 2003.
- [53] Y. Kuznetsov, I. Kuznetsov, and Y. Kuznetsov, *Elements of applied bifurcation theory*. Springer New York, 1998.
- [54] D. Jordan and P. Smith, *Nonlinear ordinary differential equations: an introduction for scientists and engineers*. Oxford University Press, USA, 2007.
- [55] R. Hilborn, *Chaos and nonlinear dynamics*. oxford university press Oxford, 2000.
- [56] G. Iooss and D. Joseph, *Elementary stability and bifurcation theory*. Springer, 1990.
- [57] M. Feigin, “Doubling the oscillation period in the presence of C bifurcations in piecewise continuous systems(Dynamic systems oscillation period doubling in presence of C bifurcations),” *Prikladnaia Matematika I Mekhanika*, vol. 34, pp. 861–869, 1970.
- [58] M. Feigin, “On the structure of C-bifurcation boundaries of piecewise continuous systems,” *Journal of Applied Mathematics and Mechanics*, vol. 42, pp. 820–829, 1978.
- [59] M. Feigin, “Forced vibrations of nonlinear systems with discontinuities,” 1994.
- [60] M. di Bernardo, C. Budd, A. Champneys, P. Kowalczyk, A. Nordmark, G. Tost, and P. Piiroinen, “Bifurcations in nonsmooth dynamical systems,” *Siam Review*, vol. 50, p. 629, 2008.

- [61] H. Nusse and J. Yorke, "Border-collision bifurcations including "period two to period three" for piecewise smooth systems," *Physica D: Nonlinear Phenomena*, vol. 57, no. 1-2, pp. 39–57, 1992.
- [62] H. Nusse, E. Ott, and J. Yorke, "Border-collision bifurcations: An explanation for observed bifurcation phenomena," *Physical Review E*, vol. 49, no. 2, pp. 1073–1076, 1994.
- [63] H. Nusse and J. Yorke, "Border-collision bifurcations for piecewise smooth one-dimensional maps," *International Journal of Bifurcation and Chaos in Applied Sciences and Engineering*, vol. 5, no. 1, pp. 189–208, 1995.
- [64] S. Banerjee and C. Grebogi, "Border collision bifurcations at the change of state-space Dimension," *Chaos*, vol. 12, pp. 1054–1069, 2002.
- [65] A. Nordmark, "Existence of periodic orbits in grazing bifurcations of impacting mechanical oscillators," *Nonlinearity*, vol. 14, pp. 1517–1542, 2001.
- [66] M. Di Bernardo, C. Budd, and A. Champneys, "Normal form maps for grazing bifurcations in n-dimensional piecewise-smooth dynamical systems," *Physica D: Nonlinear Phenomena*, vol. 160, no. 3-4, pp. 222–254, 2001.
- [67] M. Di Bernardo, C. Budd, and A. Champneys, "Corner collision implies border-collision bifurcation," *Physica D: Nonlinear Phenomena*, vol. 154, no. 3-4, pp. 171–194, 2001.
- [68] M. Di Bernardo, P. Kowalczyk, and A. Nordmark, "Bifurcations of dynamical systems with sliding: derivation of normal-form mappings," *Physica D: Nonlinear Phenomena*, vol. 170, no. 3-4, pp. 175–205, 2002.
- [69] Y. Kuznetsov, S. Rinaldi, and A. Gragnani, "One-parameter bifurcations in planar Filippov systems," *international journal of bifurcation and chaos in applied sciences and engineering*, vol. 13, no. 8, pp. 2157–2188, 2003.
- [70] P. Hartman, "A lemma in the theory of structural stability of differential equations," *Proceedings of the American Mathematical Society*, vol. 11, no. 4, pp. 610–620, 1960.
- [71] T. Parker and L. Chua, *Practical numerical algorithms for chaotic systems*. Springer-Verlag New York, Inc. New York, NY, USA, 1989.
- [72] R. Leine, *Bifurcations in discontinuous mechanical systems of Filippov-type*. PhD thesis, Technische Universiteit Eindhoven, 2000.
- [73] M. Aizerman and F. Gantmakher, "On the stability of periodic motions," *Journal of Applied Mathematics and Mechanics*, vol. 22, no. 6, pp. 1065–1078, 1958.
- [74] A. Nordmark, "Universal limit mapping in grazing bifurcations," *Physical review E*, vol. 55, no. 1, pp. 266–270, 1997.

- [75] M. Fredriksson and A. Nordmark, "Bifurcations caused by grazing incidence in many degrees of freedom impact oscillators," *Proceedings: Mathematical, Physical and Engineering Sciences*, vol. 453, no. 1961, pp. 1261–1276, 1997.
- [76] W. Levine, *The Control Handbook*. CRC Press, 1996.
- [77] L. Wang, *Adaptive fuzzy systems and control: design and stability analysis*. Prentice-Hall, Inc. Upper Saddle River, NJ, USA, 1994.
- [78] P. Liu, "Mamdani fuzzy system: universal approximator to a class of random processes," *IEEE Transactions on Fuzzy Systems*, vol. 10, no. 6, pp. 756–766, 2002.
- [79] Z. Li, *Fuzzy chaotic systems: modeling, control, and applications*. Springer, 2006.
- [80] C. Fantuzzi and R. Rovatti, "On the approximation capabilities of the homogeneous takagi-sugeno model," in *The 5th IEEE International Conference on Fuzzy Systems FUZZ-IEEE'96*, vol. 2, (New Orleans, LA), pp. 1067–72, 1996.
- [81] P. Bergsten, *Observers and Controllers for Takagi-Sugeno Fuzzy systems*. PhD thesis, Örebro university, Örebro, 2001.
- [82] M. Sugeno, "Fuzzy control," *Nikkan Kougyou Shinbunsha*, 1988.
- [83] M. Sugeno and G. Kang, "Structure identification of fuzzy model," *Fuzzy sets and systems*, vol. 28, no. 1, pp. 15–33, 1988.
- [84] H. Hellendron and D. Driankov, eds., *Fuzzy model Indentification: Selected Approaches*. Berlin: Springer-Verlog, 1997.
- [85] R. Babuska, *Fuzzy modeling for control*. Kluwer Academic Publishers Norwell, MA, USA, 1998.
- [86] P. Korba, R. Babuska, H. Verbruggen, P. Frank, A. Ltd, and S. Baden-Daettwil, "Fuzzy gain scheduling: controller and observer design based on Lyapunov method and convex optimization," *IEEE Transactions on Fuzzy Systems*, vol. 11, no. 3, pp. 285–298, 2003.
- [87] J. Shamma, "Linearization and gain-scheduling, The Control Handbook," *The Electrical Engineering Handbook Series, CRC Press, Boca Raton, FL, USA*, pp. 388–396, 1996.
- [88] T. Johansen, K. Hunt, P. Gawthrop, and H. Fritz, "Off-equilibrium linearisation and design of gain-scheduled control with application to vehicle speed control," *Control Engineering Practice*, vol. 6, no. 2, pp. 167–180, 1998.
- [89] D. Luenberger and Y. Ye, *Linear and nonlinear programming*. Springer Verlag, 2008.
- [90] D. Goldberg, *Genetic Algorithms in Search and Optimization*. Addison-wesley, 1989.
- [91] L. Davis *et al.*, *Handbook of genetic algorithms*. Citeseer, 1991.

- [92] S. Kawamoto, K. Tada, A. Ishigame, and T. Taniguchi, "An approach to stability analysis of second order fuzzy systems," in *IEEE International Conference on Fuzzy Systems, 1992.*, pp. 1427–1434, 1992.
- [93] K. Tanaka, T. Taniguchi, and H. Wang, "Generalized Takagi-Sugeno fuzzy systems: rule reduction and robust control," in *FUZZ-IEEE 2000: 9th IEEE International Conference on Fuzzy Systems*, pp. 688–693, 2000.
- [94] K. Mehran, *Takagi-Sugeno fuzzy modeling for process control*. Newcastle University, Industrial Automation, Robotics and Artificial Intelligence (EEE8005).
- [95] K. Mehran, B. Zahawi, and D. Giaouris, *Kansei Engineering and Soft Computing: Theory and Practice*, ch. Fuzzy Logic for Non-smooth Dynamical Systems. www.igi-global.com: IGI Global, 2010. To be published.
- [96] C. Hadjicostis and G. Verghese, "Monitoring discrete event systems using Petri net embeddings," *Application and Theory of Petri Nets 1999*, pp. 689–689, 1999.
- [97] C. Cassandras, "Discrete-Event Systems," *Handbook of networked and embedded control systems*, pp. 71–89, 1993.
- [98] D. Chillingworth, "Differential topology with a view to applications," *Research Notes in Mathematics*, vol. 9, 1976.
- [99] L. Tavernini, "Differential automata and their discrete simulators.," *nonlinear anal. theory methods applic.*, vol. 11, no. 6, pp. 665–683, 1987.
- [100] A. Overkamp, *Supervisory control for nondeterministic systems*, vol. 199/1994 of *Lecture Notes in Control and Information Sciences*, pp. 59–65. Springer Berlin, Heidelberg, 1994.
- [101] M. Heymann and F. Lin, "Discrete-event control of nondeterministic systems," *IEEE Transactions on Automatic Control*, vol. 43, no. 1, pp. 3–17, 1998.
- [102] J. Xu, "Digital redesign for controlling the chaotic Chua's circuit," *IEEE Transactions on Aerospace and Electronic Systems*, vol. 32, no. 4, 1996.
- [103] L. Shieh, W. Wang, and J. Tsai, "Digital redesign of H_∞ controller via bilinear approximation method for state-delayed systems," *International Journal of Control*, vol. 70, no. 5, pp. 665–683, 1998.
- [104] H. Lee, J. Park, and Y. Joo, "An efficient observer-based sampled-data control: Digital redesign approach," *IEEE Transactions on Circuits and Systems I: Fundamental Theory and Applications*, vol. 50, no. 12, pp. 1595–1600, 2003.
- [105] H. Lee, "Robust fuzzy-model-based controller design for nonlinear systems with parametric uncertainties," Master's thesis, Yonsei University, Seoul, Korea, 2000.
- [106] M. Vidyasagar, *Nonlinear systems analysis*. Society for Industrial Mathematics, 2002.

- [107] T. Johansen and B. Foss, *State-space modeling using operating regime decomposition and local models*. Universitetet i Trondheim, Norges tekniske høgskole, Institutt for teknisk kybernetikk, 1993.
- [108] Z. Li, W. Halang, and G. Chen, *Integration of fuzzy logic and Chaos Theory*. Springer, Berlin, 2006.
- [109] D. Shevits and B. Paden, “Lyapunov stability theory of nonsmooth systems,” *IEEE Transactions on Automatic Control*, vol. 39, no. 9, pp. 1910–1914, 1994.
- [110] P. Diamond and P. Kloeden, “Metric spaces of fuzzy sets,” *Fuzzy Sets and Systems*, vol. 100, pp. 63–71, 1999.
- [111] O. Kaleva, “On the convergence of fuzzy sets,” *Fuzzy Sets and Systems*, vol. 17, no. 1, pp. 53–65, 1985.
- [112] K. Lian, J. Liou, and C. Huang, “LMI-based integral fuzzy control of DC-DC converters,” *IEEE Transactions on Fuzzy Systems*, vol. 14, pp. 71–80, February 2006.
- [113] F. Lee and P. Tam, “Fuzzy control of DC-DC switching converters: stability and robustness analysis,” *Australian Journal of Electrical and Electronics Engineering*, vol. 4, no. 1, 2008.
- [114] W. So, C. Tse, and Y. Lee, “Development of a fuzzy logic controller for DC/DC converters: design, computer simulation, and experimental evaluation,” *IEEE Transactions on Power Electronics*, vol. 11, no. 1, pp. 24–32, 1996.
- [115] P. Carbonell and J. Navarro, “Local model-based fuzzy control of switch-mode DC/DC converters,” in *Proc. 14th IFAC Triennial World Congress*, pp. 237–242, 1999.
- [116] K. Mehran, D. Giaouris, and B. Zahawi, “Stability analysis and control of nonlinear phenomena in boost converter using model-based takagi-sugeno fuzzy approach,” *IEEE Transactions in Circuits and Systems - I*, vol. 57, pp. 200–212, January 2010.
- [117] K. Guesmi, A. Hamzaoui, and J. Zaytoon, “Control of nonlinear phenomena in DC-DC converters: Fuzzy logic approach,” *International Journal of Circuit Theory and Applications*, 2008.
- [118] K. Mehran, D. Giaouris, and B. Zahawi, “Modeling and stability analysis of dc-dc buck converter via takagi-sugeno fuzzy approach,” in *IEEE Conference on Intelligent Systems and Knowledge Engineering*, (Xiamen, China), IEEE, November 2008.
- [119] D. Giaouris, S. Banerjee, B. Zahawi, and V. Pickert, “Stability analysis of the continuous-conduction-mode buck converter via Filippov’s method,” *IEEE Transactions on Circuits and Systems-I*, vol. 55, pp. 1084–1096, May 2008.
- [120] K. Mehran, B. Zahawi, and D. Giaouris, “Modeling and stability analysis of nonlinear phenomena in impacting systems via model-based takagi-sugeno fuzzy approach,” *Submitted to IEEE Transactions on Fuzzy Systems*, 2010.

- [121] B. Brogliato, *Nonsmooth mechanics: models, dynamics, and control*. Springer Verlag, 1999.
- [122] M. Çamlıbel, *Complementarity methods in the analysis of piecewise linear dynamical systems*. PhD thesis, Eindhoven University of Technology, 2001.
- [123] I. Santos, *Modeling and numerical study of nonsmooth dynamical systems*. PhD thesis, Universitat Politècnica de Catalunya, Barcelona, 2006.
- [124] B. Brogliato, A. Ten Dam, L. Paoli, F. Genot, and M. Abadie, “Numerical simulation of finite dimensional multibody nonsmooth mechanical systems,” *Applied Mechanics Reviews*, vol. 55, p. 107, 2002.
- [125] P. Piiroinen and Y. Kuznetsov, “An event-driven method to simulate Filippov systems with accurate computing of sliding motions,” *ACM Transactions on Mathematical Software (TOMS)*, vol. 34, no. 3, pp. 1–24, 2008.
- [126] A. Nordmark and P. Piiroinen, “Simulation and stability analysis of impacting systems with complete chattering,” *Nonlinear Dynamics*, vol. 58, no. 1, pp. 85–106, 2009.
- [127] F. Dercole and Y. Kuznetsov, “SlideCont: An Auto 97 driver for bifurcation analysis of Filippov systems,” *ACM Transactions on Mathematical Software*, vol. 31, no. 1, pp. 95–119, 2005.
- [128] P. Thota and H. Dankowicz, “TC-HAT: A Novel Toolbox for the Continuation of Periodic Trajectories in Hybrid Dynamical Systems,” *SIAM Journal on Applied Dynamical Systems*, vol. 7, p. 1283, 2008.
- [129] W. Kang, P. Thota, B. Wilcox, and H. Dankowicz, “Bifurcation analysis of a microactuator using a new toolbox for continuation of hybrid system trajectories,” *Journal of Computational and Nonlinear Dynamics*, vol. 4, p. 011009, 2009.
- [130] J. Butcher, *Numerical methods for ordinary differential equations*. John Wiley & Sons Inc, 2008.
- [131] I. Santos, *Modeling And Numerical Study Of Nonsmooth Dynamical Systems: Applications to Mechanical and Power Electronics Systems*. PhD thesis, Universitat Politècnica de Catalunya, Barcelona, 2006.
- [132] V. Acary and B. Brogliato, *Numerical methods for nonsmooth dynamical systems: applications in mechanics and electronics*. Springer Verlag, 2008.
- [133] A. Lyapunov, “The general problem of the stability of motion,” *International Journal of Control*, vol. 55, no. 3, pp. 531–534, 1992.
- [134] A. Fuller, “Lyapunov Centenary Issue,” *International Journal of Control*, vol. 55, no. 3, pp. 521–527, 1992.

- [135] J. Zaborszky, G. Huang, B. Zheng, and T. Leung, "On the phase portrait of a class of large nonlinear dynamic systems such as the power system," *Automatic Control, IEEE Transactions on*, vol. 33, no. 1, pp. 4–15, 1988.
- [136] S. Boyd, L. E. Ghaoui, E. Feron, and V. Balakrishnan, *Linear Matrix Inequalities in System and Control Theory*. Philadelphia: SIAM, 1994.
- [137] R. Horn and C. Johnson, *Topics in matrix analysis*. Cambridge Univ Pr, 1994.
- [138] Y. Nesterov and A. Nemirovsky, "Interior point polynomial methods in convex programming," *Studies in applied mathematics*, vol. 13, 1994.
- [139] H. Wang, K. Tanaka, M. Griffin, U. Center, and E. Hartford, "Parallel distributed compensation of nonlinear systems by Takagi-Sugeno fuzzy model," in *Fuzzy Systems, 1995. International Joint Conference of the Fourth IEEE International Conference on Fuzzy Systems and The Second International Fuzzy Engineering Symposium., Proceedings of 1995 IEEE International Conference on*, vol. 2, 1995.
- [140] H. Wang, K. Tanaka, M. Griffin, U. Center, and E. Hartford, "An approach to fuzzy control of nonlinear systems: stability and design issues," *IEEE Transactions on Fuzzy Systems*, vol. 4, no. 1, pp. 14–23, 1996.
- [141] H. Wang, J. Li, D. Niemann, and K. Tanaka, "TS fuzzy model with linear rule consequence and PDC controller: a universal framework for nonlinear control systems," in *9th International Conference on Fuzzy systems*, (San Antonio, TX), pp. 549–554, Citeseer, May 2000.
- [142] K. Tanaka, T. Ikeda, and H. Wang, "Fuzzy regulators and fuzzy observers: relaxed stability conditions and LMI-based designs," *IEEE Transactions on Fuzzy Systems*, vol. 6, no. 2, pp. 250–265, 1998.
- [143] K. Tanaka, T. Ikeda, and H. Wang, "A unified approach to controlling chaos via an LMI-based fuzzy control system design," *IEEE Transactions on Circuits and Systems I: Fundamental Theory and Applications*, vol. 45, no. 10, pp. 1021–1040, 1998.
- [144] E. Kim and H. Lee, "New approaches to relaxed quadratic stability condition of fuzzy control systems," *IEEE Transactions on Fuzzy Systems*, vol. 8, no. 5, pp. 523–534, 2000.
- [145] E. Kim and S. Kim, "Stability analysis and synthesis for an affine fuzzy control system via LMI and ILMI: a continuous case," *IEEE Transactions on Fuzzy Systems*, vol. 10, no. 3, pp. 391–400, 2002.
- [146] M. Teixeira, E. Assuncao, and R. Avellar, "On relaxed LMI-based designs for fuzzy regulators and fuzzy observers," *IEEE Transactions on Fuzzy Systems*, vol. 11, no. 5, pp. 613–623, 2003.
- [147] W. Chang, J. Park, Y. Joo, and G. Chen, "Static output-feedback fuzzy controller for Chen's chaotic system with uncertainties," *Information Sciences*, vol. 151, pp. 227–244, 2003.

- [148] H. Ohtake, K. Tanaka, and H. Wang, "Switching fuzzy controller design based on switching Lyapunov function for a class of nonlinear systems," *IEEE Transactions on Systems, Man, and Cybernetics, Part B*, vol. 36, no. 1, pp. 13–23, 2006.
- [149] T. Taniguchi and M. Sugeno, "Stabilization of nonlinear systems based on piecewise Lyapunov functions," in *2004 IEEE International Conference on Fuzzy Systems, 2004. Proceedings*, vol. 3, 2004.
- [150] H. Ohtake, K. Tanaka, and H. Wang, "Piecewise nonlinear control," in *Proc. 42nd IEEE Conference on Decision and Control, Maui, HI*, 2003.
- [151] D. Xie, L. Wang, F. Hao, and G. Xie, "Robust stability analysis and control synthesis for discrete-time uncertain switched systems," in *42nd IEEE Conference on Decision and Control, 2003. Proceedings*, vol. 5, 2003.
- [152] G. Feng, "Stability analysis of piecewise discrete-time linear systems," *IEEE Transactions on Automatic Control*, vol. 47, no. 7, pp. 1108–1112, 2002.
- [153] M. Johansson, A. Rantzer, and K. Arzen, "Piecewise quadratic stability of fuzzy systems," *IEEE Transactions on Fuzzy Systems*, vol. 7, no. 6, pp. 713–722, 1999.
- [154] K. Kiriakidis, "Robust stabilization of the Takagi–Sugeno fuzzy model via bilinear matrix inequalities," *IEEE Transactions on Fuzzy Systems*, vol. 9, no. 2, p. 269, 2001.
- [155] K. Tanaka, H. Ohtake, and H. Wang, "A descriptor system approach to fuzzy control system design via fuzzy Lyapunov functions," *IEEE Transactions on Fuzzy Systems*, vol. 15, no. 3, pp. 333–341, 2007.
- [156] H. Tuan and P. Apkarian, "Low nonconvexity-rank bilinear matrix inequalities: algorithms and applications in robust controller and structure designs," *IEEE Transactions on Automatic Control*, vol. 45, no. 11, p. 2111, 2000.
- [157] H. Tuan, P. Apkarian, and Y. Nakashima, "A new Lagrangian dual global optimization algorithm for solving bilinear matrix inequalities," *International Journal of Robust and Nonlinear Control*, vol. 10, no. 7, pp. 561–578, 2000.
- [158] K. Tanaka, T. Hori, and H. Wang, "A multiple Lyapunov function approach to stabilization of fuzzy control systems," *IEEE Transactions on Fuzzy Systems*, vol. 11, no. 4, pp. 582–589, 2003.
- [159] H. Tuan, P. Apkarian, T. Narikiyo, and Y. Yamamoto, "Parameterized linear matrix inequality techniques in fuzzy control system design," *IEEE Transactions on Fuzzy Systems*, vol. 9, no. 2, p. 325, 2001.
- [160] K. Tanaka, T. Hori, and H. Wang, "A fuzzy Lyapunov approach to fuzzy control system design," in *2001 American Control Conference, Arlington, VA*, pp. 4790–4795, 2001.

- [161] B. Rhee and S. Won, "A new fuzzy Lyapunov function approach for a Takagi-Sugeno fuzzy control system design," *Fuzzy Sets and Systems*, vol. 157, no. 9, pp. 1211–1228, 2006.
- [162] B. Paden and S. Sastry, "A calculus for computing Filippov's differential inclusion with application to the variable structure control of robot manipulators," *IEEE Transaction in Circuits and Systems-I*, vol. 34, pp. 73–82, January 1987.
- [163] K. Mehran, D. Giaouris, and B. Zahawi, "Modeling and Stability Analysis of Closed Loop Current-Mode Controlled Ćuk Converter using Takagi-Sugeno Fuzzy Approach," in *CHAOS'09*, (England, London), IFAC, June 2009.
- [164] P. Peleties and R. DeCarlo, "Asymptotic stability of m-switched systems using Lyapunov-like functions," *American Control Conference*, pp. 1679–1684, 1991.
- [165] H. Ye, A. Michel, and L. Hou, "Stability analysis of discontinuous dynamical systems with applications," *Proc. of 13th IFAC*, pp. 461–466, 1996.
- [166] L. Debnath and P. Mikusiński, *Hilbert spaces with applications*. Academic Press, 2005.
- [167] G. Strang, *Linear algebra and its applications*. New York: Academic, 1976.
- [168] G. Thomas, R. Finney, and M. Weir, *Calculus and analytic geometry*. Addison-Wesley New York, 1996.
- [169] O. Krupková and O. Krupkova, *The geometry of ordinary variational equations*. Springer, 1997.
- [170] L. Xie, "Output feedback H_∞ control of systems with parameter uncertainty," *International Journal of Control*, vol. 63, no. 4, pp. 741–750, 1996.
- [171] J. Dong and G. Yang, " H_∞ controller synthesis via switched PDC scheme for discrete-time TS fuzzy systems," *IEEE Transactions on Fuzzy Systems*, vol. 17, no. 3, pp. 544–555, 2009.
- [172] Z. Liu, Y. Zhang, and Y. Wang, "A type-2 fuzzy switching control system for biped robots," *IEEE Transactions on Systems, Man, and Cybernetics, Part C: Applications and Reviews*, vol. 37, no. 6, pp. 1202–1213, 2007.
- [173] K. Ichida, K. Izumi, and K. Watanabe, "A switching control based fuzzy energy region method for underactuated robots," in *IEEE Workshop in Advanced Robotices and its Social Impacts*, pp. 190–195, June 2005.
- [174] H. Lam and F. Leung, "Fuzzy combination of fuzzy and switching state-feedback controllers for nonlinear systems subject to parameter uncertainties," *IEEE Transactions on Systems, Man, and Cybernetics, Part B: Cybernetics*, vol. 35, no. 2, p. 269, 2005.

- [175] L. Xiaodong and Z. Qingling, "New approaches to H_∞ controller designs based on fuzzy observers for TS fuzzy systems via LMI," *Automatica*, vol. 39, no. 9, pp. 1571–1582, 2003.
- [176] S. Tong and H. Li, "Observer-based robust fuzzy control of nonlinear systems with parametric uncertainties," *Fuzzy sets and systems*, vol. 131, no. 2, pp. 165–184, 2002.
- [177] M. Tittus, S. of Electrical, C. Engineering, and C. Högskola, *Control synthesis for batch processes*. Chalmers tekniska högsk., 1995.
- [178] M. Green and D. Limebeer, *Linear robust control*. Prentice-Hall, Inc. Upper Saddle River, NJ, USA, 1994.
- [179] L. Ljung, *System identification*. Springer, 1987.
- [180] J. Sjöberg, Q. Zhang, L. Ljung, A. Benveniste, B. Delyon, P. Glorennec, H. Hjalmarsson, and A. Juditsky, "Nonlinear black-box modeling in system identification: a unified overview," *Automatica*, vol. 31, no. 12, pp. 1691–1724, 1995.
- [181] P. Makila and J. Partington, "On robustness in system identification," *Automatica-oxford*, vol. 35, pp. 907–916, 1999.
- [182] J. Hespanha, *Logic-based switching algorithms in control*. PhD thesis, Citeseer, 1998.
- [183] R. Palm, D. Driankov, and H. Hellendoorn, *Model based fuzzy control: fuzzy gain schedulers and sliding mode fuzzy controllers*. Springer Verlag, 1997.
- [184] K. Åström and B. Wittenmark, *Adaptive control*. Addison-Wesley Longman Publishing Co., Inc. Boston, MA, USA, 1994.
- [185] J. Baillieul and J. Willems, *Mathematical control theory*. Springer Verlag, 1999.
- [186] G. Chen, "Chaos: Its control and generation for engineering applications," *Dynamics of Continuous Discrete and Impulsive Systems Series B*, vol. 10, pp. 235–246, 2003.
- [187] A. Fradkov and R. Evans, "Control of chaos: Methods and applications in engineering," *Annual Reviews in Control*, vol. 29, no. 1, pp. 33–56, 2005.
- [188] H. Hiew and C. Tsang, "An adaptive fuzzy system for modeling chaos," *Information Sciences*, vol. 81, no. 3-4, pp. 193–212, 1994.
- [189] H. Wang, K. Tanaka, and T. Ikeda, "Fuzzy modeling and control of chaotic systems," in *IEEE International Symposium on Circuits and Systems*, Springer, 1996.
- [190] E. Abed, H. Wang, and A. Tesi, "Control of bifurcations and chaos," *The Control Handbook*, pp. 951–966, 1996.
- [191] F. Gordillo, J. Aracil, and T. Alamo, "Determining limit cycles in fuzzy control systems," in *Fuzzy Systems, 1997., Proceedings of the 6th IEEE International Conference on*, vol. 1, 1997.

- [192] O. Calvo and J. Cartwright, "Fuzzy control of chaos," *International Journal of Bifurcation and Chaos*, vol. 8, pp. 1743–1747, 1998.
- [193] L. Chen, G. Chen, and Y. Lee, "Fuzzy modeling and adaptive control of uncertain chaotic systems," *Information Sciences*, vol. 121, no. 1, pp. 27–37, 1999.
- [194] Y. Tang, N. Zhang, and Y. Li, "Stable fuzzy adaptive control for a class of nonlinear systems," *Fuzzy sets and systems*, vol. 104, no. 2, pp. 279–288, 1999.
- [195] C. Park, C. Lee, and M. Park, "Design of an adaptive fuzzy model based controller for chaotic dynamics in Lorenz systems with uncertainty," *Information Sciences*, vol. 147, no. 1-4, pp. 245–266, 2002.
- [196] L. Wang, *Adaptive fuzzy systems and control: design and stability analysis*. Prentice-Hall, Inc. Upper Saddle River, NJ, USA, 1994.
- [197] E. Ifeachor and B. Jervis, *Digital signal processing: a practical approach*. Pearson Education, 2002.
- [198] K. Parhi, *VLSI digital signal processing systems: design and implementation*. Wiley India Pvt. Ltd., 2007.
- [199] B. Kuo, *Digital control systems*. Oxford University Press, Inc. New York, NY, USA, 1992.
- [200] J. Sunkel, L. Shieh, and J. Zhang, "Digital redesign of an optimal momentum management controller for the space station," *Journal of Guidance, Control, and Dynamics*, vol. 14, no. 4, pp. 712–723, 1991.
- [201] L. Shieh, W. Wang, and J. Zheng, "Robust control of sampled-data uncertain systems using digitally redesigned observer-based controllers," *International Journal of Control*, vol. 66, no. 1, pp. 43–64, 1997.
- [202] Y. Joo, L. Shieh, and G. Chen, "Hybrid state-space fuzzy model-based controller with dual-ratesampling for digital control of chaotic systems," *IEEE transactions on fuzzy systems*, vol. 7, no. 4, pp. 394–408, 1999.
- [203] S. Guo, L. San Shieh, G. Chen, and C. Lin, "Effective chaotic orbit tracker: a prediction-based digitalredesign approach," *IEEE Transactions on Circuits and Systems I: Fundamental Theory and Applications*, vol. 47, no. 11, pp. 1557–1570, 2000.
- [204] S. Guo, L. Shieh, C. Lin, and J. Chandra, "State-space self-tuning control for nonlinear stochastic and chaotic hybrid systems," *International Journal of Bifurcation and Chaos in Applied Sciences and Engineering*, vol. 11, no. 4, pp. 1079–1113, 2001.
- [205] W. Chang, J. Park, Y. Joo, and G. Chen, "Design of sampled-data fuzzy-model-based control systems by using intelligent digital redesign," *IEEE Transactions on Circuits and Systems I: Fundamental Theory and Applications*, vol. 49, no. 4, pp. 509–517, 2002.

- [206] H. Lee, H. Kim, Y. Joo, W. Chang, and J. Park, "A new intelligent digital redesign for TS fuzzy systems: global approach," *IEEE Transactions on Fuzzy Systems*, vol. 12, no. 2, pp. 274–284, 2004.
- [207] H. Lee, J. Park, and Y. Joo, "Digitalizing a fuzzy observer-based output-feedback control: intelligent digital redesign approach," *IEEE Transactions on Fuzzy Systems*, vol. 13, no. 5, pp. 701–716, 2005.
- [208] J. Malmberg, B. Bernhardsson, and K.J.Åström, "A stabilizing switching scheme for multi controller systems," in *13th IFAC World Congress, (San Francisco, CA)*, 1996.
- [209] F. Cuesta, F. Gordillo, J. Aracil, and A. Ollero, "Stability analysis of nonlinear multivariable Takagi–Sugeno fuzzy control systems," *IEEE Transactions on Fuzzy systems*, vol. 7, no. 5, 1999.
- [210] M. Sugeno, "On stability of fuzzy systems expressed by fuzzy rules with singleton consequents," *IEEE Transactions on Fuzzy systems*, vol. 7, no. 2, p. 201, 1999.
- [211] C. K. Tse, *Complex Behavior of Switching Power Converters*. CRC Press, 2004.
- [212] C. Tse and M. Di Bernardo, "Complex behavior in switching power converters," *Proceedings of the IEEE*, vol. 90, no. 5, pp. 768–781, 2002.
- [213] I. Daho, D. Giaouris, B. Zahawi, V. Picker, and S. Banerjee, "Stability analysis and bifurcation control of hysteresis current controlled cuk converter using Filippovs method," in *Power Electronics, Machines and Drives, 2008. PEMD 2008. 4th IET Conference on*, pp. 381–385, 2008.
- [214] P. Cabinet, A. Nemirovski, A. Laub, and M. Chilali, "LMI Control Toolbox," *The Math Works Inc*, 1995.
- [215] M. Aizerman and F. Gantmacher, "Absolute stability of control systems," *Academy of Sciences of URSS*, 1963.
- [216] A. Albert, "Conditions for positive and nonnegative definiteness in terms of pseudoinverses," *SIAM Journal on Applied Mathematics*, vol. 17, no. 2, pp. 434–440, 1969.
- [217] J. Löfberg, "YALMIP: A MATLAB toolbox for rapid prototyping of optimization problems," *Web: <http://control.ee.ethz.ch/joloef/yalmip.msql>*, 2002.
- [218] R. Nikoukhah, F. Delebecque, and L. El Ghaoui, "LMITOOL: a Package for LMI Optimization in Scilab," *Rapport technique*, vol. 170, 2008.